Feasibility of a catalytic membrane reactor for ethylene production via oxidative coupling of methane

Feasibility of a catalytic membrane reactor for ethylene production via oxidative coupling of methane

PROEFSCHRIFT

ter verkrijging van de graad van doctor aan de Technische Universiteit Eindhoven,
op gezag van de rector magnificus prof.dr.ir. F.P.T. Baaijens,
voor een commissie aangewezen door het College voor Promoties,
in het openbaar te verdedigen op maandag 5 oktober 2020 om 13:30 uur

door

Aitor Cruellas Labella

geboren te Fraga, Huesca, Spanje

Dit proefschrift is goedgekeurd door de promotoren en de samenstelling van de promotiecommissie is als volgt:

voorzitter:	prof. dr. ir. E.J.M. Hensen
1e promotor:	prof. dr. ir. M. van Sint Annaland
2e promotor:	prof. dr. Eng. F. Gallucci
leden:	dr. ir. Z. Borneman
	prof. dr. ir. W.A. Meulenberg (Universiteit Twente)
	prof. dr. ir. A. Urakawa (Technische Universiteit Delft)
	prof. dr. M. Menéndez Sastre (Universidad de Zaragoza)
	dr. Eng. V. Spallina (The University of Manchester)

Het onderzoek of ontwerp dat in dit proefschrift wordt beschreven is uitgevoerd in overeenstemming met de TU/e Gedragscode Wetenschapsbeoefening.

The research described in this thesis has been carried out in the Multiphase Reactors Group (SMR), division Chemical Process Intensification (SPI), within the Chemical Engineering and Chemistry Department of Eindhoven University of Technology, The Netherlands.

The research leading to these results has received funding from the European Union's Horizon 2020 research and innovation programme under grant agreement No 679933 (MEMERE project)

The present publication reflects only the author's views and the European Union is not liable for any use that may be made of the information contained therein.

Printed by: Gildeprint

A catalogue record is available from the Eindhoven University of Technology Library.

ISBN: 978-90-386-5020-3

Content

Summary

Ethylene is one of the most used chemicals in the petrochemical industry with a current worldwide production over 140 million tons per year. Nowadays, most of this ethylene is produced from liquid hydrocarbons, whose price is expected to increase significantly in the coming years. Therefore, a "fuel switching" scenario replacing the feedstock with other sources like natural gas is becoming increasingly interesting. Among the different alternatives to convert natural gas to ethylene, the oxidative coupling of methane (OCM) route has attracted large interest over the last decades. OCM is a catalytic process for directly converting methane into high-valued hydrocarbons. The industrial exploitation of this reaction system is, however, hampered by the low product yields achieved due to the parallel and consecutive undesired reactions occurring simultaneously in the system. Great efforts have been made to make the process more competitive with conventional technologies by improving the performance of the process at conditions feasible at large scale.

It is known that one of the possibilities to increase the reactor performance is to keep a low oxygen partial pressure along the reactor length because the OCM reaction (forming ethane from methane) has a lower reaction order in oxygen relative to undesired complete and incomplete methane combustion reactions, and is thus favored at low oxygen partial pressures. Low local oxygen partial pressures, but still considerable methane conversions, can theoretically be achieved in membrane reactors, where the oxygen is fed distributively along the reactor length through porous membranes or dense mixed ionic-electronic conducting (MIEC) membranes (also integrating oxygen separation). Moreover, in membrane reactors also heat

management issues originated from the mild exothermicity of the reactions involved in the process can also be mitigated, minimizing the formation of hot-spots that would seriously decrease the OCM process performance. The objective of this research is therefore to obtain a better understanding of the advantages and differences of the OCM membrane reactor concept in comparison with conventional OCM reactor configurations, allowing to better assess the technical and economic feasibility of the membrane reactor concept in comparison to ethylene production technologies that are nowadays dominating the market.

This research project was carried out in the context of the H2020 project MEMERE (MEthane activation via integrated MEmbrane REactors).

This thesis starts by presenting an overview of the many different reactor configurations for OCM that have been proposed in literature, highlighting the advantages and drawbacks of each of them. Special attention is paid to the integration of membrane reactors into the OCM process, briefly reviewing the main experimental works published on this topic.

Secondly, the most common and most promising reactor configurations for OCM, including different types of membrane reactors but also other concepts with different types of oxygen distribution, are quantitatively evaluated by means of phenomenological reactor models. The key reactor performance indicators, viz. methane conversion, C_2 selectivity, C_2 yield, and heat management, have been investigated in detail with the different models and thoroughly compared. The optimization of these parameters leads to the achievement of OCM membrane reactor C_2 yields up to nearly 60%, outperforming conventional configurations (maximum C_2 yields not higher than 20%) and therefore justifying their further investigation in this thesis.

After the investigation and discussion of the main alternatives which can increase the performance of OCM (from a theoretical point of view), experiments are required to corroborate this improved behavior and to demonstrate the suitability of all the

individual components (catalyst, membrane, reactor and their integration) necessary to properly design an OCM membrane reactor.

Accordingly, the thesis continues by studying one of the most often investigated OCM catalysts, viz. $Mn/Na_2WO_4/SiO_2$ since the overall performance of the OCM process highly depends on the performance of the catalyst. In particular, the behavior of this catalyst under conditions suitable for operation in a membrane reactor (i.e. very high methane/oxygen ratios) has been analyzed with a special focus on the kinetics of consecutive reactions. Experiments under differential conditions have been carried out and the kinetics of the different reactions involved in the process has been determined. Out of these experiments, the undesired secondary reactions and the C_2H_4 combustion in particular have been highlighted to be a crucial parameter for a proper optimization of the system performance. In addition, experiments under integral conditions have been performed to evaluate the activity, selectivity and stability of the catalyst when working under OCM conditions.

Subsequently, an OCM membrane reactor setup has been designed and constructed. OCM membrane reactor tests have been performed to elucidate and quantify the effects of the most important process parameters, viz. CH_4/O_2 ratio, temperature and gas residence time. The performance of the membrane reactor has been evaluated and compared with the conventional OCM packed-bed reactor configuration with premixed feed. Although relatively high yields have been obtained experimentally with the packed bed reactor (C_2 yields of around 20%), no improvements could be observed when integrating porous membranes in the reactor. Nevertheless, an even oxygen distribution in the in-house designed membrane reactor configuration could be demonstrated. The effective diffusion coefficient of the porous membrane employed in the membrane reactor tests, which was high limit effects of back-permeation, has to be better controlled and optimized to experimentally demonstrate the increase in performance expected from the simulations.

Finally, a techno-economic evaluation of the OCM technology has been carried out. This last part of the thesis allows evaluating, from a process point of view, the viability

of OCM and consequently to assess whether the large research efforts carried out at lab-scale can be somehow translated into the emergence of an alternative and competitive ethylene production technology. The cost of ethylene produced with the OCM technology, employing several different reactor configurations, has been calculated by simulating an industrial scale OCM plant in Aspen Plus. A comparison with the current ethylene market price has been made, highlighting the differences, and their origin, with conventional ethylene production technologies. The OCM competitiveness for the coming decades within the ethylene production market has also been addressed by considering the price trends of the different feedstocks that are nowadays employed for ethylene production. With this analysis it has been shown that both the porous and the dense OCM membrane reactor configurations, when designed at industrial scale, are able to compete from an environmental and economic point of view with the currently industrially applied ethylene production technologies. Therefore, the potential of the OCM membrane reactor as an alternative to produce ethylene has been demonstrated and the scale-up of one of those technologies (dense or porous membranes) is highlighted as the main challenge that still needs to be solved.

The research leading to these results has received funding from the European Union's Horizon 2020 research and innovation programme under grant agreement No 679933 (MEMERE project).

Chapter 1

Introduction

Abstract

Ethylene is one of the top five chemicals produced worldwide, and alternative technologies which can compete with conventional technologies (particularly naphtha steam cracking) could be beneficial both in terms of emissions and costs. One of these technologies, the Oxidative Coupling of Methane (OCM) process, which aims to convert natural gas into ethylene in a single step, is analyzed from different points of view to evaluate its feasibility and industrial viability. This process is detailed in this first chapter, highlighting the aspects which make it attractive for the research community. Additionally, its current constraints are also explained to emphasize the challenges and opportunities that still need to be investigated. Finally, the chapter concludes by describing the content of the rest of the thesis, giving a brief overview of each of the sections.

1.1. Introduction

1) 29th July, 2019: "*Humans have already consumed the Planet's annual resources for this year*" [1].

2) *"With Earth Overshoot Day occurring ever earlier in the year, and a big part of it being the growing amounts of CO_2 emissions, the importance of decisive action is becoming even more evident."* María Carolina Schmidt Zaldívar, Minister of Environment, Chile, and chair of the Climate COP25 [1].

These two quotes are examples showing the necessity of balancing and improving the utilization of non-renewable Earth resources if we want to maintain a healthy planet for future generations. And plastics industry plays a big role on the petrochemical industry, one of the main contributors to this consumption of the Earth resources. Plastics are nowadays essential for our daily life and it is very unlikely to be in a room, wherever it is and whatever its function is, free of plastics. And the vast majority of them are produced from fossil fuels. Therefore, its production implies the consumption of the world resources and most often the emissions of significant amounts of CO_2 into the atmosphere. One of the main contributors to this huge industry is ethylene, whose annual worldwide production exceeds 150 million tons and its annual growth rate is about 4% [2], [3]. Ethylene is used as the raw material to manufacture a very broad range of products like polyethylene, ethylene oxide, from which PET is obtained, or ethylene dichloride, used to produce PVC.

Historically, ethylene has been produced via the oil (mainly naphtha in Europe) steam cracking process which employs fossil fuels as feedstock. The close relation existing between both price trends corroborates the ethylene price dependency on naphtha, and consequently on the oil market (Figure 1.1). In the naphtha steam cracking (NSC) process the long carbon chains are broken into lighter hydrocarbons that have an added value and can be sold in the market. In addition to ethylene, also propylene, BTX and heavy oil are by-products of this reaction. However, this traditional process

is very energy intensive and the CO_2 emissions associated to it are quite high, being between 2 and 3 $ton_{CO_2}/ton_{C_2H_4}$ [4].

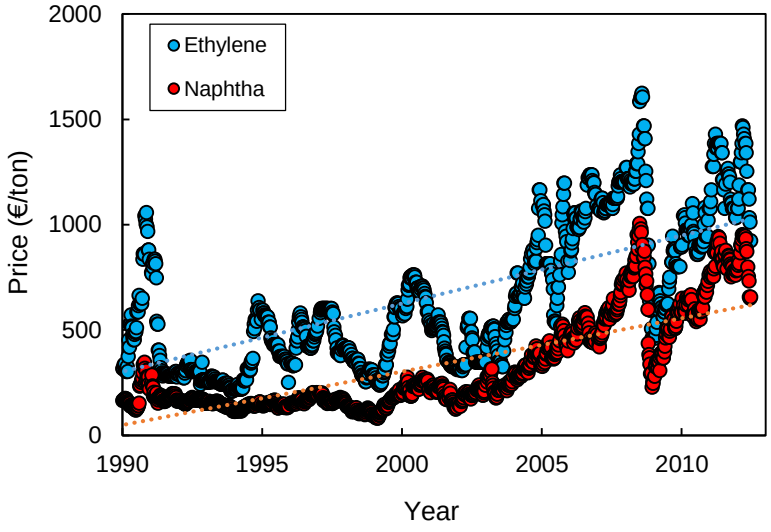

Figure 1.1. Historical prices of ethylene and naphtha [5].

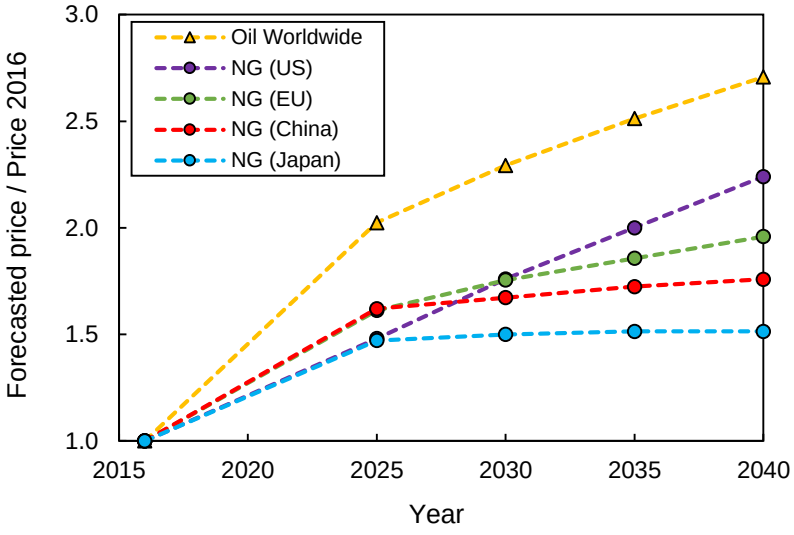

Figure 1.2. Forecast for the normalized price (respect to 2016) of oil and natural gas for the coming period [6].

Therefore, the drawbacks of this process, the fact that the price of oil in the last years has increased more than other fossil fuels like natural gas (Figure 1.2), and the forecasts showing that this tendency will continue in the coming years [6] make interesting the search for alternative processes which can produce ethylene in a cheaper and more sustainable way.

Following this statement, the oil and natural gas price projections have driven the research efforts towards diversifying the raw materials employed for the production of olefins, also known as the "fuel switching" scenario [7], [8]. Since natural gas resources are believed to be more abundant than the ones of oil and its carbon content per molecule is lower than oil, natural gas is one of the main alternatives to substitute oil, at least partially, in the production of hydrocarbons.

The production of ethylene from natural gas, containing mostly methane, can be accomplished via a direct and an indirect route, so called Fischer-Tropsch synthesis. In the indirect route, natural gas is firstly converted into syngas (a mixture of CO and H_2), while in a secondary step and by means of catalytic reactions, light hydrocarbons can be produced. On the other side, the direct route for the production of ethylene from natural gas in a single step involves the catalytic conversion of methane by reaction with an oxidizing agent, commonly oxygen, at high temperature (>750 °C), into the desired product C_2H_4 (or C_2H_6) and the main undesired by-products CO and CO_2 (see Reaction 1.1).

$$2\,CH_4 + O_2 \rightarrow C_2H_4 + 2\,H_2O \qquad \Delta H° = -141\,\frac{kJ}{mol\ CH_4} \qquad \textit{Reaction 1.1}$$

Although it may seem as a simple single reaction, this direct route, the so-called **oxidative coupling of methane (OCM)**, consists in reality of a series of parallel and consecutive steps classified in desired and undesired reactions [7]–[9]. Generally, it is well-accepted that the main mechanism of this process is the following: methane reacts firstly with oxygen to form ethane, which is subsequently dehydrogenated (oxidatively or non-oxidatively) to produce ethylene [10]. This desired OCM path competes with the combustion and/or reforming reactions occurring all along this

reaction path (methane, ethane and ethylene are prone to partial and full combustion). The three primary competing reactions of this system are shown below (Reaction 1.2, Reaction 1.3 and Reaction 1.4):

$$2\,CH_4 + \frac{1}{2}O_2 \rightarrow C_2H_6 + H_2O \qquad \Delta H° = -88.4\,\frac{kJ}{mol\ CH_4} \qquad \textit{Reaction 1.2}$$

$$CH_4 + 2\,O_2 \rightarrow CO_2 + 2\,H_2O \qquad \Delta H° = -802.6\,\frac{kJ}{mol\ CH_4} \qquad \textit{Reaction 1.3}$$

$$CH_4 + \frac{1}{2}O_2 \rightarrow CO + 2\,H_2 \qquad \Delta H° = -36.0\,\frac{kJ}{mol\ CH_4} \qquad \textit{Reaction 1.4}$$

As with many selective oxidation reactions, the competition between the parallel primary reactions results in the typical conversion-selectivity problem: high CH_4 conversions (which requires feeding a relatively large amount of O_2) are associated with a relatively poor product selectivity and a large yield towards undesired combustion products like CO_x. In addition, the highly reactive intermediate C_2H_6 may easily react to unwanted oxidation products, either via the combustion when oxygen is still present in the reactor or via other paths like reforming [11]. This is the main reason why the yield of higher hydrocarbons (C_2 and higher) is generally insufficient (<< 30%) to make the OCM concept industrially feasible.

Since the 1980's, when the first OCM articles were published [12], there have been several attempts to improve the C_2 yield by developing novel catalysts including rare-earth oxides [13], [14], resulting in some of the most promising catalysts for OCM: Li/MgO [15], [16], La_2O_3/CaO [17] and Mn/Na_2WO_4/SiO_2 [18], [19]. Although optimization of the catalyst and development of various different reactor types has led to an improved performance of the process, a single pass C_2 yield above 30-35% has never been achieved (e.g. [7], [20]) (with a stable catalyst and without large dilution). Thus, the direct conversion of CH_4 into C_2H_4 is still high on the industrial wish-list, but it remains a major scientific and technological challenge for chemical engineers. One of most interesting concepts to carry out the OCM and to achieve an industrially feasible yield is the membrane reactor (Figure 1.3) [21], [22]. With the integration of

membranes in the reactor, which could be porous or dense (often perovskite type), a distributed oxygen feeding policy is achieved, thus maintaining a low oxygen concentration along the reactor and favoring the C_2 production reactions. In the case of dense membranes, the in-situ O_2-N_2 separation can avoid the utilization of the very energy-intensive air separation unit required for other OCM concepts. On top of it, the distribution of the reaction along the reactor axial length will facilitate the heat management derived from the mild exothermicity of the reaction.

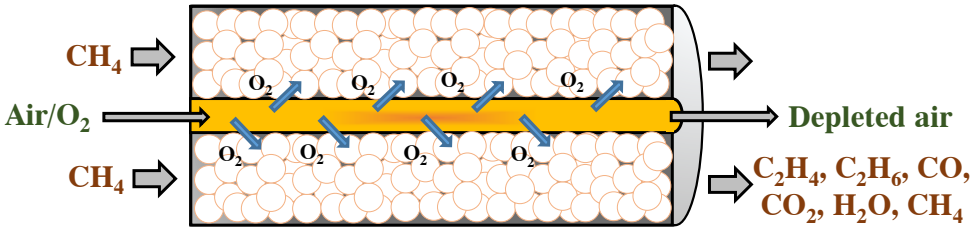

Figure 1.3. Schematic representation of an OCM membrane reactor.

Therefore, the main objective of this thesis is to evaluate the feasibility of the oxidative coupling of methane process when employing a membrane reactor and its comparison with conventional technologies. This comparison is carried out both from a reactor and process point of view, analyzing the advantages and drawbacks of each of the configurations.

To do so, in **Chapter 2** an overview of the state-of-the-art of the oxidative coupling of methane is performed, being particularly focused on the reactor configurations that researches have previously attempted. Therefore, the most promising reactor designs are highlighted from this data collection. This study is used to select the most relevant OCM reactor configurations, which are evaluated, quantified and compared in **Chapter 3**, showing the benefits and drawbacks of each individual configuration by means of phenomenological 1-D models. Out of this analysis, membrane reactors emerge as a feasible alternative to enhance the yield of the OCM reactor. Differently, **Chapter 4** experimentally investigates the behavior under OCM conditions (including membrane reactor conditions) of one of the most promising OCM catalysts, the $Mn/Na_2WO_4/SiO_2$. A kinetic model is developed based on this investigation, paying

special attention to the secondary OCM reactions, a crucial step that needs to be optimized when attempting the maximization of the C_2 yield. The knowledge gained in the previous chapters is integrated in **Chapter 5**, where the experimental demonstration of the OCM membrane reactor and its comparison with the conventional packed bed is sought. A porous membrane is used to build the packed bed membrane reactor, and the main characteristics of this configuration are analyzed and highlighted. Thereafter, **Chapter 6** and **7** relates to the techno-economic analysis of different OCM reactor configurations and how these configurations are integrated into the OCM process. The industrial viability, both from an environmental and economic point of view, of the conventional OCM packed bed reactor is evaluated in **Chapter 6**, while in **Chapter 7** two different membrane reactor concepts, employing either porous or dense membranes, are considered. The main differences among all these OCM configurations and its comparison to the conventional ethylene production technology, naphtha steam cracking, are described here, thus contributing to a deeper understanding of the overall ethylene production market and on the OCM industrial potential. Finally, **Chapter 8** summarizes the main conclusions of this work and provides recommendations for a future continuation of this study.

1.2. Bibliography

[1] "www.footprintnetwork.org," 2019.

[2] "www.ihsmarkit.com/products/ethylene-chemical-economics-handbook.html," 2019. .

[3] V. Spallina, I. C. Velarde, J. A. M. Jimenez, H. R. Godini, F. Gallucci, and M. Van Sint Annaland, "Techno-economic assessment of different routes for olefins production through the oxidative coupling of methane (OCM): Advances in benchmark technologies," *Energy Conversion and Management*, vol. 154, pp. 244–261, Dec. 2017.

[4] T. Ren, M. K. Patel, and K. Blok, "Steam cracking and methane to olefins: Energy use, CO2 emissions and production costs," *Energy*, vol. 33, no. 5, pp. 817–833, 2008.

[5] "U.S. Energy Information Administration." [Online]. Available: www.eia.gov.

[6] "World Energy Outlook," *International Energy Agency, www.iea.org/weo/*, 2017.

[7] A. Galadima and O. Muraza, "Revisiting the oxidative coupling of methane to ethylene in the golden period of shale gas: A review," *Journal of Industrial and Engineering Chemistry*, vol. 37, pp. 1–13, May 2016.

[8] C. Karakaya and R. J. Kee, "Progress in the direct catalytic conversion of methane to fuels and chemicals," *Progress in Energy and Combustion Science*, vol. 55, pp. 60–97, 2016.

[9] E. V Kondratenko *et al.*, "Methane conversion into different hydrocarbons or oxygenates: current status and future perspectives in catalyst development and reactor operation," *Catalysis Science & Technology*, vol. 7, no. 2, pp. 366–381, 2017.

[10] V. I. Lomonosov and M. Y. Sinev, "Oxidative coupling of methane: Mechanism and kinetics," *Kinetics and Catalysis*, vol. 57, no. 5, pp. 647–676, 2016.

[11] T. P. Tiemersma, M. J. Tuinier, F. Gallucci, J. A. M. Kuipers, and M. V. S. Annaland, "A kinetics study for the oxidative coupling of methane on a Mn/Na 2WO 4/SiO 2 catalyst," *Applied Catalysis A: General*, vol. 433–434, pp. 96–108, 2012.

[12] G. E. Keller and M. M. Bhasin, "Synthesis of Ethylene via Oxidative Coupling of Methane. I. Determination of active catalysts," *Journal of Catalysis*, vol. 73, pp. 9–19, 1982.

[13] K. Otsuka, K. Jinno, and A. Morikawa, "Active and selective catalysts for the synthesis of C2H4 and C2H6 via oxidative coupling of methane," *Journal of Catalysis*, vol. 100, no. 2, pp. 353–359, 1986.

[14] K. Otsuka, M. Hatano, and T. Komatsu, "Synthesis of C2H4 by Partial Oxidation of CH4 Over Transition Metal Oxides With Alkali-Chlorides," *Studies in Surface Science and Catalysis*, vol. 36, pp. 383–387, 1988.

[15] T. Ito, J. Wang, C. H. Lin, and J. H. Lunsford, "Oxidative dimerization of methane over a lithium-promoted magnesium oxide catalyst," *Journal of the American Chemical Society*, vol. 107, no. 18, pp. 5062–5068, Sep. 1985.

[16] S. J. Korf, J. A. Roos, N. A. De Bruijn, J. G. Van Ommen, and J. R. H. Ross, "Lithium Chemistry of Lithium Doped Magnesium Oxide Catalysts Used in the Oxidative Coupling of Methane," *Applied Catalysis*, vol. 58, no. 1, pp. 131–146, 1990.

[17] J. A. Sofranko, J. J. Leonard, and C. A. Jones, "The Oxidative Conversion of Methane to Higher Hydrocarbons," *Journal of Catalysis*, vol. 103, pp. 302–310, 1987.

[18] J. Wu and S. Li, "The Role of Distorted WO4 in the Oxidative Coupling of

Methane on Supported Tungsten Oxide Catalysts," *The Journal of Physical Chemistry*, vol. 99, no. 13, pp. 4566–4568, Mar. 1995.

[19] S. Pak, P. Qiu, and J. H. Lunsford, "Elementary reactions in the oxidative coupling of methane over Mn/Na2WO4/SiO2 and Mn/Na2WO4/MgO catalysts," *J. Catal.*, vol. 179, pp. 222–230, 1998.

[20] M. Makri and C. G. Vayenas, "Successful scale up of gas recycle reactor–separators for the production of C2H4 from CH4," *Applied Catalysis A: General*, vol. 244, no. 2, pp. 301–310, May 2003.

[21] S. Jašo, H. R. Godini, H. Arellano-Garcia, M. Omidkhah, and G. Wozny, "Analysis of attainable reactor performance for the oxidative methane coupling process," *Chemical Engineering Science*, vol. 65, no. 24, pp. 6341–6352, 2010.

[22] H. R. Godini, A. Gili, O. Görke, U. Simon, K. Hou, and G. Wozny, "Performance Analysis of a Porous Packed Bed Membrane Reactor for Oxidative Coupling of Methane: Structural and Operational Characteristics," *Energy & Fuels*, vol. 28, no. 2, pp. 877–890, Feb. 2014.

Chapter 2

Oxidative Coupling of Methane: State-of-the-art

Abstract

In this chapter, an overview of the main process characteristics and challenges of the oxidative coupling of methane process is presented, together with a description of different solutions proposed in the literature. From this study, both the heat management and the typically poor performance in terms of C_2 yields achieved in an OCM reactor are highlighted as the main factors hindering industrial exploitation of the OCM process. It has been also evidenced, based on the literature studies carried out so far, that membrane reactors are thought to be one of the most interesting alternative configurations which can overcome these limitations. Thus, the specific characteristics of this reactor configuration and the main experimental results achieved to date with this reactor configuration are also presented.

2.1. Introduction

This chapter summarizes the main reactor technologies proposed along the OCM "history", explaining the differences between the different concepts, how these specific challenges related to the OCM process are addressed and possibly how to improve the C_{2+} yields.

As briefly explained in Chapter 1, there are different aspects which have to be taken into account in the design and construction of an OCM reactor:

- The C_{2+} production is favored when maintaining a low oxygen concentration along the reactor.
- The OCM reaction is exothermic, so that a lot of heat must be removed from the system.
- The reaction is catalytic, so a multiphase reactor must be handled.
- The feasibility of the OCM process is highly affected by the costs of air separation and downstream separation.
- Once the C_{2+} products are formed, they can be oxidized and/or reformed, so the integration of a products separation unit can improve the yield of the reaction.

The different concepts presented in this work can be divided into different categories according to how the above-mentioned issues are handled.

2.2. Main OCM characteristics and their influence on the reactor design

The design of a reactor for the oxidative coupling of methane must consider the following aspects: type of multiphase reactor, heat management options, concepts of distributive O_2 feeding, integration of product separation and integration of O_2/N_2

separation. An overview of these aspects along with the most important options proposed in the literature is given below.

2.2.1. Types of multiphase reactors

Since OCM is a heterogeneous reaction that uses a catalyst to direct the reaction towards the desired path for the formation of C_2's, different multiphase reactors have been proposed to maximize the gas-catalyst contact and to obtain high process performance. In general, three possibilities have been studied for OCM: fixed (packed) bed reactors, fluidized bed reactors and bubble column reactors. In the first two cases, the catalyst is present in solid state, whereas in bubble columns it is assumed that it is a liquid in the form of molten salts. This is possible with some types of catalysts whose melting temperature is lower than the reaction temperature (or < 800 °C at least), which is the case for instance of lithium carbonates [1].

In fixed beds, the catalyst is present in form of solid pellets. This is the most studied configuration for OCM, and most of the catalytic studies were also carried out using this kind of reactor. In lab-scale setups, it is usually relatively easy to operate the reactor under isothermal conditions, which is also essential to evaluate the kinetic parameters at a fixed temperature. In industrial scale units, the available surface area for heat exchange is often much lower, which means that temperature profiles will be present in the reactor because of the very exothermic reactions, even when external cooling is applied (see Chapter 3, where this issue is extensively discussed). A multi-tubular configuration might be necessary in this case to ensure sufficient heat exchange. This point will be addressed in more detail in the next sections.

The catalyst can alternatively be coated on the tube walls in channels, as proposed by Kaminsky et al. [2]. In this case, a shell-and-tube configuration was also proposed. One advantage of this reactor, compared to packed bed reactors, is that the reaction can be localized directly at the location in the tubes where the heat exchange with the external coolant is most efficient. In this sense, the radial heat transfer resistance and

hence radial temperature gradients will be minimized (a radial temperature gradient could still be formed, but opposite to the one that would occur in packed beds, where the bulk temperature of the gas in the reaction section would be higher than the temperature at the tube walls). Another advantage is related to the low pressure drop. In large scale packed beds, pressure drops can set constraints on the reactor design (tube length), particle size and operating conditions (gas flow rate). Some of these constraints are often conflicting with those related to a more efficient heat management: for instance, longer tubes or higher gas flow rates can improve temperature control, but at the same time they increase the gas pressure drop. The particle size can have, on the other hand, an influence on the internal heat and mass transfer limitations in the porous pellets. While it is clear that larger particles can decrease the pressure drop and increase the internal mass transfer resistances, the effect of these resistances on the C_2 yield for the OCM reaction system is controversial [3], [4], as it may be beneficial for some type of catalysts [5]. This aspect will be further investigated in Chapter 5. When using catalytic wall reactors, on the other hand, the gas flow rate must be tuned to avoid bypass, especially if the tubes are large. In principle, part of the methane could bypass the catalytic walls, which can be avoided by enhancing gas turbulence. Finally, catalyst replacement is more difficult in catalytic wall reactors than in packed beds: basically, the whole tubes must be replaced in the first case.

Microchannel reactors were also proposed to carry out OCM [6] to increase the available surface area. Integrated heat exchange is achieved by feeding coolant fluid in some of the channels, either in co-current or countercurrent, and heat is transported through the walls separating the channels. The process can be divided in multiple stages, with multiple oxygen feedings, and intermediate product separations, that can also be arranged in microchannel modules at lower temperature, for example via gas adsorption/desorption in ionic liquids, with consequent recovery of unconverted methane, that can be fed to downstream OCM sections. This requires alternate cooling and heating of the gas that can be integrated between the different

modules. Microchannel reactors offer undoubtedly advantages in terms of temperature control, which has been proven to be much more efficient than for conventional packed beds. The scale-up of this concept can also be relatively straightforward, as it could be achieved by increasing the number of modules. Nevertheless, microchannel reactors present other problems, related to efficient gas mixing and distribution over parallel units. The catalyst replacement is expected to be much more expensive, as it can easily imply that entire modules must be changed. In general, this kind of concept could be suitable for small-scale ethylene production applications, whereas for very large scales, the size and cost of the reactor may become considerable in comparison to other options.

Another alternative to tubular and microchannel reactors is using a solid monolith, in thin honeycomb structures. This was proposed for OCM by different authors [7], [8]. Similar to the wall-coated reactor, the reaction occurs on the channel walls, where the gas is in contact with the solid catalyst. No external cooling is supplied in the monolith, but the basic idea is that the gas is fed with a rather low temperature (around 100 ^{o}C) compared to the reaction temperature (around 800 ^{o}C). The heat of reaction is used to keep the solid at the reaction temperature, taking advantage of the heat conduction across the monolith walls, countercurrent to the mass transport of gas, which is preheated. The upscaling can be performed by adding modules in parallel also for this case. High thermal conductivity for the monolith material is needed to assure avoidance of both hot spots and reaction quenching. Leyshon and Bader [7] suggested to keep the length of the channels very short (~ 0.025 m), also for large scale units. This results in a very wide and short aspect ratio for the reactor itself. The concept can be interesting as no reactor coolant needs to be handled, and no significant pressure drop is expected. It is possible that higher gas dilution ratios are necessary to assure proper thermal control of the system.

As an alternative to fixed beds, fluidized beds configurations were also studied for the application of oxidative coupling of methane considering the following regimes:

bubbling, turbulent and circulating fluidized beds. In bubbling fluidized beds, moderate gas velocities are applied (usually in the range of u/u_{mf} = 3-15, where u_{mf} is the minimum fluidization velocity). In this regime, a clear distinction is visible between bubbles, regions characterized by relatively high porosity where the gas moves from the bottom feeding section to the top free board, and an emulsion phase, with a higher solids density, continuously circulating. The inlet gas can be fed at a relatively low temperature, and directly preheated inside the bed, thanks to the very efficient heat transfer and solids mixing provided by these reactors. Most of the particles are retained in the bed, and a clear freeboard is formed on the top. Bubbling fluidized beds can be operated at a quite uniform temperature, also for the case of very exothermic reactions, like in the OCM system. The gas-solid separation can be easily handled at the gas outlet, using a disengaging area or an internal cyclone. Operation with low velocities can limit the types of catalyst that can be used in this type of bed. In particular, mechanical stability is needed for the particles to avoid agglomeration or elutriation problems. In most cases this problem can be solved using a good support for the catalyst, but for some of the catalysts problems were reported. This is especially the case for lithium-based catalysts (Li/MgO) and sodium-based catalysts (NaOH/CaO, Na_2SO_4/CaO and Na_2CO_3/CaO) [3]. For salt-based catalysts, the reaction temperature can be sufficiently high to lead to partial softening or melting of the particles, which may easily result in defluidization. The adverse effect of gas back-mixing should also be evaluated for bubbling beds. In fact, having the formed C_2's in regions with high oxygen concentrations can be detrimental for the integral selectivity of the reaction.

A solution to the problem of fluidizability of unstable catalysts was found by Santos et al. [9], using a vibro-fluidized bed. The reactor operates like a bubbling fluidized bed, with a vibration system connected to the reactor shell that makes sure that bubbles are formed even at gas velocities close to the minimum fluidization velocity. Using this apparatus, the authors succeeded in fluidizing the Li/MgO catalyst at 800 °C in a lab-scale setup. Although vibrating fluidized beds are already being used

in industrial applications, they introduce more complexity in the operability, and thus extra costs.

Fluidized beds were also studied in the turbulent regime for the OCM reaction [10]–[13]. In this case, the gas velocity is so high that particles are very well mixed with the gas itself. No clear bubbles are present in the system, which can be advantageous if a low mass transfer resistance is needed. The gas can be fed at low temperature also in this case. Even if very efficient heat exchange can be obtained inside the bed, the adiabatic temperature rise can in some cases still be too high to allow adiabatic operation. For this reason, Tjatjopoulos et al. [10] proposed a reactor design with internal steam generator heat exchangers, that must be specially designed in order to have the desired temperature in the reaction section. They also suggested a feeding system based on two separated distributors for methane and oxygen, in order to optimize the hydrodynamic performance of the reactor itself. For turbulent beds, higher costs are expected for gas/solid separation. In addition, a higher mechanical stability for the catalyst is needed in comparison with operation in the bubbling regime.

With even higher gas velocities, fluidized beds can also be operated in the circulating regime. In this case, a large fraction of the solids is directly transported with the gas out of the reactor. The two phases can be separated in a cyclone outside of the bed, and the solid catalyst is recycled at the bottom. A basic concept may include the combination with a turbulent bed at the bottom, followed by a riser on top of it, with a lower cross-sectional area and consequent increase in the gas velocity that allows pneumatic transport [10]. The riser can also have the function of carrying out the dehydrogenation reaction of ethane to ethylene, if the oxygen is completely depleted in first stage. In this case, the possible presence of C_2 side reactions like reforming must be evaluated to avoid loss of selectivity in the riser section, considering that the catalyst will be still active in the riser, even if carried out with higher dilution due to the increase in bed porosity. For a very exothermic reaction like OCM, external cooling

can be applied for the solids phase. Some alternative designs have been proposed for OCM, including an internal solid recirculation section [13]. Internals can also be added to the riser section to better avoid gas and solid back mixing [14]. Circulating fluidized beds can be a good option in terms of heat management, but can have some limitations in terms of operating pressures, because of the difficulty to handle solids at very high pressures (especially in combination with the high temperatures required for the OCM).

Finally, bubble column reactors have also been tested for OCM using in particular molten salts catalysts. Conway et al. studied lithium carbonates systems [1], and more recently, Branco et al. carried out the reaction over KCl-$LnCl_3$ eutectic mixtures [15], also using N_2O as alternative oxidizer [16]. In these particular cases, the reaction gas is fed at the bottom of the reactor and flows upwards in the medium in the form of bubbles. The reaction occurs at the interface of the bubbles, where methane and oxygen are in contact with the catalyst. Solid packing can be added to improve the phase distribution and mixing [1], which is essential to reduce the effect of mass transfer limitations. The bubbles generate internal mixing of the liquid, which contributes to have a more homogeneous temperature inside the reactor. This is highly beneficial to prevent the formation of hot spots. The gas can also be fed with a low temperature through an internal tube that acts as a pre-heater, providing simultaneously partial cooling to the gas-liquid system. In most cases, additional cooling must be provided at the reactor walls, depending on the difference between the adiabatic temperature and the desired reaction temperature. Careful reactor design is important and must take into account possible issues like plugging that can occur with viscous melts, particularly in the feeding sections.

The performance of these three kinds of reactors in their traditional forms are quite similar in terms of achievable yield of C_2 (the typical range is 15-20%). Minor optimizations can be achieved by controlling mass transfer limitations that can be present in all the three systems (gas-particle mass transfer in packed beds, gas-wall

mass transfer in monoliths or tubular reactors with wall coated catalyst, bubble-to-emulsion phase mass transfer in fluidized beds, and bubble-to-liquid mass transfer in molten salts systems). Mass transfer resistances can either have a beneficial or detrimental effect on the C_2 selectivity: on the one hand, they can decrease the local oxygen concentration at the catalyst surface, which is known to be favorable for the selectivity of the OCM reaction (this was also proven by experimental studies with different catalyst particle sizes [5], and is confirmed by the main kinetic models for OCM proposed in the literature); on the other hand the concentration of C_2's close to the catalyst can increase, which enhances the rate of unselective consecutive reactions of combustion and reforming of the formed C_2's. For this reason, controversial effects of mass transfer resistance have been reported in the literature even for the same reactor concept depending on the choice of the catalyst, as reported by Mleczko and Baerns [3].

For all the three multiphase systems, no real breakthrough was achieved in terms of C_2 yields compared to other systems. For this reason, the discrimination between fixed bed, fluidized bed or bubbling columns should be based on other factors.

2.2.2. Heat management options

In packed beds, external cooling must be applied via wall-tube heat exchange. Due to the very high heat of reaction of OCM, this is only possible by using a shell-and-tube configuration [17]. The tube diameter will be easily limited by the high surface area needed to remove the generated heat, particularly if the selectivity is not very high and the more exothermic undesired combustion reactions prevail. An easier temperature control can be achieved via microchannel configurations [6]. In reactors with a monolithic catalyst, the axial wall conductivity of the channels can be used to transport heat axially countercurrent to the flow direction. The monolith layer can work adiabatically, with the reacting gas entering the channels at a low temperature (at least 100-200 °C lower than the reaction temperature), and rapidly being heated up. This system is supposed to work with relatively short channels, which can also

limit the maximum methane conversion achievable in such a concept. For all fixed beds concepts, hot spot formation is a critical issue to be carefully considered.

Fluidized beds are probably the best choice from the point of view of heat management. Pseudo-isothermal behavior can be achieved thanks to the gas-solid mixing. Part of the produced heat can be directly removed by feeding the gas at low temperature, while the cold gas is immediately heated up. This cannot be easily achieved in a fixed bed reactor, unless a very good axial heat conduction is present. Internal heat exchangers can be used in fluidized beds, whereas in the case of circulating beds external cooling of the solids can be applied.

The gas-liquid system has the advantage of making the bed temperature more uniform than a conventional fixed bed, provided that good mixing is achieved inside the reactor. The liquid catalyst could also be used as a cooling fluid, if recirculated outside the reactor. The use of molten salts introduces the problem of dealing with slurries, which can even be problematic if the liquid catalyst is recirculated. In general, the fluid dynamics must be optimized in order to avoid clogging or heterogeneities inside the column.

As an alternative to specific concepts, the heat management can also be improved by splitting the reactor into multiple stages with intermediate cooling of the gas stream. This allows to use single packed beds in series, with a locally low methane conversion per stage [18]. Different concepts can be applied to different stages [19]. Alternatively, the final stage can be used to carry out the ethane dehydrogenation reaction by feeding additional C_2H_6 to improve the overall ethylene/ethane ratio, as proposed by Siluria [18]. According to the authors, this has the advantage that no intermediate cooling is necessary because in the final step an endothermic reaction takes place, making use of the heat produced in the previous step, and so the system can then also work adiabatically. However, it must be pointed out that complete thermal integration is possible only if the gas mixture is injected into the OCM section at quite low temperatures (~520 °C). At this temperature, no known OCM catalyst is active.

Finally, reactive cooling might be a good option to include into the ultimate concept, as an alternative to classical heat exchangers or steam generator systems. In particular, ethane dehydrogenation can be incorporated into the OCM reactor instead of being carried out in a separated unit. Nevertheless, it must be considered that the heat of reaction required to dehydrogenize ethane (144.2 kJ per mole of converted C_2H_6) is not enough to counterbalance the heat produced during the ethane formation by OCM (173.6 kJ per mole of produced C_2H_6). In practice, cooling will be even more difficult because ethylene and CO_x are also produced with more exothermic reactions. This means that additional ethane coming from another process should be introduced into the system.

2.2.3. Concepts with distributed oxygen feeding

The concepts discussed thus far operate with methane and oxygen co-fed to the reactor. One possible improvement in terms of achievable selectivity consists in distributing the oxygen fed along the reactor. The reason is that, based on many kinetics published in literature up till now [20]–[23], the reaction order in oxygen for the formation of C_2's is lower than the reaction order in oxygen for the combustion reactions. Therefore, the main advantage of this concept is that the concentration of oxygen can locally be much reduced, thus favoring the selective OCM reactions rather than the total combustion and other oxidation reactions. A more distributed reaction can also have a positive influence on the control of hot spots in fixed beds.

Distributed feeding can be achieved in different ways: the simplest one is by considering reactors with multiple oxygen inlets. The idea can be applied to a single packed bed with side inlets [24], [25], but this solution presents problems related to the mixing of the fresh oxygen with the hydrocarbon mixture in the injection points, where O_2 can be locally present in high concentrations. A technically more feasible option consists in having multistage reactors with intermediate gas mixers where the unreacted methane, C_2's, and side products coming from the previous stage are mixed with fresh oxygen or air [18], [19]. One advantage of this strategy is that external

cooling can also be applied between the stages [18], [26], which can greatly improve the heat management. The capital costs of such a concept can easily increase for a large number of stages, but the actual amount of oxygen fed to every stage can be rigorously controlled and optimized. In principle any kind of concept can be applied for the single stages, although this idea was in general proposed for packed bed concepts. It is also possible to combine different reactors in multiple stages: for instance, Shengfu and Zhang [19] proposed a packed bed, followed by a monolith, with intermediate injection of oxygen.

A second way of obtaining distributed feeding is by using membranes, either porous [27], or dense [28], [29]. In a tubular membrane reactor, the feeding policy is the same that could be obtained by splitting the reactor into an infinite number of stages with intermediate oxygen inlets. Porous membranes for OCM can be obtained from modified alumina microfiltration membranes; back-permeation of gas is possible and must be absolutely avoided in order to prevent methane from getting into contact with air/oxygen, which may result in explosive mixtures. This issue can be handled by controlling the pressure difference of the gases at the permeate and retentate side. Differently, oxygen perm-selective dense membranes working at high temperatures can be obtained from perovskite and/or fluorite materials, being considered as "mixed ionic-electronic conducting" (MIEC) type membranes. In this case, the main issues to be taken into account are the high temperature sealing, the relatively low oxygen permeation that they present and their stability under operating conditions. The main advantage of using dense membranes is that they can selectively transport oxygen, differently from porous membranes. In any case, more volume is needed in membrane reactors than in conventional beds to reach the same methane conversion. Significant improvements in the OCM performance have been already found in literature by applying this concept [30].

The third major way of realizing a distributed oxygen feed is via electrolytic cells. In this case, a membrane made of an ion conducting solid material is used. The principle

is quite similar to that controlling diffusion in dense membranes, the difference is that in this case the solid acts as an electrolyte that transports ions but is impermeable to electrons. Electrons are externally transported through an electric circuit between two electrodes at the two sides of the solid electrolyte. In this case the oxygen flux can be directly regulated by applying an electric potential to the system [31]. Alternatively, the system can be used as a fuel cell, with the oxygen permeation also resulting in a direct production of electric current [32], [33].

2.2.4. Integration of products separation

Distributed oxygen feeding can improve the C_2 selectivity by limiting the rate of parallel and consecutive reactions. Another idea to improve the selectivity is to immediately separate the produced C_2's before they have the chance to be further oxidized to CO_x. To achieve this, the concept of a simulated counter current moving bed chromatographic reactor was also applied to OCM, using solid adsorbents to selectively separate the gas products from the reagents. This concept was quite promising for OCM in the 90's [34], [35], and is still being studied [36]. Yet, the main issue related to this concept is that reaction and adsorption cannot be achieved in a single reactor, basically because of the largely different temperatures at which the catalyst and the adsorbent are active (~800 °C and ~100 °C, respectively). The reaction and separation steps must then be split and carried out in separate units with intermediate cooling and heating of the gas, where the reactor concept itself becomes more like an entire plant. The very high C_2 yield that is claimed to be obtained with this concept (> 50%) is not much different from that which could in principle be achieved in a reactor followed by separation and methane recycle.

2.2.5. Integration of O_2-N_2 separation

Another improvement to traditional reactor concepts for OCM regards the integration of air separation inside the reactor. This can be a great improvement in the overall economics of the process since the use of the very energy intensive air separation unit

can be avoided. Oxygen/nitrogen separation can be achieved by using perovskite membranes, solid electrolytic cells and by applying the chemical looping concept. The first two options have been already discussed. In a chemical looping system, the methane never gets into contact with molecular oxygen, but reacts with oxygen containing solid particles. Methane is converted to C_2 and gas side products, while the solid is reduced. Subsequently, the particles must be separately regenerated, which can be done with air. After the particles are oxidized back to their original state, they can be used to carry out the OCM reaction again. Chemical looping OCM needs at least two reactors to be operated. Packed beds or fluidized beds can be used. In the case of packed beds [37], at least one bed, containing the oxidized carrier, is fed with methane and a second one, containing the reduced solid, is fed with air. OCM takes place in the first reactor and regeneration in the second one. After complete conversion of the solids, the gas feeds are switched, and regeneration takes place in the first reactor and OCM in the second one. If fluidized beds are employed [14], the gas feedings are fixed, whereas the solids are recirculated between two interconnected reactors, being transported by the gas. In this case, one reactor is continuously used for OCM and the other one always for solids regeneration.

The option of including air separation into the reactor concept is very attractive and must be evaluated in relation to the additional capital costs that can derive from the improved configurations. Use of solid electrolytes instead of membranes could enhance the obtainable oxygen flux, but the extra cost of the electrolytic cells and electric current needs to be evaluated.

Membranes and chemical looping can be applied both to packed beds and fluidized beds. Comparative studies [17] on the application of traditional packed beds and fluidized beds for the OCM reaction system conclude that the latter can be more flexible in terms of heat management and limitation of pressure drop.

2.3. Experimental results on OCM

The quantitative performance of the different reactor concepts discussed in the previous section, resulting from experimental studies reported in the literature, are represented in Figure 2.1 in terms of C_{2+} selectivity and CH_4 conversion.

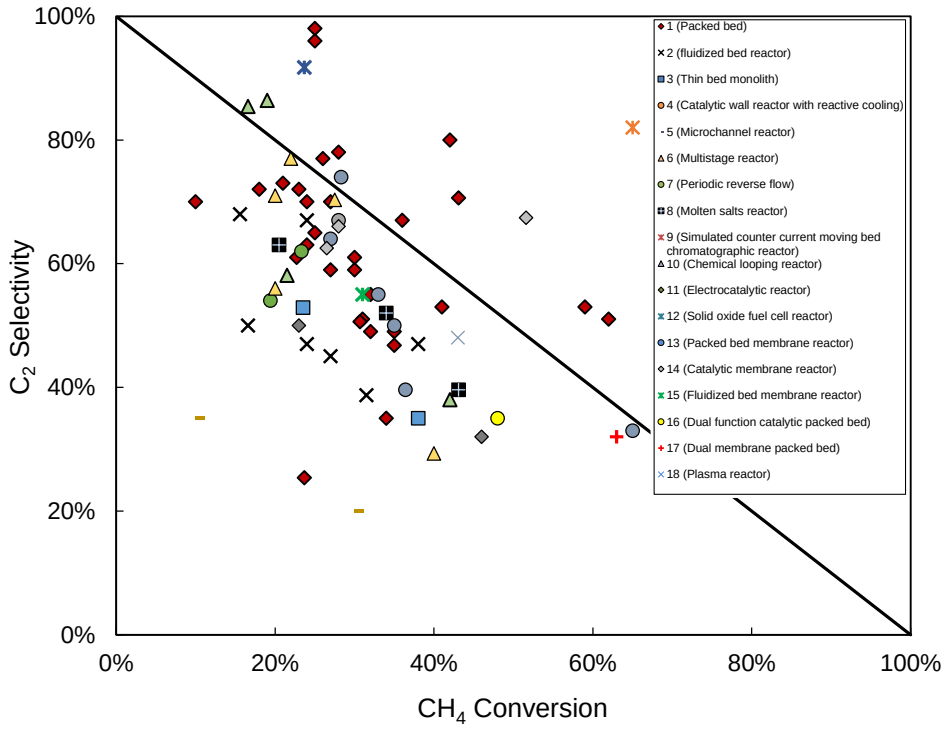

Figure 2.1. C_2 selectivities and CH_4 conversions achieved experimentally with different OCM reactor configurations.

Analyzing the data points of the graph, it can be observed that there is a trend that almost all configurations seem to obey, which can be described as an empirical correlation by:

C_{2+} selectivity + CH_4 conversion = 1

This correlation is indicated in the graph with a solid black line and indicates that it is very difficult to reach a high C_{2+} selectivity combined with a high CH_4 conversion. With the reactor configurations which are below this line, it is nowadays not

economically viable to build an industrial OCM scale plant because of the low C2 yield generally achieved.

The majority of the studied concepts are below this line, and just few reactor configurations are above. However, some of them cannot be extrapolated to real and/or industrial conditions for different reasons, including obviously the ones that have used a very high feed dilution. For example, the results achieved with the packed bed reactor configuration in which the parameter (conversion + selectivity) is above 1 have been performed with a lithium catalyst, whose stability is not good enough, provoking a decrease in the performance after some reaction time. Thus, this configuration cannot be used in real industrial applications. The simulated counter current moving bed chromatographic reactor is another configuration which reaches a high value (selectivity + conversion). Nevertheless, this configuration is really complex and different units, with intermediate cooling and heat exchange systems, would be needed for the catalyst and the adsorbent because they operate at different temperatures (800 and 100 °C respectively), making this concept extremely capital intensive. Also with the ethane injection unit a high (selectivity + conversion) can be achieved. However, in this configuration, composed of two units, the second one should be operated at around 520 °C, and currently there has not been any OCM catalyst reported in the literature with sufficient activity at this temperature. Finally, the other concepts which are above the empirical line are the ones which integrate in the reactor a system to distribute the oxygen along all the reactor, keeping a low oxygen concentration everywhere in the reactor, either with membranes or with electrolytic cells.

According to this graph, the most promising way to improve the total OCM yield and consequently to reach the necessary yield to bring this technology to industrial scale is via maintaining low oxygen concentrations along the reactor axial length, which commonly is achieved either by integrating membranes or by having several oxygen feeding points along the reactor length.

Taking into account the fact that OCM membrane reactors seem to be one of the most suitable options to increase the poor C_2 reactor yield achieved with conventional reactor configurations, a short review on the already published OCM membrane reactor works is presented in Section 2.4.

2.4. Membrane reactors for OCM

It has already been discussed that the competition between desired and undesired reactions (both primary and secondary) makes this process very complex. Because of the importance of the undesired reactions, the conventional OCM process has the common selectivity-conversion problem, resulting most of the times in a poor performance impeding the implementation of this process at industrial scales. As mentioned above, a solution can be the integration of membranes to distribute the oxygen along the reactor axial length, hence increasing the overall selectivity towards the desired products while keeping an acceptable CH_4 conversion. The most relevant OCM membrane reactor works have been summarized in Table 2.1 and are detailed below.

In 1992, Santamaría et al. [25] proposed, for the first time to the knowledge of the author, the use of a membrane reactor as an alternative to improve the yield of the process achieved with the conventional fixed bed reactor. A porous membrane was simulated to distribute the oxygen along the axial length of the reactor. Unlike the co-feeding case, the distribution of oxygen allows keeping a low oxygen partial pressure in the reactor, thus maximizing the formation of ethane among the three main primary reactions of the process (see Table 3.1). A C_{2+} yield of 29% was achieved by simulating this concept, resulting in an improvement of 20% in comparison with the also simulated conventional reactor.

In 1994 Coronas et al. [40] investigated the above described concept experimentally. Li/MgO was used as a catalyst and was placed in the inner part of a porous Al_2O_3 tube

that was selected to distribute the oxygen along the packed bed. In comparable cases, the C_{2+} selectivity increased between 10 and 15% when the oxygen was uniformly distributed. Furthermore, the temperature increase in the bed was better controlled by distributing the oxygen and consequently the reaction along the bed, reducing the maximum temperature rise reached in the bed to only 20 °C. Additionally, the authors also mentioned that the distribution of oxygen allows, contrary to the conventional co-feed packed bed reactor concept, to work below the overall explosive limits for the CH_4-O_2 mixtures, namely at lower CH_4/O_2 ratios, thereby increasing the overall CH_4 conversion of the process.

The same concept, placing the catalyst ($SrTi_{0.9}Li_{0.1}O_3$) inside the membranes and feeding the oxygen from the outer zone of the membrane, was implemented and compared with the co-feeding concept by Tan et al. [41] in 2007. In this study, a dense LSCF membrane was chosen to distribute the oxygen. By using an oxygen-selective membrane, the air separation unit that would be needed to purify the oxygen is avoided, thus significantly reducing the costs of the OCM process. Regarding the OCM performance, the maximum C_{2+} yield achieved in this work went from 12% with the conventional configuration to 21% when the membrane reactor was used. According to the authors, the selection of the catalyst was not optimal and the C_{2+} yield could have been further improved by choosing a more C_{2+} selective catalyst.

Lu et al. [42] prepared a tubular oxygen-selective $BaCe_{0.8}Gd_{0.2}O_3$ and then tested this membrane under OCM conditions. Without the use of any additional catalyst, a 16% C_{2+} yield was reached in a membrane reactor. This study thus also demonstrated the catalytic activity of some MIEC materials, resulting in similar yields to those where a separate catalyst was placed inside the reactor. According to the authors, a significant improvement of the OCM performance could be reached by increasing the activity of the species that catalyze the reaction.

In contrast to the previous work, Czuprat et al. [28], who used a BCFZ membrane, did not observe any methane conversion (below 0.3% in the best case) when attempting

the use of a membrane as catalyst. In a second batch of experiments of the same work the reactor was packed with $Mn/Na_2WO_4/SiO_2$, one of the most often used catalysts in literature for OCM [30]. A maximum yield of 17.5% was found with these operating conditions, reaching a selectivity towards C_{2+} of 50%. It was also noticed that higher residence times enhanced the CH_4 conversion, but at the expense of simultaneously decreasing the C_{2+} selectivity because of the oxidation of the desired products. The main factor hampering the process performance in these experiments was the fast formation of gaseous oxygen from the oxygen ions at the permeate side of the membrane, thus accelerating the undesired gas-phase combustion reactions. According to the authors, the deposition of a catalyst on the membrane surface could reduce this effect, leading to higher OCM performance.

The fast recombination of oxygen ions at the permeate side in comparison with the production of methyl radicals from these oxygen ions (which favors the desired path for the production of C_{2+}) was the explanation provided by Wang et al. [43] to justify their observed poor OCM reactor performance. A maximum C_{2+} yield of 15% was achieved in their study, where La-Sr/CaO was used as catalyst and BSCF as the oxygen perm-selective membrane.

Olivier et al. [44] coated the surface of a membrane with different active OCM catalysts, thus limiting the issue of the fast recombination of oxygen ions, as explained above. An oxygen-selective membrane BSCF disk was coated with three different catalysts, viz. Pt/MgO, LaSr/CaO and Sr/La_2O_3. It was noticed that the highest C_{2+} yield was obtained with the LaSr/CaO catalyst, reaching values above 18%, while the Pt/MgO catalyst showed the worst results with yields below only 3%. This work underlines that a suitable modification of the membrane surface to properly control and tune the catalytic activity of the system is critical to obtain the optimal OCM yield, although no strict correlation between oxygen permeability and C_{2+} selectivity was found.

Contrary to the findings of Olivier et al., Haag et al. [45] found a correlation between the oxygen permeation rate and the C_{2+} selectivity. Experiments where a Pt/MgO catalyst was coated onto the membrane surface of different MIEC membranes (BSCF, BSMF and BBF) were performed in this work. It was found that a proper tuning of the catalytic activity and oxygen flux across the membrane is crucial to achieve a good OCM performance. Too high oxygen membrane permeation would lead to a decrease in the C_{2+} selectivity, while too low permeation would make the catalyst inefficient, being even detrimental for the process.

Akin et al. [46] reported promising OCM results in a membrane reactor using the catalytically active $Bi_{1.5}Y_{0.3}Sm_{0.2}O_{3-\delta}$ as an oxygen-selective membrane. With a 98% helium dilution, a maximum C_{2+} yield of 35% with a C_{2+} selectivity of 54% was reached. An increase of 20% in the CH_4 conversion without any loss in the C_{2+} selectivity was observed when the experiments of this work were compared with some literature fixed bed reactor experiments performed using other typical OCM catalysts.

In agreement with Akin et al., Bhatia et al. [47] showed in their work that a catalyst coated membrane can be a good solution to significantly increase the C_{2+} yield of the OCM process. A Na-W-Mn/SiO_2 catalyst was coated on the surface of $Ba_{0.5}Ce_{0.4}Gd_{0.1}Co_{0.8}Fe_{0.2}O_{3-\delta}$ supported onto Al_2O_3. A C_{2+} yield of 34.7% was reached (with a C_{2+} selectivity of 67.4% and a CH_4 conversion of 51.6%) with a relatively low dilution (50%) in this study using the described configuration. Also in this work it was emphasized that it is necessary to carefully tune the catalyst loading and the oxygen permeation rate to hinder the fast formation of gaseous oxygen species at the permeate side of the membrane. The configuration shows a large improvement with respect to the catalytic packed bed reactor, where a maximum C_{2+} yield of only 15.2% was achieved.

Othman et al. [48] found the highest OCM performance reported so far in literature by using a membrane reactor configuration. A maximum C_{2+} yield of 39% with a 79% C_{2+} selectivity was achieved when the active specie, $Bi_{1.5}Y_{0.3}Sm_{0.2}O_{3-\delta}$ (BYS), was coated

onto the surface of the micro-channels of an oxygen selective $La_{0.6}Sr_{0.4}Co_{0.2}Fe_{0.8}O_{3-\delta}$ hollow-fiber membrane. According to the authors, another parameter that needs to be carefully controlled is the residence time; a compromise between a high CH_4 conversion, achieved with large residence times, and a high C_{2+} selectivity, found at low residence times because of the minimization of C_2 consecutive reactions, has to be found to achieve optimal performance of the system.

Table 2.1. Different membranes tested in literature for the OCM reaction.

Membrane	Temp. (°C)	Oxygen flux (mol cm^{-2} s^{-1})	Dilution (%)	Catalyst	CH_4 conversion (-)	C_{2+} selectivity (-)	C_{2+} yield (-)	Ref.
$La_{0.6}Sr_{0.4}Co_{0.2}Fe_{0.8}O_{3-\delta}$	975	-	67.5 (He)	$SrTi_{0.9}Li_{0.1}O_3$	0.3	0.7	0.21	[41]
$BaCe_{0.8}Gd_{0.2}O_{3-\delta}$	780	-	96 (He)	$BaCe_{0.8}Gd_{0.2}O_3$	0.26	0.62	0.16	[42]
$BaCo_xFe_yZr_zO_{3-\delta}$	800	-	75 (He)	$MnNa_2WO_4/SiO_2$	0.35	0.5	0.17	[28]
$Ba_{0.5}Sr_{0.5}Co_{0.8}Fe_{0.2}O_{3-\delta}$	850	$1.12 \cdot 10^{-6}$	80 (He)	La-Sr/CaO	0.22	0.67	0.15	[43]
$Ba_{0.5}Sr_{0.5}Co_{0.8}Fe_{0.2}O_{3-\delta}$	1000	$4.09 \cdot 10^{-6}$	47 (He)	Pt/MgO	0.05	0.5	0.03	[44]
$Ba_{0.5}Sr_{0.5}Co_{0.8}Fe_{0.2}O_{3-\delta}$	900	$2.60 \cdot 10^{-6}$	66 (He)	LaSr/CaO	0.25	0.7	0.18	[44]
$Ba_{0.5}Sr_{0.5}Co_{0.8}Fe_{0.2}O_{3-\delta}$	950	$1.49 \cdot 10^{-6}$	89 (He)	Sr/La_2O_3	0.25	0.37	0.09	[44]
$Bi_{1.5}Y_{0.3}Sm_{0.2}O_{3-\delta}$	900	$4.00 \cdot 10^{-8}$	98 (He)	$Bi_{1.5}Y_{0.3}Sm_{0.2}O_{3-\delta}$	0.648	0.54	0.35	[46]
$Ba_{0.5}Ce_{0.4}Gd_{0.1}Co_{0.8}Fe_{0.2}O_{3-\delta}$	850	$1.04 \cdot 10^{-6}$	50 (He)	$Na\text{-}W\text{-}Mn/SiO_2$	0.516	0.67	0.35	[47]
$La_{0.6}Sr_{0.4}Co_{0.2}Fe_{0.8}O_{3-\delta}$	900	$6.50 \cdot 10^{-6}$	25 (Ar)	$Bi_{1.5}Y_{0.3}Sm_{0.2}O_{3-\delta}$	0.49	0.79	0.39	[48]

2.5. Conclusions

This chapter has focused on the analysis of the main characteristics of the oxidative coupling of methane process, discussing in detail the most relevant parameters which influence the final performance achieved, as well as different solutions proposed in the literature. From this analysis it seems clear that, so far, only very few reactor configurations and mostly at conditions unsuitable for operation at larger scales could reach acceptable yields. Nevertheless, the large research efforts carried out in this field since the 80's have provided useful information on the process. Among the non-conventional reactor concepts proposed, those that integrate oxygen-selective membranes seem quite attractive, combining the two major advantages of improving the C_2 selectivity through distributed oxygen feeding and integrating the O_2/N_2 separation inside the reactor, thereby avoiding a costly separate air separation unit (if the membranes employed are selective for oxygen). Nevertheless, the implementation of this reactor design for conditions applicable at larger scale has not been demonstrated yet. That is the main reason why in the following chapters of this thesis, the OCM membrane reactor technology will be further investigated and analyzed.

2.6. Bibliography

[1] S. J. Conway, J. Szanyi, and J. H. Lunsford, "Catalytic properties of lithium carbonate melts and related slurries for the oxidative dimerization of methane," *Applied Catalysis*, vol. 56, no. 1, pp. 149–161, Jan. 1989.

[2] M. P. Kaminsky, G. A. Huff, N. Calamur, and M. J. Spangler, "Catalytic wall reactors and use of catalytic wall reactors for methane coupling and hydrocarbon cracking reactions," US Patent 5599510 A, 1997.

[3] L. Mleczko and M. Baerns, "Catalytic oxidative coupling of methane - reaction engineering aspects and process schemes," *Fuel Processing Technology*, vol. 42, pp. 217–248, 1995.

[4] S. Jašo, H. Arellano-Garcia, and G. Wozny, "Oxidative coupling of methane in a fluidized bed reactor: Influence of feeding policy, hydrodynamics, and reactor geometry," *Chemical Engineering Journal*, vol. 171, no. 1, pp. 255–271, Jun. 2011.

[5] G. Follmer, L. Lehmann, and M. Baerns, "Effect of transport limitations on C2+ selectivity in the oxidative methane coupling reaction using a NaOH/CaO catalyst," *Catalysis Today*, vol. 4, pp. 323–332, 1989.

[6] T. Mazanec *et al.*, "Oxidative Coupling of Methane," US Patent 20090043141 A1, 2009.

[7] D. W. Leyshon and R. A. Bader, "Thin bed cofeed reactors for methane conversion," US Patent 4876409 A, 1989.

[8] J. M. Aigler and J. H. Lunsford, "Oxidative dimerization of methane over MgO and Li+/MgO monoliths," *Applied Catalysis*, vol. 70, no. 1, pp. 29–42, Jan. 1991.

[9] A. Santos, J. Santamaria, and M. Menéndez, "Oxidative Coupling of Methane

in a Vibrofluidized Bed at Low Fluidizing Velocities," *Industrial and Engineering Chemistry Research*, vol. 34, pp. 1581–1587, 1995.

[10] G. J. Tjatjopoulos, P. T. Ketekides, D. K. Iatrides, and I. A. Vasalos, "Cold flow model and computer simulation studies of a circulating fluidized bed reactor for the oxidative coupling of methane," *Catalysis Today*, vol. 21, pp. 387–399, 1994.

[11] J. Chaouki, D. Klvana, and C. Guy, "Selective and Complete Catalytic Oxidation of Natural Gas in Turbulent Fluidized Beds," *Korean Journal of Chemical Engineering*, vol. 16, pp. 494–500, 1999.

[12] J. Chaouki, A. Gonzalez, C. Guy, and D. Klvana, "Two-phase model for a catalytic turbulent fluidized-bed reactor : Application to ethylene synthesis," *Chemical Engineering Science*, vol. 54, pp. 2039–2045, 1999.

[13] S. Ruottu, K. Kaarianen, and J. Hiltunen, "Method based on a fluidized-bed reactor for converting hydrocarbons," US Patent 6045688 A, 2000.

[14] R. A. Bader and M. G. Axelrod, "Reactor for methane conversion," US Patent 4855111 A, 1989.

[15] J. B. Branco, G. Lopes, and A. C. Ferreira, "Catalytic oxidation of methane over KCl-$LnCl_3$ eutectic molten salts," *Catalysis Communications*, vol. 12, no. 15, pp. 1425–1427, Sep. 2011.

[16] J. B. Branco, A. C. Ferreira, A. M. B. do Rego, A. M. Ferraria, G. Lopes, and T. A. Gasche, "Oxidative coupling of methane over KCl–$LnCl_3$ eutectic molten salt catalysts," *Journal of Molecular Liquids*, vol. 191, pp. 100–106, 2014.

[17] F. M. Dautzenberg, J. C. Schlatter, J. M. Fox, J. R. Rostrup-Nielsen, and L. J. Christiansen, "Catalyst and reactor requirements for the oxidative coupling of methane," *Catalysis Today*, vol. 13, pp. 503–509, 1992.

[18] W. P. Schammel *et al.*, "Oxidative coupling of methane systems and methods," WO Patent 2013177433 A2, 2013.

[19] J. Shengfu and Z. Zhang, "Method for producing ethylene and ethane and catalytic reactor," CN Patent 102659500 B, 2012.

[20] Z. Stansch, L. Mleczko, and M. Baerns, "Comprehensive kinetics of oxidative coupling of methane over the La2O3/CaO catalyst," *Industrial and Engineering Chemistry Research*, vol. 36, pp. 2568–2579, 1997.

[21] S. Jaso, H. R. Godini, H. Arellano-garcia, M. Omidkhah, and G. Wozny, "Analysis of attainable reactor performance for the oxidative methane coupling process," *Chemical Engineering Science*, vol. 65, pp. 6341–6352, 2010.

[22] T. P. Tiemersma, M. J. Tuinier, F. Gallucci, J. A. M. Kuipers, and M. V. S. Annaland, "A kinetics study for the oxidative coupling of methane on a Mn/Na 2WO 4/SiO 2 catalyst," *Applied Catalysis A: General*, vol. 433–434, pp. 96–108, 2012.

[23] A. Vatani, E. Jabbari, M. Askarieh, and M. A. Torangi, "Kinetic modeling of oxidative coupling of methane over Li/MgO catalyst by genetic algorithm," *Journal of Natural Gas Science and Engineering*, vol. 20, pp. 347–356, Sep. 2014.

[24] M. Baerns and W. Hinsen, "Process for the production of ethane and/or ethylene from methane," US Patent 4608449 A, 1986.

[25] J. Santamaria, M. Menéndez, J. A. Pena, and J. I. Barahona, "Methane oxidative coupling in fixed bed catalytic reactors with a distributed oxygen feed. A simulation study," *Catalysis Today*, vol. 13, pp. 353–360, 1992.

[26] F. Hoffmann, E. Lenget, and P. Mege, "Thin multistage catalytic reactor with internal heat exchanger, and use thereof," US Patent 6919048 B2, 2005.

[27] D. Lafarga, J. Santamaria, and M. Menéndez, "Methane oxidative coupling using porous ceramic membrane reactors—I. reactor development," *Chemical Engineering Science*, vol. 49, no. 12, pp. 2005–2013, Jun. 1994.

[28] O. Czuprat, T. Schiestel, and H. Voss, "Oxidative Coupling of Methane in a BCFZ Perovskite Hollow Fiber Membrane Reactor," *Industrial and Engineering Chemistry Research*, vol. 49, pp. 10230–10236, 2010.

[29] A. Vamvakeros *et al.*, "Real time chemical imaging of a working catalytic membrane reactor during oxidative coupling of methane," *Chem. Commun.*, vol. 51, pp. 12752–12755, 2015.

[30] T. P. Tiemersma, A. S. Chaudhari, F. Gallucci, J. A. M. Kuipers, and M. van Sint Annaland, "Integrated autothermal oxidative coupling and steam reforming of methane. Part 2: Development of a packed bed membrane reactor with a dual function catalyst," *Chemical Engineering Science*, vol. 82, pp. 232–245, Sep. 2012.

[31] A. Caravaca *et al.*, "Coupling catalysis and gas phase electrocatalysis for the simultaneous production and separation of pure H2 and C2 hydrocarbons from methane and natural gas," *Applied Catalysis B: Environmental*, vol. 142–143, pp. 298–306, 2013.

[32] V. D. Belyaev, V. A. Sobyanin, V. N. Parmon, S. Freni, and M. Aquino, "Oxidative conversion of CH_4 on Ni and Ag electrode-catalysts in molten carbonate fuel cell reactor," *Catalysis Letters*, vol. 17, no. 3, pp. 213–221, 1993.

[33] W. Kiatkittipong, T. Tagawa, S. Goto, S. Assabumrungrat, K. Silpasup, and P. Praserthdam, "Comparative study of oxidative coupling of methane modeling in various types of reactor," *Chemical Engineering Journal*, vol. 115, no. 1–2, pp. 63–71, Dec. 2005.

[34] A. L. Tonkovich, R. W. Carr, and R. Aris, "Enhanced C2 yields from methane

oxidative coupling by means of a separative chemical reactor," *Science (New York, N.Y.)*, vol. 262, pp. 221–223, Oct. 1993.

[35] A. L. Tonkovich and R. W. Carr, "A simulated countercurrent moving-bed chromatographic reactor for the oxidative coupling of methane: experimental results," *Chemical Engineering Science*, vol. 49, no. 24, pp. 4647–4656, 1994.

[36] P. K. Kundu, Y. Zhang, and A. K. Ray, "Multi-objective optimization of simulated countercurrent moving bed chromatographic reactor for oxidative coupling of methane," *Chemical Engineering Science*, vol. 64, no. 19, pp. 4137–4149, 2009.

[37] J. C. Jubin, "Fixed bed reactor system," US Patent 4751055 A, 1988.

[38] L. M. Ioffe, P. Bosch, T. Viveros, H. Sanchez, and Y. G. Borodko, "Natural manganese oxides as catalysts for oxidative coupling of methane: a structural and degradation study," *Materials Chemistry and Physics*, vol. 51, no. 3, pp. 269–275, Dec. 1997.

[39] A. Cruellas, T. Melchiori, F. Gallucci, and M. van Sint Annaland, "Advanced reactor concepts for oxidative coupling of methane," *Catalysis Reviews*, vol. 59, no. 03, pp. 234–294, 2018.

[40] J. Coronas, M. Menéndez, and J. Santamaria, "Methane oxidative coupling using porous ceramic membrane reactors–II. Reaction studies," *Chemical Engineering Science*, vol. 49, no. 12, pp. 2015–2025, 1994.

[41] X. Tan, Z. Pang, Z. Gu, and S. Liu, "Catalytic perovskite hollow fibre membrane reactors for methane oxidative coupling," *Journal of Membrane Science*, vol. 302, no. 1–2, pp. 109–114, Sep. 2007.

[42] Y. Lu, A. G. Dixon, W. R. Moser, Y. Hua, and U. Balachandran, "Oxygen-permeable dense membrane reactor for the oxidative coupling of methane," *Journal of Membrane Science*, vol. 170, pp. 27–34, 2000.

[43] H. Wang, Y. Cong, and W. Yang, "Oxidative coupling of methane in Bao.5Sro.5Coo.8Feo.2O3–δ tubular membrane reactors," *Catalysis Today*, vol. 104, no. 2–4, pp. 160–167, Jun. 2005.

[44] L. Olivier, S. Haag, C. Mirodatos, and A. C. van Veen, "Oxidative coupling of methane using catalyst modified dense perovskite membrane reactors," *Catalysis Today*, vol. 142, no. 1–2, pp. 34–41, Apr. 2009.

[45] S. Haag, A. C. van Veen, and C. Mirodatos, "Influence of oxygen supply rates on performances of catalytic membrane reactors," *Catalysis Today*, vol. 127, no. 1, pp. 157–164, 2007.

[46] F. T. Akin and Y. S. Lin, "Controlled Oxidative Coupling of Methane by Ionic Conducting Ceramic Membrane," *Catalysis Letters*, vol. 78, no. 1, pp. 239–242, 2002.

[47] S. Bhatia, C. Y. Thien, and A. R. Mohamed, "Oxidative coupling of methane (OCM) in a catalytic membrane reactor and comparison of its performance with other catalytic reactors," *Chemical Engineering Journal*, vol. 148, no. 2–3, pp. 525–532, 2009.

[48] N. H. Othman, Z. Wu, and K. Li, "An oxygen permeable membrane microreactor with an in-situ deposited Bi1.5Y0.3Sm0.2O3–δ catalyst for oxidative coupling of methane," *Journal of Membrane Science*, vol. 488, pp. 182–193, Aug. 2015.

Chapter 3

Quantitative evaluation of different OCM reactor concepts

Abstract

Based on the overview reported in Chapter 2, a quantitative comparison of the performance of the most relevant reactor configurations proposed for the oxidative coupling of methane process has been made on the basis of numerical calculations with phenomenological reactor models. The configurations that have been analyzed can be divided into two main categories, i.e. packed bed reactors (including conventional packed beds with external cooling, packed bed membrane reactors and adiabatic packed beds with post cracking) and fluidized bed reactors (bubbling fluidized bed reactor, circulating fluidized bed reactor and fluidized bed membrane reactor). The challenges of both configuration types, mainly the heat management in the case of the packed bed reactors and the low C_{2+} yields obtained in fluidized bed reactors, are evaluated and quantified. To allow for a fair comparison, La_2O_3/CaO has been chosen as the OCM catalyst for all the considered cases, mainly in view of the availability of a comprehensive kinetics model. The results show that as indicated in literature, the yields that can be reached with conventional configurations are very poor. However, the results also indicate that the C_{2+} yield can be significantly improved by feeding the oxygen distributively along the reactor axial length.

3.1. Introduction

As already discussed in previous chapters, many different OCM reactor configurations have been proposed over the last decades [1]. Specifically, an overview of the OCM reactor configurations already reported in literature has been made in Chapter 2. Modifications to conventional reactor configurations, namely packed bed and fluidized bed, can contribute to improve the OCM reactor performance. In particular, alternative configurations in which oxygen is evenly distributed along the axial reactor length are believed to be one of the most reliable options for this necessary process performance improvement. Therefore, the most often proposed configurations (packed bed and bubbling fluidized bed reactor), together with some of the most relevant alternative reactor concepts (packed bed membrane reactor, adiabatic packed bed reactor with post cracking, circulating fluidized bed reactor and fluidized bed membrane reactor), have been quantitatively evaluated in this chapter in order to quantify and compare their performance on the same footing.

To perform the simulation study, different catalysts for different configurations may have to be considered (the main characteristics and the reaction mechanism of the most important OCM catalysts are described in Chapter 4), providing each catalyst a specific performance in terms of activity and selectivity based on its kinetics [2]. One of the most often used OCM kinetics in the open literature was developed for a La_2O_3/CaO catalyst [3], [4] by Stansch et al. [3] and its behavior is well-known within the OCM community. Competing with La-based catalysts, the Mn-Na_2WO_4/SiO_2 has acquired more and more relevance in the last period. Its main characteristic is that this catalyst is more selective than the La-based catalyst, although its activity is lower. Additionally, its stability under OCM conditions makes it suitable for future OCM industrial applications. However, no fully reliable kinetic schemes were reported in the literature for this catalyst. Tiemersma et al. [5] reported some parameters for the OCM reactions, but the temperature dependency was not considered, and C_2 reforming reactions were not included. Lee et al. [6] proposed a more detailed mechanism, including some radical species and the dependency on the catalyst

coverages, but it was found to be inconsistent with respect to the total mass balance. Lomonosov et al. [7] corrected the form of the reaction rate equations for the OCM reactions, but did not report the equations and parameters for the side reactions. Other studies like the one proposed by Daneshpayeh et al. [8] need further investigations before they can be safely implemented.

Because of these reasons, and because a very broad range of conditions and reactor configurations are going to be investigated, the well-known kinetics derived from the La_2O_3/CaO catalyst has been selected to perform all the simulations [3]. This La-based catalyst kinetic model (see Table 3.1 and Table 3.2) includes both parallel side reactions (mainly total and partial combustion of methane), consecutive side reactions (combustion and reforming of C_2) and also one gas-phase reaction (ethane dehydrogenation).

Table 3.1. Reaction rate expressions for the La_2O_3/CaO kinetics [3] used for the OCM simulations carried out in this work.

	Reaction	Reaction rate expression
1	$CH_4+2\ O_2 \rightarrow CO_2+2\ H_2O$	$\frac{k_{0,1}e^{-\frac{E_{a,3}}{RT}}P_{CH_4}^{m,1}P_{O_2}^{n,1}}{\left(1+\ k_{1,CO_2}\ e^{-\frac{\Delta H_{ad,CO2}}{RT}}P_{CO_2}\right)^2}$
2	$2\ CH_4+0.5\ O_2 \rightarrow\ C_2H_6+H_2O$	$\frac{k_{0,2}e^{-\frac{E_{a,4}}{RT}}\left(k_{2,O_2}\ e^{-\frac{\Delta H_{ad,O2}}{RT}}P_{O_2}\right)^{n,2}P_{CH_4}^{m,2}}{\left(1+\left(k_{2,O_2}\ e^{-\frac{\Delta H_{ad,O2}}{RT}}P_{O_2}\right)^{n,2}+\ k_{2,CO_2}\ e^{-\frac{\Delta H_{ad,CO2}}{RT}}P_{CO_2}\right)^2}$
3	$CH_4+\ O_2 \rightarrow\ CO+H_2O+H_2$	$\frac{k_{0,3}e^{-\frac{E_{a,3}}{RT}}P_{CH_4}^{m,3}P_{O_2}^{n,3}}{\left(1+\ k_{3,CO_2}\ e^{-\frac{\Delta H_{ad,CO2}}{RT}}P_{CO_2}\right)^2}$
4	$CO+0{,}5O_2 \rightarrow CO_2$	$\frac{k_{0,4}e^{-\frac{E_{a,4}}{RT}}P_{CO}^{m,4}P_{O_2}^{n,4}}{\left(1+\ k_{4,CO_2}\ e^{-\frac{\Delta H_{ad,CO2}}{RT}}P_{CO_2}\right)^2}$
5	$C_2H_6+0.5O_2 \rightarrow\ C_2H_4+H_2O$	$\frac{k_{0,5}e^{-\frac{E_{a,5}}{RT}}P_{C2H6}^{m,5}P_{O_2}^{n,5}}{\left(1+\ k_{5,CO_2}\ e^{-\frac{\Delta H_{ad,CO2}}{RT}}P_{CO_2}\right)^2}$
6	$C_2H_4+2\ O_2 \rightarrow\ 2\ CO+2\ H_2O$	$\frac{k_{0,6}e^{-\frac{E_{a,6}}{RT}}P_{C_2H_4}^{m,6}P_{O_2}^{n,6}}{\left(1+\ k_{6,CO_2}\ e^{-\frac{\Delta H_{ad,CO2}}{RT}}P_{CO_2}\right)^2}$
7	$C_2H_6 \rightarrow\ C_2H_4+H_2$	$k_{0,7}e^{-\frac{E_{a,7}}{RT}}P_{C_2H_6}^{m,7}$
8	$C_2H_4+2H_2O \rightarrow\ 2\ CO+4\ H_2$	$k_{0,8}e^{-\frac{E_{a,8}}{RT}}P_{C_2H_4}^{m,8}P_{H_2O}^{n,8}$
9	$CO+H_2O \rightarrow\ CO_2+H_2$	$k_{0,9}e^{-\frac{E_{a,9}}{RT}}P_{CO}^{m,9}P_{H_2O}^{n,9}$

10	$CO_2 + H_2 \rightarrow CO + H_2O$	$k_{0,10} e^{-\frac{E_{a,10}}{RT}} P_{CO_2}^{m,10} P_{H_2}^{n,10}$

Table 3.2. Kinetic parameters of the La_2O_3/CaO kinetics [3] used for the OCM simulations carried out in this work.

Reaction	$\mathbf{k_{0,j}}$	$\mathbf{E_{a,j}}$	$\mathbf{k_{j,CO_2}}$	$\mathbf{\Delta H_{AD,CO_2}}$	$\mathbf{k_{O_2}}$	$\mathbf{\Delta H_{AD,O_2}}$	$\mathbf{m_j}$	$\mathbf{n_j}$
i	mol kg^{-1} s^{-1} $Pa^{-(m+n)}$	kJ mol^{-1}	Pa^{-1}	kJ mol^{-1}	Pa^{-1}	kJ mol^{-1}	-	-
1	$2.00 \cdot 10^{-3}$	48	$2.5 \cdot 10^{-13}$	-175			0.24	0.76
2	$2.32 \cdot 10^{+4}$	182	$8.3 \cdot 10^{-14}$	-186	$2.30 \cdot 10^{-12}$	-124	1	0.4
3	$5.20 \cdot 10^{-4}$	68	$3.6 \cdot 10^{-14}$	-187			0.57	0.85
4	$1.10 \cdot 10^{-1}$	104	$4.0 \cdot 10^{-13}$	-168			1	0.55
5	$1.70 \cdot 10^{+2}$	157	$4.5 \cdot 10^{-13}$	-166			0.95	0.37
6	$6.00 \cdot 10^{+1}$	166	$1.6 \cdot 10^{-13}$	-211			1	0.96
7	$1.20 \cdot 10^{+7}$	226					1	-
8	$9.30 \cdot 10^{+6}$	300					0.97	0
9	$1.90 \cdot 10^{-1}$	173					1	1
10	$2.60 \cdot 10^{+1}$	220					1	1

It should be noted that the selected kinetic model has not been validated under some of the conditions at which it will be applied in this chapter. An extension of this study may be possible in the future when more refined kinetics models for the tungsten-based catalyst system become available. However, the main conclusions/trends reported in this chapter are generally valid for different catalysts.

3.2. Packed bed reactor configurations

The performance of conventional catalytic packed bed reactors is the most widely investigated among all the experimental works published on OCM. A literature review shows that C_{2+} yields above 19% have not been reported for the conventional packed bed reactor concept [4], unless operated under particular conditions, such as the use of unstable catalysts (Li-based) or very high feed dilution [9], which are considered unsuitable for large-scale applications. What is often neglected in these studies is how the reactor temperature can be controlled when upscaling the reactor. Generally, the small dimensions of the experimental setups and the conditions used (e.g. relatively

low conversions) allow performing the reaction under nearly isothermal conditions without problems, but for large-scale reactors the relatively small available surface area for heat exchange can easily become problematic, as shown by a comparative study by Dautzenberg et al. [10]. In this section, a more detailed evaluation of these aspects is presented.

A pseudo-homogeneous plug-flow reactor model was implemented to simulate the OCM reaction in multi-tubular packed beds under non-isothermal conditions. The model includes the component and total mass balances, an energy balance and the Ergun equation in its differential form to account for the pressure drop over the reactor. It should be noted that the pressure drop over the reactor can be the limiting factor in the reactor design, particularly for relatively long tubes, high gas flow rates or small catalyst particle sizes. The model equations are summarized in Table 3.3:

Table 3.3. Equations used to simulate the packed bed reactor.

Packed bed equations		
Gas phase mass balances	$\frac{dc_i v}{dz} = r_i(c_j, T, P)$	*Equation 3.1*
	$\frac{dcv}{dz} = \sum_{j=1}^{N} r_j$	*Equation 3.2*
Total energy balance	$vcCp\frac{dT}{dz} = -\sum_{j=1}^{N} H_j(T) r_j - Ua(T - T_r)$	*Equation 3.3*
Ergun equation	$\frac{dP}{dz} = -\frac{\rho v}{d_p}\frac{(1-\varepsilon)}{\varepsilon^3}\left(\frac{150\mu(1-\varepsilon)}{\rho d_p} + 1.75v\right)$	*Equation 3.4*
Additional equations	$Cp\ (heat\ capacity) = \sum_{j=1}^{N} x_j Cp_j(T)$	*Equation 3.5*
	$\rho\ (density) = \frac{P}{RT}\sum_{j=1}^{N} x_j MW_j$	*Equation 3.6*
	Enthalpy: $H_j(T) = H_j(T_0) + \int_{T_0}^{T} Cp_j(T)$	*Equation 3.7*

In Table 3.3, *c* refers to concentrations, *v* to velocity, *r* to a certain reaction rate, *T* to temperature, *P* to pressure, *z* to axial direction, *Cp* to heat capacity, *H* to enthalpy, *a* is a ratio between area and volume (m^2/m^3), *U* to the overall heat transfer coefficient,

ε to porosity, μ to viscosity, dp to particle diameter, R to ideal gas constant, x to molar fractions and MW to the molecular weight.

The parameters to calculate the species heat capacities were taken from the NIST database [11], whereas the viscosity of the gas mixture was calculated using a mixing rule [12].

The efficiency of the cooling is assumed to be ideal outside the reactor tubes, i.e. the external heat transfer coefficient is assumed to be infinite, and the coolant temperature is constant along the axial direction (which is valid if the flow rate or the heat capacity of the coolant is very high). The effect of axial diffusion is also neglected. By specifying the inlet conditions as boundary conditions, the model can be solved with a standard ode solver (Matlab's ode15s was used), obtaining the axial profiles of the gas composition, gas velocity, temperature and pressure inside the reactor tube.

3.2.1. Conventional packed bed with external cooling

In packed beds, the very exothermic OCM and combustion reactions result in the formation of hot spots inside the reactor. With proper operating conditions and tube dimensions, the system is able to keep the temperature of the hot spot to a sufficiently low value. Otherwise, a very sharp reaction and temperature front is formed at a single point in the reactor, similar to what occurs in a premixed flame. This phenomenon is related to the exponential dependency of the reaction rates on the temperature. The runaway regime must absolutely be avoided for the OCM process, because at very high temperatures the selectivity to the desired C_{2+} is lost [13]–[16], while it poses risks to the catalyst and reactor integrity. The proposed model is able to simulate and evaluate the conditions for which the controlled or the runaway regime is present in the reactor. In this second case, a characteristic temperature profile is established with two inflection points before the maximum value. A qualitative example of a runaway case is shown in Figure 3.1.

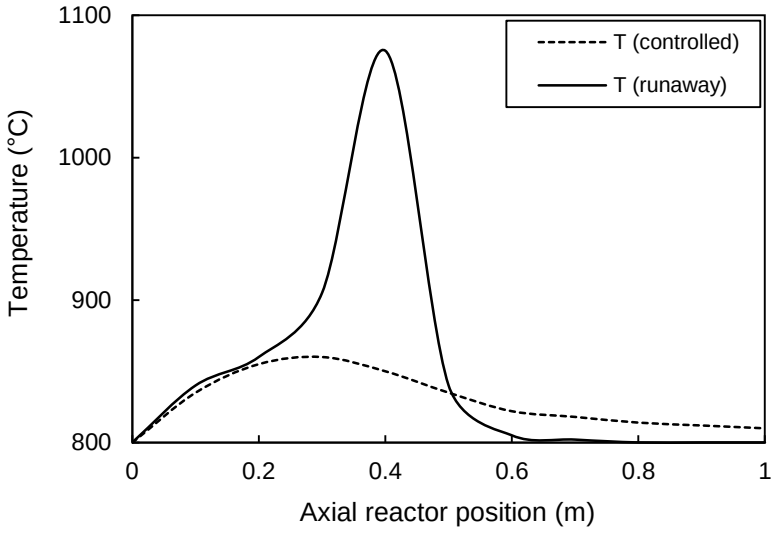

Figure 3.1: Qualitative comparison of typical temperature profiles inside the catalytic bed in the controlled and runaway regimes (inlet temperature is 800 °C).

The formation of hot spots is basically related to how the terms in the energy equation can balance each other. The source term associated to the heat of reaction depends on the values of the reaction rates. This will increase with the gas pressure and with the catalyst concentration inside the bed. The gas composition will also play a role in this. The heat transfer term depends on the efficiency of heat exchange (heat transfer coefficient), on the surface area of the tube, and on the temperature of the cooling fluid, whereas the convection term depends on the gas velocity, so on the gas flow rate. In summary, almost all process variables influence the thermal performance of the reactor.

In order to evaluate the efficiency of the heat management in tubular reactors and the influence of hot spots on the achievable C_{2+} yield, different simulations were carried out with the presented model. The tube dimensions were initially fixed (4 cm diameter, 1 m length, 3 mm particles), as well as the inlet conditions for the gas (T = 800 °C, P = 2 bar, Methane + Air co-feed, CH_4/O_2 ratio = 4). The model was used considering different amounts of catalyst in the reactor, and different values of gas hourly space velocity (GHSV). In this case the GHSV was defined as the ratio between

the inlet gas volumetric flow rate, calculated at standard conditions, and the volume occupied by the gas (reactor volume scaled by the bed porosity).

For the cooling system, a constant value for the overall heat transfer coefficient (U = 300 W/m² K), based on Dautzenberg's study [10], was selected. Moreover, a constant temperature for the coolant (T_c = 800 °C) was assumed. This approximates the situation when the coolant has a very high heat capacity, or when a very high flow rate is used. The simulations results are reported in Figure 3.2.

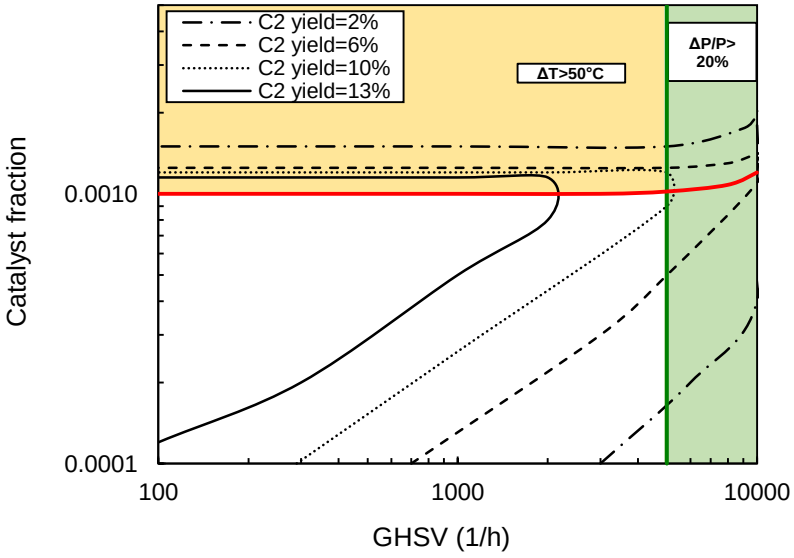

Figure 3.2: Predicted C_2 yields for different GHSVs and amounts of catalyst. Single tube simulations (4 cm diameter, 1 m length, T_{in} = 800 °C, P_{in} = 2 bar, Methane + Air co-feed, CH_4/O_2 = 4). Energy balance solved using a constant overall heat transfer coefficient U = 300 W/m²/K. Green line: simulations with $\Delta P/P_{in}$ = 20%. Red line: simulations with max(ΔT) = 50 °C.

For the selected geometry and operation conditions, the maximum C_{2+} yield that can be obtained with small catalyst fractions (10^{-4}-10^{-2}) and a GHSV in the range of 100-10000 h^{-1} is about 13-14 %, which is in agreement with most catalytic studies about OCM in packed bed reactors [3], [17], [18]. The iso-contour lines of the same C_{2+} yield are straight on logarithmic scale (indicating a small influence of ΔP or ΔT): as expected, the same yield can be obtained when increasing at the same time the gas

flow rate and the amount of catalyst. The yield decreases with an increase in the flow rate because of the reduced gas residence time and for lower catalyst fractions.

If the maximum temperature peak exceeds a certain value (around 50-80 °C), a runaway effect can be observed. This corresponds to a quick drop in the selectivity to C_{2+} and a very large temperature rise [10], [15], [16], which can lead even to catalyst melting. In Figure 3.2, the red line represents the simulations where the maximum temperature increase in the reactor is 50 °C. Above this line, the iso-contour lines are very close to each other because of the runaway regime. The green line represents the GHSV for which a relative pressure drop of 20% occurs over the packed bed. To limit the pressure drop and temperature rise it is necessary to work at a lower GHSV and catalyst fraction. In this case, the operability area is quite affected by the two constraints, but the maximum theoretical yield calculated for the isothermal and isobaric case seems still achievable (however, at the expense of a much-increased reactor volume).

The results shown in Figure 3.2 are affected by an important simplification related to the heat transfer efficiency, which was assumed constant. In particular, the overall heat transfer coefficient strongly depends on the superficial gas velocity (included in the Reynolds number). For a more accurate estimation of the constraints, the following expression for the overall heat transfer coefficient was used [19]:

$$U = \left(1 - 1.5\left(\frac{D}{d_p}\right)^{-1.5}\right)\frac{\lambda}{d_p}Pr^{1/3}Re^{0.59} \qquad \textit{Equation 3.8}$$

Where D is the diameter of the tube, λ is the thermal conductivity of the gas, d_p the particle diameter of the catalyst, Pr is the dimensionless Prandtl number (ratio between momentum and thermal diffusivities) and Re accounts for the Reynolds number (ratio between inertia and viscous forces).

The calculations were repeated with this tube correlation, and the results are shown in Figure 3.3.

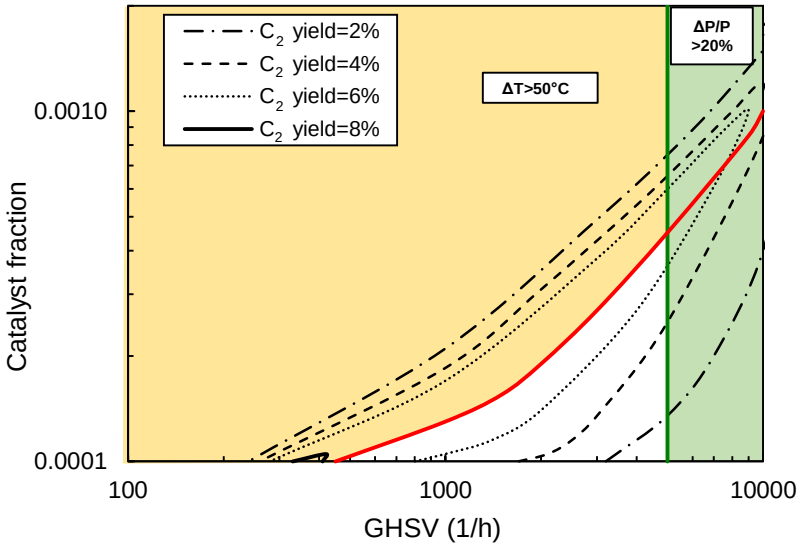

Figure 3.3: Predicted C_2 yields for different GHSVs and amounts of catalyst. Single tube simulations (4 cm diameter, 1 m length, T_{in} = 800 °C, P_{in} = 2 bar, Methane + Air co-feed, CH_4/O_2 = 4). Energy balance solved calculating the overall heat transfer coefficient from the Nusselt correlation (Equation 3.8). Green line: simulations with $\Delta P/P_{in}$ = 20%. Red line: simulations with max(ΔT) = 50 °C.

Decreasing the gas velocity has a dramatic influence on the thermal performance of the reactor. This poses quite a problem, because the best yields are theoretically achievable at low flow rates and higher residence times, or high flow rates with higher catalyst concentrations. The constraint on the pressure drop is the limiting factor to operate in the latter regime. These results demonstrate that the formation of hot spots seriously decreases the achievable C_{2+} yields in packed bed reactors, in comparison with the ideal isothermal case.

The combination of pressure and temperature effects becomes very critical for the OCM system. Very low yields are obtained when choosing this tube size. Note also that the amount of catalyst that can be used in this case is extremely low, which is consistent with the very high activity of La_2O_3/CaO.

These results shown in Figure 3.2 and Figure 3.3 are valid for the selected tube geometry and process conditions. Therefore, also the effect of the tube dimensions (diameter and length) on the achievable yield was investigated. The results of the sensitivity analyses are shown in Table 3.4.

Table 3.4. Sensitivity analysis of OCM in a packed bed reactor with different dimensions.

	Base case	Sensitivity 1 (Diameter)	Sensitivity 2 (Axial length)
Tube length (m)	1	1	10
Tube diameter (m)	0.04	0.02	0.04
Maximum yield (%)	7	9.5	12
Inlet temperature (°C)	800	800	800
Temperature increase (°C)	< 50	< 50	< 50
Inlet pressure (bar)	2	2	2
Pressure increase (bar)	ΔP/P>20%	ΔP/P>20%	ΔP/P>20%
CH_4/O_2 ratio	4	4	4

Increasing the heat exchange surface area has a beneficial effect on the temperature control. This is the reason why a higher yield can be obtained when decreasing the tube diameter and increasing its length, without exceeding the maximum temperature rise imposed by the optimization algorithm. In particular, from these results it is evident that short tubes cannot be used for OCM. Also tubes with a relatively large diameter (which is important to apply this process on an industrial scale) are not recommended, because it is not possible to control the heat management. Thus, the required small diameter of the tubes may become an important source of cost for the reactor. Another option to enhance the efficiency of the heat exchange is to operate at a higher gas velocity in the tubes, but this is limited by the allowable pressure drop, which increases with the increasing tube length. The optimum solution for this kind of reactors appears to be operating with long tubes, low flow rates and a very diluted catalyst. The results clearly indicate that a very active catalyst is not helpful for packed bed reactors, because large reactor volumes are required to achieve the desired heat exchange. For the La-based catalyst extremely high catalyst dilution ratios must be employed to balance the reaction rates with the available surface area needed to extract the produced reaction heat.

3.2.2. Packed bed membrane reactor

To investigate the performance of the packed-bed membrane reactor, a configuration has been selected where the catalyst bed was positioned around a membrane tube. Air is fed to the membrane section, which is assumed to be selective to oxygen, thus allowing to introduce pure oxygen to the catalyst bed in a distributed way along the entire length of the reactor. The catalytic section, where the OCM reaction is taking place, is located inside an external tube filled with a cooling fluid to counterbalance the exothermic behavior of OCM.

The mass (for the individual chemical species and for the overall flow) and energy balances of this system are solved for the two reactor compartments, viz. the retentate (air side) and permeate (fuel side). A mass transfer term between the two compartments is introduced in the oxygen mass balances. The energy balances also account for a heat transfer term between the air and fuel side because of conduction through the membrane. External cooling is considered through an extra term in the energy balance for the annular region, where – as before – the external cooling is considered as ideal (i.e. constant temperature of the coolant and no external heat transfer resistance). The model equations are given in Table 3.5.

Table 3.5. Equations used to simulate the packed bed membrane reactor.

Packed bed membrane reactor equations		
Equations for the fuel (^{f}) side	$\frac{dc_i^f v^f}{dz} = r_i + k_i^f a^f (c_i^{m,f} - c_i^f)$	*Equation 3.9*
	$\frac{dc^f v^f}{dz} = \sum_{j=1}^{N} (r_j + k_j^f a^f (c_j^{m,f} - c_j^f))$	*Equation 3.10*
	$v^f c^f C_P^f \frac{dT^f}{dz} = \sum_{j=1}^{N} \left[H_j (T^f) r_j\right] - U a^f (T^f - T^a)$	*Equation 3.11*
	$\frac{dP^f}{dz} = -\frac{\rho^f v^f}{d_p} \frac{(1-\varepsilon)}{\varepsilon^3} \left(\frac{150 \mu^f (1-\varepsilon)}{\rho^f d_p} + 1.75 v^f \right)$	*Equation 3.12*
	$r_i = \sum_{j=1}^{NR} v_{ij} R_j \rho_{cat} (1-\varepsilon)$	*Equation 3.13*
Equations for the air (^{a}) side	$\frac{dc_i^a v^a}{dz} = k_i^a a^a (c_i^a - c_i^{m,a})$	*Equation 3.14*
	$\frac{dc^a v^a}{dz} = -\sum_{j=1}^{N} (k_j^a a^a (c_j^a - c_j^{m,a}))$	*Equation 3.15*

	$v^a c^a C_P^a \frac{dT^a}{dz} = \sum_{j=1}^{N} Ua^a (T^f - T^a) \frac{S^f}{S^a}$	*Equation 3.16*
Equations at the membrane interface	$k_i^f \left(c_i^{m,f} - c_i^f\right) = J^m$	*Equation 3.17*
	$-k_i^a \left(c_i^{m,a} - c_i^a\right) = J^m \frac{S^f}{S^a}$	*Equation 3.18*
	$h^f (T^f - T^{m,f}) = U(T^f - T^a)$	*Equation 3.19*
	$h^a (T^{m,a} - T^a) = U(T^f - T^a) \frac{S^f}{S^a}$	*Equation 3.20*
Equation for the oxygen flux through the membrane	$J^m = \frac{D_v k_r \left(\left(p_i^{m,a}\right)^n - \left(p_i^{m,f}\right)^n\right)}{2\delta k_f \left(p_i^{m,a} p_i^{m,f}\right)^n + D_v \left(\left(p_i^{m,a}\right)^n + \left(p_i^{m,f}\right)^n\right)}$ $n = 0.5$	*Equation 3.21*
Heat and mass transfer coefficients	$k_i^f = 0.0096 \frac{D_i}{d^{eq,i}} Sc_f^{0.346} Re_f^{0.913}$	*Equation 3.22*
	$k_i^a = 0.0096 \frac{D_i}{d^{eq,a}} Sc_a^{0.346} Re_a^{0.913}$	*Equation 3.23*
	$h^f = 0.17 \frac{\lambda^f}{d_p} \left(\frac{Pr_f}{0.7}\right)^{1/3} Re_a^{0.913}$	*Equation 3.24*
	$h^a = 0.023 \frac{\lambda^a}{R^m} (Pr_a)^{1/3} Re_a^{0.8}$	*Equation 3.25*
	$U = \frac{1}{\frac{1}{h^f} + \frac{1}{h^a}\frac{S^f}{S^a} + \frac{R^m}{\lambda^m} ln\left(\frac{R^m + \delta}{R^m}\right)}$	*Equation 3.26*

The nomenclature in Table 3.5 is in line with the one detailed in Table 3.3. To complete it, it should be noted that k stands for the mass transfer coefficient, h for the heat transfer coefficient and S for the surface area. Among the membrane parameters included in Equation 3.21, J^m is the oxygen flux through the membrane, n is the exponential factor, δ is the membrane thickness, D_v is the bulk diffusion coefficient, k_f is the forward surface exchange rate constant, k_r is the reverse surface exchange rate constant and R^m is the radius of the membrane.

In addition, the superscript ^{f} refers to the fuel side (permeate) of the system, ^{a} to the air side (retentate), ^{m} to the membrane itself, ^{m,f} to the membrane interphase at the fuel side and ^{m,a} to the membrane interphase at the air side.

The flux of oxygen through the dense selective membrane is described with the generalized equation formulated by Xu and Thomson [20]. This equation presents three parameters (D_v, k_r, and k_f), which depend on temperature through an Arrhenius-

type relation. Table 3.6 shows the values of the permeability parameters used for this study [21], which corresponds to a hollow fiber BSCF perovskite membrane. These values will also be used for the simulations of the fluidized bed membrane reactor.

Table 3.6. Values of the permeability parameters resulting from the fitting of experimental data [21].

	Pre-exponential factor	Activation energy (kJ/mol)
$D_v(m^2 s^{-1})$	9.823	91.8
$k_r(mol\ m^2 s^{-1})$	15.36	56.3
$k_f(m\ s^{-1}\ Pa^{-0.5})$	308.5	267.0

For the packed bed membrane reactor simulations, it was assumed that the catalytic bed was undiluted. The high concentration of active catalyst increases the reaction rates so much, that all the oxygen is consumed as soon as it reaches the methane in the fuel section, producing a very large amount of syngas. As a consequence of this fact, plus the contribution of the ethylene reforming reaction, which is accounted for in the Stansch's OCM reaction mechanism, the methane conversion is very high (~81%), whereas the predicted C_{2+} selectivity in the outlet is quite low (~28%). Subsequently, a simulation was carried out as before (same geometry and operating conditions), but for a packed bed membrane reactor that contained only 10% active catalyst. For these simulations, 800 °C was selected as the reactor temperature with a total pressure of 2 bar, while the optimal CH_4/O_2 ratio, which was used to run these cases, was found to be 2.6. The results are reported in Figure 3.4, showing the trends of conversion, selectivity and yield, and in Figure 3.5, showing the axial temperature profiles.

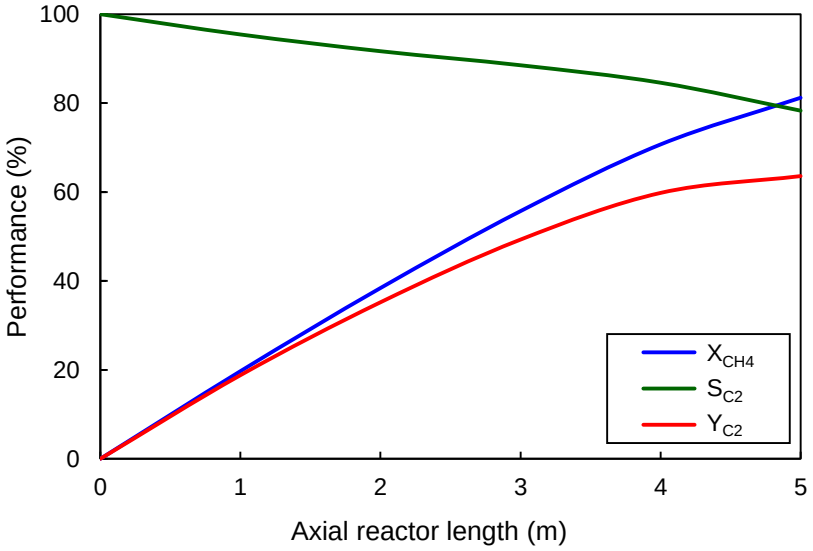

Figure 3.4: Calculated axial profiles of methane conversion, C_{2+} selectivity and C_{2+} yield at the permeate side of the membrane reactor. Simulations for the packed-bed membrane reactor with 10% La_2O_3/CaO catalyst particles in the packed bed, temperature of 800 °C, inlet pressure of 2 bar and CH_4/O_2 ratio of 2.6.

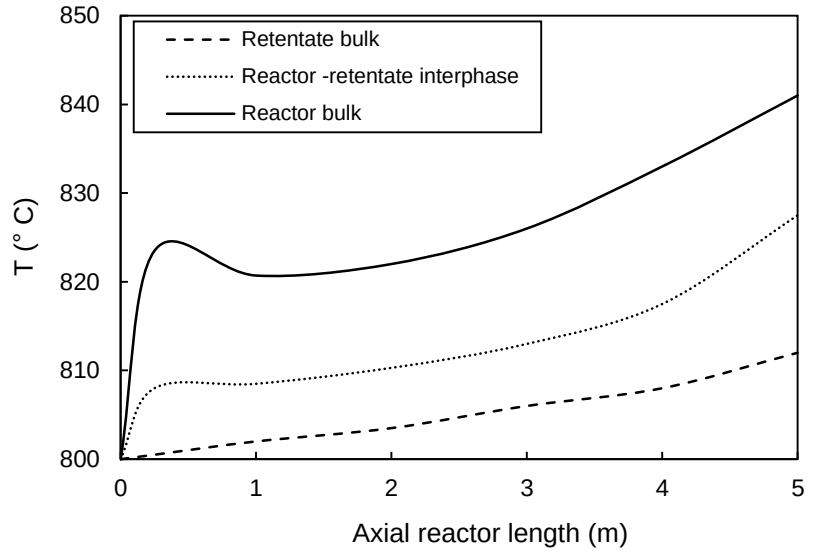

Figure 3.5: Calculated axial temperature profiles at the permeate side, retentate side and permeate-retentate interphase of the membrane reactor. Simulations for a packed bed with 10% La_2O_3/CaO catalyst particles, temperature of 800 °C, inlet pressure of 2 bar and CH_4/O_2 ratio of 2.6.

An enormous increase in the selectivity to C_{2+} can be achieved in the packed-bed membrane reactor (78% at the outlet), while also the methane conversion is slightly

higher (81%). As a result, the C_{2+} yield is increased up to 63%. The amount of produced syngas is much lower in this case, which means that a lower fraction of produced C_2's is consumed by consecutive reforming reactions. These results clearly show that the activity of the packed bed, i.e. the amount of catalyst, can be used to improve the product selectivity, because it affects the OCM reactions and consecutive reforming reactions of C_2 differently.

Despite the very high conversion obtained, the hot spot can be well controlled. The average reactor (permeate) temperature is higher in this case with the diluted catalyst bed compared to the simulation with only catalyst particles, and this is related to the decreased extent of endothermic reforming. The outlet temperature rise is only 40 °C, which also means that the combined cooling with the external fluid and with air in the retentate compartment is quite effective.

In order to directly compare the membrane reactor performance with the co-feed operation in the packed bed reactor, the same base case presented for the membrane reactor was simulated, but assuming that no permeation through the membrane is possible. As the only other difference, the catalyst was diluted with a factor 10^4, which is necessary to prevent the runaway regime (higher reaction rates result in a too high hot spot with consequent loss of all C_{2+} selectivity). Moreover, the risk associated because of working in the explosion regime has been ignored in these simulations, although it is of course a critical aspect when carrying out experimental work under these conditions. The results are summarized in Table 3.7.

Table 3.7. Comparison of the simulation results for packed beds, with co-feed and distributed oxygen feed with diluted and undiluted catalyst beds.

	Distributed feed, pure catalyst	Distributed feed, diluted catalyst	Co-feed, diluted catalyst
CH_4/O_2	2.3	2.6	2.6
% active material in solid	100%	10%	0.007%
X_{CH_4}	71%	81%	17%
$S_{C_{2+}}$	28%	78%	26%
$Y_{C_{2+}}$	20%	63%	5%
max(ΔT)	34 °C	40 °C	70 °C
$\Delta P/P_0$	8%	7%	9%

Note that the temperature rise at the hot spot is already 70 °C for strongly diluted co-feed packed bed reactor configuration, which is quite close to the transition to the runaway regime. The temperature rise is much higher than the temperature increase that was observed for the distributed feed operation, despite the much lower amount of catalyst, and the obtained C_{2+} yield is quite low, only around 5%. For the distributed O_2 feeding cases, both conversion and selectivity are increased when diluting the catalyst bed and increasing the reactor length. This example shows that, even if high reactor volumes are necessary to effectively operate membrane reactors, even higher reactor volumes are required for conventional packed beds, because of the enormous catalyst dilution needed to compensate for the inefficient heat transfer in this configuration.

3.2.2.1. Analysis of reaction rates

The three presented cases show a different operation of the reaction mechanism. The distributed feed case with pure catalyst has more or less the same C_{2+} selectivity as in co-feed operation, but with a much higher methane conversion. With distributed feeding, a major part of the selectivity loss is related to CO production, whereas in the co-feed configuration, more CO_2 is formed. A large improvement in the selectivity can be noted by diluting the catalyst in the membrane reactor. To gain more insight, the average values of the reaction rates inside the reactor were calculated for all three cases, shown in Figure 3.6.

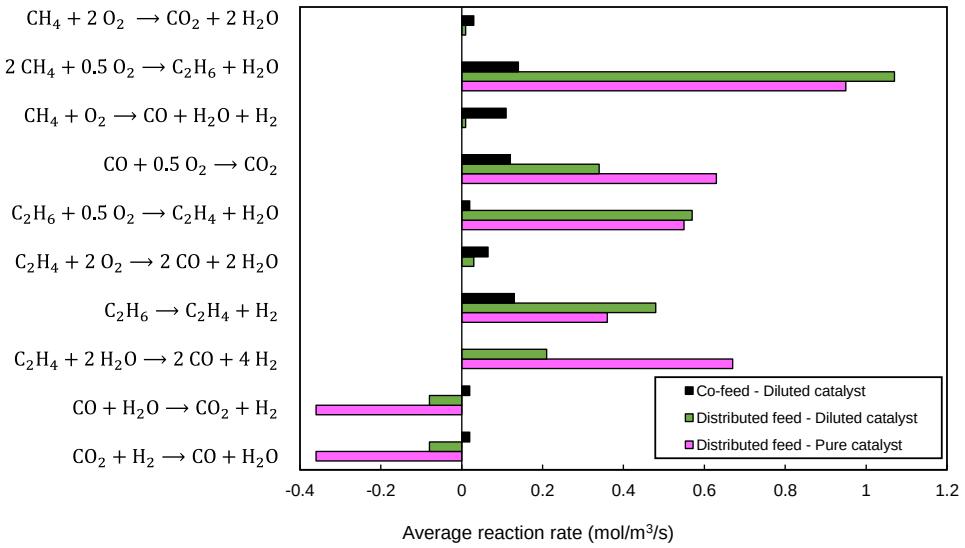

Figure 3.6: Average calculated values of the reaction rates according to the Stansch mechanism [3], for the three considered base case simulations, viz. co-feed packed bed reactor with diluted catalyst, and distributed feed in the packed bed membrane reactor with a diluted and undiluted catalyst bed.

The results show that, in case of distributed O_2 feeding, the combustions (both complete and incomplete) of methane and ethylene are relatively unimportant compared to the OCM reactions. This is quite different for the co-feed operation, where total and partial combustions are competitive and represent a major source of loss of carbon selectivity to C_{2+}. In membrane reactors, the only important side reaction involving oxygen is the CO combustion: this is not directly related to a decrease in C_{2+} selectivity, because it is only a consequence of the formation of carbon monoxide through reforming of ethylene, which is the real undesired step to be avoided in this case, whereas in co-feed operation the CO oxidation is not so important. As already indicated before, C_2 reforming is playing a much more important role when using the catalyst undiluted. The larger CO production also results in a higher O_2 consumption for its consecutive oxidation to CO_2: this is the reason why with pure catalyst the methane conversion is 10% lower, even if the amount of permeated oxygen is slightly higher than with diluted catalyst (CH_4/O_2 is lower). In summary, in membrane reactors the amount of catalyst in the bed affects the extent of reforming reactions, but not the rate of primary OCM reactions, whose

rate is controlled by the oxygen flux through the membrane. For this reason, the catalyst concentration can be tuned to optimize the C_{2+} selectivity.

In conclusion, the simulations show that the integration of membranes may lead to a large improvement in the performance of a packed bed reactor for OCM. The two key factors are the extent of the different OCM reaction rates along the reactor, which can be relatively well-controlled by means of the amount of catalyst present in the bed, the improvement in the heat management due to the distributed reaction and the additional cooling provided by the heat transfer with air.

3.2.3. Adiabatic packed bed with post cracking

In the previous sections, the problems stemming from hot spot formation in OCM tubular packed beds were addressed, and how this can be more easily handled in distributed feed configurations. Another possibility is to operate the packed bed under adiabatic conditions, which can have a clear advantage in terms of simplifying the reactor geometry (no tube and shell structure, but a single vessel), as well as its operability (no more need to handle a cooling fluid and to optimize the heat exchange).

A simple solution of this problem has been proposed by Siluria [22]. The key aspect of this concept is to operate with a relatively cold feed (~530 °C). The feed temperature should be high enough to allow reaction activation, but at the same time the adiabatic temperature rise must not be so high to cause a complete loss of selectivity (the maximum temperature should not exceed approximately 1000 °C). The OCM system is prone to exceed this limit in adiabatic operation, but one possibility to avoid this is to operate with high CH_4/O_2 ratios: in this case, the temperature rise is limited by the amount of oxygen present in the system.

In their economic analysis, Siluria proposed to use a two-stage adiabatic reactor, where the first stage consists of a catalytic bed where the OCM takes place, and the second stage a catalytic bed for the dehydrogenation. Between the two stages, extra ethane is fed, and the high temperature reached by the exothermic reactions in the

first section is used to carry out the endothermic conversion of ethane to ethylene. A methane inlet flow rate of 1065 ton/h has been selected for the simulations of this case, with an initial CH_4/O_2 ratio of 10 and without nitrogen dilution. The inlet temperature was set to 540 °C and the pressure to 9 bar. Finally, the ethane flow rate for the second stage was 90 ton/h.

For this adiabatic reactor case, the diffusion terms were added to all the conservation equations. This was done particularly to evaluate how much the axial heat dispersion influences the axial temperature profiles when no external cooling is applied to the system.

The mass balances for all the individual chemical species are given by:

$$\frac{dc_i v}{dz} = -\frac{dJ_i}{dz} + r_i \qquad \textit{Equation 3.27}$$

Where the diffusive fluxes are calculated with the generalized Fick's law:

$$J_i = -c \sum_{j=1}^{N-1} \left(D_{ij} \frac{dx_j}{dz} \right) \qquad \textit{Equation 3.28}$$

A total mass balance is added, to evaluate the gas velocity v:

$$\frac{dcv}{dz} = \sum_{j=1}^{N} (r_j) \qquad \textit{Equation 3.29}$$

The energy balance reads:

$$vcCp \frac{dT}{dz} = \frac{d}{dz}\left(\lambda \frac{dT}{dz} \right) - \sum_{j=1}^{N} H_j r_j \qquad \textit{Equation 3.30}$$

The gas diffusivities were calculated through the binary diffusion coefficients as a function of temperature and pressure. The conductivity of the bed was calculated from the contribution of the solid and gas phase:

$$\lambda = \varepsilon \lambda_g + (1 - \varepsilon)\lambda_s \qquad \textit{Equation 3.31}$$

Where λ_g was evaluated as a function of temperature and gas composition, being ε the porosity of the bed.

This model was used to simulate the two reactor sections (OCM and cracking). The Stansch kinetics was applied for both reactor sections, the only difference is that the catalyst concentration was set to zero in the second section. This automatically sets all the reaction rates to zero except for the dehydrogenation of ethane to ethylene, which is supposed to be a gas-phase reaction and thus does not depend on the concentration of La_2O_3/CaO. Figure 3.7 and Figure 3.8 show the simulation results of the two-stage bed, using the reactor dimensions and operating conditions from Siluria. A catalyst fraction of 40% was assumed to reduce hot spot formation in the bed.

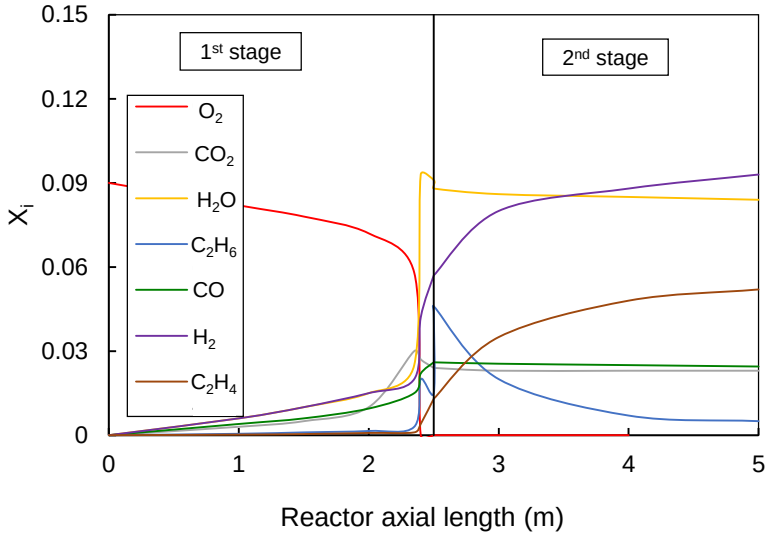

Figure 3.7: Calculated gas molar fraction profiles in a two-stage adiabatic packed bed (OCM + ethane cracking). Reactor dimensions and operating conditions according to the ones proposed by Siluria [22] (Inlet temperature is 540 °C, inlet pressure of 9 bar and initial CH_4/O_2 ratio of 10 with 40% La_2O_3/CaO catalyst particles).

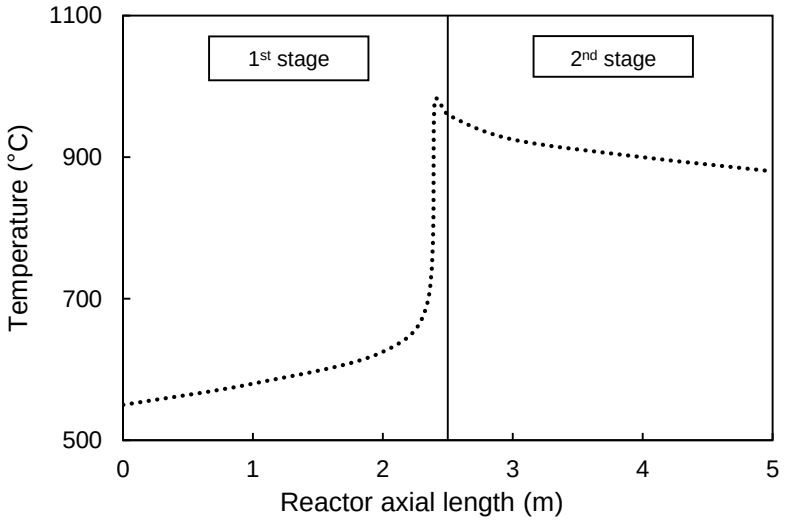

Figure 3.8: Calculated axial temperature profile in a two-stage adiabatic packed bed (OCM + ethane cracking). Reactor dimensions and operating conditions according to the ones proposed by Siluria [22] (Inlet temperature is 540 °C, inlet pressure of 9 bar and initial CH_4/O_2 ratio of 10 with 40% La_2O_3/CaO catalyst particles).

In the first reactor stage, the reaction activates at 650-700 °C, and consequently a very sharp reaction front is formed, where the temperature rises to about 980 °C. This could be considered as a kind of controlled runaway regime: even if the temperature profile is very pronounced, the temperature does not exceed 1000 °C. After the oxygen is completely consumed, neither OCM nor combustion reactions can occur anymore. At this point, only the other side reactions can take place, including C_2 dehydrogenation and reforming, according to the kinetic mechanism. Before the end of the first stage, a change in the concentration profiles can be observed, related to this.

The second stage is characterized by the formation of ethylene and hydrogen, together with a temperature decrease due to the endothermic dehydrogenation reaction. A discontinuity in the molar profiles can be noted between the first and second stage, corresponding to the addition of external gas (C_2H_6). After the first stage, the methane conversion is 12%, with a C_{2+} selectivity of 49%. This corresponds to a global C_{2+} yield of 6%. As expected, the yield is seriously limited by the very high excess of methane,

which is a necessary condition to avoid too high temperatures, and to keep the selectivity reasonably high. In their report, Siluria also suggested the possibility to split the first section into two reactors with intermediate cooling when the gas reaches a temperature in the range of 800-900 °C. This appears very difficult to achieve, because the reaction front is located exactly in correspondence of these temperatures. An even lower amount of oxygen should be fed to fulfil this condition.

3.3. Fluidized bed configurations

Fluidized bed reactor technology can overcome the heat management issues of packed bed reactors. However, the effect of mass transfer limitations between different phases of both the reactants and the products on the achievable C_{2+} yield needs to be better understood and quantified. In this section, the performance of a fluidized bed in the bubbling fluidization regime, a circulating fluidized bed system and a fluidized bed membrane reactor for OCM are investigated and compared.

3.3.1. Bubbling fluidized bed

At first, a fluidized bed reactor in the bubbling fluidization regime is considered. In a bubbling fluidized bed, assumed to consist of Geldart B type particles, the inlet gas velocity is slightly above (typically 3-15 times) the minimum fluidization velocity. As explained in Chapter 2, two separate phases are distinguished; bubbles, where the gas moves upwards in the bed, and emulsion, with a much higher solids holdup, through which the gas percolates with a velocity close to the incipient fluidization velocity. In this chapter, the bubbling fluidized bed model developed by Kunii and Levenspiel [23] was used (see also a.o. Medrano et al. [24]) and extended to include also the wake phase, which represents the region inside the bubbles (around 15% of the bubble volume) where the solids are present (solids fraction is considered to be the same as in the emulsion phase). A brief description of the model follows. Mass balances for both phases need to be calculated, being detailed in Equation 3.32 and Equation 3.33:

Bubble phase ($_b$)
$$\frac{d}{dz}\left[u_b\left(f_b + f_w\varepsilon_{mf}\right)C_{i,b}\right] = K_{i,be}\left(f_b + f_w\varepsilon_{mf}\right)\left(C_{i,e} - C_{i,b}\right) \pm R_{i,b}f_b(1-\varepsilon_{mf}) \quad \textit{Equation 3.32}$$

Emulsion phase ($_e$)
$$\frac{d}{dz}\left[u_e\left(f_e\varepsilon_{mf}\right)C_{i,e}\right] = -K_{i,be}\left(f_b + f_w\varepsilon_{mf}\right)\left(C_{i,e} - C_{i,b}\right) \pm R_{i,e}f_e(1-\varepsilon_{mf}) \quad \textit{Equation 3.33}$$

The total gas feed entering the reactor with a specified superficial gas velocity, u_o, is assumed to be distributed between the bubble phase (including the wake) at velocity u_b, and the emulsion phase (with a velocity u_e), while u_{mf} stands for the minimum fluidization velocity. The bubbles are considered to be devoid of solids, while the amount of solids contained in the wake is assumed to be constant and equal to 15% of the total bubble volume with a porosity equal to the emulsion phase porosity (ε_{mf}). Mass transfer is accounted for to describe the gas exchanged between the different phases being D_i the diffusivity of a certain chemical specie. The constitutive equations for the hydrodynamics and mass transfer processes are summarized in Table 3.8.

Table 3.8. Correlations used for hydrodynamics and mass transfer employed in the fluidized bed.

Hydrodynamics		
Minimum fluidization velocity (u_{mf})	$\frac{Ar}{Re^{mf}} = 150\frac{1-\varepsilon_{mf}}{\phi^2\varepsilon_{mf}^3} + 1.75\frac{Re^{mf}}{\phi\varepsilon_{mf}^3}$	*Equation 3.34* [25]
	with $Ar = \frac{d_p^3\rho_g(\rho_p-\rho_g)g}{\mu_g^2}$	*Equation 3.35*
	and $Re_{mf} = \frac{\rho_g u_{mf} d_p}{\mu_g}$	*Equation 3.36*
Minimum fluidization voidage	$\varepsilon_{mf} = 0.586Ar^{-0.029}\left(\frac{\rho_g}{\rho_p}\right)^{0.021}$	*Equation 3.37* [26]
Bubble diameter (d_b)	$d_b = d_{b,max} - \left(d_{b,max} - d_{b,0}\right)e^{-\frac{0.3h}{D_T}}$	*Equation 3.38* [27]
	$d_{b,max} = 1.638\left(\frac{\pi}{4}D_T^2(u_0 - u_{mf})\right)$	*Equation 3.39* [27]
	$d_{b,0} = 0.376(u_0 - u_{mf})^2$	*Equation 3.40* [27]
Bubble velocity	$u_b = u_0 - u_{mf} + 0.711(gd_b)^{0.5}$	*Equation 3.41* [28]
Emulsion velocity	$u_e = \frac{u_0 - (f_b + f_w\varepsilon_{mf})u_b}{f_{ce}\varepsilon_{mf}}$	*Equation 3.42*
Bubble fraction	$f_b \approx \frac{u_0 - u_{mf}}{u_b}$	*Equation 3.43* [23]
Wake fraction	$f_w = 0.15f_b$	*Equation 3.44* [29]
Emulsion fraction	$f_e = 1 - (f_w + f_b)$	*Equation 3.45*
Mass transfer		
Mass transfer coefficient bubble to cloud ($_{bc}$)	$K_{i,bc} = 4.5\frac{u_{mf}}{d_b} + 5.85\frac{D_i^{0.5}g^{0.25}}{d_b^{1.25}}$	*Equation 3.46* [23]

Mass transfer coefficient cloud to emulsion (ce)	$K_{i,ce} = 6.78\left(\frac{\varepsilon_{mf} D_i u_b}{d_b^3}\right)^{0.5}$	*Equation 3.47* [23]
Total mass transfer coefficient, bubble to emulsion (be)	$K_{i,be} = \frac{1}{\frac{1}{K_{i,bc}} + \frac{1}{K_{i,ce}}}$	*Equation 3.48* [23]

A part from all the described parameters, D_T refers to the reactor diameter, h to a certain height within the bed, dp to the particle diameter of the catalyst, ρ_g to the gas density, ρ_p to the solid density and g to the gravity force.

For an optimization of the OCM system, methane and oxygen need to be transported from the bubble phase to the wake and emulsion phases containing the catalyst, where they react to form C_{2+} and side products. Afterwards, these species need to be transferred back to the bubble phase, where they move upwards to the freeboard. With the developed model it is investigated whether mass transfer limitations would have an overall positive or negative effect on the OCM process performance.

As a base case, a 4 m high column with 0.6 m diameter filled with 300 µm diameter catalytic particles was considered. The temperature was kept at 800 °C and the pressure at 2 bar while using a relative fluidization velocity u/u_{mf} of 5. In this case, like in the previous reactor simulations, the catalyst fraction in the solids was set to a low value (10^{-3}) to compensate for the very high activity of the catalyst and to provide a fairer comparison with packed bed reactors. The results of the base case are depicted in Figure 3.9.

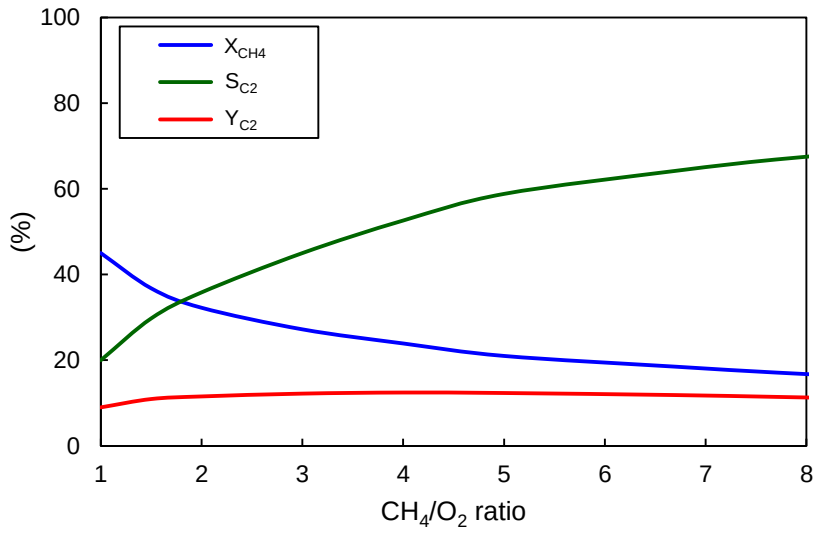

Figure 3.9. Calculated methane conversion, C_{2+} selectivity and C_{2+} yield with different CH_4/O_2 ratios in the bubbling fluidized bed reactor. Simulations at 800 °C and 2 bar with 0.1% La_2O_3/CaO catalyst particles.

The simulations indicate the relative poor performance achieved with this reactor configuration, where the best case achieves only slightly above 10% C_{2+} yield. As soon as the methane conversion starts to become high, an important loss in selectivity is observed caused by mass transfer limitations limiting the net C_{2+} production rate. Bubbles are acting like a distributed oxygen (and methane) feed to the catalytic zones, but the selectivity enhancement as found for the packed bed membrane reactor is not observed for the bubbling fluidized bed reactor with consequent quite low C_{2+} yields. In order to explain this difference, the average reaction rates along the reactor length in the bubble phase including the wake and the emulsion phase are shown in Figure 3.10 and the axial concentration profiles of the different species in each phase are represented in Figure 3.11.

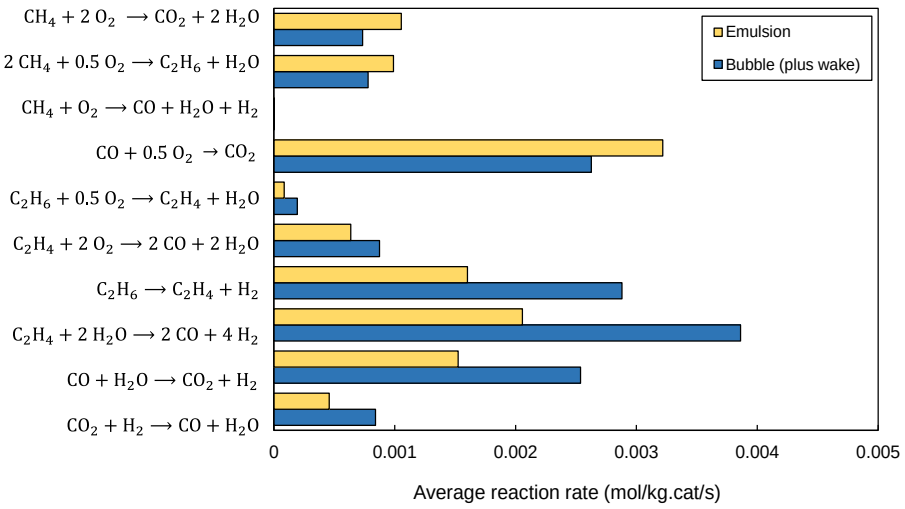

Figure 3.10: Calculated average reaction rates in the emulsion phase and the bubble phase (including the wake) in the bubbling fluidized bed reactor for the case of a CH_4/O_2 ratio of 4 (at 800 °C and 2 bar with 0.1% La_2O_3/CaO catalyst particles).

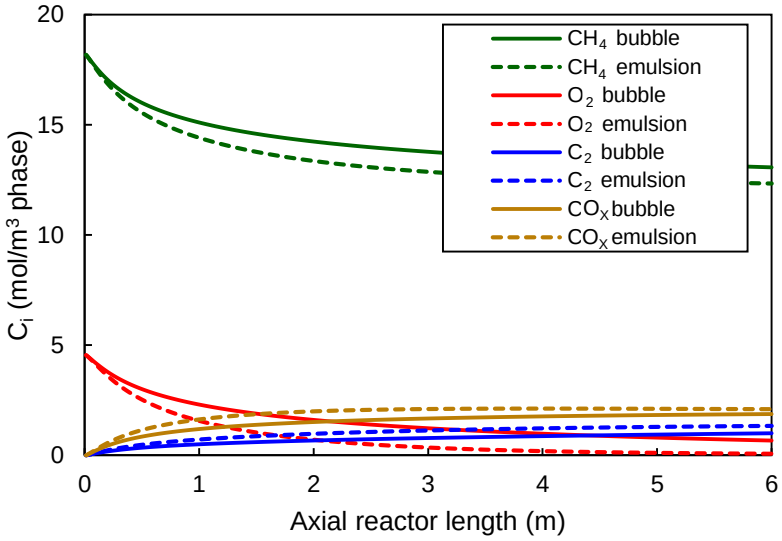

Figure 3.11. Axial concentration profiles of the relevant species (in kmol/m³ phase) in the emulsion phase and the bubble phase (including the wake) in the bubbling fluidized bed reactor for the case of a CH_4/O_2 ratio of 4 (at 800 °C and 2 bar with 0.1% La_2O_3/CaO catalyst particles).

Since the CH_4-O_2 mixture is distributed between bubble (+ wake) and emulsion phase, the concentrations are equal in both phases at the entrance of the reactor. Because of the fact that bubbles are considered to be free of solids and the only catalyst present

in the bubble phase corresponds to the wake phase (15% of the total bubble phase), the concentration profiles are steeper in the emulsion phase, leading to higher reaction rates in the emulsion phase. However, the generation of C_2's in the bubble phase together with the high reaction rates found in that phase (Figure 3.10) indicates that reactions also occur in the wake phase. On the other hand, the oxygen supply to the emulsion phase proceeds via two different mechanisms. On one side, the oxygen fed at the beginning of the reactor is distributed between bubble and emulsion phase depending on the volume fraction of each phase. In addition, oxygen can be transported from the bubbles, which is controlled by the mass transfer between both phases and this provides a distributed oxygen feeding to the emulsion phase. However, as can be deduced from Figure 3.11, the amount of oxygen transferred from the bubble phase is negligible in comparison to the amount of oxygen directly fed into the emulsion at the bottom distributor. Therefore, the concentration profiles in the bubble phase are governed by the kinetics rather than by mass exchange with the emulsion phase. Additionally, the relatively high oxygen concentration in both phases causes a relatively low C_{2+} selectivity, limiting the overall performance of the process.

The key factor to improve the reactor performance is the enhancement of the bubble-emulsion mass transfer rate while decreasing the reaction rates in the bubble wake, so that mass transfer processes govern the axial concentration profiles in the bubble plus wake phase. To do this, the amount of catalyst present in the bubble phase including the wake should somehow be limited or its activity decreased. If the conversion in the wake phase is limited, bubbles would act as a method of oxygen distribution to the emulsion phase, where the OCM could take place at low oxygen concentration levels. Moreover, it would be beneficial for the process to entirely feed the oxygen in the bubble phase, thus avoiding fast reactions in the emulsion phase close to the bottom distributor with a relatively high oxygen concentration.

In conclusion, bubbling fluidized beds may be a good solution in terms of thermal control, but suffer from a poor performance in terms of achievable yields due to the different optimal rates of intrinsic kinetics and mass transfer, as also reported in the

literature [30]. The answer to improve the performance is to try to use the bubbles as a natural way of distributing oxygen to regions with high catalyst concentrations, but the main obstacle seems to be the oxygen already present in the emulsion phase and the reactivity that the wake itself possesses.

In the next section it will be investigated whether operation in a circulating fluidized bed system could overcome these problems and achieve higher C_{2+} yields. Finally, the use of membranes in fluidized bed reactors [31], [32] will be also investigated. In this latter case, the amount of oxygen is low in all phases at the inlet, and the O_2 flux can be regulated by the membrane permeability tuned to the hydrodynamics of the gas-solid system.

3.3.2. Circulating fluidized bed

An alternative fluidization technology that could also be used for OCM is the circulating fluidized bed [33]–[35]. In this configuration, gas velocities are much higher than in bubbling fluidized beds, so that the solids are transported upwards together with the gas in the main reactor section. At the top, a system (commonly a cyclone) is used to separate the particles, which are transported back to the bottom of the reactor. Inside the bed, the solids are also partially recirculated in the regions close to the wall, where the solids naturally move downwards when operating at higher solids hold-ups.

A phenomenological model for circulating beds was proposed by Pugsley and Berruti, who applied it for different reaction systems, including OCM [36]. The model is a core-annulus model, which describes the two reactor regions that are characterized by different fluid dynamic conditions and catalyst concentrations. The model assumes that gas is transported upwards in the core section and it is stagnant in the outer region, and accounts for radial gas mass transfer between the two sections. Mass balances for both core and annulus are shown in Table 3.9:

Table 3.9. Equations for core and annulus used to solve the circulating fluidized bed mass balances.

Mass balances		
Core (c)	$\frac{dc_i^c v^c}{dx} = r_i\left(c_j^c, \gamma^c\right) - K_i^{ca}(c_i^c - c_i^a)$	*Equation 3.49*
	$\frac{dc^c v^c}{dx} = \sum_{i=1}^{N}\left[r_i\left(c_j^c, \gamma^c\right) - K_i^{bc}(c_i^c - c_i^a)\right]$	*Equation 3.50*
Annulus (a)	$0 = r_i\left(c_j^a, \gamma^a\right) + \frac{V^c}{V^a} K_i^{ca}(c_i^c - c_i^a)$	*Equation 3.51*

The volumes of the core and the annulus regions (V^c, V^a) are calculated using the position of the core-annulus interface r_c, the reactor diameter r_a and the height of the bed, H, as follows:

$$V_c = \pi r_c^2 H \qquad \textit{Equation 3.52}$$

$$V_a = \pi(r_a^2 - r_c^2)H \qquad \textit{Equation 3.53}$$

Values for r_c, γ^c and γ^a (solid fractions in core and annulus) are given by the same authors in another paper [37], summarized below (Table 3.10):

Table 3.10. Hydrodynamic correlations employed in the circulating fluidized bed.

Hydrodynamics		
Radial porosity profile	$\varepsilon(r) = 1 - \frac{G(r)}{\rho_s V_p(r)}$	*Equation 3.54*
	with $solid\ flux\ \left(G(r)\right) = \frac{G(r)}{G_s} = a\left(1 - \left(\frac{r}{r_a}\right)^5\right) + 1 - \frac{5a}{7}$	*Equation 3.55*
	and $particle\ velocity = V_p(r) = \left(1.5\frac{U_{g,c}}{\varepsilon^c} - V_t\right)\left(1 - \left(\frac{r}{r_c}\right)^2\right)$	*Equation 3.56*
Average solid fraction	$\gamma^c = 1 - \varepsilon^c = \frac{1}{r_c^2}\int_0^{r_c} 2r\varepsilon(r)dr$	*Equation 3.57*
	$\gamma^a = 1 - \varepsilon^a = \frac{1}{r_a^2 - r_c^2}\int_{r_c}^{r_a} 2r\varepsilon(r)dr$	*Equation 3.58*
	where $U_{g,c} = \frac{U_0}{\phi}$	*Equation 3.59*
	$\phi = \left(\frac{r_c}{r_a}\right)^2$	*Equation 3.60*
	$V_t = terminal\ velocity$	*Equation 3.61*
	and $a = \frac{7}{7\phi^5 - 2}$	*Equation 3.62*
Force balance	$\frac{2f_i\hat{U}_{g,c}^2}{\phi^{5/2}} + \frac{2f_w\hat{V}_{p,a}^2}{(1-\phi)^2} = (1-\phi)$	*Equation 3.63*

	where $\hat{U}_{g,c}^2 = \frac{\rho_g \varepsilon^c U_{g,c}^2}{(\rho_s - \rho_g) g 2 r_a}$	*Equation 3.64*
	$\hat{V}_{p,a}^2 = \frac{\rho_s (1-\varepsilon^a) V_{p,a}^2}{(\rho_s - \rho_g) g 2 r_a}$	*Equation 3.65*
	and $V_{p,a} = \frac{G_a}{\rho_s (1-\varepsilon^a)(1-\phi)}$	*Equation 3.66*
Friction factors	$f_i = 0.3164 \left(\frac{\mu_g}{2 r_c U_{g,c} \rho_c} \right)^{1/4}$	*Equation 3.67*
	$f_w = \frac{0.046}{V_{p,a}}$	*Equation 3.68*

In Table 3.10, ρ refers to density, ε to porosity and U to velocity while the subscript $_s$ intends for solids and subscript $_g$ intends for gas.

The hydrodynamic model by Pugsley and Berruti [36], [37] also assumes that there is an acceleration zone in the riser. This means that the values of γ^c and γ^a change along the axial coordinate until they reach the value calculated by the previous equations. Another force balance is defined to calculate the particle velocity in the acceleration zone:

$$V_{p,c} \frac{dV_{p,c}}{dz} = \frac{3}{4} C_d \frac{\rho_s V_{sl}^2}{d_p \rho_s} + g \frac{\rho_g - \rho_s}{\rho_s} \qquad \textit{Equation 3.69}$$

$$\text{Where } C_d = drag\ coefficient \qquad \textit{Equation 3.70}$$

$$V_{s,l} = \frac{U_{g,c}}{\varepsilon^c} - V_{p,c} \qquad \textit{Equation 3.71}$$

$$\text{and } \varepsilon^c(z) = 1 - \frac{G_c}{V_{p,c} \rho_s} \qquad \textit{Equation 3.72}$$

For this concept, the following conditions were selected as a base case. The column height was set to 7 m, and a particle size of 70 µm (Geldart A) was selected with a net solids flux of 100 kg/m²/s. It was assumed that undiluted catalyst particles are fed to the reactor. For the circulating fluidized bed configuration it is possible to operate without solids dilution despite the very high catalyst activity because of the very high void fractions (>90%) prevailing in the bed. The CH_4/O_2 feed ratio was set to 4 with a

bed temperature of 800 °C and a total pressure of 2 bar. The value of the mass transfer coefficient was fixed at 0.05 m/s, in agreement with the range of values proposed by the authors [36]. The computed axial mole fraction profiles of methane, oxygen and ethylene for the core and annulus regions are given in Figure 3.12.

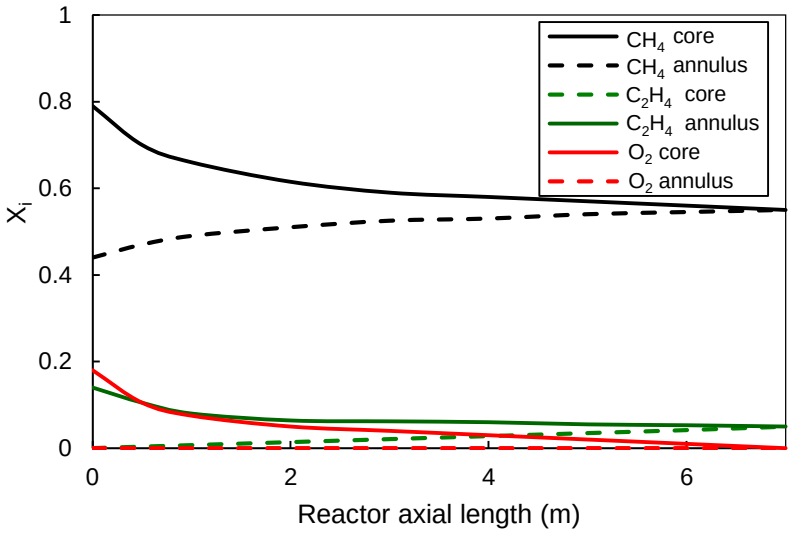

Figure 3.12: Axial mole fraction profiles of methane, oxygen and ethylene computed with the Pugsley-Berruti fluidized bed reactor model (see Appendix B) for the core (continuous lines) and annulus (dashed lines) regions (at 800 °C, 2 bar and CH_4/O_2 ratio of 4).

In the bottom part of the reactor, the gas compositions in the core and annulus regions are quite different, indicating the importance of mass transfer limitations. When the oxygen concentration in the core decreases, the compositions in the two regions get closer due to the reduced reaction rates, and the kinetic resistance becomes comparable with the mass transfer resistance. In the circulating fluidized bed reactor, the core region acts as a kind of distributed oxygen feeding to the annulus, similar to the bubbles in the bubbling fluidized bed reactor, as discussed in the previous section. At the reactor outlet almost all the oxygen from the core region has been transferred and consumed. The corresponding methane conversion amounts to 28% with a C_{2+} selectivity of 54%, giving a C_{2+} yield of 15%.

It is important to mention that the C_{2+} selectivity is enhanced in the annulus part as a result of reduced methane total and partial combustion reactions, resulting from the relatively low oxygen concentration levels. However, as was also the case in the bubbling fluidized bed reactor, the reaction kinetics predominates over the mass transfer rates at the entrance of the reactor, causing that most of the reaction takes place in the core where a relatively high oxygen concentration is still present, while most of the reaction should take place in the annulus if a maximization of the C_2 selectivity is searched. Reduced kinetics or improved core-annulus mass transfer rates are required to improve the reactor performance, limiting the reactions in the core and distributing the oxygen of the core more evenly to the annulus, where the reactions could occur at lower oxygen concentrations.

3.3.3. Fluidized bed membrane reactor

An interesting possibility to increase the overall yield of the process is to integrate oxygen membranes into a fluidized bed reactor. Therefore, the mass balances, shown in Equation 3.73 and Equation 3.74, contain the term which accounts for the reaction occurring in that phase, the mass exchanged with the other phase and the oxygen permeation from the membrane. Thus, the component mass balance for the bubble phase (b) at the permeate side is:

$$\frac{d}{dz}\left[u_b\left(f_b + f_w\varepsilon_{mf}\right)C_{i,b}\right] = K_{i,be}\left(f_b + f_w\varepsilon_{mf}\right)\left(C_{i,e} - C_{i,b}\right) \pm R_{i,b}f_b\left(1 - \varepsilon_{mf}\right) + a\left(J_{i,b}^m f_b\right) \qquad \textit{Equation 3.73}$$

While the component mass balances for the emulsion phase (e) at the permeate side:

$$\frac{d}{dz}\left[u_{g,e}\left(f_e\varepsilon_{mf}\right)C_{i,e}\right] = -K_{i,be}\left(f_b + f_w\varepsilon_{mf}\right)\left(C_{i,e} - C_{i,b}\right) \pm R_{i,e}f_e\left(1 - \varepsilon_{mf}\right) + a\left(J_{i,e}^m f_e\right) \qquad \textit{Equation 3.74}$$

$$\text{where } a = \frac{membrane\ surface\ area}{reactor\ volume} \qquad \textit{Equation 3.75}$$

The hydrodynamics and mass transfer expressions have been selected to be the same as in the case of the bubbling fluidized bed reactor. Similar to the case of the packed bed membrane reactor and detailed in Table 3.11, the membranes distribute the oxygen feed along the axial length of the reactor, keeping the oxygen partial pressure low and consequently selectively enhancing the desired reactions.

Table 3.11. Oxygen permeation through the MIEC membrane to the cloud and emulsion phase.

Membrane permeation flux [20]	
$J_{i,b}^{m} = \frac{D_v k_r \left(\left(p_i^{m,a}\right)^n - \left(p_{i,b}^{m,f}\right)^n \right)}{2\delta k_f \left(p_i^{m,a} p_{i,b}^{m,f}\right)^n + D_v \left(\left(p_i^{m,a}\right)^n + \left(p_{i,b}^{m,f}\right)^n \right)}$	*Equation 3.76*
$J_{i,e}^{m} = \frac{D_v k_r \left(\left(p_i^{m,a}\right)^n - \left(p_{i,e}^{m,f}\right)^n \right)}{2\delta k_f \left(p_i^{m,a} p_{i,e}^{m,f}\right)^n + D_v \left(\left(p_i^{m,a}\right)^n + \left(p_{i,e}^{m,f}\right)^n \right)}$	*Equation 3.77*

For the fluidized bed membrane reactor, mass transfer between bubble and emulsion phases also influences the maximum yield achievable. Mass transfer resistances could help protecting C_2's, formed in the emulsion phase and migrated to the bubble phase, from undesired consecutive reactions (reforming and combustion) because of the very low catalyst concentration in the bubbles. On the other hand, mass transfer can also have a detrimental effect, because some methane and also oxygen present in the bubbles may remain unreacted because of the low catalyst concentration in the bubble phase, leading to a much reduced conversion of the reactants.

For the simulations, the same conditions have been selected as before for the bubbling fluidized bed reactor simulations. The amount of oxygen has been varied by changing the number of membranes in the reactor, while the catalyst dilution is fixed at 10%. The membrane characteristics have been chosen identical to those in the packed bed membrane reactor simulations (see Table 3.6), with a membrane diameter of 0.01 m. The membrane length is equal to the reactor length to maximize the oxygen distribution.

In Figure 3.13 the simulation results for different CH_4/O_2 ratios have been plotted.

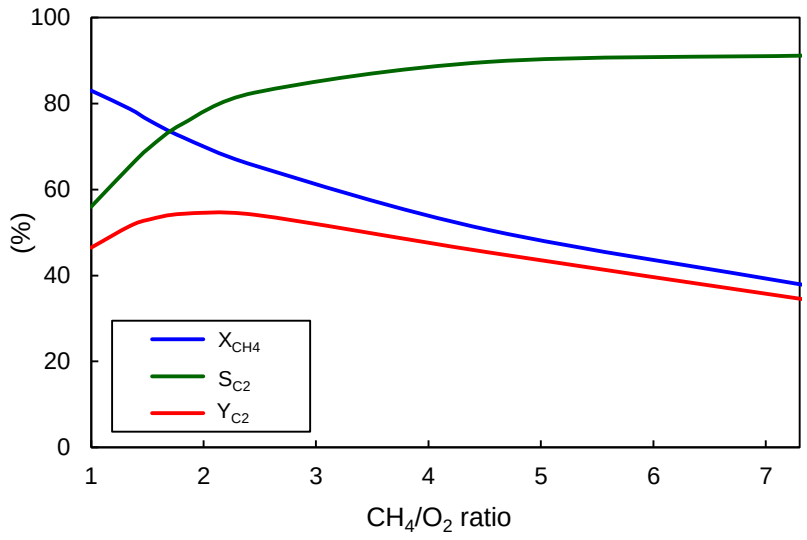

Figure 3.13. Calculated methane conversion, C_{2+} selectivity and C_{2+} yield for different CH_4/O_2 ratios in the permeate side of the fluidized bed membrane reactor (at 800 °C and 2 bar with 10% La_2O_3/CaO catalyst particles).

The figure shows that an optimal CH_4/O_2 ratio is found at around 1.5, corresponding to the integration of 50 membranes and resulting in a C_2 yield of 54%. The performance is significantly increased when compared with the other fluidized bed configurations. With this configuration indeed a good distribution of the oxygen feed is achieved along the bed, keeping a low oxygen partial pressure in both phases, particularly also in the wake phase, where most of the reactions take place.

The C_2 yield attained here is however lower than the C_2 yield that can be obtained with the packed bed membrane reactor. To better elucidate the differences in performance of the two membrane reactor configurations, the separate performance of the bubble (plus wake) and emulsion phases for the optimal CH_4/O_2 ratio are shown in Figure 3.14.

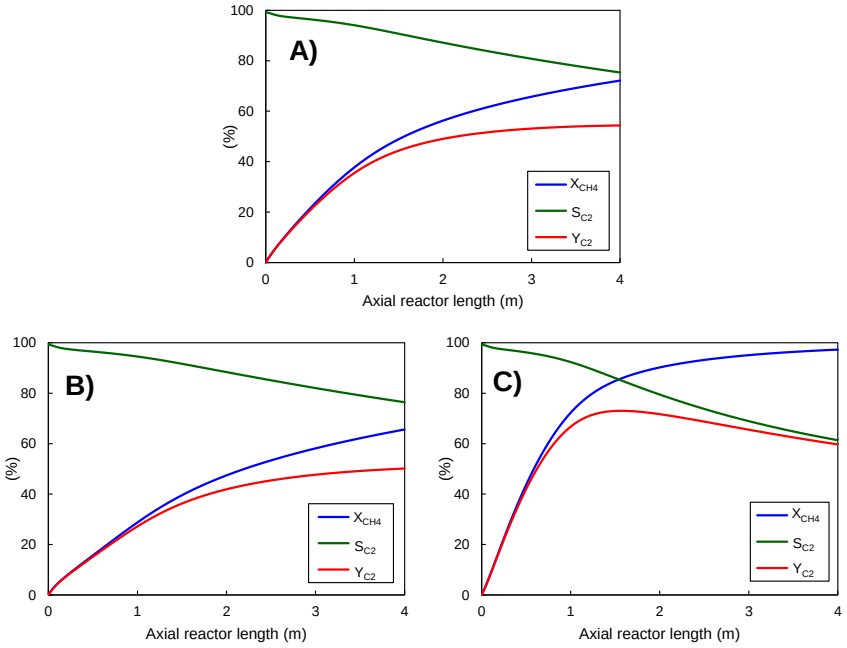

Figure 3.14. Calculated axial profiles of the methane conversion, C_{2+} selectivity and C_{2+} yield for the permeate side of the fluidized bed membrane reactor: overall reactor (A), and separate bubble (B) and emulsion (C) phase. Simulations at 800 °C and 2 bar, with 10% La_2O_3/CaO catalyst particles and with a CH_4/O_2 ratio of 1.5.

Because of the higher amount of catalyst in the emulsion phase, the methane conversion is much higher there, reaching almost 100% at the outlet, whereas in the bubble phase including the wake is much lower (about 65% at the outlet). The C_{2+} selectivity is higher in the bubble phase because of the reduced consecutive C_2 reactions, corresponding to the lower amount of catalyst present in that phase. However, the contribution of the bubble (including wake) phase to the overall performance of the OCM process is higher than the emulsion phase (in the overall reactor the profiles are more similar to the ones of the bubble phase) because of the higher superficial gas velocity in the bubble phase, being able that phase to process more gas per unit of time.

The differences in reaction rates in both phases result in a different optimal reactor length to maximize the C_2 yield in the two phases, thereby the necessity of finding a trade-off for the maximum overall yield and consequently loosing efficiency in at least

one of the two phases. The final consequence of this efficiency loss is a lower overall yield than for the comparable case of a packed bed membrane reactor, where just one compartment (phase) is considered.

To confirm this effect, the mass transfer coefficients between the different phases have been increased by 100 times for the optimal fluidized bed membrane reactor case and the simulation results are shown in Figure 3.15.

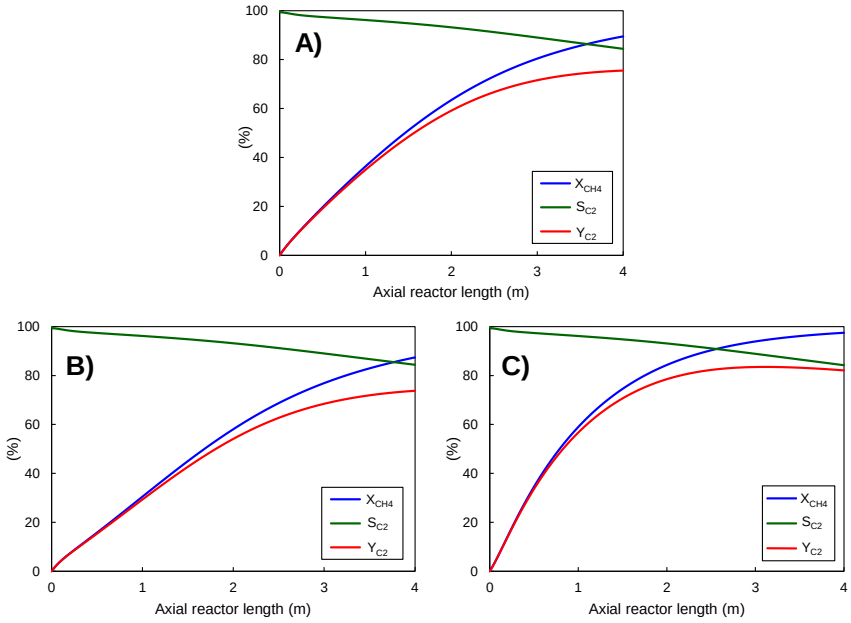

Figure 3.15. Calculated axial profiles of the methane conversion, C_{2+} selectivity and C_{2+} yield for the permeate side of the fluidized bed membrane reactor: overall reactor (A), and separate bubble (B) and emulsion (C) phase. Simulations at 800 °C and 2 bar, with 10% La_2O_3/CaO catalyst particles, with a CH_4/O_2 ratio of 1.5 and with the mass transfer coefficients multiplied by 100.

Because of the enhancement of the mass transfer between phases, the profiles of both emulsion and bubble phase get very similar, although a small difference is still discernable because of the faster reaction rates in the emulsion phase. More importantly, a very strong increase in the overall performance of the process is observed, where the C_2 yield can even be increased to values well above 70% and even surpassing the performance of the packed bed membrane reactor. By increasing the mass transfer, the methane present in the bubbles is reaching easily the emulsion

phase, thus enhancing the overall methane conversion. In addition, part of the C_2 formed in the emulsion and wake phase can migrate back to the bubbles, which are free of catalyst avoiding consecutive catalytic reactions. As a consequence, the positive effects of the use of fluidized beds are enhanced, while the negative effects are minimized.

Summing up, fluidized bed membrane reactors could indeed be a solution to improve the C_{2+} yield, and with simulations it has been demonstrated that this reactor concept can outperform conventional reactor configurations. The performance of the fluidized bed membrane reactor is lower than the packed bed membrane reactor, unless the mass transfer rates between the phases can be enhanced. However, fluidized beds provide a much easier temperature control, which is shown to be crucial for the considered reaction system.

3.4. Conclusions

In this chapter, different reactor concepts for OCM have been compared in detail with numerical simulations. With packed bed reactor configurations, a C_{2+} yield of around 20% can maximally be achieved, even when assuming isothermal operation, which is not easily accomplished in packed bed reactor configurations. Co-feeding of all reactants causes almost all conversion to take place close to the reactor inlet, leading to a very large local heat release in that region because of the strong exothermicity of the OCM reaction system, with dramatic consequences for the process performance. Optimization of several design and operating conditions, such as dilution of the catalyst with inert material and/or increase of the gas velocity, can solve the heat management issues, however at the expense of a strong decrease in the OCM performance.

Subsequently, a packed bed membrane reactor was simulated to feed the oxygen in a distributed manner along all the reactor length, thereby maintaining low oxygen partial pressures and consequently favoring the desired reactions, which also helps improving the reactor heat management and control of hot spot formation. With a

packed bed membrane reactor diluting the catalyst 10 times with inert material to minimize the effect of the C_2 reforming reactions, the C_{2+} yield can be increased up to 60%, making the OCM process economically viable and competitive with other technologies.

Another option to solve the heat management problem is the deployment of a fluidized bed reactor, with which the heat transfer is enhanced, facilitating easier thermal control of the reactor. However, the performance of both the bubbling and circulating fluidized bed configurations are rather poor, achieving C_{2+} yields of only around 12%. Again, the integration of membranes in this configuration can considerably improve the reactor performance, reaching values that – although lower than for the packed bed membrane reactor – are sufficiently high to render this process competitive with other ethylene technologies. It has been demonstrated that the mass transfer rates between the phases need to be optimized, if possible, to further increase the overall performance.

Although the results obtained for both the packed bed and fluidized bed membrane reactor concepts should be sufficiently good to satisfy the requirements for industrial exploitation of the OCM process, two important aspects that can significantly affect the computation results need to be further investigated. From one side, the reaction kinetics used for the simulations was not developed for use in a membrane reactor, and some C_2 consecutive reactions that can take place have not been accounted for in the used kinetics model. In a membrane reactor, where the desired products are formed throughout the reactor and where oxygen is fed along the entire reactor, C_2 consecutive reactions may become more important, especially towards the end of the reactor, thus decreasing the overall performance of the process. Unfortunately, so far no comprehensive reaction kinetics has been found in the literature (suited for application in a membrane reactor model) to reliably quantify the extent of the decrease in performance.

In addition, it should be considered that the La_2O_3/CaO catalyst (selected for all the simulations) is not able to completely direct the reaction towards the desired

products. As a consequence, the overall yield obtained from OCM will always be influenced by the particular characteristics of the catalyst chosen, mainly activity and selectivity, even though the reactor configuration employed could help maximizing the yield towards the desired products.

Another important assumption used here relates to the selected 1D reactor configuration. In membrane reactors lateral concentration profiles of methane, oxygen and C_2 species can significantly affect the overall reactor performance. The increased oxygen and C_2 concentrations near the membrane surface relative to the methane concentration decrease the C_2 yield, and this becomes even more important at higher methane conversion.

Summing up, from the simulations carried out in this chapter it can be concluded that membrane reactors can outperform conventional configurations and, in addition, can have the potential to reach the reactor yield target necessary to compete with the industrial technologies that are nowadays employed for the production of ethylene. Nevertheless, a proper optimization of these membrane reactor configurations has shown to be crucial and it is necessary to experimentally demonstrate the theoretical advantages of this technology.

3.5. Bibliography

[1] A. Cruellas, T. Melchiori, F. Gallucci, and M. Van Sint Annaland, "Advanced reactor concepts for oxidative coupling of methane," *Catalysis Reviews*, vol. 59, no. 3, pp. 234–294, 2017.

[2] S. Jašo, H. R. Godini, H. Arellano-Garcia, M. Omidkhah, and G. Wozny, "Analysis of attainable reactor performance for the oxidative methane coupling process," *Chemical Engineering Science*, vol. 65, no. 24, pp. 6341–6352, 2010.

[3] Z. Stansch, L. Mleczko, and M. Baerns, "Comprehensive kinetics of oxidative coupling of methane over the La2O3/CaO catalyst," *Industrial and Engineering Chemistry Research*, vol. 36, pp. 2568–2579, 1997.

[4] D. Schweer, L. Mleczko, and M. Baerns, "OCM in a fixed-bed reactor: limits and perspectives," *Catalysis Today*, vol. 21, pp. 357–369, 1994.

[5] T. P. Tiemersma, A. S. Chaudhari, F. Gallucci, J. A. M. Kuipers, and M. van Sint Annaland, "Integrated autothermal oxidative coupling and steam reforming of methane. Part 2: Development of a packed bed membrane reactor with a dual function catalyst," *Chemical Engineering Science*, vol. 82, pp. 232–245, Sep. 2012.

[6] M. R. Lee, M.-J. Park, W. Jeon, J.-W. Choi, Y.-W. Suh, and D. J. Suh, "A kinetic model for the oxidative coupling of methane over Na2WO4/Mn/SiO2," *Fuel Processing Technology*, vol. 96, pp. 175–182, Apr. 2012.

[7] V. I. Lomonosov, Y. a. Gordienko, and M. Y. Sinev, "Kinetics of the oxidative coupling of methane in the presence of model catalysts," *Kinetics and Catalysis*, vol. 54, no. 4, pp. 451–462, Jul. 2013.

[8] M. Daneshpayeh, A. Khodadadi, N. Mostou, Y. Mortazavi, R. Sotudeh-gharebagh, and A. Talebizadeh, "Kinetic modeling of oxidative coupling of

methane over Mn / Na 2 WO 4 / SiO 2 catalyst," vol. 90, pp. 403–410, 2009.

[9] A. M. Maitra, "Critical performance evaluation of catalysts and mechanistic implications for oxidative coupling of methane," *Applied Catalysis A: General*, vol. 104, no. 1, pp. 11–59, 1993.

[10] F. M. Dautzenberg, J. C. Schlatter, J. M. Fox, J. R. Rostrup-Nielsen, and L. J. Christiansen, "Catalyst and reactor requirements for the oxidative coupling of methane," *Catalysis Today*, vol. 13, pp. 503–509, 1992.

[11] "NIST Chemistry WebBook." .

[12] B. E. Poling, J. M. Prausnitz, and J. P. O'Connell, *The properties of gases and liquids - 5th edition*. McGraw-Hill, 2004.

[13] S. Sadjadi *et al.*, "Feasibility study of the Mn-Na2WO4/SiO2 catalytic system for the oxidative coupling of methane in a fluidized-bed reactor," *Catalysis Science and Technology*, vol. 5, no. 2, pp. 942–952, 2015.

[14] C. Karakaya and R. J. Kee, "Progress in the direct catalytic conversion of methane to fuels and chemicals," *Progress in Energy and Combustion Science*, vol. 55, pp. 60–97, 2016.

[15] N. Yaghobi and M. H. R. Ghoreishy, "Oxidative coupling of methane in a fixed bed reactor over perovskite catalyst: A simulation study using experimental kinetic model," *Journal of Natural Gas Chemistry*, vol. 17, no. 1, pp. 8–16, 2008.

[16] F. Raouf, M. Taghizadeh, and M. Yousefi, "Single and multi-channel reactor for oxidative coupling of methane," *International Journal of Chemical Reactor Engineering*, vol. 12, no. 1, 2014.

[17] S. Jašo *et al.*, "Experimental investigation of fluidized-bed reactor performance for oxidative coupling of methane," *Journal of Natural Gas Chemistry*, vol. 21, no. 5, pp. 534–543, 2012.

[18] H. Wang, Y. Cong, and W. Yang, "Oxidative coupling of methane in Bao.5Sro.5Coo.8Feo.2O3–δ tubular membrane reactors," *Catalysis Today*, vol. 104, no. 2–4, pp. 160–167, Jun. 2005.

[19] R. H. Perry, D. W. Green, and J. O. Maloney, *Chemical Engineers' Handbook - 7th edition*. McGraw-Hill, 1997.

[20] S. J. Xu and W. J. Thomson, "Oxygen permeation rates through ion-conducting perovskite membranes," *Chemical Engineering Science*, vol. 54, no. 17, pp. 3839–3850, 1999.

[21] V. Spallina, T. Melchiori, F. Gallucci, and M. V. S. Annaland, "Auto-Thermal Reforming Using Mixed Ion-Electronic Conducting Ceramic Membranes for a Small-Scale H2 Production Plant," pp. 4998–5023, 2015.

[22] S. Kalakkunnath, "Process Economics Program - Oxidative Coupling of Methane to Ethylene by Siluria Process," 2014.

[23] D. Kunii and O. Levenspiel, "Bubbling Bed Model. Model for Flow of Gas through a Fluidized Bed," *Industrial & Engineering Chemistry Fundamentals*, vol. 7, no. 3, pp. 446–452, Aug. 1968.

[24] J. A. Medrano *et al.*, "The membrane-assisted chemical looping reforming concept for efficient H2 production with inherent CO2 capture: Experimental demonstration and model validation," *Applied Energy*, vol. 215, pp. 75–86, 2018.

[25] S. Ergun, "Fluid flow through packed columns," *Chem. Eng. Prog.*, vol. 48, no. 2, pp. 89–94, 1952.

[26] J. R. Grace, "Contacting modes and behaviour classification of gas—solid and other two-phase suspensions," *The Canadian Journal of Chemical Engineering*, vol. 64, no. 3, pp. 353–363, Jun. 1986.

[27] S. Mori and C. Y. Wen, "Estimation of bubble diameter in gaseous fluidized

beds," *AIChE Journal*, vol. 21, no. 1, pp. 109–115, Jan. 1975.

[28] J. F. Davidson and D. Harrison, "Fluidised particles," *New York: Cambridge University Press*, 1963.

[29] I. Iliuta, R. Tahoces, G. S. Patience, S. Rifflart, and F. Luck, "Chemical-looping combustion process: Kinetics and mathematical modeling," *AIChE Journal*, vol. 56, no. 4, pp. 1063–1079, Apr. 2010.

[30] L. Mleczko and M. Baerns, "Catalytic oxidative coupling of methane - reaction engineering aspects and process schemes," *Fuel Processing Technology*, vol. 42, pp. 217–248, 1995.

[31] S. Jašo, H. Arellano-Garcia, and G. Wozny, "Oxidative coupling of methane in a fluidized bed reactor: Influence of feeding policy, hydrodynamics, and reactor geometry," *Chemical Engineering Journal*, vol. 171, no. 1, pp. 255–271, Jun. 2011.

[32] H. Arellano-Garcia, H. R. Godini, and G. Wozny, "Method for oxidatively converting alkanes and reactor assembly for carrying out said method," WO Patent 2013030084 A3, 2013.

[33] G. J. Tjatjopoulos, P. T. Ketekides, D. K. Iatrides, and I. A. Vasalos, "Cold flow model and computer simulation studies of a circulating fluidized bed reactor for the oxidative coupling of methane," *Catalysis Today*, vol. 21, pp. 387–399, 1994.

[34] S. Ruottu, K. Kaarianen, and J. Hiltunen, "Method based on a fluidized-bed reactor for converting hydrocarbons," US Patent 6045688 A, 2000.

[35] L. Mleczko and J. Marschall, "Performance of an internally circulating fluidized-bed reactor for the catalytic oxidative coupling of methane," *The Canadian Journal of Chemical Engineering*, vol. 75, no. 3, pp. 610–619, 2009.

[36] T. S. Pugsley and F. Berruti, "The circulating fluidized bed catalytic reactor:

Reactor model validation and simulation of the oxidative coupling of methane," *Chemical Engineering Science*, vol. 51, no. 11, pp. 2751–2756, 1996.

[37] T. S. Pugsley and F. Berruti, "A predictive hydrodynamic model for circulating fluidized bed risers," *Powder Technology*, vol. 89, pp. 57–69, 1996.

Chapter

4

Mn-Na_2WO_4/SiO_2 kinetics for OCM: Influence of secondary reactions

Abstract

As previously discussed, the oxidative coupling of methane holds great promise for the production of ethylene. W-based materials are widely investigated in literature to be used as OCM catalysts, but their evaluation in phenomenological models is hindered by the lack of a complete and comprehensive kinetics. In particular, reactor regions with low oxygen concentrations, which could be of high interest for the investigation of novel strategies with distributive oxygen feeding like membrane reactors, are not accurately evaluated and secondary reactions of the formed C_2's are several times not considered or underestimated with available kinetics. Therefore, in this chapter, the OCM reaction kinetics over a $Mn/Na_2WO_4/SiO_2$ catalyst is studied, paying special attention to secondary reactions. In addition, a kinetic model is developed based on experiments carried out in a micro fixed bed reactor at 800 °C and 2 bar. The accuracy of the proposed reaction kinetics model has been shown to describe the majority of the experimental data within about 20% relative error. Finally, the potential of the Mn-Na_2WO_4/SiO_2 catalyst for OCM has been demonstrated by calculations for an isothermal packed bed reactor where the developed kinetics model was implemented, showing that C_2 yields of approximately 30% are possible, provided that isothermal conditions can be achieved in the reactor.

4.1. Introduction

The combination of primary and secondary reactions, both desired and undesired, occurring in the oxidative coupling of methane process results in a dramatic decrease in the C_2 selectivity when aiming for high CH_4 conversions, and high C_2 selectivities can only be achieved at low CH_4 conversions, leading to relatively low overall C_2 yields, as shown in Figure 2.1. Therefore, the maximization of the C_2 selectivity at high CH_4 conversions still remains as the main challenge of the process. As detailed in Chapter 2 and Chapter 3, one of the possibilities proposed by previous authors to improve on this issue has been the development of novel reactor configurations, for instance using distributive oxygen feeding, thus keeping a low oxygen partial pressure along the entire reactor length, favoring the desired reactions of the process [1]–[4]. Another alternative to increase the C_{2+} selectivity is to improve the performance of currently used OCM catalysts, promoting more the reaction towards the desired products.

To do so, a deep understanding of the gas-catalyst interaction when carrying out OCM experiments is required. Going in detail into this aspect, it is usually accepted that the heterogeneous OCM reaction mechanism is independent from the specific catalyst employed in a certain experiment. Although there has been debate on this topic, it is commonly agreed that in OCM the activation of methane occurs via the so-called "Van Krevelen" mechanism [5], which describes the formation of methyl radicals (the precursor of C_2's) as the homolytic reaction of methane with oxygen-based species that have been previously adsorbed via an equilibrium reaction onto the catalyst surface. Lomonosov et al. [5] carried out a complete and extensive literature review on the OCM mechanism, including the steps involved from the methane activation up to the final ethylene production. The very broad range of experiments and the diversity of hypotheses that have been formulated in literature to accurately describe the complete OCM mechanism are a fair indication of the complexity of this reaction system. Generally, it is thought that the mechanism develops as follows; the process initiates with the formation of highly reactive methyl radicals via the Van Krevelen mechanism. These oxygen-free intermediates (free radicals) combine with each other

to produce firstly ethane, and then ethylene. At the same time, they can also react with oxygen species adsorbed on the catalyst surface to form undesired carbon oxides via heterogeneous reactions. The selectivity towards these undesired reactions depends on many parameters, such as the morphology of the catalyst and its actives sites, the specific conditions at which a certain experiment is conducted or the concentration of all the species involved in those reactions. In addition, the role that gas-phase oxidation reactions play in the OCM secondary reactions is also a matter of discussion, since in most of the OCM conducted experiments oxygen is also present in the gas-phase. Actually, it is believed that the rate of molecular oxygen in the gas-phase versus oxygen species on the catalyst surface is governed by an equilibrium reaction. Therefore, the role of molecular oxygen that has not been adsorbed on the catalyst cannot be underestimated, since it can enhance homogeneous combustions, especially of the C_2's, which are much more reactive than CH_4 at the typical OCM temperatures. Finally, heterogeneous and homogeneous OCM reactions cannot be studied independently since, as previously mentioned, the catalyst influences the amount of oxygen available in the gas-phase (as it is in equilibrium with the adsorbed oxygen) and also, as commented in some other works, by the ability of some OCM catalysts of capturing ethane and ethylene into their structure, hence hindering the amount of these species available in the gas-phase [6].

Along the OCM history, many OCM catalysts have been attempted for the activation of methane towards higher-weight hydrocarbons. Already in 1982, Keller and Bhasin [7] tested different metal oxides for their application in the OCM reaction. Even though from that point on many different options have been considered [8], [9], the screening of catalysts has been progressively narrowed, being Li, La and W based-catalysts the most studied. However, a lot of research on this field is still ongoing, trying to further improve their suitability towards the production of C_2's by, among others, modifying their preparation method (sol-gel technique [10]–[12] has become quite popular), by doping them with other active species [13], [14] or by having a deeper understanding of the heterogeneous reaction mechanism [15]–[17].

In particular, the Li-based catalysts group attracted a lot of interest in the first years of investigation of OCM [18]–[20]. The high C_2 selectivity that this group of catalysts provides coupled with a sufficient activity made Li-based catalysts the preferred option for OCM scientists at that time. However, the poor stability of the Li, which tends to migrate out of the catalyst because of its volatility [21] and affects the overall catalytic performance, especially in long term tests, hampers the scaling up of the experiments and strongly limits their applications.

Differently, La-based catalysts are considered to be stable under OCM conditions. They are also very active and their main drawback is the relatively low selectivity towards C_2's, below 50% in most of the published works [22], [23]. Despite this, they have been widely investigated. Specifically, the La_2O_3/CaO catalyst acquired a crucial relevance and it had a great impact for OCM since Stansch et al. [24] published their kinetics (shown in Table 3.1 and Table 3.2) in 1997, still nowadays the most reliable and used kinetic rate expressions to simulate OCM reactors. This kinetic rate model consists of a set of 10 individual reactions, including desired and undesired reactions occurring both in series and in parallel, aiming for an accurate description of the path that all the species involved in OCM follow.

Lastly, W-based catalysts appeared later, but they are currently one of the most investigated catalysts for OCM applications, since they combine a reasonably high C_2 selectivity, above 60% under certain conditions [25], with an acceptable stability under OCM conditions (although the W-based catalysts are much less active than the La-based catalysts). Large research efforts have been given to develop a deep understanding of the complex reaction mechanism and to determine the actual active sites of this catalyst when interacting with the OCM gas reaction mixture [26]–[28]. The complexity of its composition makes difficult the development of a comprehensive and accurate description of the reaction rates over W-based catalysts. Some researchers have attempted to use micro-kinetics models accounting for the presence of free radicals to develop a good description of the OCM mechanism when employing a W-based catalyst [29], [30]. However, the large number of species

(including radicals) accounted for in this type of models makes its application into simplified phenomenological models complicated. Following another approach, Daneshpayeh et al. [31], in 2009, took the reaction path described by Stansch et al. for the La_2O_3/CaO catalyst and adapted the main parameters, viz. activation energies, pre-exponential factors and reaction orders, to the Mn-Na_2WO_4/SiO_2 catalyst by means of fitting to experimental data. The result of this kinetics is however doubtful, bringing even inconsistent results in some of the standard OCM conditions. Similar to this work, Tiemersma et al. [25] proposed a simplified reaction mechanism, including just two primary and three secondary reactions to describe the reaction kinetics of a W-based catalyst for OCM. However, this work focused on the primary reactions and only the main secondary consecutive reactions. Particularly, the combustion and reforming of C_2's were not included, and hence not suited to describe the performance of the catalyst under integral reactor conditions.

Concluding, despite the fact that W-based catalysts have been shown to be very interesting catalyst systems for OCM applications, the lack of a comprehensive reaction kinetics model for this catalyst hinders the modeling and thereby the development of novel reactor configurations for OCM applications. In the development of novel reactor designs it is of high relevance to accurately predict the catalyst behavior and quantify the advantages that this catalyst is expected to bring in comparison to other OCM catalysts.

Therefore, the aim of the work described in this chapter is to find a more accurate kinetic model to describe the performance of the Mn-Na_2WO_4/SiO_2 catalyst under integral OCM conditions, paying special attention on the description of consecutive reactions involving C_2's. A complete kinetic model will be derived afterwards based on the experimental data, thus proposing a new reaction network for OCM over a Mn-Na_2WO_4/SiO_2 catalyst. To do so, the kinetics developed by Tiemersma et al. [25] over the Mn-Na_2WO_4/SiO_2 catalyst (summarized in Table 4.1), which includes only two primary reactions and three consecutive reactions, is taken as the initial point and this

kinetics model is in this work further extended with experiments in a micro-packed bed reactor including experiments at integral conditions.

Table 4.1. Kinetic model for OCM over a Mn-Na_2WO_4/SiO_2 catalyst proposed by Tiemersma et al. [25].

(i)	Reaction	Expression	k_i ($\frac{mmol}{kg*s*kPa^{n_i+m_i}}$)	n_i	m_i
		Based on measurements			
(1)	$2\,CH_4 + \frac{1}{2}O_2 \rightarrow C_2H_6 + H_2O$	$r_1 = k_1 P_{CH_4}^{n_1} P_{O_2}^{m_1}$	0.0118	1.0	0.36
(2)	$CH_4 + 2\,O_2 \rightarrow CO_2 + 2H_2O$	$r_2 = k_2 P_{CH_4}^{n_2} P_{O_2}^{m_2}$	0.00702	0.59	1.0
(3)	$C_2H_6 + \frac{1}{2}O_2 \rightarrow C_2H_4 + H_2O$	$r_3 = k_3 P_{C_2H_6}^{n_3} P_{O_2}^{m_3}$	0.2008	1.0	0.58
		Based on (Takanabe and Iglesia, 2008)			
(4)	$C_2H_4 + 3\,O_2 \rightarrow 2\,CO_2 + 2\,H_2O$	$r_4 = k_4 P_{C_2H_4}^{n_4} P_{O_2}^{m_4}$	0.052	1.0	1.0
(5)	$C_2H_6 + \frac{7}{2}O_2 \rightarrow 2\,CO_2 + 3\,H_2O$	$r_5 = k_5 P_{C_2H_6}^{n_5} P_{O_2}^{m_5}$	0.0331	1.0	1.0

In order to develop a more extensive and accurate (lumped) kinetics model, first a qualitative analysis on the relative importance of the different secondary reactions will be carried out. Subsequently, experimental results at integral conditions will be used to fit all the reactions involved in the OCM reaction system, obtaining a comprehensive OCM kinetics model accounting for 11 different reactions. After the validation of this fitting, the developed kinetics model will be integrated in a 1D phenomenological reactor model to evaluate the performance of the OCM process and particularly the importance of the secondary reactions.

4.2. Experimental

4.2.1. Catalyst preparation

The Mn-Na_2WO_4/SiO_2 catalyst used in this work was prepared by Johnson Matthey via incipient wetness impregnation. The final formulation of the catalyst was 1.6%Mn-5%Na_2WO_4. The catalyst was crushed and sieved to obtain the desired particle size, between 250 and 355 μm. The BET surface area of the catalyst was measured with a ThermoFischer Surfer and found to be 17.01 m^2/g, while its skeleton particle density was 1693 kg/m^3.

4.2.2. Experimental procedure

The experiments have been performed in a setup containing a feeding system, a micro fixed bed reactor, a post reaction zone and finally a gas analysis section.

The feeding system contains individual mass flow controllers for all the gases, CH_4, air, N_2, C_2H_4, C_2H_6 and CO_2, whereas a CEM (controlled evaporator mixer) is used for steam feeding. After all the mass flow controllers, the gases are pre-mixed and traced in order to preheat the gas mixture before entering the micro-packed bed reactor. The feed composition can be measured by by-passing the reactor.

The tubular micro reactor is made of quartz to withstand temperatures above 900 °C. Two thermocouples are used to measure the temperature, one in the post catalytic zone and the other one in the center of the reactor bed. The catalyst is placed on top of glass wool and it is mixed with quartz of the same particle size. The purpose of this mixing is to decrease the extent of reaction and therefore the temperature rise during the experiments. On top of the fixed bed, some bigger quartz particle are placed in order to ensure heating of the gas until the reaction temperature. The gas arrives from the upper part of the reactor, thus keeping the catalyst packed against the glass wool. Depending on the inlet flow rate, the pressure drop caused by the fixed bed has to be taken into account. The reactor is placed inside a tubular furnace to maintain the reaction temperature.

After the reactor, the outlet gas is chilled, and liquids are condensed in two condensers. The feed and dry product streams are analyzed by online gas chromatography (GC), with a Varian Micro-GC 4900 containing three columns, two 5A molsieve columns to separate oxygen, nitrogen, methane, carbon monoxide and hydrogen and a PoraPLOT Q column to separate H_2O, CO_2, C_2 and C_3 components. The columns are equipped with thermal conductivity detectors. Nitrogen is used as internal standard.

Oxygen and carbon atom mass balances of the results reported hereafter are within 2% and in most cases even within 1%. All experiments have been conducted under

differential conditions and in absence of internal and external mass transfer limitations (see Chapter 5).

In Figure 4.1 a scheme of the setup is shown, while in Table 4.2 the main operating conditions are summarized:

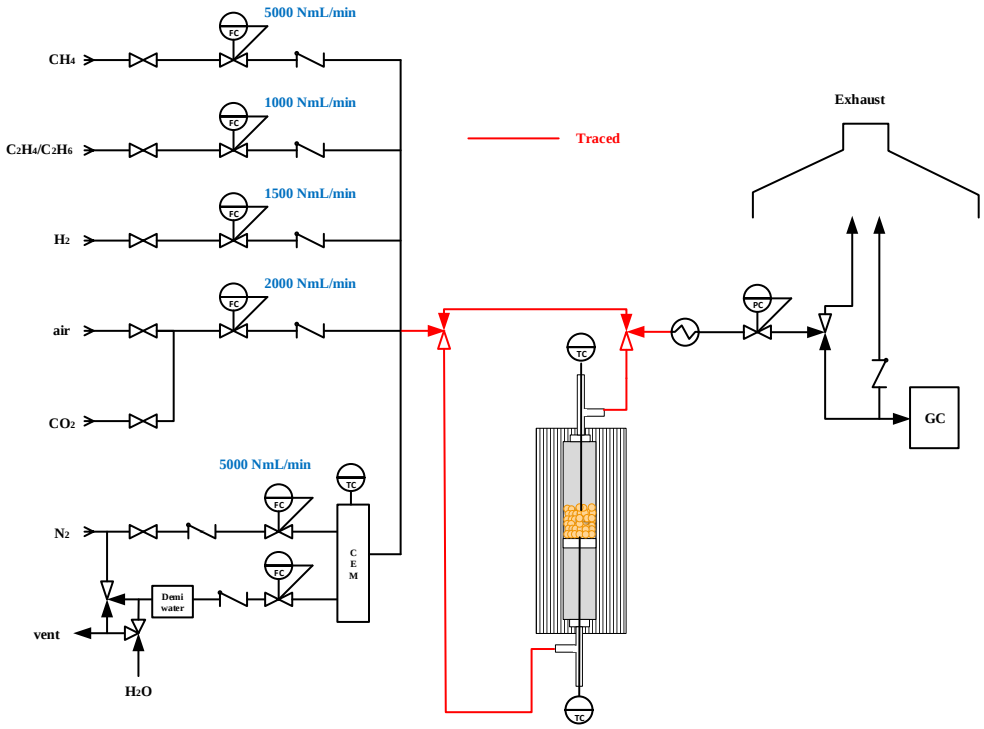

Figure 4.1. Scheme of the setup used for the kinetic experiments.

Table 4.2. Operating conditions used for the kinetic experiments.

Description	Value
Reactor diameter [mm]	7
Bed height [mm]	10-20
Amount of catalyst [mg.]	200-250
Amount of inert [mg.]	200-250
GHSV [1/h]	20-40
Inlet flow [L/min]	0.2-0.8
Temperature [°C]	800
Pressure [bar]	2

4.2.3. Catalyst stability

While the different experiments were taking place, a standard OCM mixture was fed to periodically check the activity of the Mn-Na_2WO_4/SiO_2 catalyst. The results of these experiments are shown in Figure 4.2.

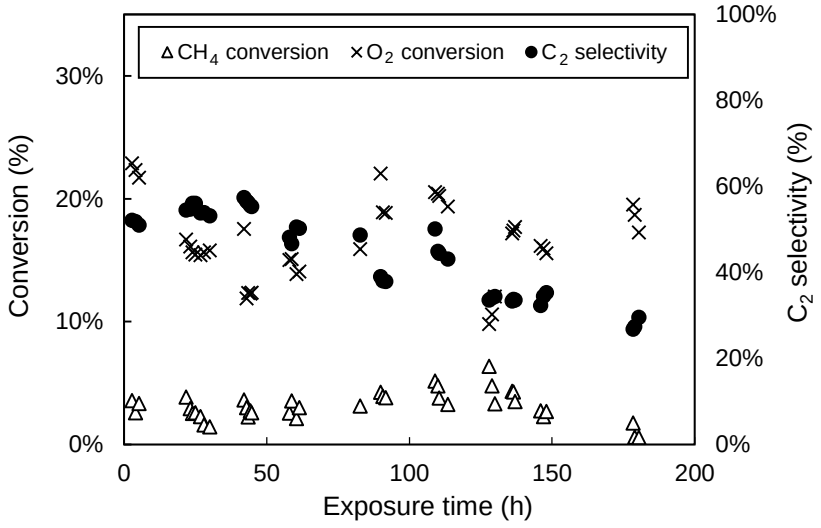

Figure 4.2. CH_4 conversion, O_2 conversion and C_2 selectivity of an experiment performed periodically with a CH_4/O_2 of 5 at 800 °C and 2 bar with a total flow rate of 360 mL/min.

First, it should be clarified that the exposure time refers to the time in which the catalyst has been exposed to an OCM mixture, that is, to the total reaction time. This time is much shorter than the total time that the catalyst has been kept at high temperatures (800 °C).

Different aspects can be discussed from this figure. It is evident that the catalyst needs some time under OCM conditions (at least 30 hours) to reach a steady state, mainly to stabilize the oxygen conversion. Once this steady state is achieved, the catalyst is exposed to different conditions to study other properties. The standard experiment is repeated for each batch of experiments to assess its stability. It can be seen that during the time in which the activity of the catalyst was monitored, the conversion of both reactants remains similar, even with a slightly increase in the case of the oxygen

conversion. In the case of the selectivity towards C_2's, a slow decrease could be observed over time, being somewhat steeper after 100-150 operating hours.

This is the main reason why each batch of catalyst, which corresponds to a batch of experiments, has been kept under reaction for no more than 100 hours, thus assuming a reasonably constant behavior of the catalyst during the experiments.

4.3. Results

The analysis of all the OCM experiments carried out with the Mn-Na_2WO_4/SiO_2 is organized as follows. First, a closer look at the individual secondary reactions is presented, assessing the importance of each of these reactions. Subsequently, a kinetic model is developed, where the kinetic parameters of the relevant OCM reactions are fitted using the obtained experimental data. Finally, the influence of the developed kinetic expressions on the OCM performance is discussed using calculations with a phenomenological 1-D model in which the developed kinetics model was implemented.

4.3.1. Description of secondary reactions

Secondary OCM reactions, particularly the ethane and ethylene reforming and oxidation reactions, have been investigated by carrying out experiments where the number of reactants, and consequently the number of possible reactions that need to be accounted for, are limited. Therefore, the mixtures shown in Table 4.3, which will later be individually analyzed, have been tested. The design of experiments has been performed such that the reactants and mixtures expected to prevail in an OCM reactor are replicated. The anticipated reactions in each batch have also been included in Table 4.3.

Table 4.3. Feed mixtures for the analysis of the secondary reactions together with the reactions that are accounted for when feeding these mixtures.

Feed mixture	Reactions considered based on products distribution
$C_2H_6 + H_2O$	$C_2H_6 + 2\,H_2O \rightarrow 2\,CO + 5\,H_2$ $C_2H_6 \rightarrow C_2H_4 + H_2$

$C_2H_6 + O_2$	$C_2H_6 + \frac{1}{2}\ O_2 \rightarrow C_2H_4 + H_2O$ $C_2H_6 \rightarrow C_2H_4 + H_2$ $C_2H_6 + O_2 \rightarrow 2\ CO + 3\ H_2$ $C_2H_6 + \frac{7}{2}\ O_2 \rightarrow 2\ CO_2 + 3\ H_2O$
$C_2H_4 + H_2O$	$C_2H_4 + 2\ H_2O \rightarrow 2\ CO + 4\ H_2$
$C_2H_4 + O_2$	$C_2H_4 + O_2 \rightarrow 2\ CO + 2\ H_2$ $C_2H_4 + 3\ O_2 \rightarrow 2\ CO_2 + 2\ H_2O$

The main objective of these experiments is to investigate and assess the relative importance of the aforementioned secondary reactions.

It should be mentioned that all these experiments have been performed under differential conditions, limiting the conversion of the carbon-based reactant, allowing to assume that further consecutive reactions are hardly taking place. This assumption is especially important for the cases where C_2H_6 has been used as reactant.

In addition, the OCM conditions summarized in Table 4.2 are also valid for these experiments.

4.3.1.1. $C_2H_6 + H_2O$

Since steam is generated in the primary OCM reactions (see Table 3.1), the reforming of ethane could take place during OCM (especially at low oxygen concentrations and high methane conversions), leading to a decrease in the overall OCM performance. Because of this, experiments have been carried out with a C_2H_6/H_2O ratio of 3.6, 2.4, 1.8 and 1.4, respectively. Higher C_2H_6/H_2O ratios could not be tested because of limitations in the setup. The results are presented in Table 4.4.

Table 4.4. Partial pressure of the reactants, reaction rates of consumption and production and C_2H_4 selectivity during the C_2H_6 reforming experiments with catalyst and with quartz performed at 800 °C and 2 bar with a total flow rate of 720 mL/min.

Type of experiment	P_{C2H6}	P_{H2O}	RR C_2H_6	RR CO	RR C_2H_4	RR H_2	C_2H_4 Selectivity
	[kPa]	[kPa]		[µmol/g_{solids}/s]			(%)
Catalytic	46.0	13.9	90.7	56.2	66.4	130.9	70.3

Catalytic	46.0	20.1	79.1	74.2	52.3	97.8	58.5
Catalytic	46.0	27.8	81.8	26.2	70.7	129.0	84.3
Catalytic	46.0	34.7	77.2	13.2	70.0	91.6	91.4
Catalytic	72.0	21.0	186.1	29.9	162.3	300.6	91.6
Catalytic	45.9	21.0	91.3	4.5	82.6	115.6	97.4
Catalytic	32.1	21.0	71.2	11.7	59.2	110.9	91.0
Catalytic	24.4	21.0	58.0	7.1	44.6	88.0	92.7

As expected, CO and H_2, the typical reforming products, are formed in these experiments. Nevertheless, it is interesting to observe that this reactant mixture also results in a high formation rate of ethylene, even higher than the formation rate of CO. Selectivities towards C_2H_4 above 60-70% are found in all the cases. The C_2H_4 formation can be attributed only to the non-oxidative dehydrogenation of ethane, which competes with the reforming reaction to consume C_2H_6. The experimental data also provide information to determine the main route by which the C_2H_6 is converted into C_2H_4. The results indicate that the C_2H_4 production predominates even in absence of oxygen, indicating that the non-oxidative C_2H_6 dehydrogenation plays a significant role in the production of C_2H_4. Indeed, these results indicate that the ethane reforming rate is much slower than the formation rate of C_2H_4, which is beneficial for OCM since few carbon-based reactants will be lost at this step to produce CO. In addition, the experiments carried out in this section are performed with relatively high concentrations of steam (it was not possible to feed lower amounts of steam because of limitations with the setup), meaning that, in conditions in which lower amounts of steam are present, as to be expected in the actual OCM process, the ratio of the non-oxidative dehydrogenation rate versus the reforming rate is expected to be even higher and more favorable towards the desired reaction.

4.3.1.2. $C_2H_6 + O_2$

To perform the C_2H_6 oxidation experiments, C_2H_6 and O_2 were co-fed and oxygen was selected as the limiting reactant in the oxidation experiments. Four different experiments have been performed (C_2H_6/O_2=7, C_2H_6/O_2=10, C_2H_6/O_2=12 and

C_2H_6/O_2=14) by varying the partial pressure of both reactants. A lower C_2H_6/O_2 ratio could not be used to avoid explosive conditions of this mixture. The results have been summarized in Table 4.5:

Table 4.5. Partial pressure of the reactants, reaction rates of consumption and production and C_2H_4 selectivity during the C_2H_6 oxidation experiments with catalyst and with quartz performed at 800 °C and 2 bar with a total flow rate of 720 mL/min.

Type of experiment	$P_{C_2H_6}$	P_{O_2}	RR C_2H_6	RR O_2	RR CO_2	RR CO	RR C_2H_4	RR H_2	C_2H_4 Selectivity
	[kPa]	[kPa]			[μmol/g_{solids}/s]				(%)
Catalytic	47.0	3.4	119.4	12.3	2.9	30.4	97.8	90.0	85.5
Catalytic	47.0	4.0	129.9	14.9	3.2	35.0	107.8	102.7	85.0
Catalytic	47.0	4.8	139.4	17.4	3.8	38.0	115.7	103.8	84.7
Catalytic	47.0	6.6	162.2	26.7	5.0	48.0	130.1	106.4	83.1
Catalytic	31.0	4.8	85.4	27.8	3.6	9.0	68.4	62.0	91.6
Catalytic	47.0	4.8	135.8	36.5	4.6	10.4	108.5	100.5	93.5
Catalytic	58.0	4.8	156.2	45.3	7.5	15.6	129.3	128.0	91.8
Catalytic	69.0	4.8	157.8	44.9	7.1	16.0	129.0	127.3	91.8

As can be observed, the selectivity towards the desired product is above 80% in all the experiments performed, showing that the main product is the desired C_2H_4. However, this 20% total selectivity towards undesired products (CO and CO_2) does affect the final performance of the process, because it consumes, in a secondary step, part of the C_2H_6 produced with the primary reactions. It has to be mentioned that the selectivity decreases with increasing C_2H_6/O_2 ratios, thus indicating that higher concentrations of oxygen lead to a decrease in the C_2H_4 selectivity because of an increase in the importance of the C_2H_6 combustion over its route towards C_2H_4.

The high production rate of H_2, together with the relatively low consumption rate of O_2, indicates that the non-oxidative dehydrogenation (independent from the partial pressure of oxygen) is the main route for the production of C_2H_4 in almost all the cases studied. The predominance of the non-oxidative C_2H_6 dehydrogenation over the oxidative dehydrogenation is also proven with the C_2H_6 reforming experiments, since

in these experiments the C_2H_4 production rate is also significant even in absence of oxygen feeding.

In any case, the oxidative dehydrogenation of C_2H_6 also plays a role, since the amount of C_2H_4 produced is higher when more oxygen is fed into the reactor. Considering that the non-oxidative C_2H_6 dehydrogenation does not depend on the amount of oxygen present in the bed, the oxidative dehydrogenation becomes more important when high oxygen partial pressures are applied, reaching even levels of production similar to the ones of the non-oxidative dehydrogenation (all the increase in C_2H_4 production from the experiment with P_{O_2} = 3 kPa to the one with P_{O_2} = 7 kPa has to be related to the enhancement of the oxidative dehydrogenation). These findings are especially interesting for the specific "membrane reactor" conditions. In that case, where low local oxygen concentrations in the reactor are expected, higher selectivities towards C_2H_4 are anticipated because of the high relevance of the non-oxidative dehydrogenation.

4.3.1.3. $C_2H_4 + H_2O$

The approach employed to analyze the C_2H_6 consecutive reactions has also been used for the C_2H_4 reactions. In particular, C_2H_4 reforming experiments have been carried out with C_2H_4/H_2O ratios of 3.6, 2.4, 1.8 and 1.4. Table 4.6 shows the results obtained in these experiments.

Table 4.6. Partial pressure of the reactants and reaction rates of consumption and production during the C_2H_4 reforming experiments with catalyst and with quartz performed at 800 °C and 2 bar with a total flow rate of 720 mL/min.

Type of experiment	$P_{C_2H_4}$	P_{H_2O}	RR C_2H_4	RR CO	RR C_2H_6	RR H_2
	[kPa]	[kPa]		[µmol/g_{solids}/s]		
Catalytic	48.0	13.9	2.1	2.5	0.5	8.3
Catalytic	48.0	20.1	4.7	4.3	0.5	12.3
Catalytic	48.0	27.8	4.9	5.1	0.6	15.6
Catalytic	48.0	34.7	4.8	15.3	0.9	39.6
Catalytic	72.3	21.0	14.9	18.1	2.1	49.0
Catalytic	48.3	21.0	9.7	13.0	0.9	36.3
Catalytic	36.1	21.0	4.2	7.3	0.4	19.3

Catalytic	29.2	21.0	8.7	12.9	0.4	34.4

The reaction rates of this sequence of experiments indicate that the C_2H_4 reforming is the slowest among all the secondary OCM reactions investigated, even when high steam concentrations are present in the bed. This fact is supported by the low production rates of both CO and H_2. Similar to the C_2H_6 reforming, this finding affects the overall OCM behavior positively, since the "damage" that C_2H_4 reforming can cause on the final C_2 selectivity has been shown to be rather low. Since it has been demonstrated that the rate of both C_2 reforming reactions is relatively low, it can therefore be concluded that the presence of steam in the reaction mixture, as is likely to occur during OCM, is not a large impediment to achieve high C_2 selectivities, as was reported in other works for other OCM catalysts [5].

4.3.1.4. $C_2H_4 + O_2$

Experiments with C_2H_4/O_2=7, C_2H_4/O_2=10, C_2H_4/O_2=12 and C_2H_4/O_2=14 have been performed by varying the partial pressure of both reactants to quantify the importance of the C_2H_4 oxidation, and the obtained results are shown in Table 4.7.

Table 4.7. Partial pressure of the reactants and reaction rates of consumption and production during the C_2H_4 oxidation experiments with catalyst and with quartz performed at 800 °C and 2 bar with a total flow rate of 720 mL/min.

Type of experiment	$P_{C_2H_4}$	P_{O_2}	RR C_2H_4	RR O_2	RR CO_2	RR CO	RR C_2H_6	RR H_2
	[kPa]	[kPa]			[µmol/g_{solids}/s]			
Catalytic	47.0	3.4	40.3	59.0	18.0	29.6	2.1	8.1
Catalytic	47.0	4.0	27.2	48.7	14.6	21.4	1.7	8.1
Catalytic	47.0	4.8	24.9	31.9	11.4	16.2	1.2	6.0
Catalytic	47.0	6.6	16.9	29.7	10.8	15.8	1.2	5.8
Catalytic	31.0	4.8	61.7	72.0	31.3	37.3	5.4	39.1
Catalytic	47.0	4.8	53.5	69.8	29.4	34.2	4.4	35.0
Catalytic	58.0	4.8	50.3	69.4	30.7	34.3	2.3	36.2
Catalytic	69.0	4.8	42.5	69.1	30.4	32.4	1.6	28.1

Even though it is not shown in Table 4.7, it should be remarked that this sequence of experiments was the only one where one of the reactants (oxygen) was fully consumed. This fact indicates that the ethylene oxidation is very fast, which can also be seen from the high consumption and production rates obtained in these experiments. However, it should also be noted that the concentrations of the products selected for these experiments are not likely to prevail in an OCM reactor, since it is very unlikely that the concentration of C_2H_4 is as high as the one employed in these experiments. However, the concentration of both reactants could not be better adjusted because of limitations in the setup. The experiments clearly show that the further oxidation of ethylene is very fast and should be avoided as much as possible. To do so, different strategies could be employed. Firstly, an even oxygen distribution along the axial reactor coordinate can limit the amount of oxygen in contact with the ethylene molecules, thus limiting also the amount of ethylene combusted. Secondly, a reactor design in which ethylene is removed from the reactor as soon as it is formed could also be a solution to limit this combustion. And finally, a deeper investigation should be carried out to some catalytic materials which posse the ability of reducing the ethylene oxidation reaction rate by capturing in their structure the radicals that are formed during the oxidation, as was already proposed in the literature [6], [32]–[34], contributing to mitigate the negative effect of the C_2H_4 oxidation.

4.3.2. General comments

The rates of all the above described reactions have been determined separately. Consequently, the interaction between the different reactants, mainly between the carbon-based species that coexist during OCM, has not been accounted for. This means that, for instance, methane, ethane and ethylene will have to compete for the oxygen available at each single region in the reactor, since the three main carbon-components (methane, ethane and ethylene) can consume it, and therefore the reaction rates will be affected. That is why it is necessary to derive the complete kinetics from integral experiments and therefore the above-described secondary reactions have been just considered as starting point for the fitting.

During the oxidation experiments, the carbon specie-oxygen ratio has been selected by considering oxygen as the limiting reactant. This approach was selected with particular interest in the application of distributive oxygen feeding in membrane reactors in mind. As mentioned before, the local oxygen concentration is expected to be low in membrane reactors, and thus this specie has been considered as the limiting reactant for all the individual experiments carried out. Therefore, the generalization of the results obtained in this section should be done carefully since the ratio of both reactants can strongly modify the conclusions of a certain experiment.

4.3.3. Kinetic model for the Mn-Na_2WO_4/SiO_2 catalyst

A kinetic model of the oxidative coupling of methane to C_{2+} hydrocarbons over a Mn-Na_2WO_4/SiO_2 catalyst has been developed. As explained before, the base of this model relies on the one developed by Tiemersma et al. [25]. However, this kinetics model is extended by adding more secondary reactions that are relevant and can contribute to better predict the outlet reactor stream composition.

Based on the results and observations analyzed in Section 4.3.1, it has been considered that the OCM system can be described by a set of 3 primary and 8 consecutive reactions. Hence, the kinetic model proposed here, consisting of these 11 steps, is shown in Figure 4.3:

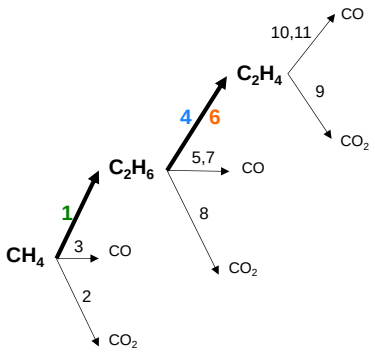

Step	Reaction
1	$2\,CH_4 + 0.5\,O_2 \rightarrow C_2H_6 + H_2O$
2	$CH_4 + 2\,O_2 \rightarrow CO_2 + 2\,H_2O$
3	$CH_4 + 0.5\,O_2 \rightarrow CO + 2\,H_2$
4	$C_2H_6 \rightarrow C_2H_4 + H_2$
5	$C_2H_6 + 2\,H_2O \rightarrow 2\,CO + 5\,H_2$
6	$C_2H_6 + 0.5\,O_2 \rightarrow C_2H_4 + H_2O$
7	$C_2H_6 + O_2 \rightarrow 2\,CO + 3\,H_2$
8	$C_2H_6 + 3.5\,O_2 \rightarrow 2\,CO_2 + 3\,H_2O$
9	$C_2H_4 + 3\,O_2 \rightarrow 2\,CO_2 + 2\,H_2O$
10	$C_2H_4 + O_2 \rightarrow 2\,CO + 2\,H_2$
11	$C_2H_4 + 2\,H_2O \rightarrow 2\,CO + 4\,H_2$

Figure 4.3. Proposed reaction scheme of primary and secondary OCM reactions, including desired (in colour) and undesired (in black) ones.

It should first be remarked that a description of the complex OCM mechanism is not the aim of this study, which would require a different type of work including all the free-radicals reactions that are formed and consumed during OCM, but instead the goal is to have a general set of reaction rate expressions that can adequately describe the distribution of the products and can be used in phenomenological models to evaluate the performance of the OCM process.

After the definition of all the reactions playing a role in OCM (for the particularities of the system investigated), the quantification of each of the reactions to build the kinetics model has been performed as follows. Firstly, the values (reaction constant and reaction orders) of the reactions accounted for by Tiemersma et al. have been taken as starting point. For the reactions that were not considered by Tiemersma et al. in their work but that are present in this kinetics model, the reaction constants and reaction orders have been found by carrying out a separate fitting to each individual reaction (based on the data analyzed in Section 4.3.1). Lastly, the so called "initial values" of all OCM reactions (the ones considered by Tiemersma and the ones obtained via the individual reaction fitting) have been improved by performing a global fitting (11 reactions at once) to extra OCM experimental data developed under integral conditions, as detailed below, thereby accounting for the coexistence of different carbon-based species in the reactor bed. In the experiments used for this final fitting, and with the purpose of generating sufficient data points to obtain decent results, the CH_4/O_2 ratio and the total flow rate (so residence time) have been varied. The rest of the operating conditions, including temperature, have been kept as described in Table 4.2. Because of working at a constant temperature during all the experiments, the pre-exponential factor and activation energy of all the reactions could not be determined in this work. The results of these integral conditions experiments are shown in Table 4.8:

Table 4.8. Results of the packed bed OCM experiments carried out under integral conditions at 800 °C and 2 bar.

	Flow rate 1					Flow rate 2					Flow rate 3				
Total feed flow rate (NmL/min)	250	250	250	250	250	350	350	350	350	350	450	450	450	450	450
Feed flow rate CH_4 (NmL/min)	65	63	63	63	62	90	90	89	88	89	113	113	111	113	113
Feed flow rate O_2 (NmL/min)	21	11	7	5	3	26	16	11	7	5	33	20	14	10	6
Feed flow rate N_2 (NmL/min)	164	177	180	182	185	235	244	250	254	256	304	318	325	327	331
CH_4/O_2 ratio	3.1	5.9	8.4	12.2	18.2	3.5	5.7	8.4	11.9	19.5	3.4	5.7	7.9	11.7	17.5
CH_4 conversion	0.28	0.20	0.16	0.16	0.09	0.21	0.17	0.14	0.11	0.09	0.16	0.11	0.10	0.09	0.07
O_2 conversion	0.75	0.78	0.89	0.89	0.87	0.51	0.61	0.69	0.65	0.84	0.37	0.37	0.39	0.50	0.59
C_2 selectivity	0.63	0.68	0.73	0.77	0.77	0.68	0.74	0.76	0.78	0.81	0.70	0.74	0.74	0.78	0.80
C_2 yield	0.18	0.14	0.12	0.12	0.07	0.14	0.13	0.11	0.08	0.07	0.11	0.08	0.07	0.07	0.05
C_2H_4/C_2H_6 ratio	1.4	1.0	1.0	0.80	0.6	1.0	0.8	0.7	0.5	0.5	0.7	0.5	0.4	0.4	0.4

The experimental results shown in Table 4.8 are consistent for OCM. A maximum C_2 yield of 18% is reached, a reasonable value for OCM in packed bed reactors [35]. Note the high selectivity achieved in some cases, attaining values above 80% when high CH_4/O_2 ratios are employed. In addition, the increasing reactants conversion and the decreasing C_2 selectivity when lowering the CH_4/O_2 ratio, a typical OCM behavior, support the validity of these experiments. Because of the reliability of the experiments, these data points could be used, as just described, to quantitatively calculate the parameters of the OCM kinetic expressions.

To carry out this optimization procedure, the error which has been minimized is defined as follows:

$$\varepsilon = \frac{\left|x_{exp} - x_{model}\right|}{x_{exp}} \qquad \textit{Equation 4.1}$$

Being "x" either CH_4 conversion, C_2 selectivity or C_2 yield, the three parameters accounted for during the optimization.

The complete scheme, including all the kinetic parameters calculated from the fitting at 800 ˚C for the Mn-Na_2WO_4/SiO_2 catalyst, is detailed in Table 4.9:

Table 4.9. Complete OCM kinetics for the Mn-Na_2WO_4/SiO_2 catalyst derived from the kinetics experiments at 800 ˚C and 2 bar.

Step	Reaction	Kinetic expression $[\frac{\mu mol}{g_{solids}*s}]$
1	$2\,CH_4 + 0.5\,O_2 \rightarrow C_2H_6 + H_2O$	$r = 0.0241 * P_{CH_4}^{1} * P_{O_2}^{0,36}$
	$CH_4 + 2\,O_2 \rightarrow CO_2 + 2\,H_2O$	$r = 0.0143 * P_{CH_4}^{0,59} * P_{O_2}^{1}$
3	$CH_4 + 0.5\,O_2 \rightarrow CO + 2\,H_2$	$r = 0.0122 * P_{CH_4}^{0,93} * P_{O_2}^{0,73}$
4	$C_2H_6 \rightarrow C_2H_4 + H_2$	$r = 1.5219 * P_{C_2H_6}^{1,66}$
5	$C_2H_6 + 2\,H_2O \rightarrow 2\,CO + 5\,H_2$	$r = \frac{0.1811 * P_{C_2H_6}^{0,59}}{(1 + (0.055 * P_{H_2O}^{1,59}))^2}$

6	$C_2H_6 + 0.5\ O_2 \rightarrow C_2H_4 + H_2O$	$r = \frac{0.7570 * P_{C_2H_6}^{1,38} * P_{O_2}^{1,05}}{(1 + (0.017 * P_{O_2}^{7}))^2}$
7	$C_2H_6 + O_2 \rightarrow 2\ CO + 3\ H_2$	$r = 0.0499 * P_{C_2H_6}^{0,08} * P_{O_2}^{1,13}$
8	$C_2H_6 + 3.5\ O_2 \rightarrow 2\ CO_2 + 3\ H_2O$	$r = 0.0001 * P_{C_2H_6}^{1,35} * P_{O_2}^{0,74}$
9	$C_2H_4 + 3\ O_2 \rightarrow 2\ CO_2 + 2\ H_2O$	$r = 0.0694 * P_{C_2H_4}^{0,18} * P_{O_2}^{0,6}$
10	$C_2H_4 + O_2 \rightarrow 2\ CO + 2\ H_2$	$r = 0.0347 * P_{C_2H_4}^{0,33} * P_{O_2}^{0,8}$
11	$C_2H_4 + 2\ H_2O \rightarrow 2\ CO + 4\ H_2$	$r = 0.0002 * P_{C_2H_4}^{1,11} * P_{H_2O}^{0,83}$

Two reactions, viz. ethane reforming and ethane oxidative dehydrogenation, have been found to be influenced by the adsorption of one of the reactants into the catalyst pores, lowering consequently the rate of the mentioned reactions. The inclusion of a Hougen-Watson type equation in these two reactions considerably improved their fitting, reaching a significantly higher accuracy. For the other reactions, a simple power-law expression has been found sufficient.

This developed kinetic model has been subsequently integrated in an isothermal 1-D reactor model. The model considers the reactor to be in plug-flow, where mass balances of all the species involved in the OCM are solved along the reactor axial coordinate. The dimensions of the simulated reactor have been set equal to the experimental conditions (see Table 4.2). Therefore, the results achieved with both the model (with the kinetics developed here) and the experiments can be fairly compared. All the parameters selected to perform the integral experiments, such as gas dilution, catalyst dilution, temperature and pressure have been taken for the simulations.

The quality of the kinetics expressions developed has been evaluated by comparing the experimental results (shown in Table 4.8) with the output of the model (with the kinetics parameters shown in Table 4.9). The three most relevant indicators to analyze the performance of an OCM reactor, i.e. CH_4 conversion, C_2 selectivity and C_2 yield,

have been selected for this evaluation. A comparison between the experimental data with the simulation results using the kinetic model is shown in Figure 4.4:

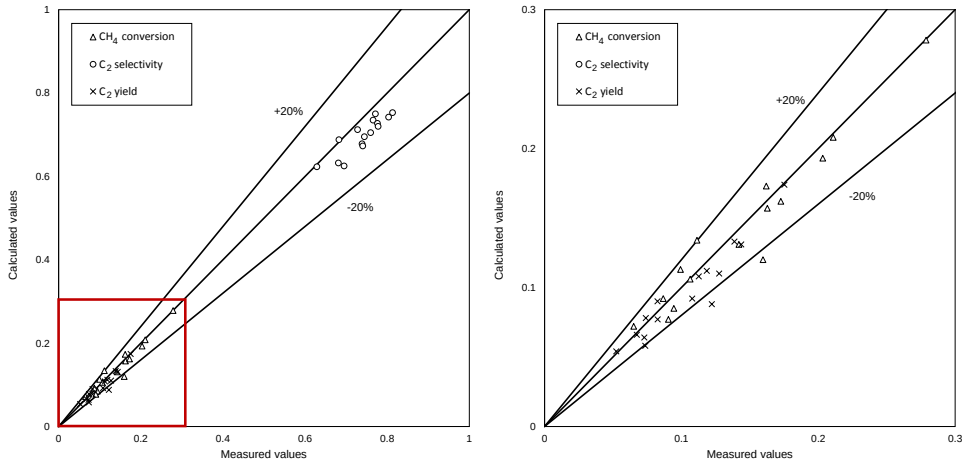

Figure 4.4. Comparison of experimental and calculated reaction rates of the primary OCM reactions.

As shown in Figure 4.4, the deviation of the model (with the indicators selected) are within a standard deviation of ±20%, showing that the model can replicate, by means of 11 reactions, the OCM results obtained experimentally. This is expected since the experimental data used for this comparison is the same than the one taken to build the kinetic model. However, it is anyway remarkable that the fitted model is relatively accurate at very different methane conversions (from 8 to 28%) and especially at low CH_4 conversions, where the deviation was expected to be higher because of the larger experimental errors under those conditions.

4.3.4. Discussion

The proposed kinetics model has been implemented in the aforementioned phenomenological 1D reactor model to investigate its behavior under OCM conditions and to validate it. Thereby, a sensitivity analysis on the CH_4/O_2 ratio, one of the most important OCM parameters, has been carried out. These simulations have been performed at "lab scale" conditions, meaning that the dimensions described in Table 4.2 have been used. However, and differently to the experiments, the length of the

reactor has been modified to 0.15 m in order to assure full conversion of the limiting reactant (oxygen in most of the cases). Full oxygen conversion was never achieved during the experiments because of the impossibility of increasing further the residence time of the gases in the bed caused by the constraints of the setup (lower flow rates or longer reactors could not be used). The data of these simulations obtained with the in-house developed kinetics has been compared to the one in which Stansch kinetics [24] has been employed (keeping constant the rest of the OCM parameters), thus allowing for a comparison between the behavior of both catalysts. In particular, the activity of both catalysts and the main OCM parameters, that is, CH_4 conversion, C_2 selectivity and C_2 yield, have been selected as the indicators to evaluate the systems. These comparisons are shown in Figure 4.5 and Figure 4.6:

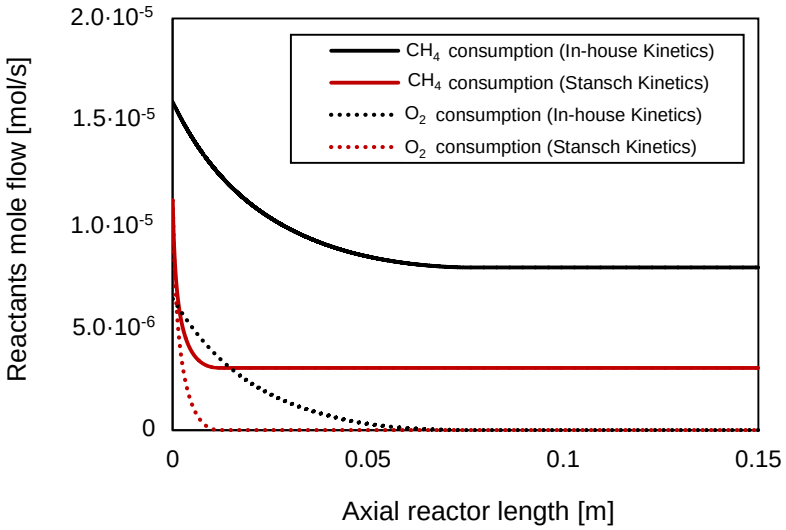

Figure 4.5. CH_4 and O_2 consumption rates along the axial reactor length obtained with the 1D reactor model using the in-house developed kinetics (black) and Stansch et al. [24] kinetics (red). Simulations carried out at 800 °C and 2 bar.

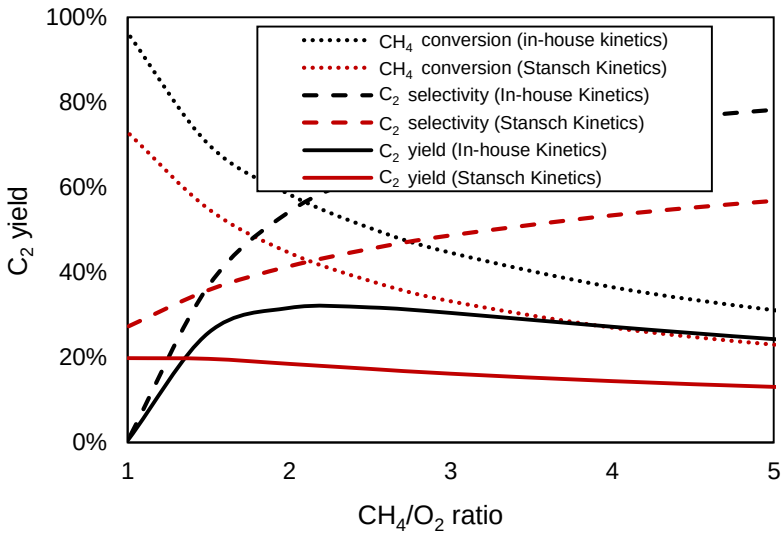

Figure 4.6. CH_4 conversion, C_2 selectivity and C_2 yield versus CH_4/O_2 ratio obtained with the 1D reactor model using the in-house developed kinetics (black) and Stansch et al. [24] kinetics (red).

It has been explained in the introduction that La-based catalysts, as the one employed in the kinetics developed by Stansch et al., are expected to be more active but less selective than the W-based catalysts (used in the in-house developed kinetics). The activity of both catalysts is compared in Figure 4.5. There, the red lines, corresponding to the La-based catalyst, are much steeper than the black ones (in-house kinetics based on a W-based catalyst), meaning that the reactions occur much faster along the axial reactor length when employing the La-based catalyst. In Figure 4.6 it can be observed that, as theoretically expected, a higher C_2 selectivity is reached for most of the CH_4/O_2 ratios with the W-based catalyst in comparison to the La-based one. It is also remarkable how the CH_4/O_2 ratios affect the performance of both catalysts differently: the maximum C_2 yield is found for a CH_4/O_2 ratio of 2 for the W-based catalyst (in-house kinetics), whereas the La-based catalyst (Stansch kinetics) shows a much flatter profile reaching its maximum at a CH_4/O_2 ratio of around 1.2. When optimizing the CH_4/O_2 ratio, one can notice that the La-based catalyst with the Stansch kinetics reaches a maximum C_2 yield of only around 20%, and this value is consistent with other works in which this kinetics has been used [4]. A maximum of

around 30% C_2 yield is reached for the W-based catalyst with the developed kinetics instead. This value is very interesting and, if this can be experimentally demonstrated, it would strongly decrease the gap to find an industrial application of the OCM technology (see Chapters 6 and 7).

It is however worth mentioning that none of the experimental works in which a Mn-Na_2WO_4/SiO_2 packed bed has been employed has reached this 30% C_2 yield calculated in the simulations. The discrepancy between the modelling results found here and the experimental results reported in the literature could be explained by the assumption of isothermal conditions in the reactor model. Due to the high exothermicity of the consecutive reactions, the experimental data may be adversely affected by the unavoidable temperature profile created along the reactor bed. This reaction exothermicity is very high when reaching high CH_4 conversions, as the case of the simulations where 30% C_2 yield was reached, leading to large discrepancies with the experimental results.

Nonetheless, the calculated maximum of 30% C_2 yield also shows the potential of this catalyst. If a reactor design allows to keep the temperature inside the optimal range for OCM (800 to 820 °C for this catalyst) all along the axial reactor length while reaching full conversion of methane, it is expected that higher yields than the ones experimentally obtained in this work can be attained. This reactor design could include either a catalyst dilution tuning with some inert material to have a closer control of the reaction behavior and thus of the temperature profile all along the bed, or could include some extra cooling to be able to better deal with the heat management in the bed.

4.4. Conclusions

The different reactions playing a role during the oxidative coupling of methane over a Mn-Na_2WO_4/SiO_2 catalyst have been identified and their kinetics investigated. Special attention has been given to the secondary C_2 reforming and oxidation reactions. The non-oxidative dehydrogenation has been shown to be the main route for the

production of ethylene from ethane. It is also clear from the experimental results that for the OCM reaction system the further oxidation of ethylene is the most relevant undesired reaction among all the investigated reactions. Since these reactions (both the complete and incomplete ethylene combustion) have been shown to be very fast, it is likely that they significantly hamper the C_2 yield. Therefore, by means of optimizing the reactor design, the ethylene-oxygen contact at OCM conditions should be avoided as much as possible. A possibility to minimize this detrimental C_2H_4-O_2 contact could be the integration of membranes to selectively separate the C_2H_4 or an optimization of all the reactor parameters (reaction temperature, residence time, catalyst dilution along the bed…) so that consecutive ethylene reactions are minimized.

Based on the knowledge acquired in the study of the individual secondary reactions, a kinetics model for OCM over a Mn-Na_2WO_4/SiO_2 catalyst has been developed. Reaction rate constants and reaction orders of all the relevant OCM reactions have been obtained (at 800 °C and 2 bar with a catalyst dilution of 50%) by carrying out a fitting procedure using experiments at integral reactor conditions. It has been shown that the 11-reaction developed kinetics model developed can adequately describe the integral conditions packed bed OCM experiments (within 20% error in most of the cases). In addition, a comparison with the well-known Stansch kinetics has corroborated the expected behavior, namely that the W-based catalyst is less active but more selective than the La-based catalyst. The model has also shown the great potential of this catalyst, showing that it is possible to reach C_2 yields of around 30%. However, the reactor design should be further improved to achieve close to isothermal conditions and actually reach these promising model results.

The kinetics developed in this work should be further extended to include the temperature dependency of the reaction rates (i.e. pre-exponential factors and activation energies of all involved reactions), an essential parameter to accurately predict the performance of actual reactor designs where temperature gradients cannot be (completely) avoided. This is the main reason why other kinetic models have been

used to develop the phenomenological models employed in this thesis (Chapters 3, 6 and 7).

4.5. Bibliography

[1] A. S. Chaudhari, J. J. F. E. Ramakers, F. Gallucci, and M. van S. Annaland, "Design of a Packed Bed Membrane Reactor for the Oxidative Coupling of Methane," *Procedia Engineering*, vol. 44, pp. 1724–1725, 2012.

[2] S. Jašo, H. Arellano-Garcia, H. R. Godini, and G. Wozny, "Method for oxidatively converting gaseous alkanes in a fluidized bed membrane reactor and a reactor for performing said method," WO Patent 2013017664 A3, 2014.

[3] A. Cruellas, T. Melchiori, F. Gallucci, and M. Van Sint Annaland, "Advanced reactor concepts for oxidative coupling of methane," *Catalysis Reviews*, vol. 59, no. 3, pp. 234–294, 2017.

[4] A. Cruellas, T. Melchiori, F. Gallucci, and M. van Sint Annaland, "Oxidative Coupling of Methane: A Comparison of Different Reactor Configurations," *Energy Technology*, vol. 0, no. 0, p. 1900148, May 2019.

[5] V. I. Lomonosov and M. Y. Sinev, "Oxidative coupling of methane: Mechanism and kinetics," *Kinetics and Catalysis*, vol. 57, no. 5, pp. 647–676, 2016.

[6] V. I. Lomonosov, T. R. Usmanov, M. Y. Sinev, and V. Y. Bychkov, "Ethylene oxidation under conditions of the oxidative coupling of methane," *Kinetics and Catalysis*, vol. 55, no. 4, pp. 474–480, 2014.

[7] G. E. Keller and M. M. Bhasin, "Synthesis of Ethylene via Oxidative Coupling of Methane. I. Determination of active catalysts," *Journal of Catalysis*, vol. 73, pp. 9–19, 1982.

[8] Y. Gambo, A. A. Jalil, S. Triwahyono, and A. A. Abdulrasheed, "Recent advances and future prospect in catalysts for oxidative coupling of methane to ethylene: A review," *Journal of Industrial and Engineering Chemistry*, vol. 59, pp. 218–229, 2018.

[9] E. V Kondratenko *et al.*, "Methane conversion into different hydrocarbons or oxygenates: current status and future perspectives in catalyst development and reactor operation," *Catalysis Science & Technology*, vol. 7, no. 2, pp. 366–381, 2017.

[10] G. Lee, I. Kim, I. Yang, J.-M. Ha, H. Bin Na, and J. C. Jung, "Effects of the preparation method on the crystallinity and catalytic activity of LaAlO3 perovskites for oxidative coupling of methane," *Applied Surface Science*, vol. 429, pp. 55–61, 2018.

[11] H. Habibpoor, M. Taghizadeh, and F. Raouf, "Oxidative coupling of methane over Li/MgO catalysts prepared by sol-gel and impregnation methods," *Inorganic and Nano-Metal Chemistry*, vol. 47, no. 10, pp. 1449–1456, Oct. 2017.

[12] A. G. Dedov *et al.*, "Oxidative coupling of methane to form ethylene: Effect of the preparation method on the phase composition and catalytic properties of Li-W-Mn-O-SiO2 composite materials," *Petroleum Chemistry*, vol. 55, no. 2, pp. 163–168, 2015.

[13] L. Cong, Y. Zhao, S. Li, and Y. Sun, "Sr-doping effects on La2O3 catalyst for oxidative coupling of methane," *Chinese Journal of Catalysis*, vol. 38, no. 5, pp. 899–907, 2017.

[14] R. T. Yunarti, S. Gu, J.-W. Choi, J. Jae, D. J. Suh, and J.-M. Ha, "Oxidative Coupling of Methane Using Mg/Ti-Doped SiO2-Supported Na2WO4/Mn Catalysts," *ACS Sustainable Chemistry & Engineering*, vol. 5, no. 5, pp. 3667–3674, May 2017.

[15] A. Vamvakeros *et al.*, "Real time chemical imaging of a working catalytic membrane reactor during oxidative coupling of methane," *Chem. Commun.*, vol. 51, pp. 12752–12755, 2015.

[16] D. Matras *et al.*, "Operando and Postreaction Diffraction Imaging of the La–Sr/CaO Catalyst in the Oxidative Coupling of Methane Reaction," *The Journal*

of Physical Chemistry C, vol. 123, no. 3, pp. 1751–1760, Jan. 2019.

[17] D. Matras *et al.*, "Real-Time Operando Diffraction Imaging of La–Sr/CaO During the Oxidative Coupling of Methane," *The Journal of Physical Chemistry C*, vol. 122, no. 4, pp. 2221–2230, Feb. 2018.

[18] S. J. Korf, J. A. Roos, N. A. de Bruijn, J. G. van Ommen, and J. R. H. Ross, "Oxidative coupling of methane over lithium doped magnesium oxide catalysts," *Catalysis Today*, vol. 2, no. 5, pp. 535–545, 1988.

[19] G. J. Hutchings, M. S. Scurrell, and J. Woodhouse, "Oxidative coupling of methane using Li/MgO catalyst: Re-appraisal of the optimum loading of Li," *Catalysis Letters*, vol. 5, no. 3, pp. 301–308, 1990.

[20] S. J. Korf, J. A. Roos, N. A. De Bruijn, J. G. Van Ommen, and J. R. H. Ross, "Lithium Chemistry of Lithium Doped Magnesium Oxide Catalysts Used in the Oxidative Coupling of Methane," *Applied Catalysis*, vol. 58, no. 1, pp. 131–146, 1990.

[21] S. Arndt *et al.*, "A Critical Assessment of Li/MgO-Based Catalysts for the Oxidative Coupling of Methane," *Catalysis Reviews*, vol. 53, no. 4, pp. 424–514, Oct. 2011.

[22] V. R. Choudhary, S. A. R. Mulla, and V. H. Rane, "Surface basicity and acidity of alkaline earth-promoted La2O3 catalysts and their performance in oxidative coupling of methane," *Journal of Chemical Technology & Biotechnology*, vol. 72, no. 2, pp. 125–130, 1998.

[23] C. Karakaya and R. J. Kee, "Progress in the direct catalytic conversion of methane to fuels and chemicals," *Progress in Energy and Combustion Science*, vol. 55, pp. 60–97, 2016.

[24] Z. Stansch, L. Mleczko, and M. Baerns, "Comprehensive kinetics of oxidative coupling of methane over the La2O3/CaO catalyst," *Industrial and Engineering Chemistry Research*, vol. 36, pp. 2568–2579, 1997.

[25] T. P. Tiemersma, M. J. Tuinier, F. Gallucci, J. A. M. Kuipers, and M. V. S. Annaland, "A kinetics study for the oxidative coupling of methane on a Mn/Na 2WO 4/SiO 2 catalyst," *Applied Catalysis A: General*, vol. 433–434, pp. 96–108, 2012.

[26] M. Y. Sinev, Z. T. Fattakhova, V. I. Lomonosov, and Y. a. Gordienko, "Kinetics of oxidative coupling of methane: Bridging the gap between comprehension and description," *Journal of Natural Gas Chemistry*, vol. 18, no. 3, pp. 273–287, Sep. 2009.

[27] Y. Gordienko *et al.*, "Oxygen availability and catalytic performance of NaWMn/SiO2 mixed oxide and its components in oxidative coupling of methane," *Catalysis Today*, vol. 278, pp. 127–134, 2016.

[28] V. I. Lomonosov, Y. a. Gordienko, and M. Y. Sinev, "Kinetics of the oxidative coupling of methane in the presence of model catalysts," *Kinetics and Catalysis*, vol. 54, no. 4, pp. 451–462, Jul. 2013.

[29] C. Karakaya, H. Zhu, C. Loebick, J. G. Weissman, and R. J. Kee, "A detailed reaction mechanism for oxidative coupling of methane over Mn/Na2WO4/SiO2 catalyst for non-isothermal conditions," *Catalysis Today*, vol. 312, pp. 10–22, 2018.

[30] J. Sadeghzadeh Ahari, S. Zarrinpashne, and M. T. Sadeghi, "Micro-kinetic modeling of OCM reactions over Mn/Na2WO4/SiO2 catalyst," *Fuel Processing Technology*, vol. 115, pp. 79–87, Nov. 2013.

[31] M. Daneshpayeh, A. Khodadadi, N. Mostoufi, Y. Mortazavi, R. Sotudeh-Gharebagh, and A. Talebizadeh, "Kinetic modeling of oxidative coupling of methane over Mn/Na2WO4/SiO2 catalyst," *Fuel Processing Technology*, vol. 90, no. 3, pp. 403–410, 2009.

[32] J. Sanchez-Marcano, C. Mirodatos, E. E. Wolf, and G. A. Martin, "Inhibition of the gas phase oxidation of ethylene by various solids and influence of their

addition on the catalytic properties of lanthanum oxide towards the oxidative coupling of methane," *Catalysis Today*, vol. 13, no. 2, pp. 227–235, 1992.

[33] L. Yu, W. Li, V. Ducarme, C. Mirodatos, and G. A. Martin, "Inhibition of gas-phase oxidation of ethylene in the oxidative conversion of methane and ethane over CaO, La2O3/CaO and SrO–La2O3/CaO catalysts," *Applied Catalysis A: General*, vol. 175, no. 1, pp. 173–179, 1998.

[34] S. Parishan *et al.*, "Investigation into Consecutive Reactions of Ethane and Ethene Under the OCM Reaction Conditions over MnxOy–Na2WO4/SiO2 Catalyst," *Catalysis Letters*, vol. 148, no. 6, pp. 1659–1675, 2018.

[35] S. Jaso, H. R. Godini, H. Arellano-garcia, M. Omidkhah, and G. Wozny, "Analysis of attainable reactor performance for the oxidative methane coupling process," *Chemical Engineering Science*, vol. 65, pp. 6341–6352, 2010.

Chapter

5

Proof-of-concept of OCM in a packed bed (membrane) reactor

Abstract

The potential of the OCM membrane reactor technology has been shown in Chapters 2 and 3. In this chapter, the advantages of this configuration will be experimentally evaluated, and the results obtained will be confronted to the ones of the conventional packed bed reactor. The Mn-Na_2WO_4/SiO_2 catalyst investigated in Chapter 4 and a porous symmetric MgO membrane have been selected for their integration in a packed bed membrane reactor. The conventional packed bed reactor showed good performance for the OCM reaction (C_2 yield of around 20%), but the potential benefit of an axial distribution of oxygen along the reactor via the porous membrane for the membrane reactor concept could not be experimentally demonstrated and no significant improvement in the performance could be observed. It was shown that back-permeation of hydrocarbons caused a non-uniform oxygen permeation flux, deteriorating the reactor performance. A theoretical sensitivity study carried out on the effective dispersion coefficient of the porous membrane has clearly indicated the necessity of further fine-tuning of membrane properties to be able to achieve the promising theoretical results. This study has highlighted how to address this issue for future research.

5.1. Introduction

As extensively discussed in Chapters 2 and 3, an even and fine oxygen distribution along the axial length of the reactor can contribute to increase the performance that can be reached during the OCM reaction compared to pre-mixed feed reactor configurations. This effect is caused by the preferential enhancement of the desired reactions over the undesired ones during the OCM process when keeping the oxygen partial pressure low, because of the lower reaction order in oxygen of the desired reactions. Thus, a distributed oxygen feeding along the reactor contributes to keep the local oxygen partial pressure low (yielding high C_2 selectivities), while maintaining an overall high CH_4 conversion, hence resulting in an improvement of the C_2 yield [1]. Many alternative reactor configurations have been experimentally proposed and tested based on this principle, e.g. the chemical looping concept [2]–[6], the packed bed reactor with multiple oxygen feedings [7], [8] or membrane reactors [9]–[18].

As extensively described in Chapter 3, both the packed bed membrane reactor and the fluidized bed membrane reactor have the potential to substantially improve the performance of the process and are currently believed to be the most suitable alternatives to improve the unsatisfactory results obtained with conventional reactor concepts. Even though the advantages that fluidized beds possess, especially the enhanced heat transfer that they can provide to the system, packed bed membrane reactors can slightly outperform fluidized bed membrane reactors (according to the calculations carried out in Chapter 3) for the specific OCM application, and that is why the simpler packed bed configuration has been further studied in this thesis.

Even though this packed bed membrane reactor emerges as one of the most promising solutions to realize high C_2 yields during OCM, in Chapter 3 also the difficulties encountered thus far to experimentally replicate the attractive performance values based on model calculations have been mentioned and remarked. The aim of the study reported in this chapter is to give an experimental proof-of-concept of OCM membrane reactors.

Therefore, an experimental study has been carried out to compare the performance of a packed bed and a packed bed membrane reactor. First, the design of an experimental OCM packed bed membrane reactor is detailed, highlighting the main parameters that need to be optimized to maximize and achieve the theoretical OCM performance expected from the membrane reactor simulations. Different oxygen feeding policies and operating conditions have been tested in order to better understand the functioning of the OCM membrane reactor and to search for the most relevant reactor parameters that are crucial for the further development of this technology.

5.2. Materials and methods

5.2.1. Catalyst preparation

The Mn-Na_2WO_4/SiO_2 catalyst used here is identical to the one described in Chapter 4 (Section 4.2.1) with a final formulation of 1.6%Mn-5%Na_2WO_4 with all other specifications the same. For all the experiments carried out, the catalyst was 50% diluted with quartz of the same particle size. By doing this, the reaction rates are slowed down and consequently the amount of heat released per surface area of the reactor tube is also decreased, making the temperature profile in the bed more homogeneous and simplifying the reactor heat management.

5.2.2. Membrane preparation

A porous symmetric MgO tube was selected as membrane material for the experiments. Their extensive availability and the simplicity of their sealing, when compared to MIEC membranes, have been the two main reasons for the selection of this membrane. These membranes were supplied by Rauschert and were sealed to a metallic tube, which then is connected to the reactor, by using the RAB sealing technique [19]. A picture of the sealed membrane can be seen in Figure 5.1:

Figure 5.1. Picture of the sealed (by means of the RAB sealing technique) MgO porous membrane used to carry out the membrane reactor experiments.

5.2.3. Experimental procedure

The setup used to carry out the experiments is composed by different sections: a feeding section, a reactor section and finally an analysis section. In general, four streams are considered for this system, that is, permeate inlet, permeate outlet, retentate inlet and retentate outlet. The scheme of the setup is depicted in Figure 5.2:

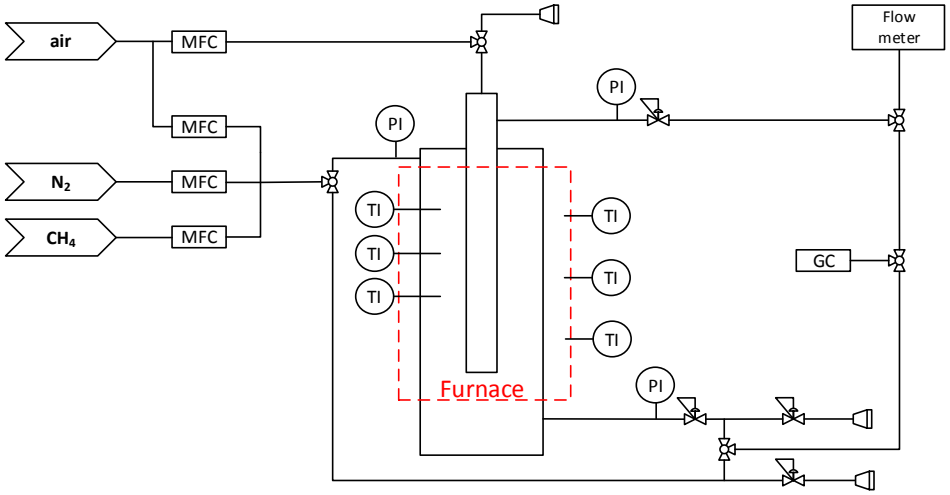

Figure 5.2. Scheme of the setup used for the experiments both in packed bed and packed bed membrane reactor configuration.

The design of the system was done, by means of a set of valves, such that all the streams could be independently sent to the analysis section to determine their composition (in a micro-GC) and/or to a flow-meter. In particular, the inlet streams could be characterized by by-passing the reactor, as shown in Figure 5.2, while the outlet streams could be sent directly to the analyzer and/or flow-meter. This strategy

allows to calculate the carbon balance in each of the experiments and to determine whether the experiment was successful and to obtain all the required information to understand the system.

Similar to the experiments described in Chapter 4, the carbon atom mass balances of the experimental results reported hereafter are within 2% and in most cases even within 1% relative error.

5.2.3.1. Feeding section

The feeding section is composed of individual mass flow controllers for CH_4, N_2 and air. A system of valves is designed such that the inlet can be divided into a permeate and retentate. In addition, both retentate and permeate inlet can be by-passed to the analyzer in order to quantify their flow rate and to know their compositions. Subsequently, both permeate and retentate gases are fed into the reactor section, where the OCM takes place.

5.2.3.2. Reactor section

The reactor consists of a tube made of quartz, expected to be inert and sufficiently resistant to the temperatures required for OCM, sealed by means of graphite to two metal connections. A picture of the empty reactor and its scheme are shown in Figure 5.3:

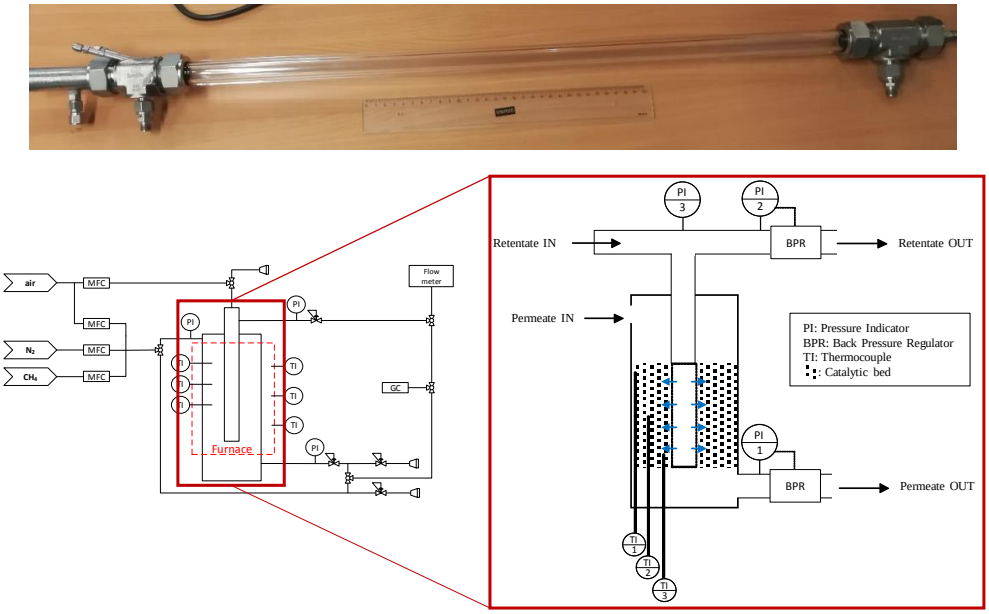

Figure 5.3. Picture of the empty reactor used to carry out the experiments (top) and zoom of the reactor from the setup scheme with the inlet and outlet streams (bottom).

The reactor, with a length of 70 cm, is longer than required to make sure that both metal-quartz sealings are cold and gas-tight. Three thermocouples are introduced in the reactor bed at different axial positions to monitor the temperature along the reactor, while another thermocouple is placed in the retentate side (inside of the membrane). The pressure at both sides is controlled by means of back pressure regulators, while the pressure indicators at different reactor sections are used to control the pressure drop in these regions. In addition, the back-pressure regulator of the retentate side is used to adjust the retentate-permeate pressure difference. This transmembrane pressure difference is the driving force that governs the system and determines the amount of gas permeating via the membrane from retentate to permeate side. The membrane is firstly sealed independently to a metallic tube, and afterwards this metallic tube is connected to the reactor via its correspondent Swagelok connection. Subsequently, the catalyst is placed inside the reactor, where glass wool is used to hold the catalytic bed. Four pictures of the assembling of the catalytic bed are shown in Figure 5.4:

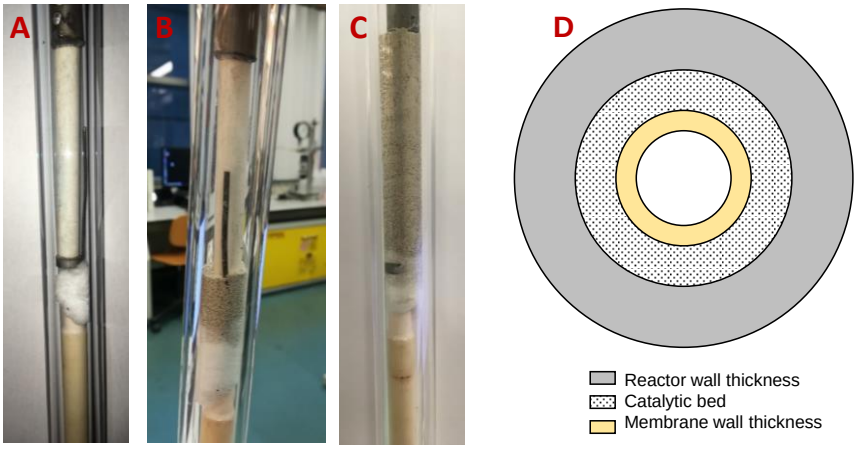

Figure 5.4. Pictures of the membrane reactor without catalyst (A), when part of the catalyst is placed (B) and when the catalytic bed is completed (C) and scheme of the view of the reactor in cross-section (D).

In addition, bigger quartz particles are placed on top of the bed, from where the inlet gas comes, in order to pre-heat the gas up to the desired temperature. Finally, the reactor is located inside a furnace, where the temperature is monitored and controlled via a computer.

5.2.3.3. Analysis section

The analysis of the gases is performed with the same GC that was described in Chapter 4 (Section 4.4.2). The only difference is that, since nitrogen is permeating to the reactor side together with oxygen (as will be explained later, air is fed at the retentate side of the system), He is used as internal standard.

5.2.4. Reactor configurations

The above described setup has been used to carry out tests with different reactor configurations. A summary of the experimental conditions is given in Table 5.1:

Table 5.1: Summary of conditions and parameters used for the experiments carried out in this work.

Condition	Value
Temperature [°C]	800
Gas dilution [%]	70 (N_2)
Catalyst dilution [%]	50 (quartz)

Type of catalyst	$Mn\text{-}Na_2WO_4/SiO_2$
Amount of solid in the bed [g.]	3-6
Permeate pressure [bar]	2
Retentate pressure [bar]	2.1-2.3
Total flow rate [mL/min]	250-750
CH_4/O_2 ratio	2-10
Membrane type	Porous MgO
Membrane length [mm]	50
Membrane outer diameter [mm]	10
Membrane inner diameter [mm]	7
Reactor diameter [mm]	16

The temperature is controlled such that none of the three thermocouples placed inside the bed exceeds 800 °C, hence assuming that temperatures above this preset maximum do not occur in the catalyst bed. The reactants, methane and in case of the conventional packed bed reactor also air, are always 70% mixed with N_2 to dilute the reaction and to minimize the effect that the exothermicity of the OCM reaction can cause on the axial temperature profile in the reactor. Because of the same reason, the catalyst is also diluted for 50% with quartz particles of the same particle size. To assure a permeation from the retentate to the permeate, the retentate pressure has been always kept higher than the permeate pressure. As will be explained later, the pressure in the retentate has been controlled to determine the amount of air permeating into the reaction side, which was maintained during all the experiments at 2 bar. Flow rates have been adjusted to provide reasonable residence times of the gases into the reactor, while the CH_4/O_2 ratio has been varied, as this is one of the most important parameters to be analyzed in this work. The dimensions of both the membrane and the reactor have been selected in order to limit radial concentration profiles when the membrane reactor configuration is used. Finally, the thick wall of the quartz reactor was chosen to avoid problems when increasing the pressure and to increase the mechanical strength of the reactor.

With all these conditions, the aim of this work is to compare the conventional (co-fed) packed bed reactor with the packed bed membrane reactor. To do so, three different reactor configurations have been employed, which are detailed in Figure 5.5:

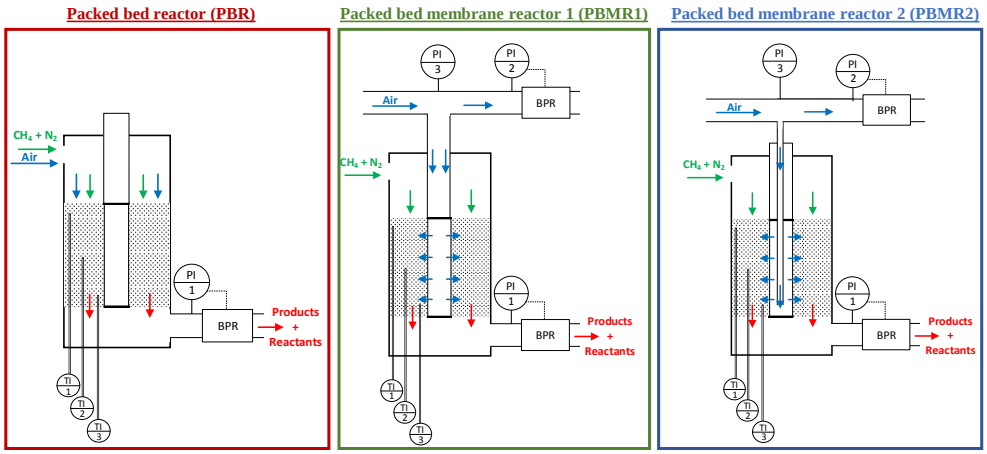

Figure 5.5. Scheme of the different reactor configurations (packed bed reactor (PBR), packed bed membrane reactor 1 (PBMR) and packed bed membrane reactor 2 (PBMR2) used for this study.

The packed bed reactor (PBR) configuration has been considered as the reference configuration for this work, that is, other reactor configurations will be always compared to the conventional packed bed. For the PBR case, the so called "retentate side" remains closed (no gas is fed from there), and all the reactants are co-fed from the "permeate" side. Subsequently, the gases go through all the catalyst bed.

In packed bed membrane reactor 1 (PBMR1), methane and gas diluent (N_2) are fed from the permeate side, while air is fed to the retentate side. The back-pressure regulator (BPR) located at the retentate outlet allows to control the amount of air permeating to the permeate side. Differently to PBMR1, where the air flows freely inside the membrane, a thin tube is introduced into the retentate side of packed bed membrane reactor 2 (PBMR2) to direct the air flow until the end of the membrane. At that point, the air reaches the retentate side and can start to permeate. The reason behind carrying out experiments with the PBMR1 and PBMR2 configurations is to determine whether the way in which air is introduced into the retentate side (at the beginning or at the end of the membrane) affects the results, thereby providing extra

information for the analysis of the experiments. In other words, these different configurations will contribute to understand how homogeneous the membrane permeation is along the axial length.

5.3. Results

5.3.1. Mass and heat transfer limitations

The relevance of heat and mass transfer in a catalytic bed should be quantified to verify that the observed reaction rates match with the reaction rates predicted from the determined reaction kinetics. When reactants are transported from the bulk reactor phase to the active sites of the catalyst, two different steps can be identified, as schematically shown in Figure 5.6. The first step is the transfer from the bulk phase to the external particle surface, often assumed to take place in a film layer around the particle, and this is referred to as external mass transfer. The second step, the so-called internal mass transfer, relates to the diffusion of molecules from the catalyst particle surface into the pores of the catalyst, where on their surface the active sites are located.

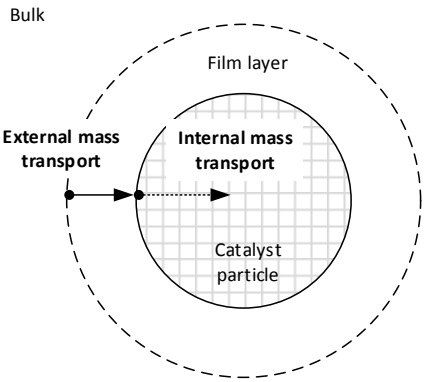

Figure 5.6. Scheme of mass transport steps occurring around/inside a catalyst particle.

The (potential) role of these mass transfer steps occurring in the system can be determined from several criterions for mass and heat transfer in and around the catalyst particle, as detailed in Table 5.2.

Table 5.2. Criterions used to identify mass and heat transfer limitations.

Mears criterion (external mass transfer)	$C_M = \frac{R_i^{obs} r_p}{k_{ext} c_i} < 0.15$
Weisz-Prater criterion (internal mass transfer)	$C_{WP} = \frac{-R_i^{obs} r_p^2}{D_{eff}\, c_i} < 1.0$
Thiele modulus (internal mass transfer)	$\phi_1^2 = \frac{k_1 r_p^2}{D_{eff}}$
Effectiveness factor (internal mass transfer)	$\eta = \frac{3}{\phi_1^2}(\phi_1 \coth \phi_1 - 1)$
Mears criterion (internal heat transfer)	$\frac{-\lvert\Delta H\rvert R_i^{obs} r_p^2}{\lambda T_0} < 0.75 \frac{T_0 R}{E_a}$
Mears criterion (external heat transfer)	$\frac{-\lvert\Delta H\rvert R_i^{obs} r_p}{h T_0} < 0.15 \frac{T_0 R}{E_a}$

Where R_i^{obs} (mol·s^{-1}·m^{-3}) and c_i (mol·m^{-3}) are the observed (experimentally) rates of conversion per unit of catalyst volume and the bulk concentration of the specie i, r_p (m) is the particle radius and k_{ext} (m·s^{-1}) the external mass transfer coefficient.

For the calculation of the Weisz-Prater criterion, D_{eff} (m^2·s^{-1}) refers to the effective diffusion coefficient, and it accounts for both the contributions of molecular and Knudsen diffusion.

In addition, the Thiele modulus uses instead k_1 (s^{-1}) for its determination, the ratio between R_i^{obs} and c_i.

For the heat transfer limitations, ΔH (J·mol^{-1}) refers to the reaction enthalpy, λ (W·m^{-1}·K^{-1}) is the thermal conductivity of the catalyst particle and h (J·m^{-2}·K^{-1}) is the external heat transfer coefficient. R (J·mol^{-1}·K^{-1}) is the universal gas constant, E_a (J·mol^{-1}) is the activation energy and T_0 (K) is the bulk temperature.

In the calculations regarding mass and heat transfer, oxygen was considered as the potentially limiting reactant and thus the most important specie. The mass and heat transfer criteria were checked for a standard case of OCM in a conventional packed bed reactor. Conditions of this "standard" case are listed in Table 5.3:

Table 5.3. Conditions and performance parameters of the standard experiment used to evaluate possible mass and heat transfer limitations.

Condition	Value
Inlet flow rate [mL/min]	360
CH_4/O_2 ratio	5
Gas dilution	70% (N_2)
Temperature [°C]	800
Pressure [bar]	2
Observed CH_4 conversion [%]	14.5
Observed O_2 conversion [%]	45.8

The calculated values for the mass and heat transfer criterions are summarized in Table 5.4. Each criterion is determined for two different situations to investigate its sensitivity towards some of the assumptions that were done. Cases with different assumptions are indicated with letters a-f. Besides the different criterions, also the intra particle effectiveness factor was estimated.

Table 5.4. Results of mass and heat transfer calculations.

Criterion	Value		Restriction
Mears criterion (external mass transfer)	0.056[a]	0.11[b]	< 0.15[a,b]
Weisz-Prater criterion (internal mass transfer)	0.41[c]	0.086[d]	< 1[c,d]
Effectiveness factor (intra particle)	0.974[c]	0.994[d]	–
Mears criterion (external heat transfer)	$6.38 \cdot 10^{-4}$ [e]	$7.23 \cdot 10^{-4}$ [f]	< 0.0063 [e] < 0.0136 [f]
Mears criterion (internal heat transfer)	$1.53 \cdot 10^{-5}$ [e]	$1.74 \cdot 10^{-5}$ [f]	< 0.0315 [e] < 0.0679 [f]

[a] Calculation of external mass transfer using Sherwood correlation (Equation 5.1)
[b] Calculation of external mass transfer using worst-case scenario of Sh = 2
[c] Calculation of internal mass transfer using mesopore size
[d] Calculation of internal mass transfer using macropore size
[e] Calculation of heat transfer using methane coupling reaction
[f] Calculation of heat transfer using methane combustion reaction

The Mears criterion for external mass transfer coefficient (k_{ext}) was determined using the following Sherwood correlation.

$$\mathrm{Sh} = 2 + 1.1\,\mathrm{Sc}^{\frac{1}{3}}\,\mathrm{Re}^{0.6} \quad \text{for } 3.0 < \mathrm{Re} < 10{,}000 \qquad \text{Equation 5.1}$$

However, the calculated Reynolds number of 1.51 exceeds the provided accuracy limits of the Sherwood correlation [20]. To put this in perspective, a worst-case scenario was also used for the Mears criterion. This worst-case scenario (case b) is the case where external mass transfer is fully diffusional, leading to a Sherwood number (ratio between convective mass transfer and diffusive mass transfer) of 2. A look at the results of the Mears criterion calculation shows that even in the worst-case scenario (case b), external diffusion limitations are absent.

Secondly, the presence of internal mass transfer limitations was checked using the Weisz-Prater criterion. Since the nano-scale structure of the catalyst particle is not known, the cases were purposively chosen. Case c calculates the effective diffusivity for a catalyst pore size (6.5 nm) in the mesoscale regime, since this was reported for a similar type of catalyst, while case d uses a catalyst pore size (50 nm) in the macroscale regime [21]. For both case c and d, it was found that internal mass transfer limitations can be neglected. In addition to the Weisz-Prater criterion, the effectiveness factors were also calculated for both cases, obtaining values of 97.4% and 99.4%, confirming that internal mass transfer limitations hardly influence the results.

The above mentioned results of the mass transfer analysis, showing the absence of any mass transfer limitations, corresponds to what Tiemersma et al. [22] showed using both calculations and experiments for a similar system.

The heat transfer criterions were also verified for two different cases and the results are summarized in Table 5.4. Firstly for case e, where the coupling reactions are considered, and for the second case (case f) where all reactions taking place are considered to be the methane combustion reactions, verifying absence of significant heat transfer limitations.

5.3.2. Packed bed vs. packed bed porous membrane reactor

The performance of the conventional packed bed configuration will be compared to the packed bed membrane reactor with the integrated MgO porous tube.

5.3.2.1. Membrane characterization

First, experiments without reactions were carried out to quantify the membrane permeation rate as a function of the trans-membrane (permeate-retentate) pressure difference. The membrane flux was measured both with PBMR1 and PBMR2 configurations. The results are shown in Figure 5.7:

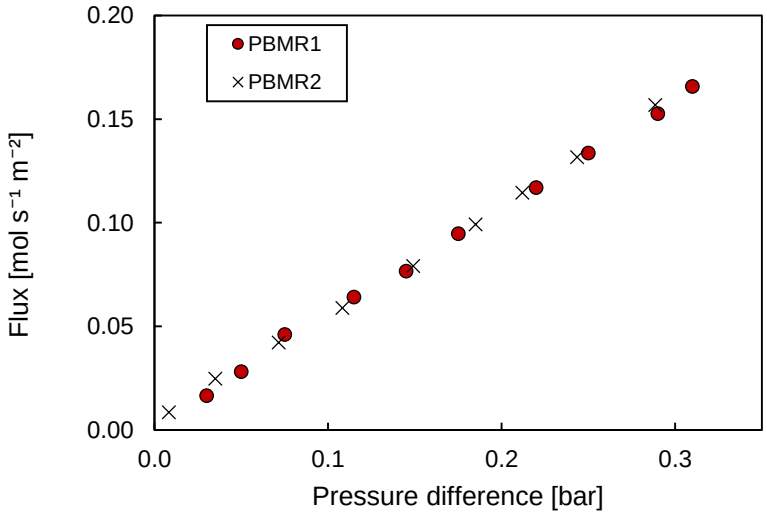

Figure 5.7: Flux of the symmetric MgO porous membrane plotted against the trans-membrane pressure difference.

The first conclusion that can be extracted from this figure is that the way in which air is fed to the retentate side does not influence the total membrane flux that is achieved when no reactions take place. Thus, in absence of reactions prevailing in the reactor, the pressure is constant along the axial coordinate of the retentate side (otherwise differences between the PBMR1 and PBMR2 configurations would have been observed). Moreover, the pressure drop caused by the thin tube introduced in PBMR2 is negligible.

The results of these tests are relevant for the design of the OCM reaction tests discussed in the next section, where the transmembrane pressure difference required

to obtain the desired CH_4/O_2 ratios for the OCM reaction experiments is calculated based on the information acquired in this section.

5.3.2.2. Membrane reactor experiments

As extensively discussed, the main aim of this chapter is to experimentally investigate the effect of the integration of a membrane in the reactor to the performance of the OCM process. To do so, experiments with the conventional packed bed were first carried out, which were then compared to both membrane reactor configurations (PBMR1 and PBMR2). The results of this comparison on the basis of CH_4 conversion, O_2 conversion, C_2 selectivity and C_2 yield as a function of the CH_4/O_2 ratio are summarized in Figure 5.8:

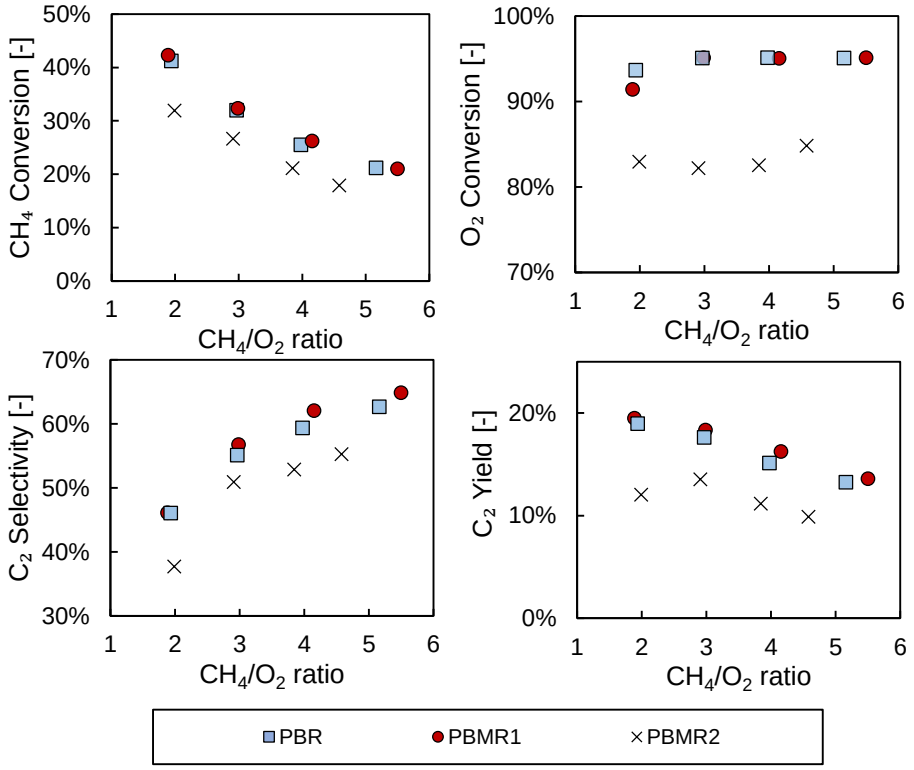

Figure 5.8. CH_4 conversion (top left), O_2 conversion (top right), C_2 selectivity (bottom left) and C_2 yield (bottom right) of the different reactor configurations (PBR, PBMR1 and PBMR2) employed for OCM in experiments carried out at 800 °C, 2 bar and with a CH_4 inlet flow of 105 mL/min.

In general, the obtained performance follows the expected trend as a function of the CH_4/O_2 ratio. The selectivity towards the desired products decreases while both reactants conversions increase when operating at low CH_4/O_2 ratios. At lower CH_4/O_2 ratios, more oxygen is available to react with the methane, thereby increasing its conversion. However, the higher oxygen concentration favors undesired reactions (undesired reactions are enhanced when high oxygen partial pressure is high), resulting in a decrease in the overall C_2 selectivity. In terms of the C_2 yield, an optimum is observed at a CH_4/O_2 ratio of around 2-3, depending on the reactor configuration, balancing the C_2 selectivity and CH_4 conversion.

It is remarkable that with the conventional packed bed reactor relatively good performance was reached. The obtained results are in agreement with literature [1], [23] and they indicate both that the catalyst works properly at the conditions at which the experiments were conducted, and that the operating conditions employed in this study are reasonable and lead to consistent results. Specifically, 20% C_2 yield using a packed bed reactor is already better than many other experimental works reported in literature (see Table 2.1 of this thesis). In addition, this work is carried out with a relatively large packed bed, i.e. using reaction beds longer than 5 cm and with an amount of catalyst that exceeds 5 grams in most of the cases.

The difference in the results of both membrane reactor experiments (PBMR1 vs. PBMR2) was however not expected, as the measured membrane flux was the same for the two configurations. All the studied parameters are worsened when PBMR2 is applied. These results highlight the fact that the way in which air is fed into the retentate side of the system does have a significant influence on the OCM performance. The lower conversion of the reactants in the PBMR2 configuration could indicate that, in this case, the permeation of air is not uniform and is higher towards the end of the catalytic bed, where the O_2 has a much reduced residence time to react with the available CH_4, thereby decreasing both the CH_4 and O_2 conversion. This non-uniform air permeation could also influence the thermal behavior of the reactor, since in these conditions most of the heat will be generated at the end of the bed. The

difference in this thermal behavior could well be the origin of the lower C_2 selectivity achieved with this configuration. To study these effects in more detail, the temperatures have been monitored during all the experiments and these are shown in Figure 5.9:

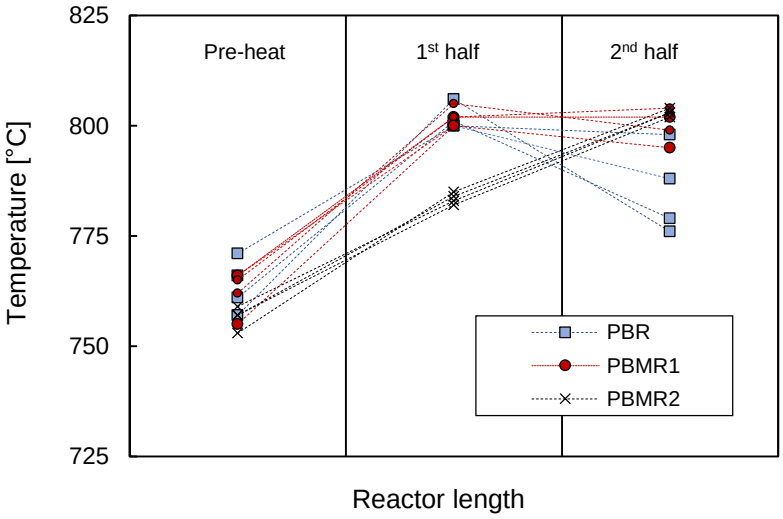

Figure 5.9. Temperature distribution in the reaction bed for all the experiments carried out in this work, divided in PBR, PBMR1 and PBMR2.

The non-uniformity of the air permeation can be easily inferred from this graph, thus corroborating the hypothesis made before. The axial temperature profile in the PBMR2 shows that the bed is heated most towards the end of the bed, most likely because of the heat released during the exothermic OCM reaction. On the other side, PBMR1 shows the highest temperature point in the first half of the bed, where most of the oxygen is expected to permeate. In addition, it can also be noted that the temperature profile of PBMR1 differs to the one of PBR. The temperature profile of PBMR1 is more flattened, indicating that reaction and consequently heat is being distributed more evenly along the bed. On the contrary, for the PBR the temperature profiles are steeper, and most of the reaction occurs at the very beginning of the bed due to the co-feeding of methane and oxygen. Therefore, the differences in these

temperature profiles corroborate the idea of having (at least to some extent) a more even oxygen distribution in the PBMR1 and PBMR2.

However, the differences in temperature profiles and thus the oxygen distribution along the bed, does not seem to correspond to the results shown in Figure 5.8, where there is not a significant difference between PBR and PBMR1. A more homogeneous oxygen distribution (PBMR1) should have led to higher C_2 selectivities, especially at lower CH_4/O_2 ratios. This indicates that the permeation rate was not uniform along the reactor, and this has limited the maximum performance that can be achieved with PBMR1. The non-uniformity of the permeation flux along the reactor is investigated in more detail in the next section.

5.3.2.3. Permeation mechanisms through the porous membrane

From the temperature profiles discussed so far it is clear that when employing the porous membrane reactor, the permeation of oxygen is not homogeneous along the reactor length, despite the fact that it has been demonstrated that the pressure is constant along the retentate side of the system. The pressure along the retentate side could be measured because of the thin tube placed there and indeed a uniform permeation profile was obtained (see Figure 5.7) when no reactions were taking place, independent from where the oxygen was fed. The non-uniformity of the membrane permeation during the reactive experiments, and the lack of differences in observed PBR-PBMR1 performances, is related to the different permeation mechanisms that can occur through a porous membrane. The equation governing the permeation flux through a porous membrane is given by:

$$J_i = \frac{1}{RT}\left(D_{eff}\frac{\partial(x_i P)}{\partial r} + \frac{B_0 x_i P}{\mu}\frac{\partial P}{\partial r}\right) \qquad \textit{Equation 5.2}$$

Where J_i (mol·s^{-1}·m^{-2}) is the permeation flux of component i, D_{eff} (m^2·s^{-1}) the effective diffusion coefficient of the specie i in the membrane and B_o (m^2) the convective permeability constant. D_{eff} was assumed to be 10^{-6} m^{2}s^{-1} and B_o was fitted using the measured permeation data and was determined at 2·10^{-14} m^2. The effective diffusion

coefficient depends on the membrane morphology and combines Knudsen and molecular diffusion into one lumped coefficient, D_{eff}. P refers to the pressure, T to the temperature, R is the universal gas constant, x_i is the fraction of the component I, μ (Pa·s) is the dynamic viscosity and r refers to the radial direction.

This equation, known as extended Fick's law, is a simplification for the description of the permeation through a porous membrane which considers a diffusive term (1st term on the right hand side of the equation), governed by the partial pressure of component i at both sides of the membrane, and a convective term (drift flux), which is driven by the total pressure difference between both sides.

In a work by Aseem et al. it was stated that "In the absence of a sufficient transmembrane pressure gradient, back diffusion of tube side reactant to the feed side can occur" [25]. In addition, it was also shown that the morphology of the membrane should be tailored in order to minimize back diffusion [26]. Because the membranes used in this work have relatively high permeances, the permeate-retentate pressure difference needed to reach the desired flux is generally small, and therefore it could indeed allow for some back diffusion to occur.

In the system of study, there is firstly a convective term with direction retentate to permeate, a diffusive O_2 flux going to the permeate side and a diffusive flux of methane (also products) back-permeating into the membrane. This back-permeation of CH_4 is not just removing one of the OCM reactants from the catalytic bed, but it is also burning part of the oxygen intended to be fed to the reaction side (the retentate side is still at high temperature and combustion will happen if CH_4 and O_2 encounter). Actually, two O_2 molecules are needed to burn (combust) a single CH_4 molecule. On top of it, as soon as the OCM reaction takes place in the permeate side, C_2 and CO_x start to be formed. These molecules could also, at a certain point, back permeate into the retentate side, where they could be oxidized further by the oxygen still present there. Therefore, it can be said that the combustion of back-permeated species amplifies the effect of back diffusion on the oxygen distribution. If the fraction of oxygen in the retentate decreases because of combustions taking place, the oxygen

content of the convective permeation term will also decrease, leading to a non-uniform oxygen permeation profile. All these phenomena are schematically represented in Figure 5.10:

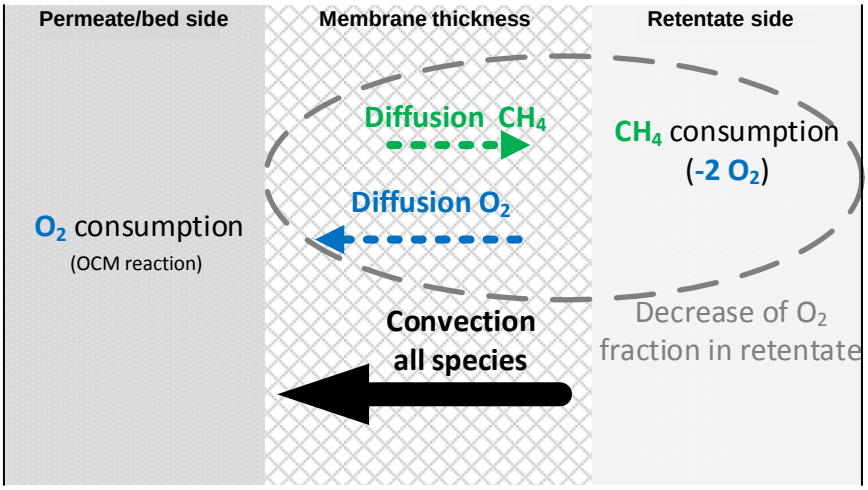

Figure 5.10. Schematic summary of the effect of diffusion and convection on the membrane permeation.

Based on the extended Fick's law equation and all the extra phenomena taking place in the system of study, a 1D model with reactor-membrane exchange of species has been built to study the evolution of the species concentration profiles at both the retentate and permeate side, trying to explain the behavior that was experimentally observed. In Figure 5.11, the normalized hydrocarbon and oxygen fluxes are plotted for three different cases. In the first case, just convection is considered (diffusion going through the membrane is set to zero). Subsequently, in the second case diffusion inside the membrane is described by the extended Fick model, but without combustion at the retentate side. Finally, the third case includes the full extended Fick equation and the instantaneous combustion inside the membrane (retentate side). All the fluxes have been normalized by dividing through the average net permeation flux $\bar{J}_{tot}$.

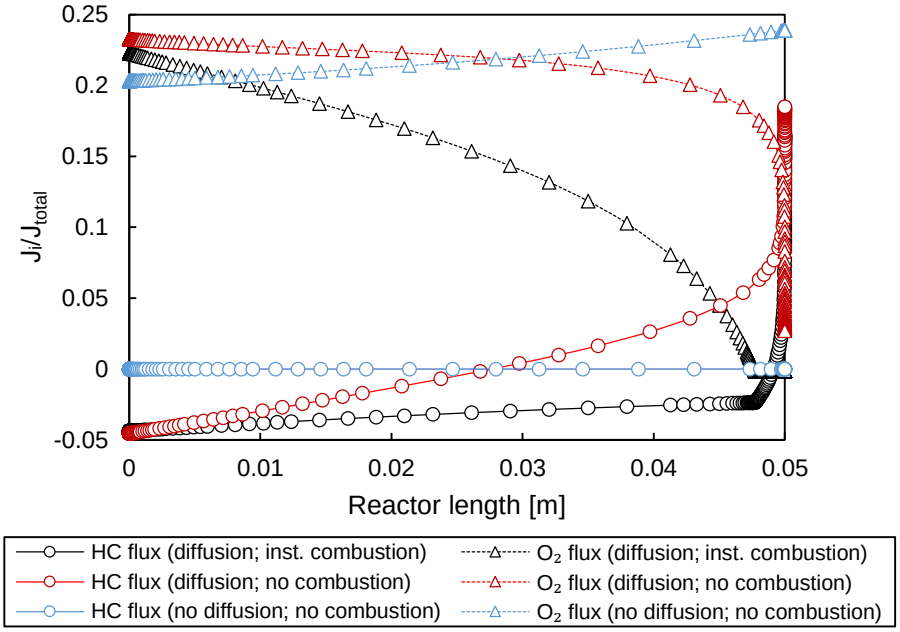

Figure 5.11. Normalized oxygen and hydrocarbons (HC) fluxes obtained from the 1D PBMR model for three cases; just convection (blue), convection and diffusion (red) and convection, diffusion and combustion in the retentate side (red).

It can be clearly seen that the diffusive contribution changes the oxygen flux profile significantly. For the case where just convection is accounted for, the only active mechanism is the convective transport of oxygen from the retentate to the permeate side. This oxygen flux increases when moving along the axial length of the reactor because the pressure drop of the permeate side (where the catalyst is present) increases the driving force (i.e. the pressure difference between the retentate and permeate sides). In the second case, where diffusion is included, the oxygen flux decreases towards the end of the membrane as a result of a decrease in the oxygen fraction throughout the membrane. In parallel, there is also back-permeation of OCM species, both reactants and products, from the permeate to the retentate (this permeate-retentate direction is the cause of the negative value shown in the graph). Lastly, when instantaneous combustion of hydrocarbons is included in the retentate side, the non-uniformity of the oxygen flux is even more pronounced than in the other two cases. As a result, the flux of hydrocarbons into the membrane is increased since

differently to the case in which combustion in the retentate was not considered, the driving force for hydrocarbons diffusion remains due to their instantaneous reaction at the retentate side.

It can be concluded that the observed trends in Figure 5.11 show that back permeation could indeed make the oxygen distribution profiles non-uniform, corresponding to the observations from the experiments. The rather small difference in performance between the PBR and PBMR shown in Figure 5.8 and the altered behavior for the different feeding strategies can qualitatively be explained.

5.3.2.4. Influence of effective diffusion coefficient

In the calculations discussed in the previous section, the contribution of diffusion to the overall flux was estimated and qualitatively described. Therefore, a sensitivity study was performed to provide a more quantitative indication of the diffusional effect. Four different values of the effective diffusion coefficient were tested in the 1D PBMR model with the extended Fick description of the permeation flux. The results of the model are shown in Figure 5.12, where an inlet flow rate of 370 NmL/min (70% N_2 diluted), a bed pressure (permeate side) of 2 bar, a membrane pressure (retentate side) of 2.15 bar and a CH_4/O_2 ratio of 3 was used.

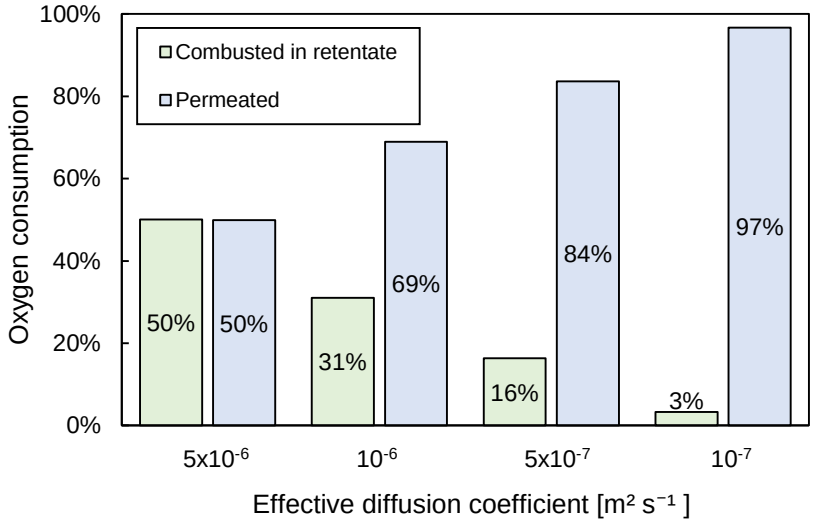

Figure 5.12. Sensitivity of the effective diffusion coefficient on the distribution of oxygen consumption.

It can be clearly seen that the effective diffusion coefficient can play a major role in the system. The higher the effective diffusion coefficient is, the larger the contribution of oxygen consumption in the retentate will be. In the range of 10^{-7} to $2{\cdot}10^{-6}$ m^2s^{-1}, the consumption of oxygen via combustion in the retentate increases from 3% to 50%. This indicates that the diffusion mechanism can significantly hinder the maximum achievable performance in the bed, that is, part of the oxygen which was fed into the retentate side to permeate to the catalytic side (permeate) would instead be consumed in the retentate side because of the diffusive back-permeation of both reactants (CH_4) and products (C_2H_6, C_2H_4) of the OCM. Therefore, since the retentate is free of catalyst and just gas-phase combustion is considered in that compartment, the selectivity of the overall OCM process could be strongly decreased.

Summarizing, the fact that the C_2 selectivity is lower than the theoretical predictions assuming a uniformly distributed feed was found to be partially caused by a maldistribution of the oxygen feed over the bed, and it was argued that the origin of this maldistribution is the back-permeation of hydrocarbon reactants and products. The consequence of back-permeation is that species move from the permeate side to the retentate side, causing a non-uniform oxygen flux profile. In addition, combustion

reactions caused by back-permeation were found to amplify this effect due to the consumption of oxygen in the retentate side. The non-uniformity in the oxygen flux profile causes a lower selectivity towards C_2's and a higher oxygen conversion, which is further aggravated by their influence on the temperature profile.

5.4. Conclusions

The main objective of this work has been an experimental comparison of the performance of packed bed and packed bed membrane reactors for the oxidative coupling of methane (OCM) process over a Mn-Na_2WO_4/SiO_2 catalyst. With theoretical calculations absence of internal and external mass transfer limitations has been verified, demonstrating that the conversion in the catalyst bed is governed by reaction kinetics.

Subsequently, the OCM performance achieved with the conventional packed bed has been compared with two different reactor configurations in which a porous symmetric MgO membrane was integrated. The experiments in the packed bed reactor with co-feed of the reactants have shown the suitability of the used catalyst, reaching C_2 yields of around 20%. Even though improved results were expected with the integration of a membrane in the reactor, no significant improvement was observed in comparison with the packed bed. The differences in temperature profiles along the three reactor configurations employed indicated that the oxygen permeation flux was non-uniform along the reactor.

The cause of the absence of improvements in the performance when using the membrane reactor has been found by investigating the transport mechanism of the gas through the porous membranes employed for this work. The relatively large pore size of these membranes has resulted in a significant effect of diffusive back-permeation of hydrocarbon species to the retentate side, there combusting part of the oxygen which should have been permeated to the catalyst bed, where the OCM reaction takes place. These results highlight the crucial importance of carefully tuning the effective diffusion coefficient, depending mainly on the morphology of the porous

membrane selected, in order to avoid back-permeation hindering the benefits of the membrane reactor configuration. Membranes with a much smaller pore size, or the use of asymmetric membranes, which commonly have a small layer with a very small pore size, could help decreasing the effective diffusion coefficient, and thereby to minimize the effect of back-permeation and consequently attain higher C_2 yields. Alternatively, dense membranes can be integrated, provided that sealing issues can be overcome and leakages or pinholes can be avoided.

5.5. Bibliography

[1] A. Cruellas, T. Melchiori, F. Gallucci, and M. van Sint Annaland, "Oxidative Coupling of Methane: A Comparison of Different Reactor Configurations," *Energy Technology*, vol. 0, no. 0, p. 1900148, May 2019.

[2] Z. Cheng, D. S. Baser, S. G. Nadgouda, L. Qin, J. A. Fan, and L.-S. Fan, "C2 Selectivity Enhancement in Chemical Looping Oxidative Coupling of Methane over a Mg–Mn Composite Oxygen Carrier by Li-Doping-Induced Oxygen Vacancies," *ACS Energy Letters*, vol. 3, no. 7, pp. 1730–1736, Jul. 2018.

[3] E. Y. Chung, W. K. Wang, S. G. Nadgouda, D. S. Baser, J. A. Sofranko, and L.-S. Fan, "Catalytic Oxygen Carriers and Process Systems for Oxidative Coupling of Methane Using the Chemical Looping Technology," *Industrial & Engineering Chemistry Research*, vol. 55, no. 50, pp. 12750–12764, Dec. 2016.

[4] V. Fleischer, P. Littlewood, S. Parishan, and R. Schomäcker, "Chemical looping as reactor concept for the oxidative coupling of methane over a Na2WO4/Mn/SiO2 catalyst," *Chemical Engineering Journal*, vol. 306, pp. 646–654, Dec. 2016.

[5] S. Parishan, P. Littlewood, A. Arinchtein, V. Fleischer, and R. Schomäcker, "Chemical looping as a reactor concept for the oxidative coupling of methane over the MnxOy-Na2WO4/SiO2 catalyst, benefits and limitation," *Catalysis Today*, vol. 311, pp. 40–47, 2018.

[6] V. Fleischer *et al.*, "Investigation of the role of the Na2WO4/Mn/SiO2 catalyst composition in the oxidative coupling of methane by chemical looping experiments," *Journal of Catalysis*, vol. 360, pp. 102–117, 2018.

[7] J. Santamaría, M. Menéndez, J. A. Peña, and J. I. Barahona, "Methane oxidative coupling in fixed bed catalytic reactors with a distributed oxygen feed. A simulation study," *Catalysis Today*, vol. 13, no. 2, pp. 353–360, 1992.

[8] M. Baerns and W. Hinsen, "Process for the production of ethane and/or ethylene from methane," US Patent 4608449 A, 1986.

[9] A. Arratibel Plazaola *et al.*, "Mixed Ionic-Electronic Conducting Membranes (MIEC) for Their Application in Membrane Reactors: A Review," *Processes* , vol. 7, no. 3. 2019.

[10] D. Lafarga, J. Santamaria, and M. Menéndez, "Methane oxidative coupling using porous ceramic membrane reactors—I. reactor development," *Chemical Engineering Science*, vol. 49, no. 12, pp. 2005–2013, Jun. 1994.

[11] X. Tan, Z. Pang, Z. Gu, and S. Liu, "Catalytic perovskite hollow fibre membrane reactors for methane oxidative coupling," *Journal of Membrane Science*, vol. 302, no. 1–2, pp. 109–114, Sep. 2007.

[12] Y. Lu, A. G. Dixon, W. R. Moser, Y. Hua, and U. Balachandran, "Oxygen-permeable dense membrane reactor for the oxidative coupling of methane," *Journal of Membrane Science*, vol. 170, pp. 27–34, 2000.

[13] O. Czuprat, T. Schiestel, and H. Voss, "Oxidative Coupling of Methane in a BCFZ Perovskite Hollow Fiber Membrane Reactor," *Industrial and Engineering Chemistry Research*, vol. 49, pp. 10230–10236, 2010.

[14] H. Wang, Y. Cong, and W. Yang, "Oxidative coupling of methane in Bao.5Sro.5Coo.8Feo.2O3–δ tubular membrane reactors," *Catalysis Today*, vol. 104, no. 2–4, pp. 160–167, Jun. 2005.

[15] L. Olivier, S. Haag, C. Mirodatos, and A. C. van Veen, "Oxidative coupling of methane using catalyst modified dense perovskite membrane reactors," *Catalysis Today*, vol. 142, no. 1–2, pp. 34–41, Apr. 2009.

[16] F. T. Akin and Y. S. Lin, "Controlled Oxidative Coupling of Methane by Ionic Conducting Ceramic Membrane," *Catalysis Letters*, vol. 78, no. 1, pp. 239–242, 2002.

[17] S. Bhatia, C. Y. Thien, and A. R. Mohamed, "Oxidative coupling of methane (OCM) in a catalytic membrane reactor and comparison of its performance with other catalytic reactors," *Chemical Engineering Journal*, vol. 148, no. 2–3, pp. 525–532, 2009.

[18] N. H. Othman, Z. Wu, and K. Li, "An oxygen permeable membrane microreactor with an in-situ deposited Bi1.5Y0.3Sm0.2O3–δ catalyst for oxidative coupling of methane," *Journal of Membrane Science*, vol. 488, pp. 182–193, Aug. 2015.

[19] H. Chen *et al.*, "Reactive air brazing for sealing mixed ionic electronic conducting hollow fibre membranes," *Acta Materialia*, vol. 88, pp. 74–82, 2015.

[20] N. Wakao and T. Funazkri, "Effect of fluid dispersion coefficients on particle-to-fluid mass transfer coefficients in packed beds," *Chemical Engineering Science*, vol. 33, pp. 1375–1384, 1978.

[21] W. Appamana, S. Charojrochkul, S. Assabumrungrat, and W. Wiyaratn, "Synthesis of Na2WO4-Mn Supported YSZ as a Potential Anode Catalyst for Oxidative Coupling of Methane in SOFC Reactor," *Engineering Journal*, vol. 19, no. 1, pp. 13–20, Jan. 2015.

[22] T. P. Tiemersma, M. J. Tuinier, F. Gallucci, J. a. M. Kuipers, and M. V. S. Annaland, "A kinetics study for the oxidative coupling of methane on a Mn/Na2WO4/SiO2 catalyst," *Applied Catalysis A: General*, vol. 433–434, pp. 96–108, Aug. 2012.

[23] S. Jašo, H. R. Godini, H. Arellano-Garcia, M. Omidkhah, and G. Wozny, "Analysis of attainable reactor performance for the oxidative methane coupling process," *Chemical Engineering Science*, vol. 65, no. 24, pp. 6341–6352, 2010.

[24] A. Cruellas, T. Melchiori, F. Gallucci, and M. van Sint Annaland, "Advanced

reactor concepts for oxidative coupling of methane," *Catalysis Reviews*, vol. 59, no. 03, pp. 234–294, 2018.

[25] A. Aseem and M. P. Harold, "C2 yield enhancement during oxidative coupling of methane in a nonpermselective porous membrane reactor," *Chemical Engineering Science*, vol. 175, no. Supplement C, pp. 199–207, 2018.

[26] V. Papavassiliou, C. Lee, J. Nestlerode, and M. P. Harold, "Pneumatically Controlled Transport and Reaction in Inorganic Membranes," *Industrial and Engineering Chemistry Research*, vol. 36, no. 11, pp. 4954–4964, 1997.

Chapter

6

Techno-economic evaluation of the conventional OCM packed bed reactor concept

Abstract

To evaluate the economic feasibility of the OCM packed bed reactor technology, the ethylene price has been taken as the main indicator and has been estimated under different conditions. An entire OCM industrial-scale plant, including all the units required for its proper functioning, has been simulated in Aspen Plus. The performance of the OCM reactor and its impact on the overall OCM plant have been quantified from a techno-economic point of view. It has been shown that a very high ethylene price (above 1500 €/ton C_2H_4) is estimated with the current OCM technology, with a single-pass C_2 reactor yield of around 15%. With the simulation of the entire plant, it has also been demonstrated that a single-pass C_2 yield of at least 25-30% is required to obtain an ethylene cost below 1000 €/ton C_2H_4. Finally, it has been shown that, based on the forecast of costs for natural gas and naphtha, the gap between the ethylene price obtained with conventional technologies and the one obtained with the current OCM state-of-the-art is expected to progressively become smaller, forecasting OCM to be competitive with traditional technologies in around 20 years, provided that the conditions remain the same.

6.1. Introduction

Most of the research carried out in the OCM field has been focused on improving the C_2 yield in order to make this process feasible at larger scales. Specifically, big efforts have been made on developing novel reactor configurations (Chapters 2, 3 and 5), such as membrane reactors [1], and more suitable OCM catalysts (Chapter 4), meaning a better compromise between its selectivity, activity and stability [2]. These efforts are based on the fact that model calculations have shown promising results [3]–[5] demonstrating that a proper optimization of the reactor design and operating conditions can lead to OCM reactor yields well above this 30% target (which is generally believed in the OCM community to be the minimum to make the process economically interesting). Nevertheless, the OCM experimental work reported in the literature over the last years has not resulted in the significant improvements that are necessary to make the process economically viable. Just few of these experimental works, and with conditions not feasible at industrial scales, have reached results near the values obtained in the simulations of modelling works [6]–[8].

Even though in several works a 25-35% C_2 is mentioned as the yield target, the specific value to make the OCM industrially viable is not clear. Some authors, however, have suggested in literature values for the C_2 reactor yield necessary to make the process competitive with the conventional technologies. Particularly, Roos et al. [9] in 1987 and Lange et al. [10] in 1997 proposed 24% as the minimum C_2 yield to make OCM a potential alternative to other C_2H_4 production technologies. More recently, Parishan et al. [11] and Jaso et al. [12] claimed in their works that a 30% C_2 yield is necessary to make OCM competitive, although they do not justify the value neither with a reference nor a calculation. In addition, Spallina et al. [13] compared, from an economical point of view, different OCM scenarios with the benchmark ethylene production technology (NSC). They found a gap of at least 350 €/ton C_2H_4 between both processes in the most OCM optimistic case (1209 versus 834 €/ton C_2H_4).

Therefore, it seems that there is a lack of up-to-date information regarding the overall OCM performance required to consider OCM as a feasible alternative for C_2H_4 production. Despite the efforts made in the last decades for a maximization of the C_2 yield in a single OCM reactor, the reactor conditions which would lead to a minimization of the ethylene price via the OCM have not yet been defined. A clear definition of this target value together with the selection of the optimal reactor conditions would contribute to place the current state-of-the-art OCM technology within the global ethylene production framework.

Thereby, this chapter aims at providing a detailed forecast of the potential of the conventional OCM technology, focusing on the trend of the prices of different feedstocks used for the production of ethylene. In other words, the objective is to identify (as a function of time) the yield needed in the reactor in order to produce ethylene with OCM at a cost similar to benchmark technologies. This also allows to identify if and when the state-of-the-art OCM technology would be preferred over other technologies as a consequence of the variability in feedstock prices. To this end, a techno-economic analysis of the OCM process has been carried out, identifying the optimal reactor conditions that will result in the lowest ethylene price. This cost is then compared to the benchmark case (in Europe, the naphtha steam cracking), and the yield required for the OCM technology to fill the gap between the different technologies will be determined. Finally, and based on the forecasts for oil and natural gas prices, the price prediction for ethylene using different technologies will be analyzed for the coming decades.

In the coming sections of this chapter, the selected methodology, the OCM reactor model and the overall OCM process technology used will be described. Afterward, the results obtained at different operating conditions and process yields, as well as forecasted scenarios, will be evaluated and discussed. Finally, the main outcomes will be summarized and guidelines on how to increase process yields will be provided.

6.2. Methodology

Despite of the fact that other technologies are nowadays emerging, naphtha steam cracking has been historically the most applied technology for ethylene production (at least in Europe). That is the main reason why it has been considered as the benchmark technology for this work. This benchmark technology has been compared to the OCM process, whose process scheme plant has been designed and will be explained in the following sections. The methodology here presented can be extended to any other ethylene production technology, but this is out of the scope of the present study.

The core of the process will be the OCM reactor, which has been modelled by means of an in-house developed 1D plug-flow model. From this OCM reactor, the main indicators employed to quantitatively evaluate the performance are the ones introduced in equations 6.1-6.3:

CH_4 conversion

$$X_{CH_4} = \frac{F_{in_{CH_4}} - F_{out_{CH_4}}}{F_{in_{CH_4}}} \qquad \textit{Equation 6.1}$$

C_2 selectivity

$$S_{C_2} = 2 * \frac{\left(F_{out_{C_2H_4}} + F_{out_{C_2H_6}} - F_{in_{C_2H_4}} - F_{in_{C_2H_6}}\right)}{F_{in_{CH_4}} - F_{out_{CH_4}}} \qquad \textit{Equation 6.2}$$

C_2 yield

$$Y_{C_2} = X_{CH_4} * S_{C_2} \qquad \textit{Equation 6.3}$$

In order to integrate the OCM reactor model in the overall process, a set of assumptions are required to solve the mass and energy balances of all the process units. To do that, the assumptions used by Spallina et al. [13] in their work have been considered.

Similarly, a techno-economic model has been integrated in the OCM process to investigate how the different parameters affect the distribution of costs of the different units and the leveled production cost of ethylene. This ethylene cost has been calculated in the model as the sum of both capital (CAPEX) and operational (OPEX) costs, as reported in Equation 6.4.

$$Cost\ of\ ethylene\ \left[\frac{€}{ton}\right] = \frac{(OPEX_{variable} + CAPEX_{C_2H_4} + C_{O\&M,fixed})_y}{\left(\dot{m}_{C_2H_4}\right)_y} \qquad \textit{Equation 6.4}$$

Where $\left(\dot{m}_{C_2H_4}\right)_y$ is the flow rate of ethylene produced per year (ton$_{C_2H_4}$/year) and $C_{O\&M,fixed}$ are the yearly operating and maintenance fixed costs.

The equations used for the CAPEX calculations are summarized in Table 6.1. The costs of all the units considered in the OCM plant, which will be used later to calculate the bare erected costs, have been estimated based on the scale-up factor correlation, shown in Equation 6.5:

$$C = nC_0 * \left(\frac{S}{nS_0}\right)^f \qquad \textit{Equation 6.5}$$

where C_0 is the cost of the component based on literature data, S_0 is the capacity of the scaling parameter, which is also based on literature data, S is the capacity that has to be scaled, n is the number of units to be considered and f is the scaling factor. The prices and scaling parameters of all the units are taken from the work by Spallina et al. [13].

Table 6.1. Capital (CAPEX) costs calculations from NETL [14].

Capital costs (CAPEX)	
Plant Components	Cost (M€)
Component A	A
Component B	B
Component C	C
Component D	D
BEC (Bare Erected Costs)	A+B+C+D
Direct costs as percentage of BEC	
Total Installation Cost (TIC)	80% of BEC
Total Plant Costs (TPC)	BEC + TIC
Indirect Costs (IC)	14% of TPC
Engineering Procurement and Construction (EPC)	TPC + IC
Contingency	10% of EPC

Owner's Cost	5% of EPC
Total contingencies and owner's costs (TCOC)	15% of EPC
Total Overnight Costs (TOC)	EPC + TCOC
CCF (Capital charge factor)	0.1
$CAPEX_{C_2H_4}$ [M€/year]	TOC*CCF

Differently, the operational expenses (OPEX) can be differentiated between the fixed, which mostly refer to labor costs, maintenance and insurance, and the variable costs, which include the feedstock, electricity, etc. Thus, the OPEX costs of the plant have been calculated as described in Equation 6.6:

$$OPEX = \left(\sum OPEX_{variable} + \sum OPEX_{O\&M}\right) = (OPEX_{feedstock} + OPEX_{el} + \sum OPEX_{O\&M} + OPEX_{catalyst}) \left[\frac{M€}{y}\right] \quad \textit{Equation 6.6}$$

And:

$$OPEX_{feedstock} = C_i * \dot{m}_i * 3600 * h_{year} * 10^{-6} \left[\frac{M€}{y}\right] \quad \textit{Equation 6.7}$$

$$OPEX_{electricity} = D_i * \dot{m}_i * 3600 * h_{year} * 10^{-6} \left[\frac{M€}{y}\right] \quad \textit{Equation 6.8}$$

Where C_i is the specific cost of natural gas per kilogram of ethylene produced (€/kg), D_i is the specific cost of electricity per kilogram of ethylene produced (€/kg), m_i is the flow rate of ethylene produced in the plant (kg/s) and h_{year} are the number of hours per year in which the plant is assumed to be running (7884 effective hours per year are considered).

For the CAPEX and OPEX calculations, some assumptions regarding the operation and maintenance (O&M) costs and the price fixed for consumables are required. The assumed values are summarized in Table 6.2:

Table 6.2. Assumptions for the O&M costs calculations and consumables.

O&M Fixed		
Labor	M€/year	1.5
Maintenance	% TOC	2.5
Insurance	% TOC	2.0
O&M Variable		
Catalyst	€/kg	50.0
Diluent	€/kg	9.45
Catalyst Replacement	Years	5
Diluent Replacement	Years	5
Plant Lifetime	Years	25
Consumables		
Cooling Water	€/ton	0.35
Natural Gas price (Europe)	€/GJ_{LHV}	5
Electricity	€/MWh	85
CO_2	€/ton_{CO_2} emitted	0

In addition, for all these calculations the following two assumptions have been made:

- Europe has been considered to be the scenario for all the calculations. That is, the assumptions and prices of the consumables have been taken from the current European market. Furthermore, this selection is based on the fact that the NSC is the typical process for ethylene production in Europe.
- The OCM plant has been designed to produce 31.9 kg/s of ethylene, which is the equivalent to a C_2H_4 production of 1 million-ton/year.

6.3. OCM Reactor model

The reactor is one of the most important units of the OCM technology since small variations in the reactor yield will largely impact the downstream separation

processes. Therefore, before building up a complete process scheme, it is of high relevance to accurately describe and simulate the OCM reaction network. Because of that, a 1D reactor model has been developed using a set of assumptions within the state-of-the-art technology. Subsequently, this reactor model is fully integrated in the overall OCM process scheme using the process design software Aspen Plus.

6.3.1. Assumptions

The reactor has been designed to fulfill the necessities of an industrial scale OCM process. To do so, the main reactor parameters have been defined and fixed and are listed in Table 6.3:

Table 6.3. Characteristics assumed for the simulation of the 1D OCM reactor model.

OCM Reactor characteristics		
Diameter [m]	3	
Inlet gas velocity [m/s]	1	
Bed porosity [-]	0.5	
Inlet pressure [bar]	10	
Pressure drop in the reactor [bar]	1	
Catalyst type	La_2O_3/CaO	[15]
Catalyst density [kg particle/m^3 reactor]	3600	[15]
Active weight fraction	0.27	[15]
Catalyst dilution $[\frac{Catalyst\ weight\ [kg]}{Total\ solid\ weight\ [kg]}]$	0.01	
Maximum axial reactor length [m]	15	
Cooling tubes diameter [m]	$12.7 \cdot 10^{-3}$	[16]
Cooling tubes material	Stainless steel 316	[16]

The OCM reactor diameter has been selected based on reactor standards for industrial scale chemical plants. Similarly, the values for inlet gas velocity, bed porosity and total pressure chosen are also well-accepted when working with industrial scale packed bed reactors. Additionally, the defined pressure drop is consistent with the operation of large-scale packed beds. Regarding the OCM catalyst, different alternatives can be considered as presented in several OCM reviews available in the open literature [12],

[17]–[20]. Since their characteristics vary significantly, the selection of the catalyst can strongly influence the reactor performance (see Chapter 4). The knowledge acquired over the years on the La_2O_3/CaO catalyst [21], [22], together with the fact that its kinetics is the most reliable and comprehensive (as discussed in section 4.4 of this thesis, the in-house kinetics developed in Chapter 4 is not sufficiently completed to be applied in this reactor model), has been the main reason for its selection to simulate the OCM reactor. Specifically, the data provided by Stansch et al. [15] in their work has been used (see Table 3.1 and Table 3.2 of this thesis). The system is assumed to be kinetically limited, that is, it has been assumed that there are not mass and heat transfer limitations (see section 5.3.1).

In order to achieve a better heat management inside the OCM reactor, the catalyst should be diluted with inert particles to slow down the reaction rate. This is a consequence of the highly exothermic reactions occurring inside the catalyst bed, and overall results in the need of longer reactors to fully convert the oxygen introduced in the system. An accurate temperature control, derived from a proper heat management, is crucial to keep a high C_2 selectivity. A deviation from the optimal temperature, most likely caused by hotspots, would lead to a dramatic loss of C_2 selectivity, hampering the desired outcome of the reaction.

The 1D reactor model developed here assumes isothermal conditions, where the cooling needed to remove the heat generated by the reactions is provided by evaporating high pressure water inside cooling tubes passing through the catalytic bed. The number of cooling tubes is calculated by comparing the total heat released during the reaction and the heat that a single tube can take. Subsequently, by fixing the inlet gas velocity of the reactants in a single reactor and the area of a single reactor (cross-sectional reactor area minus area occupied by the cooling tubes), the number of parallel reactors required to process the specified amount of reactants needed to satisfy the C_2H_4 production target can be calculated. Additionally, the number of cooling tubes required is properly considered in the techno-economic analysis when calculating the capital costs of the process.

The last assumption concerns the total length of the reactor. A reactor length is selected such that at the end of the reactor one of the reactants is fully consumed. However, the maximum reactor length has been limited to 15 meters to avoid excessively long reactors that may be not industrially attractive. Hence, a different reactor length is obtained for each set of operating conditions investigated.

6.3.2. Results

After the definition of some reactor parameters, a sensitivity analysis has been carried out on the OCM operating conditions. In particular, the operating temperature and CH_4/O_2 ratio. An overview of the yields obtained from this sensitivity analysis is shown in Figure 6.1:

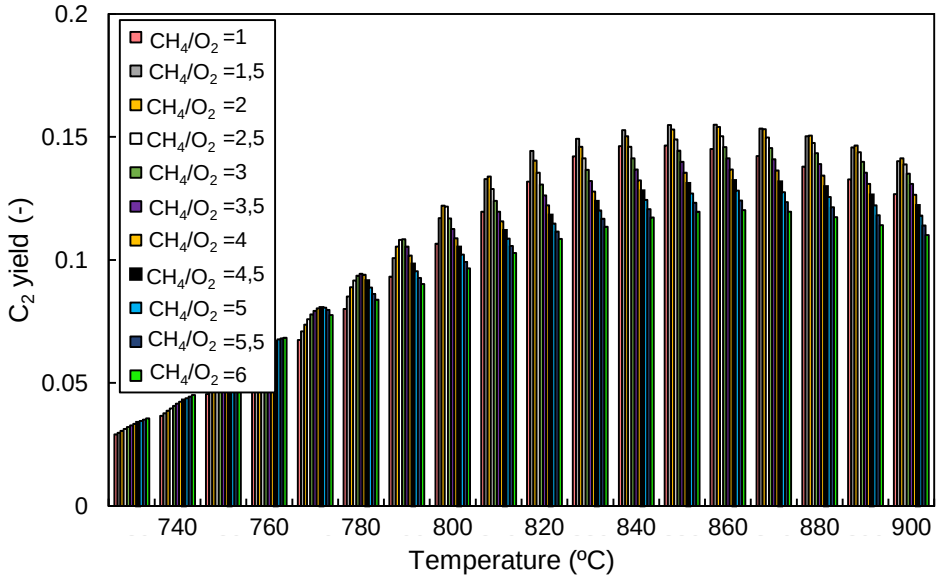

Figure 6.1. C_2 yield obtained in the OCM reactor for different temperatures and CH_4/O_2 ratios.

As can be observed in Figure 6.1, the optimal temperature for the OCM reactor is in between 830 and 870 °C. Lower temperatures do not activate the methane molecules sufficiently, hence limiting the CH_4 conversion and consequently the C_2 yield. At higher temperatures, the CH_4 combustion reactions prevail, thus hampering the achievement of a high selectivity towards the desired products. When giving a closer

look at the effect of the CH_4/O_2 ratio, a compromise should be found. Feeding larger amounts of oxygen results in a higher CH_4 conversion at the expense of a lower C_2 selectivity. On the other hand, high CH_4/O_2 ratios yield high C_2 selectivities, although acceptable CH_4 conversions cannot be achieved. With all this, the best yield obtained is 15.5 %, corresponding to a CH_4 conversion of 51.1 % and a C_2 selectivity of 30.3 %. This maximum yield is reached at 860 °C with a CH_4/O_2 ratio of 1.5. These model results are consistent with many experimental works reported in the literature for the same packed bed reactor configuration and the same catalyst as the one simulated in this study [1], [15], [23].

However, the conditions giving the highest yields do not automatically imply a minimization of the cost of the plant. As can be seen in Figure 6.1, other operating conditions give a yield close to the optimal one, which could significantly influence the cost of the ethylene produced when integrated in the overall process.

To illustrate this statement, Figure 6.2 compares the C_2 yield obtained from all the simulations presented in Figure 6.1 with the required reactor length for each case.

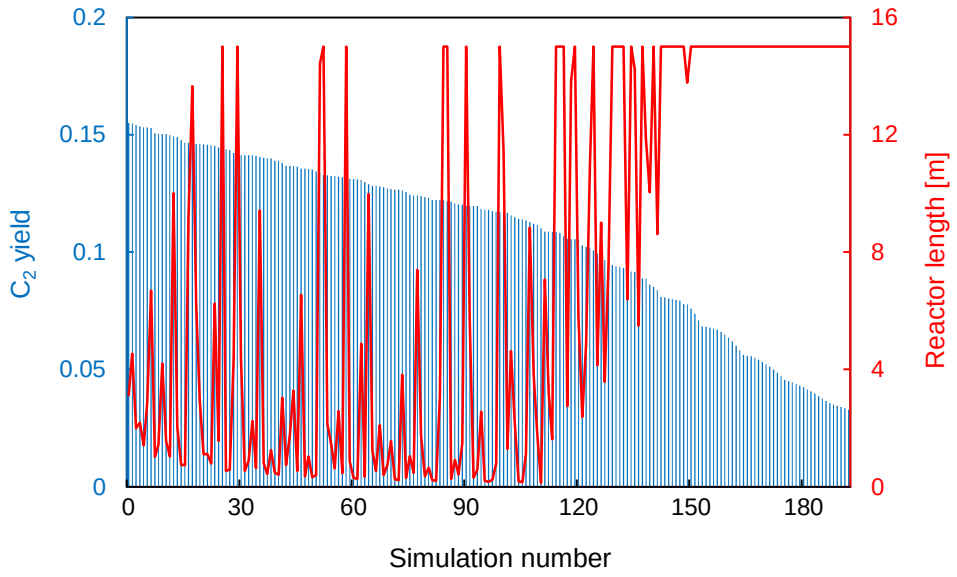

Figure 6.2. C_2 yield and reactor length obtained in each of the OCM reactor simulation performed.

As depicted in Figure 6.2, similar yields can be reached with very different reactor lengths. This implies a large variation in capital costs for similar efficiencies, as bigger amounts of catalyst and larger reactor volumes will be required for the cases that employ a long OCM reactor. Furthermore, the need for a very energy intensive air separation unit (ASU) to produce pure oxygen for the OCM process should also be considered in the overall process and can affect considerably the final ethylene cost. In particular, the lower the CH_4/O_2 ratio, the more oxygen needs to be supplied to the reactor, resulting in higher energy demands, and consequently in an increase in the total cost of the OCM plant.

Summarizing, a maximization of the OCM reactor performance will not directly imply a minimization of the total plant costs, as upstream and downstream processes have a large influence on the cost of ethylene. Therefore, all these variables should be properly accounted for in the optimization of the C_2 yield, as they can play a very important role in the economics of the process. In the next section, a detailed description of the overall OCM process and the economic evaluation of all the cases simulated at a reactor level will be highlighted. This preliminary economic evaluation will help defining optimized reactor parameters that minimize the ethylene production costs.

6.4. OCM Process

The developed reactor model has been integrated and linked with the OCM plant designed in Aspen Plus. This integration allows the optimization of the OCM technology by paying special attention to the influence of the reactor variables on the process economics.

6.4.1. Plant description and assumptions

The OCM plant used in this chapter has been previously described by Spallina et al. [13]. In Figure 6.3, a scheme of the simulated plant is given.

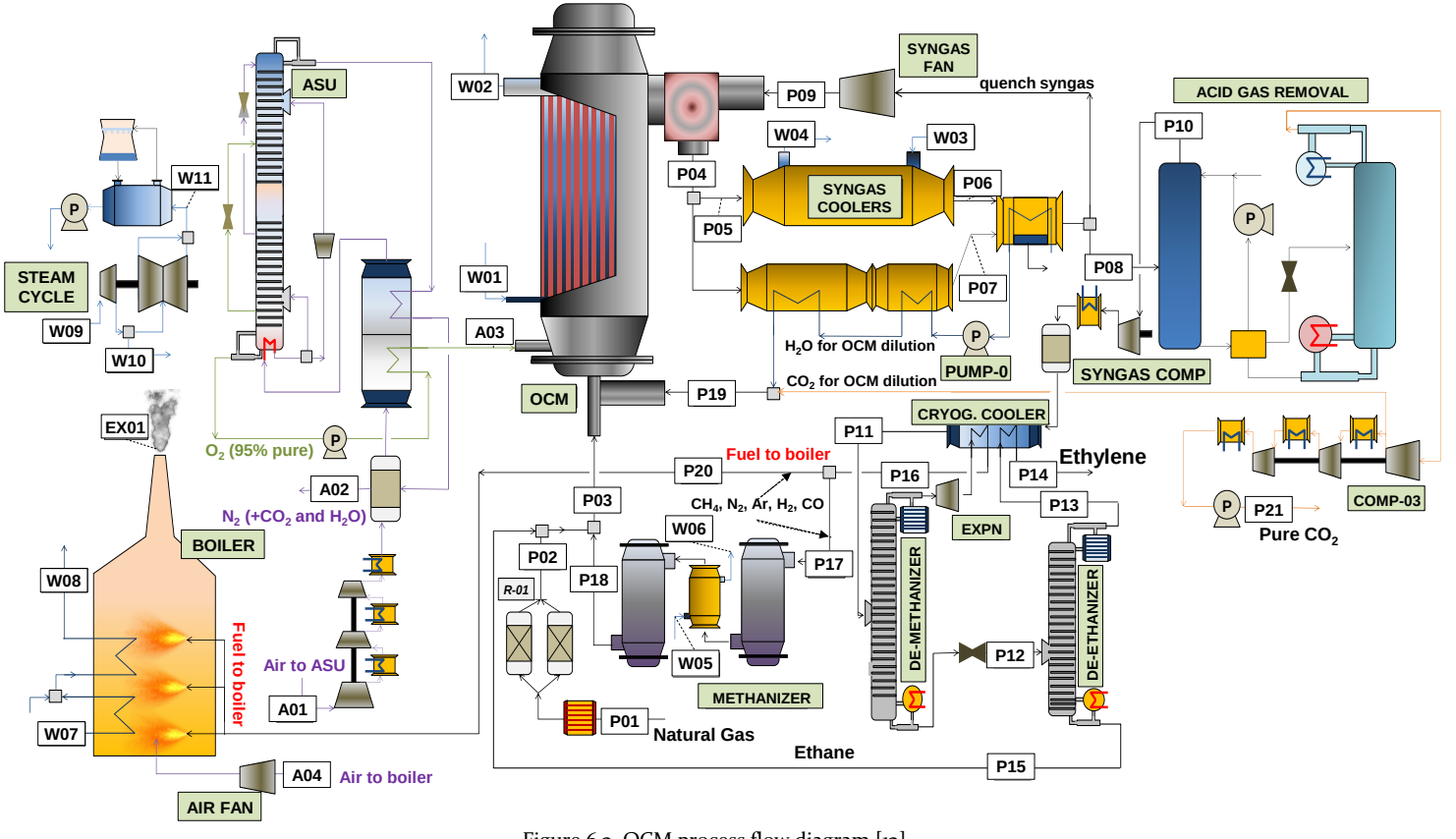

Figure 6.3. OCM process flow diagram [13].

In this technology, oxygen is first purified in a cryogenic air separation unit (ASU). This oxygen is mixed afterwards with desulfurized natural gas, and both are fed to the reactor, where the very exothermic OCM reactions take place and where the desired products of the plant are formed. High-pressure water is evaporated inside the cooling tubes integrated in the reactor to compensate for the heat produced during the reaction, hence assuring isothermal operation. To restrict the consecutive gas-phase reactions, in which the desired products can further react leading to a significant decrease of the reactor performance, the outlet of the reactor is rapidly quenched with a dry recycled stream and further cooled down in a series of heat exchangers, where high-pressure steam is also produced. Subsequently, the steam in the products stream is condensed and separated in a flash unit, and the CO_2 is removed from the cooled gas stream by means of an amine-based acid gas removal unit. Afterward, the gas is pressurized and enters the cryogenic distillation units, where first the light gases are separated from the C_2's in the de-methanizer distillation column. Thereafter, the ethane and the ethylene are separated in the de-ethanizer, which works at milder conditions compared to the de-methanizer. To reach these cryogenic temperatures, a refrigeration cycle is required. The pure ethylene is obtained from the top of the de-ethanizer, while the bottom stream, which contains mostly ethane, is recirculated to the reactor where it can be further converted into ethylene.

The light gases coming from the top of the de-methanizer, containing mainly unreacted CH_4, CO and H_2, are sent to a reactor for methanation in which the CO and H_2 are converted back to CH_4. The outlet of this unit, comprised mostly of methane, is then divided; part of the flow is directed to a boiler, where methane is burnt to provide heat and high pressure steam to the plant, while the rest of the stream is recirculated to the OCM reactor to maximize the conversion of CH_4. This syngas stream could be used in different ways, such as for a FTS process, for H_2 production or for electricity production. The optimization of the processing of this stream has been left out from this study.

The main assumptions and the methods used for the calculation of the different units are adopted from the ones given in the work of Spallina et al. [13]. The size of the plant is also the same as the one taken from Spallina et al. [13], having an production capacity of 31.9 kg C_2H_4/s (equivalent to 1 million tons of ethylene per year) with a purity of 99.5%, allowing also a direct comparison with literature results.

6.4.2. Results

6.4.2.1. Optimization of OCM process

Among the different approaches that can be taken (energy consumption minimization, CO_2 emissions minimization etc.), the price of ethylene has been selected as the target to be minimized during the sensitivity analysis of the plant. The same parameters as in the previous section, that is, reactor temperature and CH_4/O_2 ratio, have been varied for this optimization. The results of the simulations are presented in Figure 6.4:

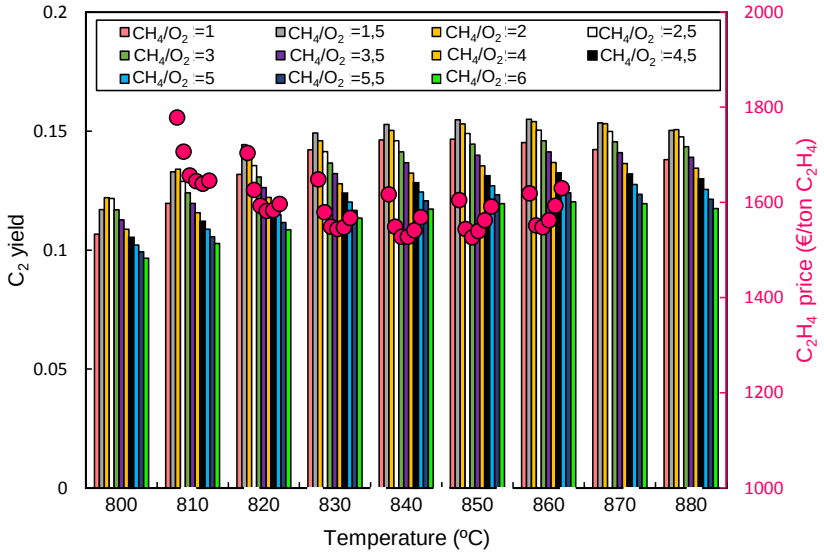

Figure 6.4. OCM reactor yield and overall C_2H_4 cost for the results of the simulations carried out when varying temperature (from 800 to 880 °C) and CH_4/O_2 ratio (from 1 to 6).

As anticipated in the previous section, the results of this analysis reveal that the conditions that yield the cheapest ethylene are not necessarily the ones that correspond to the highest reactor yield. Actually, the lowest price (1541 €/ton C_2H_4) is obtained at 850 °C with a CH_4/O_2 ratio of 3, while the best reactor conditions are achieved at 860 °C and a CH_4/O_2 ratio of 1.5 (C_2 yield of 15.5%). In more detail, the cost of a single reactor, which mainly relates to the cost of the reactor vessel and the cooling tubes, is affected by the reactor operating conditions. However, different reactor conditions lead to a variation in the composition of the reactor outlet stream, which can afterwards influence the size and consequently the cost of all the separation train. Thus, a compromise between the costs of all these units and not just a reactor optimization needs to be found to optimize the ethylene price.

To study in more detail the origin and the behavior of these costs, a disaggregation of the unit costs is reported in Figure 6.5.

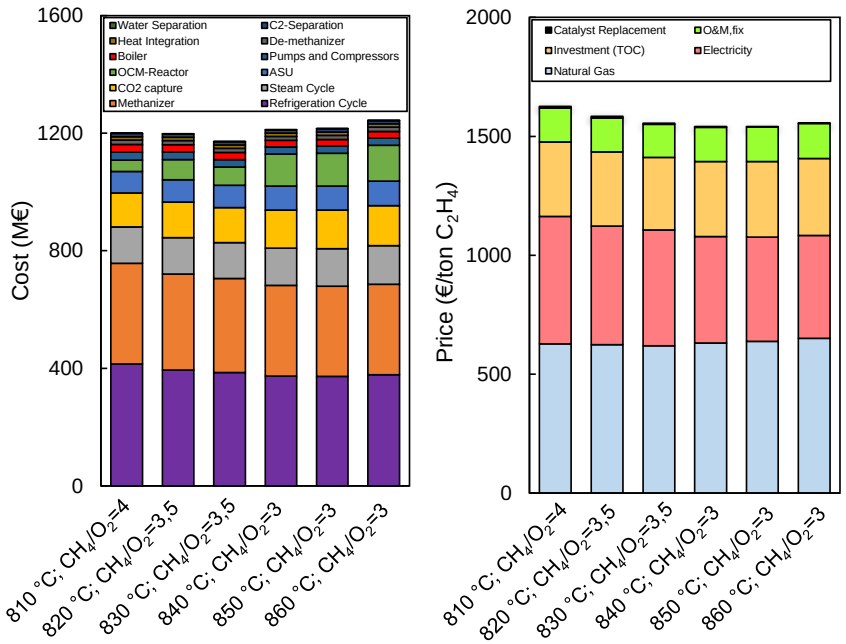

Figure 6.5. Detailed cost of the units of an OCM plant, CAPEX, (left) and disaggregated ethylene cost, CAPEX and OPEX, (right) for the minimum C_2H_4 price case at different temperatures.

In the left part of the graph, the CAPEX cost is detailed. Because of the energy intensive units that are required to separate products like oxygen from nitrogen, C_2 from methane or ethylene from ethane (cryogenic temperatures are required in these three examples), the biggest contribution to the CAPEX is given by the refrigeration cycle, which includes all the pumps, compressors, condensers and evaporators that need to be integrated to assure a proper functioning of the mentioned units. This unit is barely affected by the changes in temperature. However, the methanizer, the second most important contributor to the CAPEX, is more sensitive to temperature. When employing lower temperature in the reactor, its cost increases significantly. This effect can be caused by the fact that at lower temperatures the selectivity of the reactor decreases (methane coupling is considered not to be sufficiently activated at low temperatures with the reactor kinetics implemented for these simulations), having more undesired products like CO which then need to be processed in the methanizer to be converted back to methane. The other remarkable variation in the CAPEX with temperature relates to the OCM reactor itself. Its cost increases when having elevated temperatures because at such conditions more reaction, and consequently more heat, is produced. To overcome this heat production and to keep a controlled and optimal temperature in the reactor, a larger cooling area is required, hence increasing the number of the cooling tubes and consequently the overall reactor cost. In any case, the overall influence of the CAPEX on the final ethylene price is much lower than the OPEX, where the costs of the raw material (natural gas) and the electricity required for the process are the main contributors. The cost of natural gas, the factor which weights the most in the OPEX, is relatively constant when varying the temperature. Nevertheless, there is a significant electricity cost variation when varying the reactor temperature. The increase in the in-house electricity production derived from the fact that, as explained previously, more reaction and consequently more heat is released at higher temperatures, is translated into a decrease in the need of importing electricity when applying higher reactor temperatures.

Looking at the overall values obtained from the simulations, it can be clearly understood that the actual OCM process cannot compete in any case with the

conventional C_2H_4 technologies. Although the price of ethylene can remarkably fluctuate depending on the region and on the resources available, its current value does not exceed 1000 €/ton. In particular, the C_2H_4 price calculated by Spallina et al. [13] for the benchmark technology (naphtha steam cracking with a naphtha price of 450 €/ton) was 834 €/ton, that is, almost half of the C_2H_4 price obtained with packed-bed reactor OCM technology.

The expensive ethylene price derived from the OCM process is mainly caused by the low C_2 yield attained with the OCM reactor. The techno-economic evaluation shows the consequences of this poor yield. Firstly, large amounts of electricity need to be imported to operate all the separation train units to separate the very large and broad variety of by-products that are formed in the reactor, thus impacting notably both OPEX and CAPEX. Another important cost contribution relates to the feedstock that the process employs. A large quantity of natural gas is required to meet the ethylene production target since most of it is not converted into the desired product but into CO and CO_2, having this effect a major impact on the OPEX.

6.4.2.2. Sensitivity analysis on the reactor performance

From the previous section it is clear that OCM is not economically viable with the current state of the art. Nevertheless, large research efforts are still spent on this topic. Thus, it would not be surprising to see further improvements on the process performance in the coming period.

To quantify the relevance of the improvement of the reactor performance on the overall ethylene price, the yield of the OCM reactor has been modified and the updated ethylene price obtained with such a modification has been analyzed.

To do so, the OCM simulation giving the lowest ethylene price has been taken as base case. Its main conditions are summarized in Table 6.4:

Table 6.4. Main characteristics of the base case simulation obtained with Aspen Plus.

Base case simulation	
Temperature [°C]	850
Pressure [bar]	10
CH_4/O_2 [-]	3
Reactor length [m]	1.56
CH_4 conversion (%)	31.8
C_2 selectivity (%)	43.8
Ethylene price (€/ton)	1541

From this base case, the reaction rates of the primary OCM reactions (according to the kinetics provided by Stansch et al. [15]) have been manually modified to increase the CH_4 conversion and/or the C_2 selectivity as a way to simulate improvements in the reaction path. With this strategy, both an improvement on the OCM reactor performance and a decrease on the C_2H_4 final price are expected in every simulation. In Figure 6.6, the different OCM simulations are represented and the change in the overall process performance for each of them is quantified:

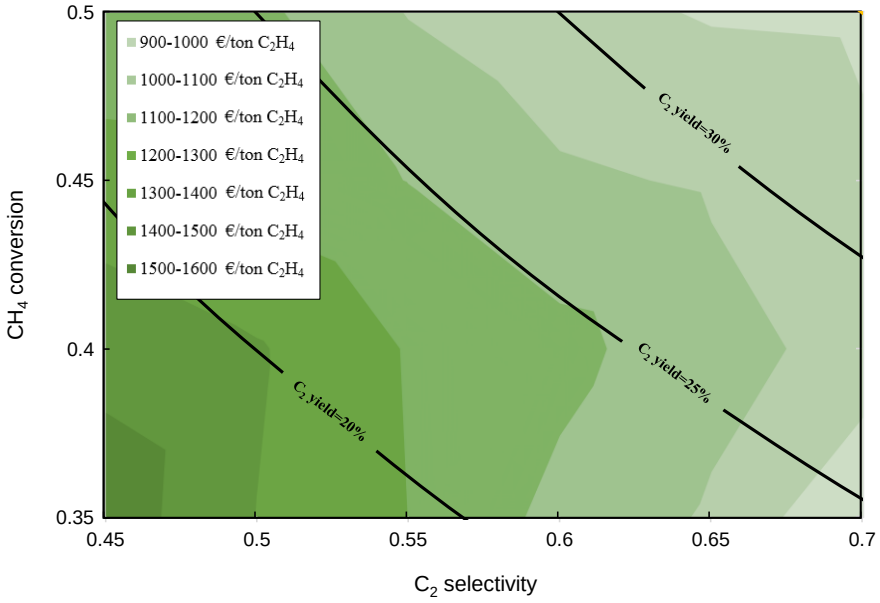

Figure 6.6. "Iso-C_2H_4 prices" obtained from the OCM process for different reactor C_2 selectivities and CH_4 conversions.

It is clear from the graph that a significant increase in C_2 yield in the OCM process plant is needed to become competitive with the conventional ethylene production technologies. A yield of 30% at conditions applicable at industrial scale is the target to decrease the ethylene price below 1000 €/ton$_{C_2H_4}$, which can be set as the objective to be competitive with conventional technologies. Two main technical options can be considered to reach this target in the coming years; the development of a novel reactor configuration and the improvement of the characteristics of the OCM catalyst. Many reactor designs have been attempted at small scale, showing some advantages with respect to the conventional packed bed in terms of reactor performance (see Chapter 2 and Chapter 3). Specifically, the advantages of membrane reactors as an alternative to improve the OCM reactor performance have been extensively discussed in this thesis. Therefore, an individual techno-economic analysis of this technology will be carried out in the next chapter (Chapter 7), keeping the conventional packed bed as the only configuration under study in this chapter.

The improvement of the catalyst performance is another alternative to increase the OCM reactor yield. If the performance of the catalyst is sufficiently increased, there would be no need of changing the reactor configuration to become competitive at large scale. There are two main factors affecting the behavior of the catalyst; its activity and its selectivity. The selectivity influences mostly the primary reactions, and it has a major contribution to the overall process performance. A more selective catalyst would decrease the percentage of undesired products, enhancing the production of ethane (in the primary step) and resulting at the reactor outlet in an increase in the ethylene yield even though the undesired gas-phase consecutive reactions (C_2 combustion and reforming) could still play a role. However, high selectivities are commonly related to relatively low CH_4 conversions. Similarly, a more active catalyst would increase the CH_4 conversion, although in most of the cases it is accompanied by a significant decrease in the C_2 selectivity.

In literature it can be found that in a conventional lab-scale packed-bed reactor, the yield that can be currently achieved with a stable catalyst, commonly W, La or Sr

based, remains around 15-20% [1]. Therefore, the challenge is to develop a better OCM catalyst, either by increasing its activity and/or its selectivity, such that the overall reactor yield reaches the target fixed to be competitive with the conventional ethylene technologies.

To study in more detail how the different parameters affecting the ethylene cost change when the OCM reactor performance is improved, three different cases have been evaluated. The first one is the so-called reference case, which accounts for the conditions derived from the process performance optimization. Subsequently, in Case 2 the reactor performance has been improved by increasing the C_2 selectivity while keeping the same CH_4 conversion as in the reference case. For Case 3, the CH_4 conversion has been increased and the C_2 selectivity has been kept as in the reference case. The objective behind this comparison is to determine whether an increase in conversion is preferred over an increase in selectivity, or vice versa, for further OCM catalyst improvements. The details of the three cases are listed in Table 6.5:

Table 6.5. Simulations selected to analyze the effect of the reactor performance improvement in the ethylene cost distribution.

	Reference case	Case 2 (higher C_2 selectivity)	Case 3 (higher CH_4 conversion)
CH_4 conversion (%)	31.8	31.8	40.8
C_2 selectivity (%)	43.8	56.2	43.8
C_2 yield (%)	13.9	17.9	17.9
Ethylene price (€/ton)	1541	1223	1460

The ethylene cost distribution in the cases selected is presented in Figure 6.7:

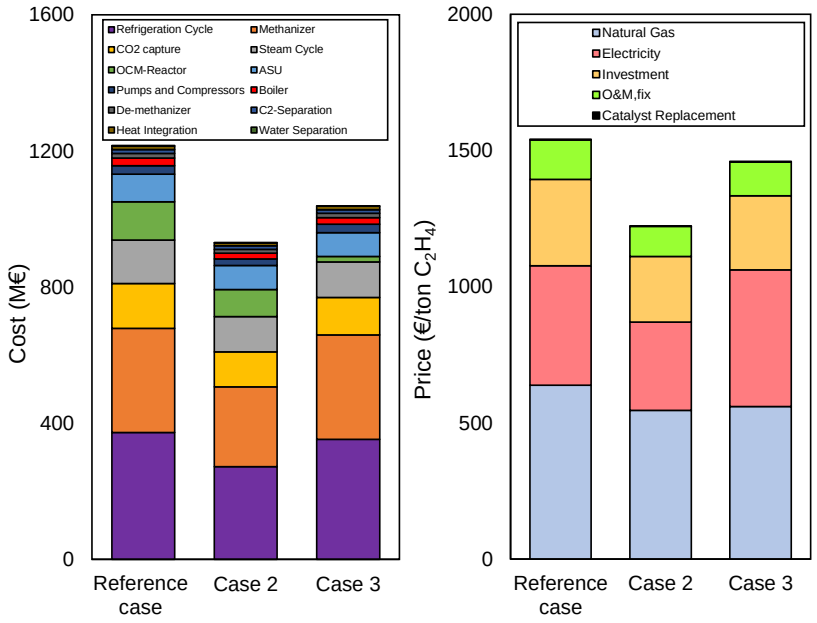

Figure 6.7. Cost distribution of an OCM plant, CAPEX, (left) and disaggregated ethylene cost, CAPEX and OPEX, (right) for the reference case, Case 2 (higher C_2 selectivity) and Case 3 (higher CH_4 conversion).

It can be seen in Figure 6.7 that both CAPEX and OPEX show better results when the C_2 reactor yield is improved by increasing the C_2 selectivity rather than by increasing the CH_4 conversion (Case 2 has lower costs than Case 3). The variation in the separation train units cost (CAPEX) emanates from the fact that the outlet of the OCM reactor is influenced by the achieved C_2 selectivity and CH_4 conversion, getting in each case a specific by-products distribution. Particularly, Case 2 will have a separation train with more unreacted CH_4 while Case 3 will face more undesired carbon products (CO and CO_2). Actually, the low CAPEX cost obtained in Case 2 relates mainly to the cost of the refrigeration cycle, which accounts for all the energy required for the cryogenic units, and of the methanizer. The low production rate of undesired carbon (mainly CO) because of the high C_2 selectivity achieved in the OCM reactor will result in a lower methanizer cost, since this unit is used to convert back the CO into CH_4. Furthermore, the increase in ethane and ethylene mole fractions at the inlet of the cryogenic distillation columns, as a consequence of increased selectivities, will result in lower amounts of condensable gases at the condenser of the de-methanizer. This

will lead to lower energy requirements in the condenser which will result in the reduced power consumption of the compressors for the refrigeration cycle, with a positive impact on both CAPEX and OPEX.

Another remarkable cost change is associated with the OCM reactor. The cost of this unit in Case 2 and 3 is much smaller than in the reference case. The endothermic C_2H_6 dehydrogenation becomes more important when more C_2H_6 is produced during the primary reactions, as it happens in Cases 2 and 3. As a consequence, the overall system is less exothermic, thus reducing the required number of cooling tubes with a concomitant decrease in the cost of this reactor.

Correspondingly, the OPEX is also largely influenced by the reactor performance. A better reactor performance leads to a reduction in the carbon footprint of the process, since less natural gas is needed to achieve the same production capacity. However, even if the total electricity consumption is also decreased when increasing the OCM reactor performance (especially in Case 2), it still remains an important factor on the final ethylene price and it evidences the need to import electricity. This power generation is still associated with large CO_2 emissions derived from the electricity production, and can be understood as a drawback of this process.

Summing up and knowing that an increase of the OCM reactor performance is always beneficial for the process, it has been demonstrated that the effect of increasing the C_2 selectivity has a larger (and positive) impact on both the CAPEX and the OPEX of the process than when the CH_4 conversion is increased (reaching the same C_2 yield).

6.4.3. OCM Forecast

Different aspects such as location, politics or economics can have a large influence on the ethylene market price. Therefore, it remains challenging to properly predict the ethylene price for the coming future. However, based on the historical ethylene price trend for the last 30 years (in US, since there was no data available from Europe) [24], a linear trend line has been extrapolated to foresee the ethylene price for the coming years. The results of this analysis are plotted in Figure 6.8:

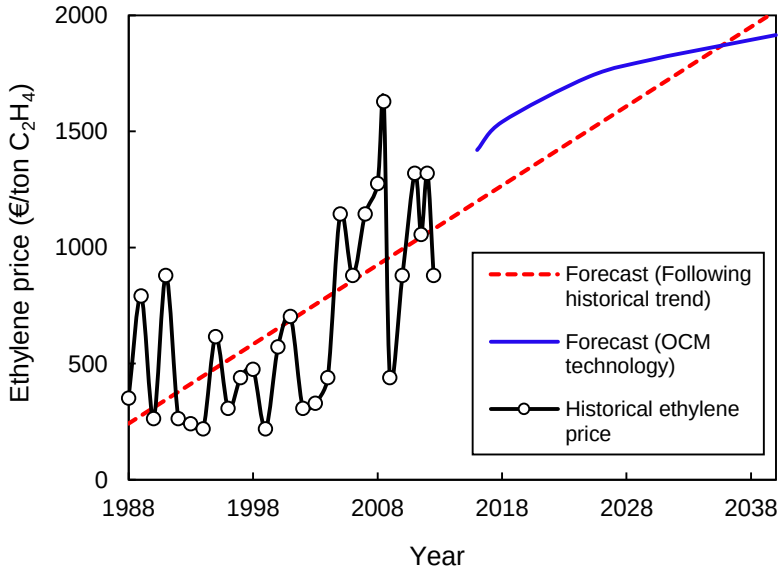

Figure 6.8. Historical ethylene price (black) [24], ethylene price forecast based on historical data (red) and ethylene price forecast using OCM (blue) for the coming period.

In Figure 6.8 it can be seen that, with the currently achieved C_2 yield of 14%, conventional OCM can become competitive with the traditional process in the near future because the naphtha price is expected to increase faster than the natural gas one. When considering accurate the predictions for natural gas [25] and cost of ethylene for the coming years from benchmark technologies, the currently developed OCM technology (C_2 yield=14%) for the ethylene production is expected to be able to compete with conventional technologies from 2030-2035 in the EU. Since the increase in the oil price is anticipated to be steeper than the natural gas price (see Figure 1.2 of this thesis), and the price of ethylene in each technology is strongly affected by the cost of the feedstock used, the increase in the ethylene price when using conventional technologies is also expected to increase faster than when applying OCM. Additionally, OCM could become competitive even earlier if improvements in the process performance can be achieved. In Figure 6.9, the OCM reactor yield required at each of the coming years to reach with OCM the same ethylene price than with conventional technologies is presented:

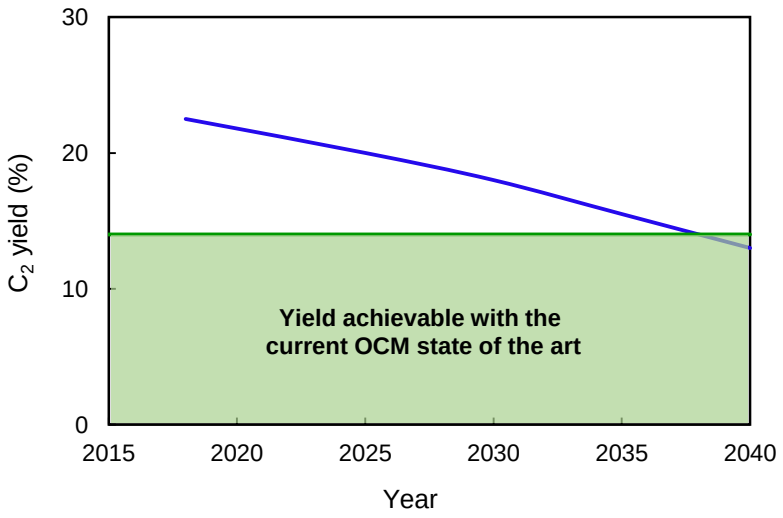

Figure 6.9. OCM reactor yield necessary to achieve the same ethylene price with OCM as with the conventional ethylene production technologies in Europe for the next period. The green area represents the C_2 reactor yield that can be currently achieved with OCM.

Because of the explained trend of the different fuels cost from which ethylene can be produced, the OCM performance required to make this technology competitive is expected to decrease in the coming years.

This can be translated into the fact that a technological breakthrough in the OCM technology, that is, a significant increase in the current OCM performance, would make OCM viable for its application at industrial scale even before 2035. As extensively stated in previous sections, two are the most likely options to achieve this breakthrough: reaching a high maturity level with a novel reactor configuration which can provide a higher C_2 reactor yield, and/or with the development of a better catalyst which would also result in the desired reactor performance increase.

It should be in any case considered at this point that other already fully-developed technologies, like ethane dehydrogenation, can also play a very significant role in this future scenario (especially if natural gas becomes much more attractive than naphtha), competing also to be the most cost-effective alternative to naphtha steam cracking. Actually, ethane dehydrogenation has already been implemented in some regions whose characteristics make the process especially convenient.

6.5. Conclusions

The results reported in this chapter show that the OCM reactor performance (CH_4 conversion and C_2 selectivity) has a large influence on the ethylene price, but that the lowest ethylene price is not necessarily obtained with the highest C_2 product yield. Moreover, by using the most often researched OCM reactor technology, the packed bed, and by assuming the most trustable OCM kinetics, it has been demonstrated that the current OCM state of the art is not yet competitive with traditional C_2H_4 production technologies, particularly naphtha steam cracking.

In order to understand how to close the existing gap between OCM and benchmark technologies, the OCM reactor performance has been manually modified to increase the reactor yield and to investigate its effect on the behavior of the overall plant. As a result, a C_2 reactor yield of at least 25-30%, at conditions applicable at industrial scale, is nowadays needed to obtain an ethylene price below 1000 €/ton$_{C_2H_4}$, which could be set as the threshold to become industrially competitive. This can be translated into the fact that a breakthrough in the OCM technology is required to reach this C_2 yield, either by means of an improvement of the catalyst characteristics and/or the development of novel reactor configurations (as will be discussed in the next chapter). It has been demonstrated that an improvement in the selectivity of the catalyst towards the products is more beneficial than an increase in feedstock conversion. In addition, it should be considered that the improvements should be mature and validated by long-term tests to ensure a proper industrial application of such a novel catalyst or reactor configuration. Considering that the assumptions formulated are relatively accurate, it can be highlighted that the OCM technology is expected to become competitive within a period of around 20 years if the oil price has a steeper increase than the natural gas price, as expected. If the foreseen situation is accomplished, a "fuel switching" scenario for the ethylene production with the emergence of alternative technologies, like OCM, will be likely to happen.

6.6. Bibliography

[1] A. Cruellas, T. Melchiori, F. Gallucci, and M. Van Sint Annaland, "Advanced reactor concepts for oxidative coupling of methane," *Catalysis Reviews*, vol. 59, no. 3, pp. 234–294, 2017.

[2] L. Olivier, S. Haag, H. Pennemann, C. Hofmann, C. Mirodatos, and A. C. van Veen, "High-temperature parallel screening of catalysts for the oxidative coupling of methane," *Catalysis Today*, vol. 137, no. 1, pp. 80–89, 2008.

[3] W. Wiyaratn, S. Manundawee, A. Arpornwichanop, S. Assabumrungrat, A. Watanapa, and C. Worawimut, "Two-dimensional mathematical modeling of the oxidative coupling of methane in a membrane reactor," *Engineering Journal*, vol. 20, no. 1, pp. 17–33, 2016.

[4] N. Holst *et al.*, "Two-Dimensional Model for Oxidative Coupling of Methane in a Packed-Bed Membrane Reactor," *Chemical Engineering & Technology*, vol. 35, no. 2, pp. 294–301, Feb. 2012.

[5] A. Cruellas, T. Melchiori, F. Gallucci, and M. van Sint Annaland, "Oxidative Coupling of Methane: A Comparison of Different Reactor Configurations," *Energy Technology*, vol. 0, no. 0, p. 1900148, May 2019.

[6] S. Bhatia, C. Y. Thien, and A. R. Mohamed, "Oxidative coupling of methane (OCM) in a catalytic membrane reactor and comparison of its performance with other catalytic reactors," *Chemical Engineering Journal*, vol. 148, no. 2–3, pp. 525–532, 2009.

[7] F. T. Akin and Y. S. Lin, "Controlled Oxidative Coupling of Methane by Ionic Conducting Ceramic Membrane," *Catalysis Letters*, vol. 78, no. 1, pp. 239–242, 2002.

[8] N. H. Othman, Z. Wu, and K. Li, "An oxygen permeable membrane microreactor with an in-situ deposited $Bi_{1.5}Y_{0.3}Sm_{0.2}O_{3-\delta}$ catalyst for

oxidative coupling of methane," *Journal of Membrane Science*, vol. 488, pp. 182–193, Aug. 2015.

[9] J. A. Roos, A. G. Bakker, H. Bosch, J. G. van Ommen, and J. R. H. Ross, "Selective oxidation of methane to ethane and ethylene over various oxide catalysts," *Catalysis Today*, vol. 1, no. 1, pp. 133–145, 1987.

[10] J.-P. Lange and P. J. A. Tijm, "Processes for converting methane to liquid fuels: Economic screening through energy management," *Chemical Engineering Science*, vol. 51, no. 10, pp. 2379–2387, 1996.

[11] S. Parishan, P. Littlewood, A. Arinchtein, V. Fleischer, and R. Schomäcker, "Chemical looping as a reactor concept for the oxidative coupling of methane over the MnxOy-Na2WO4/SiO2 catalyst, benefits and limitation," *Catalysis Today*, vol. 311, pp. 40–47, 2018.

[12] S. Jašo, H. R. Godini, H. Arellano-Garcia, M. Omidkhah, and G. Wozny, "Analysis of attainable reactor performance for the oxidative methane coupling process," *Chemical Engineering Science*, vol. 65, no. 24, pp. 6341–6352, 2010.

[13] V. Spallina, I. C. Velarde, J. A. M. Jimenez, H. R. Godini, F. Gallucci, and M. Van Sint Annaland, "Techno-economic assessment of different routes for olefins production through the oxidative coupling of methane (OCM): Advances in benchmark technologies," *Energy Conversion and Management*, vol. 154, pp. 244–261, Dec. 2017.

[14] NETL, "Cost Estimation Methodology for NETL Assessments of Power Plant Performance," Pittsburgh, USA, 2011.

[15] Z. Stansch, L. Mleczko, and M. Baerns, "Comprehensive kinetics of oxidative coupling of methane over the La2O3/CaO catalyst," *Industrial and Engineering Chemistry Research*, vol. 36, pp. 2568–2579, 1997.

[16] Dutch Network and Knowledge center for Cost Engineering and Value, Ed.,

DACE Price booklet, 32nd ed. Mieke Stkkelorum, 2017.

[17] V. I. Alexiadis, M. Chaar, A. van Veen, M. Muhler, J. W. Thybaut, and G. B. Marin, "Quantitative screening of an extended oxidative coupling of methane catalyst library," *Applied Catalysis B: Environmental*, vol. 199, pp. 252–259, 2016.

[18] A. Galadima and O. Muraza, "Revisiting the oxidative coupling of methane to ethylene in the golden period of shale gas: A review," *Journal of Industrial and Engineering Chemistry*, vol. 37, pp. 1–13, May 2016.

[19] V. I. Lomonosov, Y. a. Gordienko, and M. Y. Sinev, "Kinetics of the oxidative coupling of methane in the presence of model catalysts," *Kinetics and Catalysis*, vol. 54, no. 4, pp. 451–462, Jul. 2013.

[20] C. Karakaya and R. J. Kee, "Progress in the direct catalytic conversion of methane to fuels and chemicals," *Progress in Energy and Combustion Science*, vol. 55, pp. 60–97, 2016.

[21] D. Matras *et al.*, "Real-Time Operando Diffraction Imaging of La–Sr/CaO During the Oxidative Coupling of Methane," *The Journal of Physical Chemistry C*, vol. 122, no. 4, pp. 2221–2230, Feb. 2018.

[22] D. Matras *et al.*, "Operando and Postreaction Diffraction Imaging of the La–Sr/CaO Catalyst in the Oxidative Coupling of Methane Reaction," *The Journal of Physical Chemistry C*, vol. 123, no. 3, pp. 1751–1760, Jan. 2019.

[23] D. Schweer, L. Mleczko, and M. Baerns, "OCM in a fixed-bed reactor: limits and perspectives," *Catalysis Today*, vol. 21, pp. 357–369, 1994.

[24] "U.S. Energy Information Administration." [Online]. Available: www.eia.gov.

[25] "World Energy Outlook," *International Energy Agency, www.iea.org/weo/*, 2017.

Chapter

7

Techno-economic evaluation of the OCM packed bed membrane reactor concept

Abstract

In Chapter 6, a significant increase in the OCM reactor performance to an overall C_2 yield of about 30% was shown to be the main prerequisite to make the OCM process economically competitive. Membrane reactors are a real possibility to accomplish this objective. Thus, a techno-economic analysis for the packed bed membrane technology for OCM has been developed in Chapter 7. The higher OCM reactor yields obtained with the membrane reactor have indeed a very positive impact on the economics and performance of the downstream separation of the simulated OCM plant, resulting in a cost of ethylene production of 595-625 €/ton$_{C_2H_4}$ depending on the type of membranes employed, 25-30% lower than the benchmark technology (naphtha steam cracking). Despite the use of a cryogenic separation unit, the porous membranes configuration shows generally better results than the configuration employing selective dense membranes because of the much larger membrane area required when using dense membranes. In addition, the CO_2 emissions of the OCM processes are also much lower than the benchmark technology (total CO_2 emissions are reduced by 96% when using dense membrane and by 88% when using porous membranes with respect to naphtha steam cracking). However, the scalability and the issues associated to it seem to be the main constraints to the industrial exploitation of the packed bed membrane OCM process.

7.1. Introduction

The conventional OCM process, in which a packed bed reactor with a C_2 yield of 15% is considered, has been evaluated from an economic point of view in Chapter 6. Although it was shown that this technology cannot compete with the traditional ethylene production technology (the cost of ethylene from this technology is almost double than the one achieved with the reference naphtha steam cracking process), it has been verified that an increase in the OCM reactor performance could make the process competitive with NSC. Indeed, and according to the calculations performed in Chapter 6, a reactor yield of at least 25-30% would be needed to make OCM industrially viable. However, these calculations are made by using the process flowsheet designed for a packed bed reactor, while the feasibility of alternative configurations which could also contribute to this C_2 yield enhancement are not considered. As explained and justified in detail in Chapters 2, 3 and 5, membrane reactors emerge as a solution for this required yield increase.

Therefore, a techno-economic analysis on the membrane reactor configuration for OCM has been carried out in this chapter, following a very similar methodology. To the authors' knowledge, the analysis that will be carried out here represents the first time that the industrial viability of this packed bed membrane OCM configuration, widely investigated experimentally, will be evaluated from a process performance point of view. In addition, the membrane reactor configuration will be compared with the conventional OCM (with a packed bed reactor), highlighting the changes that the different reactor configurations require in the process and analyzing the influence of these modifications. Because of their suitability to operate in a similar temperature range of the OCM reactions, dense oxygen (MIEC) membranes are, in principle, the most interesting to be implemented in this process, since the O_2 separation from air occurs in-situ in the reactor by the membranes themselves, thus avoiding the use of the energy-intensive air separation unit. However, their O_2 flux is relatively low [1] and can deteriorate in presence of CO_2 or H_2O. Therefore, not just these membranes have

been considered for this comparison, but also the use of porous tubes for distributive feeding of pure O_2.

In the following section the methodology selected for this techno-economic comparison will be given, followed by a detailed description of the OCM plants considered for the analysis. Subsequently, the results of this study will be presented, and a sensitivity analysis on the main variables discussed. Finally, the main conclusions of this chapter, as well as potential improvements for the OCM technology, will be given.

7.2. Methodology

The methodology followed in this chapter is identical to the one described in Chapter 6, where the feasibility of the conventional OCM packed bed reactor was evaluated. Thereby, all the methodology and indicators detailed there are also valid for Chapter 7 (Table 6.1 and 6.2).

To allow for a fair comparison with the analysis carried out in Chapter 6, the size of the plant has also been kept the same, that is, the target of the simulations is to produce 31.9 $kg_{C_2H_4}/s$, which corresponds to a production capacity of 1 million-ton of ethylene per year. Similarly, the plant is assumed to be located in Europe.

In addition to all the performance indicators described in Chapter 6, which mainly focuses on the economic viability of the OCM packed bed concept, the environmental impact of each of the studied configurations will also be evaluated in this chapter, and the related definition of performance indicators is shown in Table 7.1:

Table 7.1. Definition of the indices used for the evaluation of the environmental performance of the process.

Environmental performance indexes		
Direct CO_2 emissions	$E_{CO_2,direct} = \frac{\dot{m}_{CO_2,direct}}{\dot{m}_{C_2H_4}}$	*Equation 7.1*
Indirect CO_2 emissions (*)	$\dot{m}_{CO_2,indirect} = +W_{electr,imported/exported} * E_{CO_2,CC} + W_{heat,imported/exported} * E_{CO_2,TH}$	*Equation 7.2*
	$E_{CO_2,indirect} = \frac{\dot{m}_{CO_2,indirect}}{\dot{m}_{C_2H_4}}$	*Equation 7.3*

CO_2 captured	$CC\ (\%) = \frac{\dot{m}_{CO_2,captured}}{\dot{m}_{CO_2,captured} + \dot{m}_{CO_2,direct} + \dot{m}_{CO_2,indirect}}$	*Equation 7.4*

(*)$E_{CO_2,CC} = 96 \frac{g_{CO_2}}{MJ_{el}}$; $E_{CO_2,TH} = 63 \frac{g_{CO_2}}{MJ_{el}}$

The direct CO_2 emissions refer to the fuel that is burnt in the plant, which is used in the plant for heat integration and electricity generation. Differently, the indirect CO_2 emissions refer to the net production/consumption of energy in the plant. If electricity needs to be imported in the plant, this will bring along the CO_2 emissions during the electricity generation. Similarly, if the plant has a surplus of electricity that can be exported, this will result in a decrease in carbon emissions (considered as negative CO_2 emissions) as this electricity is already produced. The same analogy is considered for the case of heat import/export. The carbon emission values are taken from the work of Spallina et al. [2], where it is assumed that the imported/exported electricity comes from a natural gas combined cycle plant (NGCC) with an efficiency of 58% emitting 96 g_{CO_2}/MJ ($E_{CO_2,CC}$) [3]. In the case of the imported/exported heat, it is assumed that it is produced in an industrial boiler (90% efficiency) with 63 g_{CO_2}/MJ ($E_{CO_2,TH}$) emissions[4], [5].

Finally, the undesired reactions prevailing in the OCM reactor are another source of CO_2 (CO_2 captured). This CO_2, together with the rest of the products and unconverted reactants, goes subsequently to the separation train, where all this CO_2 is captured by means of an acid gas removal ($\dot{m}_{CO_2,captured}$).

7.3. Model descriptions

In this section, first the reactor model used for the OCM simulations is presented, and subsequently the overall processes is shortly outlined for both the dense and porous membranes.

7.3.1. OCM membrane reactor model

The OCM reactor has been simulated by means of a 1D plug-flow reactor model. The core of the model is identical to one described and used in Chapter 6 (Section 6.3 of

this thesis), where also the selected main characteristics and parameters, included again in Table 7.2, were justified.

Table 7.2. Reactor characteristics assumed for the simulation of the 1D OCM reactor model.

OCM Reactor characteristics		
Diameter [m]	3	
Inlet gas velocity [m/s]	1	
Bed porosity [-]	0.5	
Inlet pressure [bar]	10	
Pressure drop in the reactor [bar]	1	
Catalyst type	La_2O_3/CaO	[6]
Catalyst density [kg particle/m³ reactor]	3600	[6]
Active weight fraction	0.27	[6]
Catalyst dilution $[\frac{Catalyst\ weight\ [kg]}{Total\ solid\ weight\ [kg]}]$	1	
Reactor length [m]	2	
Type of porous membrane	Asymmetric Al_2O_3	[7]
Porous membrane diameter [m]	0.01	
Porous membrane length [m]	2	
Porous membrane price [€/m²]	700	
Type of dense membrane	BSCF	[1]
Dense membrane layer [m]	$5 \cdot 10^{-5}$	
Dense membrane length [m]	2	
Dense membrane price [€/m²]	1000	
Number of reactors needed for the process	10-40 (*)	
Membrane lifetime [years]	5	

(*) Depending on the simulation and its conditions

The reactor model developed in Chapter 6 has been expanded by adding the membranes from where oxygen will be fed into the OCM reactor. Both the selective dense membranes and unselective porous membranes have been considered.

As explained during this thesis, perovskites and fluorites are the most common MIEC membranes investigated in literature [8]. Perovskites achieve generally higher O_2 permeation fluxes since they are able to transport both ions and electrons. Differently, fluorites present a high ionic conductivity, but a very poor electronic conductivity. That is why they are often mixed with some electronic conductors (which can be

ceramic or metallic) to form the so-called "dual-phase" O_2 membranes. BSCF membranes are one of the often used perovskite materials and, although it is known that they can suffer from stability issues when in contact with some species produced during OCM (like CO_2) [8], this type of mixed ionic-electronic conducting (MIEC) membranes has been selected for the simulations using the dense membranes, as it was done in Chapter 3 (sections 3.2.2 and 3.3.3) due to its well-known permeation behavior [1]. The oxygen flux to describe these membranes is given again in Equation 7.5:

$$J^m = \frac{D_v k_r \left(\left(p_i^{m,a}\right)^n - \left(p_i^{m,f}\right)^n \right)}{2\delta k_f \left(p_i^{m,a} p_i^{m,f}\right)^n + D_v \left(\left(p_i^{m,a}\right)^n + \left(p_i^{m,f}\right)^n \right)} \qquad \text{Equation 7.5}$$

where $p_i^{m,a}$ is the pressure of the specie i (oxygen) in the air side (retentate), $p_i^{m,f}$ is the pressure of the specie i (oxygen) in the fuel side (permeate) and the exponent n is set to 0.5. δ is the thickness of the membrane and D_v, k_r and k_f are parameters characteristic of the membrane (oxygen vacancy diffusion coefficient and surface exchange reaction rate constants), which depend on temperature through an Arrhenius-type relation. The permeability parameters for the BSCF membrane selected were listed in Table 3.6 [9].

As shown in Equation 7.5 [1], the permeation of the selected membranes, at a given temperature, is constant and independent from their thickness and applied pressure difference when the oxygen partial pressure at the reactor side is close to zero, a phenomena occurring during the OCM reaction because of the fast oxygen consumption in the permeate (reaction) side, which impedes its accumulation. In this case, most of the terms in the equation are cancelled out, and the oxygen permeation rate is only determined by k_r, the constant of the reaction rate for the oxygen recombination after its permeation (in form of ions) through the membrane bulk.

Differently, porous membranes are not selective to oxygen, and the driving force for these membranes is governed by the total pressure difference between retentate and permeate side. For simplicity of the model, a uniform permeation profile along the

reactor axial length has been considered (back permeation and other phenomena that can reduce the performance of the porous membrane reactor are not considered in this 1D model). These membranes have been assumed to be asymmetric Al_2O_3 tubes with a constant oxygen flux of 0.25 mol/m²/s ($5 \cdot 10^{-6}$ mol/m²/s/Pa with an assumed constant pressure difference of 0.5 bar between the retentate and permeate sides). These values are typically found in the literature for this type of porous membranes [7]. Since the optimization of the membranes formulation and operating condition is out-of-the-scope of this work, the selected assumptions to calculate the oxygen permeation lead to a fixed reactor performance in terms of CH_4 conversion, C_2 selectivity and C_2 yield for both the porous and the dense membranes case, while major differences still remain in the process scheme due to their different integration.

The lifetime of all the membranes employed to run the simulations shown here has been set to 5 years, a realistic target for an industrially-applied process.

Differently to the conventional packed bed OCM reactor evaluation (Chapter 6), where the optimized length of the reactor depends on the inlet conditions, in this case the reactor length has been fixed to 2 m for simplicity of all the calculations. It will be shown in the following sections that this parameter (englobed within the reactor costs) is not relevant for the calculations of the economics.

7.3.2. Dense membrane reactor OCM process scheme

The process scheme of the dense membrane reactor OCM process, where dense BSCF membranes are integrated in the OCM reactor, is shown in Figure 7.1:

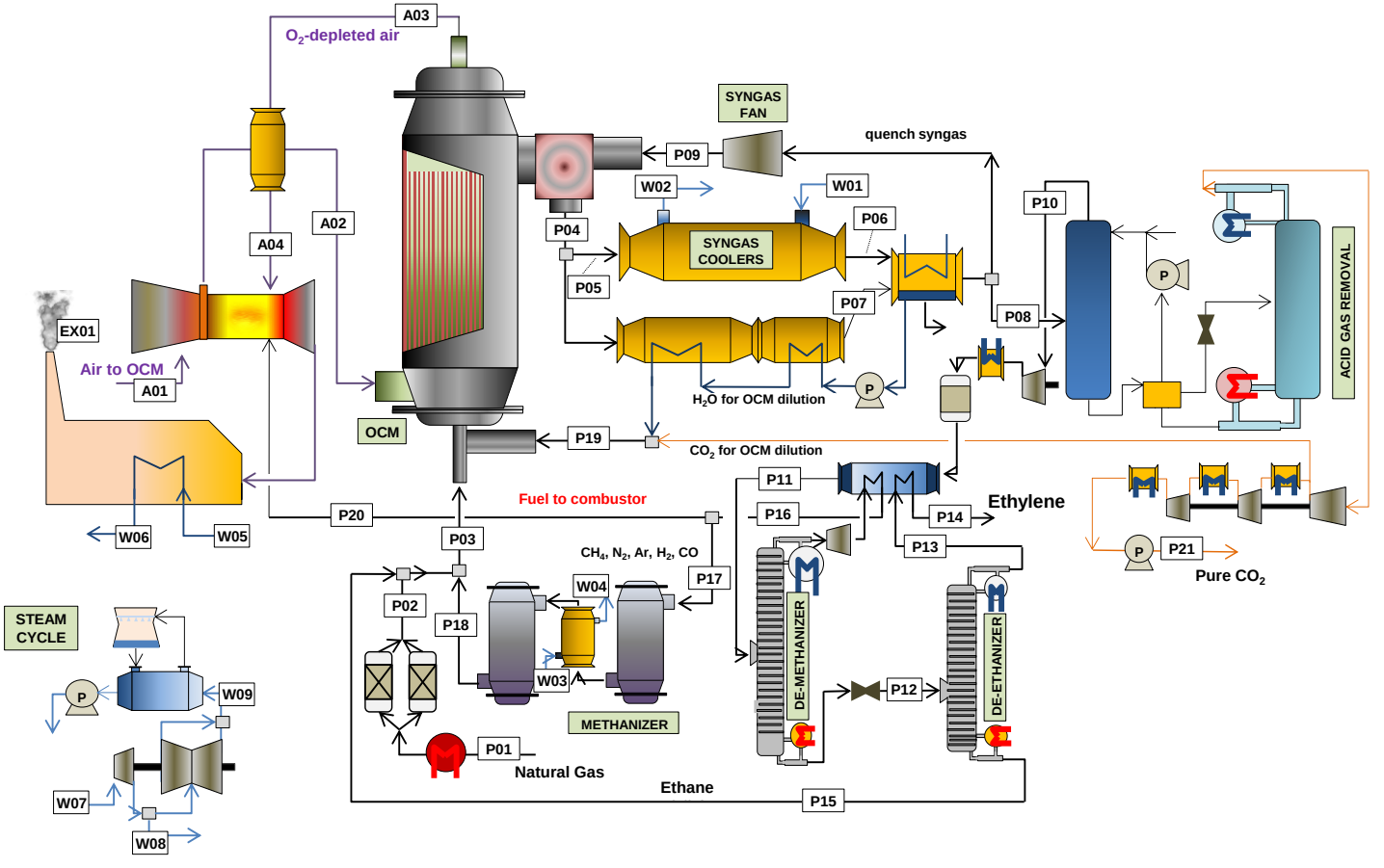

Figure 7.1. Dense membrane reactor OCM process flow diagram.

In this process scheme, air is first compressed up to 10 bar and pre-heated before being fed through the membranes, where oxygen will permeate towards the reaction section. Subsequently, the mid pressure and high temperature depleted air stream leaving the reactor from inside the membranes is used to burn the purge of the recycle stream in the combustion chamber of a gas turbine to generate part of the electricity required in the plant. Differently to other OCM configurations, no cooling tubes inside the reactor are installed, since the air inside the membranes acts as coolant. That is, the heat released because of the exothermic reactions is taken by the air fed through the membranes. Thus, the dense membranes are also acting as cooling tubes. The amount of air injected into the retentate side (from which subsequently oxygen permeates) is adjusted in each of the simulations to balance the heat released by the reactions and to assure isothermal conditions in the reactor. This OCM reactor configuration does not have any influence on the configuration of the separation train (but only on its CAPEX/OPEX) [10]. Firstly, the outlet reactor stream is quenched to stop the gas-phase reactions that can negatively affect the selectivity of the process. Subsequently, the gas is cooled to ambient temperature and fed to the acid gas removal absorption unit, where CO_2 is purified. The next step is the purification of ethylene by means of two cryogenic distillation columns: in the first one (de-methanizer), C_2 components are separated from the other incondensable species, while in the second one (de-ethanizer) pure ethylene is obtained while ethane is recycled back to the reactor. The remaining species coming from the de-methanizer are fed into the methanizer, in which CO and H_2 are converted back to methane before recycling them back to the OCM reactor. Part of this recirculation stream is purged to be burnt in a boiler, thus producing electricity required for the system. In this process scheme, heat is integrated by producing high pressure steam to be fed in a steam cycle, and the cryogenic temperatures are obtained by means of a refrigeration cycle.

7.3.3. Porous membrane reactor OCM process scheme

The process flow diagram for the plant with porous membranes integrated in the OCM reactor is shown in Figure 7.2:

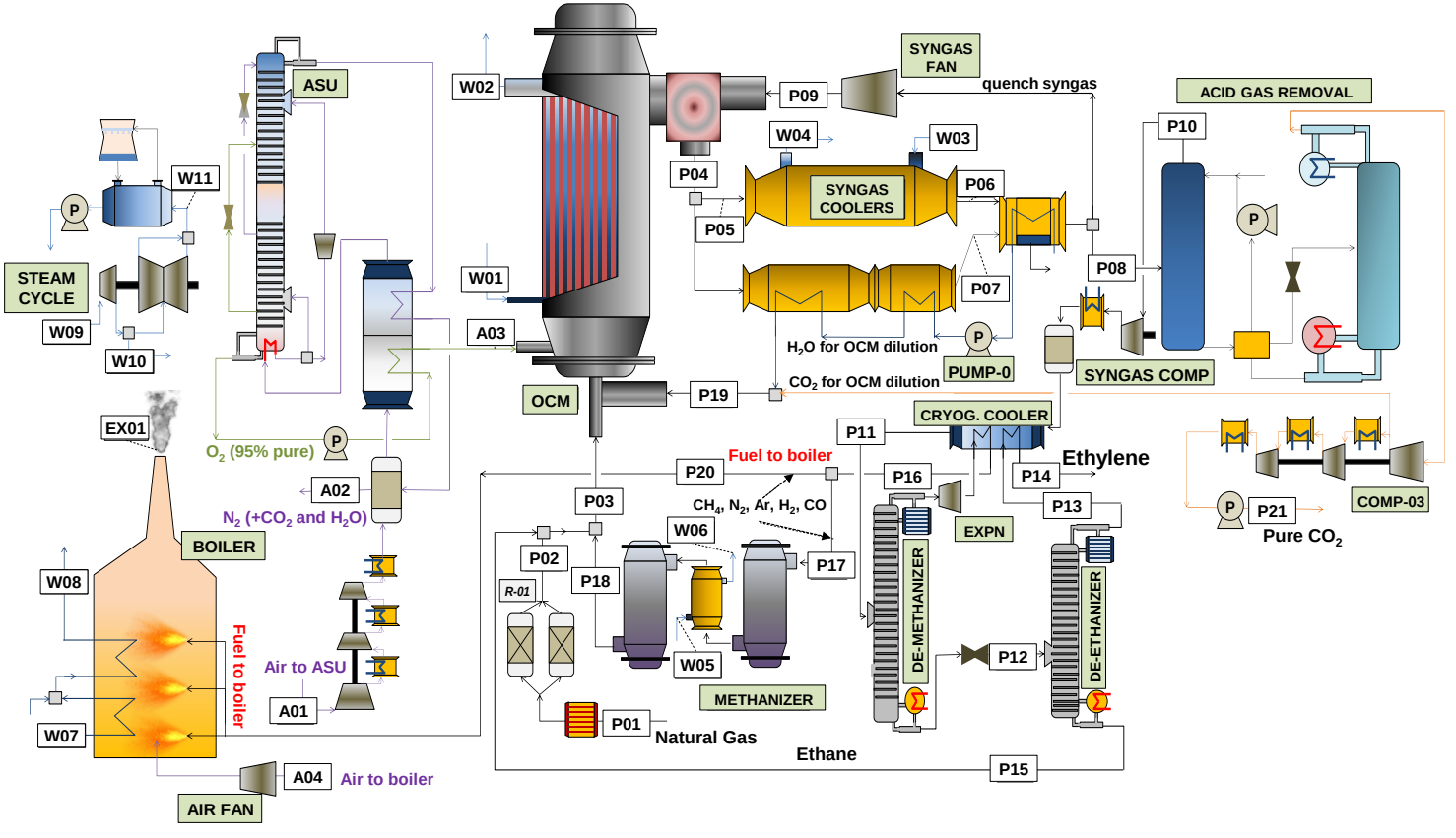

Figure 7.2. Porous membrane reactor OCM process flow diagram.

In this case, the air separation is carried out in a cryogenic air separation unit. The separated oxygen, with a purity of 95% (the remaining 5% is N_2 and Ar), is evenly fed by means of the porous membranes into the catalyst bed, where the OCM reactions take place. The integration of porous membranes in the reactor is combined with the integration of cooling tubes (assumed to have a heat transfer coefficient of 100 $W/m^{2}*K$ [11]) to remove the heat released when performing OCM. High pressure liquid water is fed through these tubes, producing steam when carrying out the reaction. As can be seen in the scheme, the steam produced is further used in the steam cycle to produce electricity. Since the heat of the reaction is managed differently to the dense membranes case, no gas turbine is included in this process scheme. The rest of the process is identical to the one explained below (section 7.3.2).

7.4. Results

The different process schemes previously described will be analyzed and compared. The processes employing a membrane reactor will first be detailed. Subsequently, a techno-economic comparison between the selected process schemes will be carried out, focusing on the differences that the different reactor configurations imply on the rest of the plant.

7.4.1. Membrane reactor OCM scheme

As previously explained, two different configurations (employing a dense and a porous membrane reactor), have been considered to study the feasibility of the OCM membrane reactor technology. The integration of membranes is expected to increase the C_2 reactor yield because of the even distribution of the oxygen along the reactor length, hence favoring the desired reactions over the undesired ones. To do so, a complete sensitivity analysis has been carried out on the reactor level, where the reaction temperature and the CH_4/O_2 ratio were varied. Since the economic evaluation calculator is embedded in the Aspen software, through this sensitivity also the economic indicators could be obtained. The results for both configurations have been combined in Figure 7.3. Since both dense and porous membranes distribute the

oxygen homogeneously along the reactor length (see assumptions in Section 7.3.1), no significant differences in reactor performance have been found for these two configurations and therefore the C_2 yield reported in Figure 7.3 is valid for both the dense and porous membrane reactor cases. However, the ethylene price obtained for each case differ for the porous and dense membrane reactor configuration.

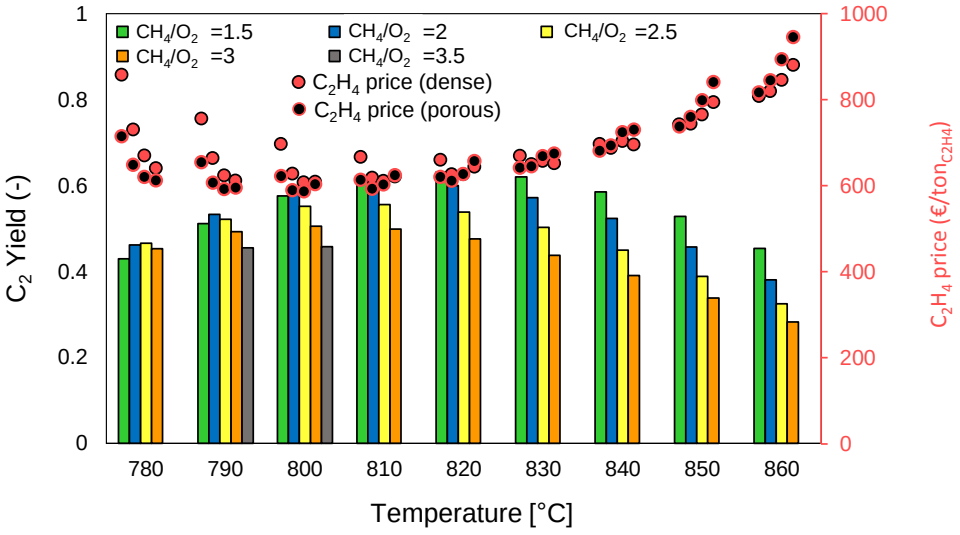

Figure 7.3. OCM reactor yield at different reactor temperatures and operating CH_4/O_2 ratios (valid for both porous and dense membrane reactor cases represented with bars), and overall C_2H_4 price obtained based on the process scheme for the porous and the dense membrane reactor cases.

It can be observed in the graph that the reactor yield achieved with the OCM membrane reactor configurations (both porous and dense), is ranging from approximately 30% to above 60%, and it clearly overcomes the maximum reactor yield obtained with the conventional packed bed reactor (around 14% in the case in which the lowest ethylene price was obtained) (see Chapters 2, 3 and 6). This increase in the reactor performance is translated into a steep decrease in the ethylene price calculated accounting for the entire plant. When reaching higher yields, like in this case, the process becomes more efficient, reducing the energy requirement for the refrigeration in the separation train and decreasing the amount of natural gas required to reach the selected C_2H_4 production (1 MTPY) because of the higher conversion and selectivity reached in the reactor towards the desired products.

The maximum C_2 reactor yield is found to be 63.1% (84.8% CH_4 conversion with 74.5% C_2 selectivity), achieved at 820 °C and with a CH_4/O_2 ratio of 1.5. The temperature at which this maximum is found maximizes the C_2 selectivity, as it is known to be in the range of "optimal operating conditions" while the large amounts of oxygen fed (low CH_4/O_2 ratio) maximizes the conversion of CH_4. However, the highest reactor yield does not correspond to a minimum in the ethylene price. This conclusion was also drawn in the economic evaluation of the OCM conventional packed bed reactor plant (see Chapter 6), meaning that the final ethylene price is not just a function of the C_2 reactor performance, but also related to all the equipment associated to the process plant and the utilities required.

The lowest ethylene price for the case of the MIEC membranes reactor is found to be 625 €/ton$_{C_2H_4}$ at 800 °C and a CH_4/O_2 ratio of 2.5, while for the porous membranes case a price of 595 €/ton$_{C_2H_4}$ (again at 800 °C and CH_4/O_2 ratio of 2.5) was found. As shown in Figure 7.3, the ethylene price is generally 30-70€ more expensive when employing dense membranes compared to the porous membranes' configuration. In order to identify the differences between the two plants, the CAPEX and price distribution of the optimal cases have been investigated. In terms of CAPEX, the disaggregated unit costs are shown in Figure 7.4:

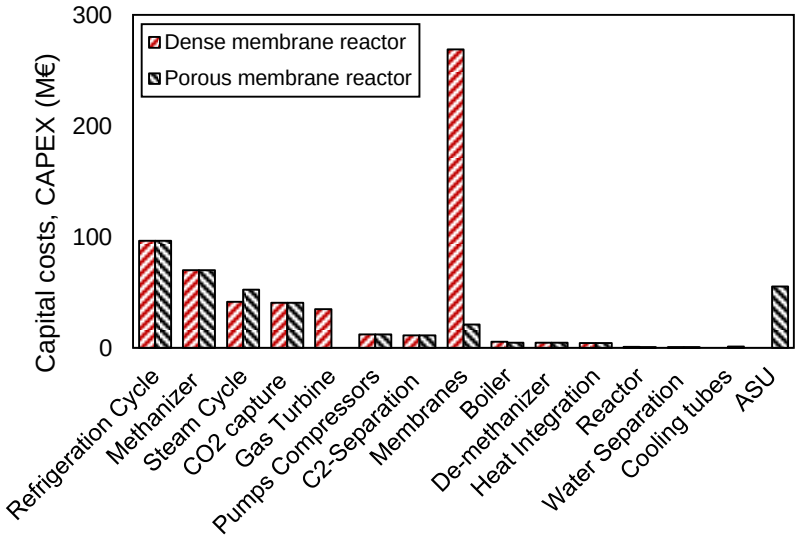

Figure 7.4. Disaggregated capital costs (BEC), CAPEX, for the OCM plant employing a dense membrane reactor (red) and a porous membrane reactor (black).

The total plant cost (BEC) of the two plants is 367 M€ for the porous configuration and 590 M€ for the dense configuration. It is clearly seen that the biggest difference between both configurations relates to the membrane cost. Dense membranes are considered to be supported, namely a porous support in which a dense layer of a material selective to oxygen is coated. Because of that, they will always be more expensive than the porous membranes (assumed to be respectively 1000 €/m² and 700 €/m²). However, this price difference cannot explain the large difference in the total cost of the membranes. This remarkable difference is instead associated with the permeation flux of oxygen that dense and porous membranes can offer. The oxygen flux of porous membranes is roughly one order of magnitude higher than the flux through dense membranes, which translates in a reduction of the membrane area required to feed the desired amount of oxygen into the reactor (the membrane area required for the optimal porous membranes case is 6010 m², whereas for the dense membrane case the required membrane area is 53812 m²). Considering that BSCF membranes are employed for these calculations and that these membranes are known to have relatively high oxygen fluxes among oxygen-selective membranes, the

differences shown here could even be more pronounced when employing the permeation flux of a CO_2-tolerant dense membrane.

Therefore, the repercussion of the membrane cost part in the total CAPEX cost is major in the case of the dense membranes, accounting for almost 50% of the total CAPEX, while it decreases to 6% when porous membranes are employed.

The second important difference between both configurations is the need of an air separation unit (ASU) to feed pure oxygen into the reactor in the case of the porous membrane reactor. This unit accounts in this specific case for roughly 15% of the total plant cost (≈55 M€) although in some conditions this can increase up to 30% of all the CAPEX. The need of an ASU does not just impact the investments, but also the utilities, as electricity needs to be supplied to this unit in order to operate at cryogenic conditions.

Differently, the cost associated with the integration of cooling tubes in the porous membrane reactor is negligible when compared to the total CAPEX cost. Through these tubes, heat is recovered by producing high pressure steam, which is subsequently used in the steam cycle, posing a benefit in the net electricity generation compared to the dense membrane case. This argumentation is supported by the fact that the cost of the steam cycle in the porous membrane case is larger, meaning that a larger steam turbine and larger heat rejection units are required.

On the other hand, in the dense membranes case, the heat removed from the reactor is taken by the depleted air at the outlet of the MIEC membranes. This high temperature-high pressure air burns part of the recycle stream, increasing the temperature and accelerating the gas velocity to drive the gas turbine, where electricity is produced. Opposite to the porous membrane case, the heat management strategy for the dense membranes case is translated into a gas turbine cost, and a surplus of electricity generated.

The disaggregated ethylene cost, containing OPEX (electricity, natural gas and catalyst replacement) and CAPEX (investment and O&M), is shown in Figure 7.5:

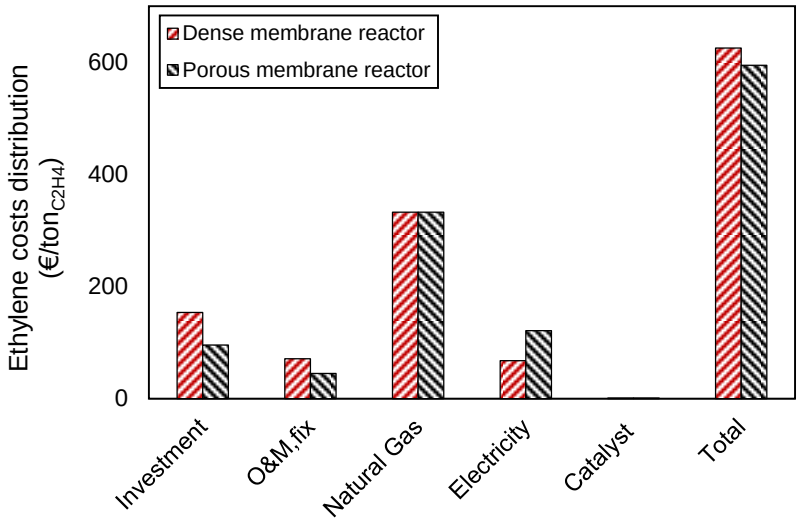

Figure 7.5. Disaggregated ethylene costs, including CAPEX and OPEX, for the OCM plant employing a dense membrane reactor (red) and a porous membrane reactor (black).

In both membrane reactors, the cost of the raw material emerges as the main contributor to the final ethylene cost. It should be mentioned here that this fact is strongly influenced by the selection of the location of the plant (Europe), which subsequently determines the price and composition of natural gas. As typically happens for chemical plants, and as presented in Chapter 6 for the conventional OCM packed bed case [10], the OPEX cost weights more than the CAPEX (shown in the graph as "investment", referring to the cost of all the units shown in Figure 7.4, and "O&M$_{fix}$"). The higher yearly fixed costs are related to a higher cost of maintenance for the dense membranes case and, overall, it can be concluded that the cost of the dense membranes is the main contributor to the higher price for the dense configuration.

7.4.1.1. Sensitivity on membrane costs

To analyze in detail how the cost of the membranes affects the overall ethylene price calculated in each of the selected configurations, a sensitivity analysis has been carried out.

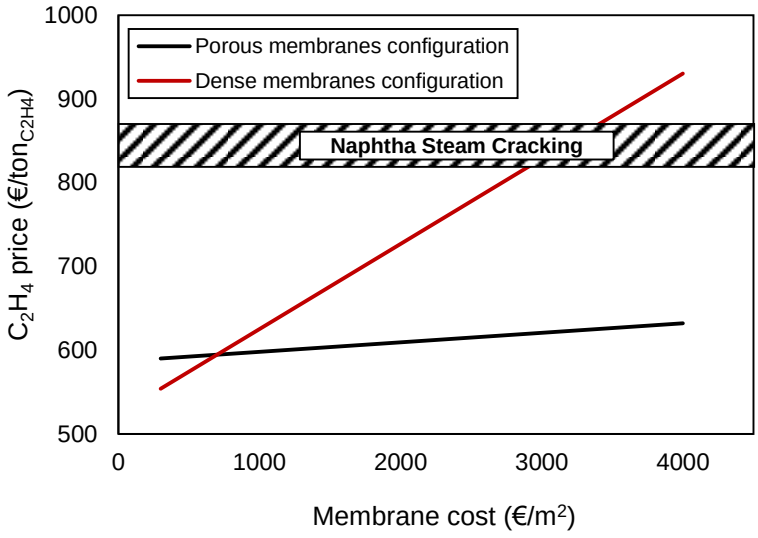

Figure 7.6. Calculated C_2H_4 price for the OCM porous and dense membrane reactor configurations when changing the cost of the membranes (in €/m²) and C_2H_4 price achieved with the conventional NSC.

As shown in Figure 7.6, the cost of the membranes in both configurations has been varied over a wide range to investigate its effect on the final ethylene price. This sensitivity is essential because of lack of accurate data regarding this parameter when considering industrial applications, since none of the membranes simulated here have been produced at industrial scale for the specific OCM process in such large quantities.

The fact that the trend line in the dense membranes case is much steeper than the porous one indicates that this configuration is more impacted by the membranes price. As explained before, this mostly relates to the larger membrane area required for this configuration. Differently, the porous membrane configuration remains (almost) unaffected by an increase in the membrane price, since the increase in price considered for this sensitivity is not sufficient to significantly influence the relatively low membrane area required. Subsequently, it can be concluded that the porous membranes case is independent from the membranes price (in the price range analyzed), and this factor is especially relevant because of the uncertainty in their industrial scale price.

Going to the specific values, it is noticeable that both dense and porous membranes are competitive in most of the cases analyzed compared with the conventional naphtha steam cracking, resulting in an ethylene price lower than 1000 €/ton$_{C_2H_4}$. It is also remarkable to note the different trend for both configurations: the lower the price of the membranes, the more competitive the dense membranes case in comparison with the porous membranes case. Actually, if the fabrication of dense membranes does not exceed 1000 €/m², this technology can already compete with the porous membranes case, while if the price becomes below 500 €/m² it starts to be even more economic because the investment cost will drop significantly while no relevant effects are found for the porous configuration where the ASU dominates the overall costing.

As previously mentioned, the absence of a large-scale producer of dense membranes gives uncertainty to the predicted cost of the dense membranes, and it is very important to stress that the characteristics of the employed membranes in the OCM reactor can strongly modify the economics of the process. For instance, the performance of the dense membranes is currently limited by the relatively low O_2 flux achieved with this type of membranes. If the oxygen flux considered initially here is doubled because of the employment of a different and better membrane, the membrane area required in the process would already be halved and consequently also the cost associated with these membranes. A detailed optimization of the membrane characteristics can make the oxygen flux through the membrane to vary in even more than one order of magnitude, thus affecting the total required membrane area and the total cost of the membranes. In particular, the type of membrane (supported or self-supported), membrane material (fluorite, perovskite), membrane thickness, membranes lifetime (currently set to 5 years) or recyclability to a certain extent are examples of parameters that need to be addressed for a proper membrane reactor design, given their effect on the final total plant cost. A trade-off between high oxygen flux, low cost and membrane stability and durability under OCM conditions (both chemical and mechanical) should be made to find the most suitable membrane for this specific application.

7.4.1.2. Analysis of electricity production/consumption

Besides the differences in investment and fixed costs, the other OPEX variables seem to be very similar when comparing the porous and dense membranes configurations, although some differences caused by the modifications in the plant scheme can be highlighted. Even if the net electricity demand is very similar for both configurations, there is a different distribution of the energy demand throughout the plant as presented in Table 7.3:

Table 7.3. Production (positive) and consumption (negative) of electricity (in MW) in the OCM plant for the dense membrane reactor and porous membrane reactor configurations.

ELECTRICITY PRODUCTIONS/CONSUMPTIONS (in MW)		
	Dense membranes	Porous membranes
Steam cycle	102.9	159.6
Refrigeration cycle	-201.7	-201.7
Syngas Compressor	-24.7	-24.7
CO_2 Capture	-7.8	-7.8
Gas turbine	45.3	0.0
Air Compressor	0.0	-15.8
Air Fan	0.0	-1.8
Air Separation Unit (ASU)	0.0	-43.3
Other Auxiliaries	-4.9	-4.9
TOTAL	-91.0	-163.4

The steam cycle in the porous membrane configuration produces almost twice the amount of electricity than in the dense membranes case. In the porous membranes process scheme, the cooling tubes placed inside the OCM reactor allow the generation of an additional amount of HP steam, thus increasing the power produced in the steam cycle. On the contrary, the heat of reaction is taken by the depleted air in the dense membranes process case. This hot stream is used to burn part of the recirculated gases, hence producing electricity in a gas turbine. Therefore, the electricity production/consumption distribution clearly follows the different approaches taken for the heat management inside the reactor in both configurations. The second relevant difference relates, as aforementioned, to the air separation unit. It can be seen

in the table that the air separation unit does not only affect the CAPEX, but also has a significant influence on the electricity balance of the process, being responsible for around 30% of the total electricity that needs to be imported in the porous membranes case (43 MW out of 163 MW).

7.4.2. Comparison of different reactor configurations

One of the main assumptions taken to perform the economic evaluation described in Section 7.2 relates to the reaction kinetics selected to describe the OCM reactor (see Chapter 4 for more information) [6]. These OCM kinetics were initially developed and validated for specific packed bed lab-scale reactor conditions, and its validation when integrating membranes was not carried out. Nevertheless, the high C_2 reactor yields (up to 60%) achieved with the membrane reactor are in agreement with other modelling OCM membrane reactor works (see Chapter 3). However, these yields have never been validated with experiments. As a matter of fact, the discrepancies in results between modelling and experimental works are significant and should be carefully considered. Therefore, and in order to make a more reliable evaluation, two extra scenarios have been considered here. The reactor performance obtained with the membrane reactors has been reduced by manually decreasing the reaction rate of the desired primary reaction (oxidative production of ethane from methane) such that a lower C_2 yield is obtained, better corresponding to experimental results in a packed bed membrane reactor is achieved. The kinetics has been adjusted in such a way, that a C_2 yield of around 30% is obtained, which is in line with the best OCM experimental results for a membrane reactor (see Chapter 2). This modification has been applied to the dense and the porous membrane reactor cases. The techno-economic evaluation of the previously mentioned membrane based processes and the experimental state-of-the-art membrane reactor configurations (indicated as lower yield) have been also compared with the conventional OCM packed bed process [10] and to the NSC process [2] in order to have a broader framework of the ethylene production market.

A summary of all the selected configurations together with the main operating parameters of each of them is listed in Table 7.4:

Table 7.4. Main parameters of the different OCM configurations and the naphtha steam cracking (NSC) considered to carry out the economic analysis.

Process		OCM					NSC
Configuration		**Classic PBR**	**Dense PBMR**	**Dense PBMR (lower yield)**	**Porous PBMR**	**Porous PBMR (lower yield)**	-
Natural Gas	kg/s	88.0	45.9	59.8	45.9	59.8	0.0
Naphtha	kg/s	0	0	0	0	0	97.2
Ethylene	kg/s	31.9	31.9	31.9	31.9	31.9	31.9
Other products	kg/s	0	0	0	0	0	34.3
Electricity production/consumption							
Steam cycle	MW	609.5	102.9	239.4	159.6	367.8	-
Gas turbine	MW	0.0	45.3	111.6	0.0	0.0	-
Refrigeration cycle	MW	-908.0	-201.7	-308.5	-201.7	-308.5	-
Syngas Compressor	MW	-106.4	-24.7	-37.7	-24.7	-37.7	-
CO_2 Capture	MW	-36.3	-7.8	-20.1	-7.8	-20.1	-
ASU	MW	-136.8	0.0	0.0	-82.0	-144.1	-
Other Auxiliaries	MW	-13.4	-4.9	-8.1	-6.7	-12.2	-
Net Electricity	**MW**	**-591.4**	**-91.0**	**-23.5**	**-163.4**	**-154.8**	**62.2**
Reactor							
Temperature	°C	850	800	800	800	800	850
CH_4/O_2	mol basis	3	2.5	2.5	2.5	2.5	-
Pressure	bar	10	10	10	10	10	1
CH_4 conversion	-	31.8%	64.0%	45.2%	64.0%	45.2%	-
C_2 selectivity	-	43.8%	86.3%	67.3%	86.3%	67.3%	-
C_2 Yield	-	13.9%	55.2%	30.5%	55.2%	30.5%	33%
Membrane area	m^2	0	53813	94500	6010	10554	-
Investment							

Membranes	M€	0.0	269.1	472.5	21.0	36.9	-
Refrigeration Cycle	M€	372.9	96.3	141.1	96.3	141.1	-
Methanizer	M€	306.1	69.9	99.1	69.9	99.1	-
CO_2 capture	M€	131.7	40.5	84.0	40.5	84.0	-
Steam Cycle	M€	127.9	41.4	69.3	52.3	89.3	-
Reactor	M€	111.7	0.7	1.1	1.5	3.7	-
ASU	M€	81.7	0.0	0.0	49.3	72.8	-
Gas Turbine	M€	0.0	34.7	62.9	0.0	0.0	-
Pumps and Compressors	M€	24.5	12.0	15.8	12.0	15.8	-
Boiler	M€	22.2	5.4	12.0	4.5	9.2	-
De-methanizer	M€	13.9	4.5	6.4	4.5	6.4	-
C_2-Separation	M€	11.1	11.1	11.1	11.1	11.1	-
Heat Integration	M€	11.0	4.1	5.8	4.1	5.8	-
Water Separation	M€	1.1	0.4	0.6	0.4	0.6	-
Total Costs (BEC)	**M€**	**1215.7**	**590.0**	**981.9**	**367.4**	**575.9**	**409.9**
				CO_2 Emissions			
Direct	$ton_{CO_2}/ton_{C_2H_4}$	1.3	0.2	0.5	0.2	0.5	2.8
Indirect	$ton_{CO_2}/ton_{C_2H_4}$	1.8	0.3	0.1	0.5	0.5	-0.2
CO_2 capture	$ton_{CO_2}/ton_{C_2H_4}$	2.6	0.4	1.2	0.4	1.2	0.0
Net emission	**$ton_{CO_2}/ton_{C_2H_4}$**	**0.5**	**0.1**	**-0.6**	**0.3**	**-0.2**	**2.6**
				Costs distribution			
Investment	€/$ton_{C_2H_4}$	317	154	256	96	150	206
$O\&M_{fix}$	€/$ton_{C_2H_4}$	148	72	118	46	71	78
Feedstock	€/$ton_{C_2H_4}$	636	332	433	332	433	1273
Electricity	€/$ton_{C_2H_4}$	438	67	17	121	115	-723
C_2H_4 price	**€/$ton_{C_2H_4}$**	**1540**	**625**	**824**	**595**	**768**	**834**

7.4.2.1. Ethylene price

The first index chosen to evaluate all these configurations is the final ethylene price that comes out from the process, disaggregated into the main cost contributors. The results of this comparison can be seen in Figure 7.7:

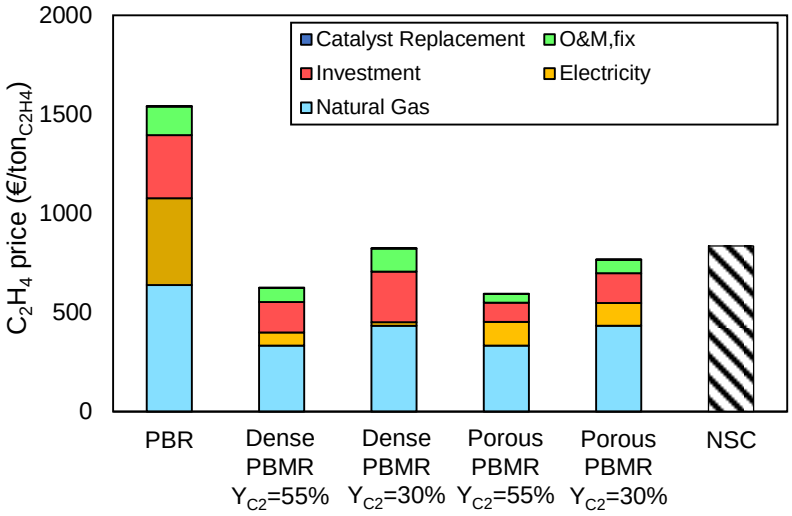

Figure 7.7. Cost distribution of the OCM process when using four different reactor configurations; packed bed (PBR), dense membranes reactor, dense membranes reactor with a reduced yield, porous membranes reactor and porous membranes reactor with a reduced yield, and of the conventional naphtha steam cracking (NSC).

Among the different OCM technologies, the maturity of the packed bed is the main advantage of the conventional packed bed configuration. However, it seems clear that a breakthrough in the technology is required to industrially compete with conventional ethylene production technologies, represented in this graph by the naphtha steam cracking. One of the most promising options to reach this necessary breakthrough is the integration of membranes in the reactor. It has already been widely explained that with this reactor modification the C_2 reactor yield can be increased, increasing the profitability of the process. The first consequence of this performance improvement relates to the decrease in the cost related to the raw material, natural gas. The more optimized methane conversion occurring in the OCM reactor decreases the total feed inlet requirement, thus reducing the costs associated

to the purchase of raw material. Secondly, the electricity demand and investment are strongly reduced when employing a membrane reactor. The higher yields in all the membrane reactor cases also makes the separation train cheaper. For instance, the stream comprising the incondensable gases that still remain after the C_2 separation, which actually contains some of the undesired products formed in the OCM reaction (stream P16 in Figure 7.1 and Figure 7.2) is reduced from 20.6 in the conventional OCM packed bed reactor to 3.9 kmol/s when the membrane reactor is employed. This is reflected in the investment cost, since the size of all the units downstream of the reactor could be lowered, including also a lower electricity demand due to the lower amount of energy required to separate the species involved in the various distillation columns.

The ethylene price in the cases in which the C_2 reactor yield has been decreased are still comparable to the price calculated by Spallina et al. [2] for the conventional naphtha steam cracking. This means that if the membrane reactor experiments, in which the 30% C_2 yield has been overcome [12]–[14], can be extrapolated at industrial conditions without any lose in performance, the OCM technology could be located within the range of industrial viability for ethylene production. However, this step is not as straight-forward as it may seem, since most of these experimental works are carried out at very specific conditions. Commonly, in the experiments at lab scale the extent of reaction is controlled by diluting the feed with an inert (usually N_2) and by using low flow rates (in the range of mL/min) in small reactors. With these actions, the reaction temperature can be easily kept within the optimal temperature range, where the selectivity towards the desired products is maximized. Instead, these shortcuts cannot be applied in an industrial application of the process, since they will significantly hinder its efficiency. As a result, the upscaling of the OCM membrane reactor process can be complex and it has not been yet experimentally tested.

When confronting the dense-porous cases, it turns out that the ethylene price obtained from the porous configurations (for both reduced and non-reduced C_2 reactor yield) is just slightly lower. In terms of technology maturity, MIEC membranes

are still very far from commercialization and most of the research has been devoted to pure O_2 production or to solid oxide fuel cells, in which the presence of an electric field improves the oxygen transfer rate [15]. If the fact that the maturity of porous membranes is much larger than the one of dense (MIEC) membranes is taken into account, porous membranes like the ones simulated in this chapter are commercially available, whereas MIEC dense membranes are certainly not produced at industrial scale yet (and it remains doubtful that in a relatively short timeframe the large number of membranes required to run the OCM dense membrane reactor plant can actually be produced), it comes out that the feasibility of the porous membrane reactor configuration clearly overcomes the one of the dense membranes case. In addition, possible extra issues of dense membranes that have not been tested yet, like the long term stability of the membranes (CO_2 tolerance) and sealings, possible interaction with the catalyst, etc. can direct more the decision towards the implementation of porous membranes, where several material aspects can be simplified, provided that problems with back-permeation can be overcome by applying a sufficiently large pressure drop over the membrane.

7.4.2.2. CO_2 emissions

Another relevant parameter to study in detail, especially considering all the political-environmental aspects that are currently being discussed in the society, is the environmental impact and the carbon footprint of the process. Because of that, the CO_2 emissions derived from all the processes have been evaluated and are shown in Figure 7.8:

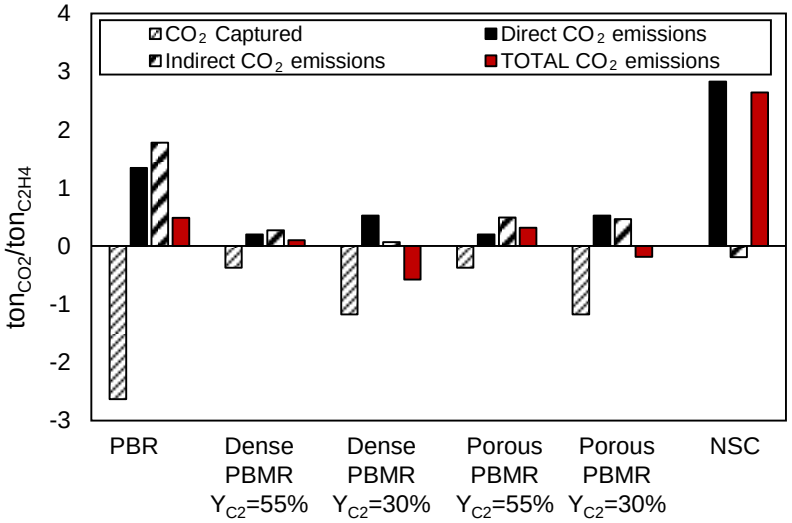

Figure 7.8. CO_2 captured, direct CO_2 emissions, indirect CO_2 emissions and total CO_2 emissions (all of them in $tonCO_2/tonC_2H_4$) for the five cases considered; packed bed (PBR), dense membranes reactor, dense membranes reactor with a reduced yield, porous membranes reactor and porous membranes reactor with a reduced yield, and conventional naphtha steam cracking (NSC).

Differently to the conventional NSC where the need of a fuel to supply heat to the reaction cracking reaction impacts directly the CO_2 emissions, the OCM technology requires a CO_2 separation unit in the plant which is able to deliver a stream of pure CO_2 which can be sent for long-term storage or used as carbon feedstock without being emitted to the atmosphere. This comes from the fact that CO_2 is produced itself in the process (as a by-product of the OCM reaction), necessitating its removal from the outlet reactor stream in order to be able to obtain pure ethylene. That is also the reason why the CO_2 capture rate in the conventional OCM case, that is, packed bed reactor (PBR), is much larger than in all the other cases because of the more C_2 unselective reactions taking place in this configuration.

In the case of NSC, CO_2 is not produced in the cracking process itself, but as off-gas from the combustion of light alkanes derived from the cracking technology to provide heat and/or electricity to the process. As a result, no CO_2 is captured in the NSC process and all the positive CO_2 emissions are direct and originated by the combustion of these hydrocarbons. The negative value shown in the indirect CO_2 emissions relies on the fact that, when combusting these hydrocarbons, the heat produced is recovered

by high pressure steam to power steam cycle, resulting in a large production of electricity, larger than required in the plant itself, thus creating a surplus of electricity that can be exported. Therefore, the negative emissions refer to the CO_2 that is saved when exporting electricity.

When comparing the different OCM configurations, it can be observed that the direct CO_2 emissions, related to the CO_2 emitted within the process (in the particular of OCM in the boilers used to supply energy for the plant), are much higher in the PBR configuration than in all the other cases. The large unconverted methane stream of this particular configuration, which partially goes to the burner to produce electricity, is the main cause of this big contribution. Since the reaction is more selective towards the desired products, this stream gets strongly reduced when integrating membranes in the reactor.

Similarly, the indirect CO_2 emissions, which account for the import/export of electricity and/or heat, are also much larger in the PBR in respect to all the other OCM cases. These emissions come from the need of electricity import because of the very energy intensive separation train required to separate the big amounts of undesired products formed in the OCM reactor from ethylene. In case of an integrated renewables plant to account for the electricity demand, the indirect CO_2 emissions could be removed, reducing significantly the footprint of the process. In the medium-long term scenario this is likely to happen, although several technical and policy related aspects are still open to guarantee that the required amount of electricity will be available for more than 8000 hours per years.

Overall, the total CO_2 emissions (accounting for direct, indirect and captured) are much lower for the OCM cases than for the NSC. In particular, the total CO_2 emissions in the OCM dense membranes configuration case are reduced by 96% and in the OCM porous membranes configuration by 88% when compared to the NSC. This factor is especially relevant if taxes are applied to CO_2 emissions, as it is likely to happen in the coming future. The conventional packed bed is still CO_2 positive because of the requirement of importing electricity, while the cases in which membranes are

integrated are roughly CO_2 neutral. In addition, these cases have the potential to become CO_2 emissions-negative, if the electricity that they require comes from a renewable source, hence removing the indirect CO_2 emissions contribution.

7.5. Conclusions

A techno-economic evaluation of different OCM membrane reactor configurations has been carried out. Two types of membrane reactor, which subsequently imply two different OCM process schemes, have been simulated. In the first of these two options, which integrates dense oxygen-selective membranes, the O_2-N_2 separation is carried out in-situ in the reactor, avoiding the utilization of an energy intensive air separation unit to purify O_2. The second membrane reactor configuration is based on the integration of porous membranes, and this has shown slightly better results (even though a separate air separation unit is required in this case), reducing the ethylene cost of production between 5 and 10% with respect to the dense membranes case. The reason of this finding is the larger membrane area required in the dense membranes case because of the lower flux of this type of membranes (membrane area required in the dense membranes configuration is around one order of magnitude higher than the porous one). The unfavorable economics and the current status of technology development of the dense membranes case lead to the conclusion that OCM using porous membranes is more convenient and currently more reliable. Nevertheless, the effective performance of the membrane reactor could possibly modify these results. A one-dimensional reactor model has been used to simulation all the reactor configurations, consequently assuming that, in the reactor, radial dispersion is infinitely fast. Therefore, the local oxygen concentration in the region close to the porous membrane wall has not been properly calculated. As a consequence, the fact that porous membranes employ higher oxygen fluxes, thus increasing the local oxygen concentrations more than in the dense membrane case, has not been considered. Higher local oxygen concentrations would mean a lower selectivity towards the desired products, reducing the reactor performance. An exhaustive evaluation of this situation, which would consist on linking the Aspen process scheme simulation to a

two-dimensional reactor model accounting for radial dispersion, would be necessary to study the influence/clarify this aspect.

Both configurations lead to a much lower ethylene price compared with the reference naphtha steam cracking, so that this price is competitive with conventional technologies. In particular, the viability of the process has been shown for the cases in which the reactor performance has been matched to experimental works reported in literature, where the ethylene price is still below the one calculated for the naphtha steam cracking technology. These promising results should concentrate the efforts towards the achievement of a larger prototype and push the development of the OCM membrane reactor technologies. In particular, issues that are "hidden" at small scales, such as heat management or reliability of the reaction kinetics need to be dealt with. In addition, the price of the membranes (both dense and porous) has been shown to be crucial in the economics of the OCM process, reaching in some cases even 50% of the total CAPEX cost. Therefore, an accurate evaluation/study of the membrane cost is necessary to continue with the scale-up of the process.

Finally, the results are also promising from an environmental point of view. In all the OCM cases, the overall CO_2 emissions are much lower than in the conventional NSC. Specifically, the independency of the electricity (the OCM membrane reactor technologies are almost neutral in electricity demand), translated into low indirect CO_2 emissions, helps balancing the CO_2 emissions. Thereby and in contrast to NSC, the OCM membrane cases are very close to reach the "zero" CO_2 emissions target, something which could be accomplished in the near future, if the electricity that these processes demand is obtained from renewable sources.

7.6. Bibliography

[1] S. J. Xu and W. J. Thomson, "Oxygen permeation rates through ion-conducting perovskite membranes," *Chemical Engineering Science*, vol. 54, no. 17, pp. 3839–3850, 1999.

[2] V. Spallina, I. C. Velarde, J. A. M. Jimenez, H. R. Godini, F. Gallucci, and M. Van Sint Annaland, "Techno-economic assessment of different routes for olefins production through the oxidative coupling of methane (OCM): Advances in benchmark technologies," *Energy Conversion and Management*, vol. 154, pp. 244–261, Dec. 2017.

[3] I. Martínez, M. C. Romano, P. Chiesa, G. Grasa, and R. Murillo, "Hydrogen production through sorption enhanced steam reforming of natural gas: Thermodynamic plant assessment," *International Journal of Hydrogen Energy*, vol. 38, no. 35, pp. 15180–15199, 2013.

[4] *Cleaver Brooks. Boiler efficiency guide*. 2010.

[5] *Iea - Energy Technology Group. Industrial Combustion Boilers*. 2010.

[6] Z. Stansch, L. Mleczko, and M. Baerns, "Comprehensive kinetics of oxidative coupling of methane over the La2O3/CaO catalyst," *Industrial and Engineering Chemistry Research*, vol. 36, pp. 2568–2579, 1997.

[7] A. Arratibel, U. Astobieta, D. A. Pacheco Tanaka, M. van Sint Annaland, and F. Gallucci, "N2, He and CO2 diffusion mechanism through nanoporous YSZ/γ-Al2O3 layers and their use in a pore-filled membrane for hydrogen membrane reactors," *International Journal of Hydrogen Energy*, vol. 41, no. 20, pp. 8732–8744, 2016.

[8] A. Arratibel Plazaola *et al.*, "Mixed Ionic-Electronic Conducting Membranes (MIEC) for Their Application in Membrane Reactors: A Review," *Processes* , vol. 7, no. 3. 2019.

[9] V. Spallina, T. Melchiori, F. Gallucci, and M. V. S. Annaland, "Auto-Thermal Reforming Using Mixed Ion-Electronic Conducting Ceramic Membranes for a Small-Scale H2 Production Plant," pp. 4998–5023, 2015.

[10] A. Cruellas, J. J. Bakker, M. van Sint Annaland, J. A. Medrano, and F. Gallucci, "Techno-economic analysis of oxidative coupling of methane: Current state of the art and future perspectives," *Energy Conversion and Management*, vol. 198, p. 111789, 2019.

[11] Y. A. Çengel, *Introduction to Thermodynamics and Heat Transfer*. 2008.

[12] F. T. Akin and Y. S. Lin, "Controlled Oxidative Coupling of Methane by Ionic Conducting Ceramic Membrane," *Catalysis Letters*, vol. 78, no. 1, pp. 239–242, 2002.

[13] S. Bhatia, C. Y. Thien, and A. R. Mohamed, "Oxidative coupling of methane (OCM) in a catalytic membrane reactor and comparison of its performance with other catalytic reactors," *Chemical Engineering Journal*, vol. 148, no. 2–3, pp. 525–532, 2009.

[14] N. H. Othman, Z. Wu, and K. Li, "An oxygen permeable membrane microreactor with an in-situ deposited Bi1.5Y0.3Sm0.2O3–δ catalyst for oxidative coupling of methane," *Journal of Membrane Science*, vol. 488, pp. 182–193, Aug. 2015.

[15] J. Sunarso, S. S. Hashim, N. Zhu, and W. Zhou, "Perovskite oxides applications in high temperature oxygen separation, solid oxide fuel cell and membrane reactor: A review," *Progress in Energy and Combustion Science*, vol. 61, pp. 57–77, 2017.

Chapter

8

Epilogue

Abstract

In the epilogue, the most relevant findings of the thesis have been listed and the main challenges that still need to be overcome to experimentally demonstrate the potential of the OCM technology are described.

8.1. Conclusions and Recommendations

The search for a competitive alternative to the very energy-consuming naphtha steam cracking process for the production of ethylene has been the motivation for the study described in this PhD thesis. In particular, the feasibility of the oxidative coupling of methane for the direct production of ethylene from natural gas has been evaluated.

The overview and discussion of the current status of the OCM technology, including the description of most of the OCM reactor concepts proposed in literature (including patents), has evidenced the main issue for the industrial viability of the process, namely the poor C_2 yield attained during the reaction. Nevertheless, in this literature review most of the authors agree on the fact that, theoretically, a uniform distribution of oxygen along the reactor length can contribute to maintain a high selectivity towards the desired products at relatively high reactants conversions, improving the reactor performance when compared to the conventional reactants co-feeding strategies.

In order to evaluate and compare different oxygen feeding policies and to quantify the expected improvements that the oxygen distribution should bring, phenomenological one-dimensional models have been developed. The results of these models show the expected behavior, that is, the C_2 yield is significantly increased when the oxygen is distributed along the reactor. In addition, these models also highlight the necessity of obtaining a proper reactor heat management to keep the temperature within the optimal OCM range to avoid side reactions. Among all the studied configurations, membrane reactors (both packed bed and fluidized bed) arise as the concepts showing the largest improvements with respect to the conventional packed bed, reaching (calculated) C_2 yields of around 60%. However, the reliability of the model results is hindered by the fact that radial profiles (both of heat and mass transfer) are neglected. Even though the benefits of the membrane reactor have been clearly highlighted, the implementation of a two-dimensional model (which could be realized in future research works) would contribute to have a better understanding of the system and to

better predict the concentration profiles of all the species, which can influence the overall OCM reactor performance, therefore allowing for a further optimization of the reactor design. Nevertheless, the promising modelling results for the OCM membrane reactors are the main reason why this reactor concept was selected for further experimental studies.

The experimental part of this thesis has started by evaluating the performance of the Mn-Na_2WO_4/SiO_2 catalyst, which is nowadays considered to be the most suitable catalyst for OCM when balancing activity, stability and selectivity. When employing the conventional packed bed reactor configuration, experimental C_2 yields of around 20% have been achieved with such a catalyst, where this value exceeds the performance reported in many other published experimental work, thus corroborating its suitability for OCM. In addition, special attention has been paid to the secondary reactions, especially in the specific conditions employed in a membrane reactor, because of their high relevance on the overall process performance. One of the main findings of this study is the strong influence that the combustion of ethylene, the fastest in the conditions of study among all the undesired secondary reactions, can have in the system. Because of that, a specific reactor in which this reaction is minimized, either by optimizing the most relevant reaction parameters such as catalyst dilution, residence time etc. or via the implementation of alternative reactor configuration such as membrane reactors, should be carefully designed. Even though the reaction orders of all the reactions have been determined in the in-house developed kinetics, additional experiments at different temperatures are required to determine all activation energies and pre-exponential factors. This fact hampers a wider application of this kinetics model (as aforementioned, heat management is a relevant aspect for OCM) and impedes its application in non-isothermal models.

With the information gained from the analysis of the non-conventional reactor configurations and from the tests carried out with the Mn-Na_2WO_4/SiO_2 catalyst, experiments using membrane reactors have performed. The promising membrane reactor performance predicted by simulations together with its relative simple

operation, especially when compared to the fluidized bed membrane reactor (where high mechanical resistance of all the elements comprised in the reactor is needed), has led to the selection of the packed bed membrane reactor concept.

Porous membranes have been selected to carry out these packed bed membrane reactor experiments because of the complexity, mainly sealing and mechanical and chemical stability, of the integration of MIEC membranes. A packed bed membrane reactor has been designed and tests were carried out with symmetric MgO porous membranes. In these tests, the desired distribution of oxygen along the reactor length was corroborated by analyzing the temperature profiles observed in the different experiments. As expected, flatter profiles in the membrane reactor experiments (when compared to the co-feeding strategies) were obtained. Nevertheless, this oxygen distribution did not result in an improvement in the reactor performance. The experiments have revealed that back-permeation of hydrocarbon reactants and products impeded the improvement that was theoretically predicted. A study on the effect of the effective diffusion coefficient of the porous membrane has shown the necessity to tune the membrane parameters (mainly thickness and pore size) and accomplish an optimal OCM membrane reactor design. A further optimization of the porous membrane characteristics, for example by employing asymmetric membranes, is required to maximize the benefits of these membranes when integrated within an OCM reactor. Even though all the benefits of the packed bed membrane reactor concept could not be experimentally demonstrated, the tests carried out could show experimentally the most critical parameters that need to be optimized in this configuration, being this information very useful for a better design of further experiments.

Finally, the potential of the OCM technology has also been evaluated from a process point of view. Although the specific values obtained in this study may have some uncertainty because of the many strong assumptions taken, the observed trends and tendencies are very illustrative to place the OCM technology within the ethylene production market. To the knowledge of the author, this has been the first time that

the OCM reactor technology has been compared by evaluating the ethylene price by simulating an industrial scale OCM plant. It has been shown that the lowest ethylene price is not realized at the optimal reactor C_2 yields, and that also other plant costs, upstream and downstream the OCM reactor, should be accounted for. Although the conventional packed bed reactor cannot compete with the conventional ethylene production technologies, the simulations have shown that the potential of OCM becomes interesting when C_2 yields of around 25% can be achieved (especially if obtained at high C_2 selectivities). Below this target value, the separation train of the process becomes too expensive, since many undesired by-products and/or unconverted reactants need to be processed.

Contrary to the conventional OCM packed bed case, the results are completely changed when employing membrane reactors. In the techno-economic evaluation, the industrial viability of the OCM membrane reactor (both with porous and dense membranes) concept has been confirmed, and quite competitive ethylene prices have been obtained. In addition, also from an environmental point of view (in terms of CO_2 emissions) the different OCM membrane technologies outperform conventional technologies.

One of the most important next steps that need to be taken is a more detailed experimental validation of all the employed phenomenological models. The experimental work reported in this thesis has provided interesting results and important insights for the OCM technology and form a good basis for further experimental studies. However, the improvements expected from the simulations of membrane reactors over conventional OCM technologies could not yet be explicitly demonstrated by experiments, and this should be the focus of future experimental work.

8.2. Outlook

The main objective of this thesis was the development of a more efficient and sustainable technology for the production of ethylene. According to the author, the potential of the oxidative coupling of methane when employing a packed bed membrane reactor configuration has been shown. Several steps in the further development of this technology have been taken, viz. reactor simulations, lab-scale experiments and process simulations focusing both on the economic and environmental impact of the technology, and the results have been investigated in detail. Moreover, the complexity of the technology, which currently hampers the industrial exploitation of the process, and the obstacles encountered to experimentally demonstrate the promising results achieved with simulations, have also been extensively discussed. Therefore, the main challenge that still remains to be addressed is the experimental demonstration of the OCM membrane technology on lab or pilot scale to clearly show the advantages of this process. In addition (in the opinion of the author), more research should already focus on scaling-up of the technology, since several experimental works carried out up-to-date just focused on achieving high yields under conditions that cannot be used for larger industrial scale systems. The scaling-up should focus on industrial-scale conditions, such as the utilization of undiluted gas feeds, the employment of large gas volumes and large reactors, and the validation of long-term mechanical and chemical stability of all the elements contained in the OCM system under industrial conditions (i.e. high pressures or recirculation of certain species into the reactor). Moreover, the use of larger reactors could also result in steeper radial concentration and temperature profiles in the reactor, an effect demonstrated to be of high relevance for the OCM process. All these factors should be carefully controlled, analyzed and optimized to avoid or minimize a decrease in the reactor performance when going from lab-scale to industrial-scale OCM experiments.

Publications and contributions

PUBLICATIONS

A. Cruellas, T. Melchiori, F. Gallucci, and M. Van Sint Annaland, "Advanced reactor concepts for oxidative coupling of methane," *Catalysis Reviews*, 2017.

A. Arratibel, **A. Cruellas**, Y. Liu, N. Badiola, D.A. Pacheco Tanaka, M. Van Sint Annaland, F. Gallucci, "Mixed ionic-electronic conducting membranes (MIEC) for their application in membrane reactors: a review," *Processes (MDPI),* 2019.

A. Cruellas, T. Melchiori, F. Gallucci, and M. Van Sint Annaland, "Oxidative Coupling of Methane: A Comparison of Different Reactor Configurations," *Energy Technology*, 2019.

A. Cruellas, J.J. Bakker, M. Van Sint Annaland, J.A. Medrano, F. Gallucci, "Techno-economic analysis of oxidative coupling of methane: Current state of the art and future perspectives," *Energy Conversion & Management*, 2019.

A. Cruellas, J. Heezius, V. Spallina, M. Van Sint Annaland, J.A. Medrano, F. Gallucci, "Oxidative coupling of methane in membrane reactors; a techno-economic assessment," *Processes (MDPI)*, 2020.

A. Cruellas, M. H. Khalinle, V. Varughese, F. Gallucci, M. Van Sint Annaland, "Mn-Na2WO4/SiO2 kinetics for oxidative coupling of methane; influence of secondary OCM reactions," in preparation, 2020.

A. Cruellas, W. Ververs, F. Gallucci, M. Van Sint Annaland, "Experimental investigation of the oxidative coupling of methane porous membrane reactor concept and its comparison with the conventional packed bed," in preparation, 2020.

A. Cruellas, M. De Keizer, M. Martínez, F. Layo, J. A. Medrano, F. Gallucci, M. Van Sint Annaland, "Effect of elevated temperatures in fluidized beds by means of the experimental ePIV/DIA technique," in preparation, 2020.

CONFERENCE CONTRIBUTIONS

A. Cruellas, T. Melchiori, F. Gallucci, M. Van Sint Annaland, "Oxidative coupling of methane: A comparison of diferent reactor configuraitons" in Third European Workshop on Membrane reactors: Membrane reactors for Process Intensification (MR4PI2017) in Verona, **Poster presentation**, 2017.

A. Cruellas, V. Middelkoop, M. Van Sint Annaland, F. Gallucci, "Oxidative coupling of methane in a catalytic membrane reactor: Membrane development and reactor design" in International Conference on Catalysis in Membrane Reactors (ICCMR13) in Houston, **Oral presentation**, 2017.

A. Cruellas, F. Gallucci, M. Van Sint Annaland, "Novel catalytic membrane reactor for oxidative coupling of methane: reactor modelling and design" in 10th World Congress of Chemical Engineering (WCCE10) in Barcelona, **Oral presentation**, 2017.

A. Cruellas, V. Spallina, J.A. Medrano, H.R. Godini, M. Van Sint Annaland, F. Gallucci, "Techno-economic assessment for C_2H_4 production using OCM integrated with membrane and membrane reactor" in 10th World Congress of Chemical Engineering (WCCE10) in Barcelona, **Oral presentation**, 2017.

A. Cruellas, M. Van Sint Annaland, F. Gallucci, "Mn-Na_2WO_4/SiO_2 kinetics for oxidative coupling of methane; Influence of secondary reactions" in 25th International Symposium on Chemical Reaction Engineering (ISCRE25) in Florence, **Poster presentation**, 2018. **Awarded as best poster presentation**.

A. Cruellas, F. Fabbricatore, F. Gallucci, M. Van Sint Annaland, "Study of MIEC membranes for their application in an OCM membrane reactor" in 15th International Conference on Inorganic Membranes (ICIM15) in Dresden, **Oral presentation**, 2018.

A. Cruellas, M. Martinez, F. Layo, M. De Keizer, F. Gallucci, M. Van Sint Annaland, "Experimental investigation of high-temperature fluidization using the ePIV/DIA technique" in Fluidization XVI conference in Guilin, **Oral presentation**, 2019.

A. Cruellas, W. Ververs, J.A. Medrano, D. Frank, U. Werr, F. Gallucci, M. Van Sint Annaland, "Oxidative coupling of methane: comparison of performance between different reactor configurations" in International Conference on Catalysis in Membrane Reactors (ICCMR14) in Eindhoven, **Oral presentation**, 2019.

A. Cruellas, J. Bakker, J. Heezius, J.A. Medrano, V. Spallina, M. Van Sint Annaland, F. Gallucci, "Feasibility of oxidative coupling of methane via membrane reactors" in Netherlands Process Technology Symposium (NPS19) in Eindhoven, **Oral presentation**, 2019.

Acknowledgements

When I decided to come to the Netherlands, I could not imagine learning as many things as I have learnt, and to grow as much as I have grown. I feel I am a completely different person from the one that arrived the first day to TUE, and this is something I will be grateful to many people I have met all along these years. With many people we started being colleagues, but after so many good and not so good moments we ended up being friends.

I would like to start by thanking my supervisors for all the help that have provided to me during this time. Fausto and Martin, thank you for giving me the opportunity of doing this PhD and for the confidence you have placed on me to develop this project. I am very happy and thankful about your decision of choosing me to carry out the research within the MEMERE European project. You have brought continuously nice ideas to the table and you have helped and supported me to solve many problems and issues that we have encountered during this process, thank you very much for that. During all the time and situations we have shared, I have learnt a lot and this has had a major impact on my development from a scientific point of view but more important from a personal point of view.

My PhD belongs to a European project formed by 12 institutions. All the meetings, calls and discussions we have had during this time have enriched me in many aspects, and some people of this big team have been essential for me during this time. I have learnt from all of you. In particular, thanks to all the people from Tecnalia and to Hamid, you have been always willing to selflessly spend part of your time with me.

I am also grateful to the staff members within our group that have helped me during these years. Especially, I would like to thank Joost, Joris, Thijs and Herbert because of all the support given to me. I appreciate your creativity and initiative when facing experimental issues. Besides them, the secretaries of the group, Ada and Judith, have been dealing with all the administrative part of my PhD, something especially valuable at the beginning.

On top of it, this PhD would not have been possible without the help of many other people. I would like to start by thanking all the students I have had over this period. This book is here in part because of you, the great contribution of all of you has been fundamental for this work. Gabriel, Mohamed, Katia, María, Anouk, Huib, Fátima, Vandhana, Federico, Johnno, Marthijn, Wout and Jelle, thank you very much.

I would like to continue by thanking all the colleagues I have met in TUE, you are a key part of this story. First of all, many THANKS to my office mates. I can now say that I was very lucky to be placed in that office. We have had many useful discussions but I have also enjoyed a lot our "non-working" conversations. Jose, you have been there since the beginning and you have helped me a lot, and still you do it, something that I really appreciate. Alba, you still don't know how important you were at the beginning of my PhD, I will be always grateful for that. And Niek, I have learnt a lot from you and your personality, especially towards the end of the PhD.

But a part from my office mates, there are some people here that, as I said, became my friends. Here I want to specifically mention 3 people which made (and make) much easier my stay here in different ways, being all of them very valuable for me. Many thanks to Maria, Giulia and Francesco, sometimes you don't realize the value of the support you are constantly giving to me. But not just them have been important in this trip, I also want to thank Alessandro, Milan, Nerea, Jon, Solomon, Leon, Stefan, Evan, Tim, Dario, Kai, Marian, Arash H., Vincenzo, Alvaro, Mohammad, Ildefonso, Michela, Arash R., Camilla, Olivia, Morteza, Wendy and Kun. Moreover, people from outside the university are also a big part of this story. Many thanks to Carmen, Luca,

Hossein and Kelly. Y por supuesto, Elisa, Isabel y Luis (y a vuestra antena parabólica ;)). Habéis sido un gran apoyo durante todo este tiempo y eso es algo que siempre os agradeceré, muchas gracias por todo!

Y para terminar, desde aquí también quiero dar las gracias a toda la gente que está en España y que me ha apoyado (y visitado en muchos casos) durante este tiempo.

Dar las gracias en particular a los amigos de Fraga, y en especial a Jesús y Ángel por encontrar siempre tiempo para vernos. Gracias también a la gente de Madrid con la que siempre es un placer organizar viajes. Y gracias al grupo de la Universidad (Edu, Edu, Juan, Juan, Juanma y Javi) por juntarnos de vez en cuando para recordar tiempos pasados.

Y por último, María, Carlos y Rubén. Me lo habéis dado todo y siempre me habéis apoyado y ayudado. Y aunque no lo digo a menudo, quiero que sepáis que es una suerte tener unos padres como vosotros. Rubén y yo estamos orgullosos de vosotros. Y por qué no decirlo también, Rubén, es una suerte tener un hermano como tú. Pero no sólo gracias a vosotros, también al resto de la familia. Seguir compartiendo momentos con todos vosotros es una de las principales razones por las que cada vez que vuelvo a Fraga lo hago con mucha ilusión. Este tipo de momentos son los que se echan de menos y se ven con envidia cuando uno está lejos. Todas estas cosas, que se van apreciando más y más con los años, no las cambiaría por nada y te llenan de fuerza y ánimos para coger el avión de vuelta.

Gracias a todos!

Aitor Cruellas Labella, Eindhoven, March 2020

About me

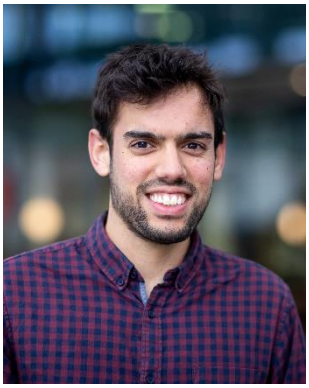

Aitor Cruellas Labella was born in Fraga, Huesca, Spain, the 15th of August of 1991. He started his studies in Fraga, where he remained until the age of 18. At that age he moved to Zaragoza to enroll in the University of Zaragoza to start a 5-year degree in Chemical Engineering. He coursed the 4th year of this degree in Torino, Italy, using an Erasmus exchange student scholarship. He graduated in 2015 after developing his degree Thesis (*Study of the recirculation gas in a pyrolysis process of sewage sludge carried out in a fluidized bed reactor*) within the "Thermo-chemical Processes" group of the University of Zaragoza. After his graduation, he obtained a scholarship given by the SAMCA group which allowed him to carry out a 4 month-internship in the R&D department of NUREL S.A, a polymers factory located in Zaragoza.

The 1st of October of 2015 he moved to Eindhoven to start his PhD in the "Chemical Process Intensification" (SPI) group of the Eindhoven University of Technology (TUE) under the supervision of Professor Fausto Gallucci and Professor Martin Van Sint Annaland. The title of the PhD is "*Feasibility of a catalytic membrane reactor for ethylene production via oxidative coupling of methane*", is funded by the European Union and it belongs to the MEMERE European project. The research work executed during this PhD is presented in this dissertation ceremony. In 2018, Aitor was awarded as the best Poster presentation at the "International Symposium on Chemical Reaction Engineering" (ISCRE18) in Florence. From April 1st he is employed as researcher in the Sustainable Process Engineering (SPE) group under the supervision of Professor Fausto Gallucci.